The Bedrock Geology of the Wallingford Quadrangle, New Haven County, Connecticut, with a Map and Cross-section.

Randolph Steinen [1,3]

Allison B. Charney[2]

Assisted by

James Bogart [1]

Rebecca VandeerLeest [3]

Heidi Salg [2]

Kaitlin Taylor [2]

STATE GEOLOGICAL AND NATURAL HISTORY SURVEY OF CONNECTICUT
Department of Energy and Environmental Protection

QUADRANGLE REPORT NO. 42

2021

1. Connecticut Geological and Natural History Survey, Department of Energy and Environmental Protection, 79 Elm Street, Hartford, Connecticut.
2. Department of Geological Sciences, Central Connecticut State University, New Britain, Connecticut.
3. Center for Integrative Geosciences, University of Connecticut, Storrs, CT.

TABLE OF CONTENTS:

List of Figures:

Appendix I Figures:

Bedrock Geology of the Wallingford Quadrangle with a map and cross-sections.

Randolph Steinen (1, 2), Allison B. Charney (3)

(1) State Geological Survey of Connecticut, Department of Energy and Environmental Protection, Hartford, CT; (2) Center for Integrative Geosciences, University of Connecticut, Storrs, CT; (3) Department of Geological Sciences, Central Connecticut State University, New Britain, CT.

SUMMARY

This report discusses observations and interpretations made during construction of a detailed geological map (1:12000) of the Wallingford quadrangle (Plate I) in Connecticut. Our map more accurately plots the location of rock bodies and their contacts with adjacent rock bodies than previous maps (Sanders, 1972a; Rodgers, 1985). The entire quadrangle lies within the Central Valley of Connecticut and Massachusetts (Bell, 1985) and is underlain by Mesozoic sedimentary, volcanic, and intrusive igneous rocks of the Hartford Basin.

Most of the quadrangle is underlain by New Haven Arkose which consists of A) medium- to coarse-grained pebbly arkosic sandstone and conglomerate and B) pinkish-gray to brick-red sandstone and siltstone. The conglomerate and sandstone beds are lenticular and typically have sharp erosional, channel-like bases. The conglomerates that we have seen occupy the deepest parts of the channel topography; they grade upward to pebbly sandstone. Cross-bedding is rarely seen but where interpretable indicates northwesterly to southerly flowing depositional currents. The coarse facies is ridge-forming and more abundant in the eastern parts of the quadrangle. The red, finer grained facies is less resistant and is exposed in stream valleys and artificial exposures along highways. It is composed of coarse- to fine-grained sandstone and siltstone that are bedded and cross-bedded. Mudstones are rarely exposed.

The Talcott Basalt conformably overlies New Haven Arkose. The magma that fed the basalt flows was erupted through a number of dikes and intruded into associated sills. The Talcott Basalt is altered everywhere in the quadrangle, but is so strongly altered in the central portion of the quadrangle that it does not crop out. The basalt is composed of clinopyroxene and calcic plagioclase feldspar with minor amounts of magnetite/ilmenite. It consists in some places of pillowed basalt and in other places of basaltic agglomerate. At one location, near the southern boundary of the quadrangle, agglomerate overlies the pillowed basalt, but otherwise a stratigraphy was not observable.

Intrusive West Rock Diabase forms dikes and sills referred to as the Fairhaven dikes (also referred to as the Higganum dike where it intrudes crystalline rocks to the east of the quadrangle) that are interpreted as the feeder dikes to the Talcott Basalt (Philpotts and Martello, 1986). The West Rock Diabase dikes have the same composition as the Talcott Basalt, but in addition, the chilled margins contain olivine microcrysts. Pyroxenes commonly form glomeroporphyritic aggregates.

Overlying the Talcott Basalt with apparent conformity is the Shuttle Meadow Formation, which crops out in the valley of Gulf Brook and the valley of an unnamed stream immediately

north of Totoket Mountain. Outcrops of the Shuttle Meadow Formation consists of fine- to medium-grained feldspathic sandstone.

The Holyoke Basalt occupies the southeastern corner of the quadrangle overlying the Shuttle Meadow Formation and forms an impressive ridge with up to 100 m (200-300 feet) of relief. The ridge is cuesta-form with north and northwest facing cliffs and a gentle southeasterly dip-slope. It consists of clinopyroxene and calcic plagioclase feldspar with minor amounts of magnetite/ilmenite.

The Buttress Dike, thought to be the feeder dike for the Holyoke Basalt (Philpotts and Martello, 1986), crops out in the northwest corner of the quadrangle. The Buttress Diabase consists of massive fine- and medium-grained diabase and breccia consisting of clasts of diabase mixed with clasts and disaggregated grains of sandstone.

The East Berlin Formation does not crop out in the Wallingford quadrangle, but is likely present in the subsurface of the extreme southeastern corner. Closest outcrops of East Berlin Formation are several hundred meters south of the southern quadrangle boundary.

Thin, near vertical, dikes (1-2m in width) of finely crystalline lamprophyre intrude the West Rock Diabase in the east central part of the quadrangle (Taylor and others, 2019). The dikes contain phenocrysts, up to 3 cm diameter, of biotite, amphibole and clinopyroxene. These dikes are similar to previously described lamprophyre dikes (Eppler, 1999, Charney and Philpotts, 2004; Philpotts and Philpotts, 2010) and possibly are Cretaceous in age (Armstrong and Besancon, 1970; Armstrong and Stump, 1971).

We have made detailed petrographic observations of the diabase and basalt in the area and analyzed whole rock chemistry to confirm that the dikes and sills in all but the northwest corner of the quadrangle are not Buttress Diabase (Buttress Dolerite; Jb) as mapped by Rodgers (1985). Rather, the dikes and sills in the Wallingford quadrangle have affinities to the Fairhaven dikes in the Branford quadrangle (Philpotts and Martello, 1986) that have been shown to be feeders of the Talcott flows (Philpotts and Asher, 1992).

We cannot confirm the mapped extent of the Talcott Basalt interpreted by Sanders (1972a) and we cannot recognize the Foxon Fault (Sanders and others, 1963; Sanders, 1970) in the Wallingford quadrangle. Sanders (1972a) mapped a fault cutting out the Talcott Basalt in the northern part of the quadrangle, an interpretation carried to the State Geological map by Rodgers (1985). We on the other hand find the Talcott Basalt in that area (and in the Durham quadrangle) to be so altered that it does not crop out (Steinen and others, 2017). A fault is not needed to explain the disappearance of the typical basalt-ridge exposure.

We have confirmed many of the structural interpretations of the nineteenth and early twentieth century geologists (Davis, 1898; Krynine, 1936), notably that the major faults are oriented northeast/southwest and are down to the northwest with possible strike-slip (dextral) movement. These observations further cast doubt on the existence of the Foxon Fault (Sanders and others, 1963), a down to the southeast fault, hypothesized on the west side of the Gaillard graben. We, therefore, also question the existence of the graben structure proposed by Sanders.

INTRODUCTION

The Wallingford quadrangle is one of the few quadrangles in Connecticut without a published bedrock geological map at a scale of 1:24,000. A surficial geological map was published by Porter (1960) that shows many of the outcrop areas we visited. The bedrock was mapped by John Sanders and his students in the 1960s and several preliminary compilations of his field data (Sanders, 1972a) are available in the files of the State Geological Survey. Based on Sanders' compilations, Rodgers (1985) showed the geology of the quadrangle at a scale of 1:125,000. These maps were consulted in constructing the map included with this report (Plate I). Most of the outcrops indicated on both the Sanders and Porter maps were visited. Some, however, are overgrown or covered by colluvium or otherwise could not be located. Others have been obliterated or covered during intense urban development, much of which has occurred since both prior maps were constructed. At least two of the outcrops we visited have been lost since in a similar manner.

Acknowledgements. This geologic map was funded in part by the USGS National Cooperative Geologic Mapping Program under StateMap award number G16AS00006, 2016. Matching funds were met by the Connecticut Department of Energy and Environmental Protection which also provided abundant logistic support as well as helping to fund chemical analyses.

Erin O'Hare, Environmental Planning, Town of Wallingford, provided us with maps of town owned property and information about rock outcrops in Wallingford. Carey Duques, Town Planner, and Kurt Weiss, Town Engineer, North Branford provided us maps and information about location of town owned property.

Numerous institutions allowed us access to their property or records. The South Central Regional Water Authority granted us a permit (and issued us a key) to repeatedly access their land. The East Shore Health District and Quinnipiac Valley Health District provided access to water-well completion reports. Leslie Peters and the ACES School District allowed our access to school property in North Branford. Capasso Construction allowed us access to outcrops on their storage yard; Mineri Timberwood Homes in North Haven gave us permission to study rock outcrops in their development on Patten Road in North Haven. The Wallingford Rod and Gun Club provided us access to their land on numerous occasions. Ochenkowski Excavation allowed access to their property on Village Road, North Haven.

Numerous individuals gave us permission to study outcrops on private property. Several individuals refused permission to map their property; outcrop distribution and geological interpretations on such properties were made by pattern recognition on hillshaded LiDAR digital elevation models (DEMs).

Several students from local universities accompanied us in the field. James Bogart, a student (Southern Connecticut State University) intern at the Department of Energy and Environmental Protection from 2015-2017 participated in the field mapping and also was the

principal cartographer for our early results. Rebecca VanderLeest, University of Connecticut, worked with us during the summer 2016 field season. Heidi Salg, a volunteer from Central Connecticut State University helped us in the field numerous times during 2017. Kaitlin Taylor, a volunteer from Central Connecticut State University, accompanied us in the field during 2018-19 and helped our analysis of a lamprophyre dike (see Taylor and others, 2019). Earl Manning, then a student at Central Connecticut State University conducted observations with Steinen on the Buttress Dike during 2006-8. Alan Tanwi, a student intern from Central Connecticut State University, and Taryn Isenburg, a recent graduate of Mt. Holyoke College, provided cartographic assistance with the final map.

Mark Evans, allowed us the use of department equipment at Central Connecticut State University. Lisa Park Boush granted us access to the rock preparation equipment at the Center for Integrative Geosciences at the University of Connecticut. Anthony Philpotts, Emeritus Professor at the University of Connecticut, provided advice, help with interpretation, encouragement, and accompanied us in the field on occasion. Thomas Nosal provided cartographic support, without which the final map would not have been completed.

Detailed reviews of our preliminary manuscript by Jean Crespi, (University of Connecticut), Phil Resor (Wesleyan University), and Paul Olsen (Lamont-Doherty Earth Observatory, Columbia University) improved this report immeasurably by pointing out an embarrassing number of our errors in grammar and spelling but more importantly in our interpretative overstatements.

Finally, special thanks to Margaret Thomas, State Geologist of the State of Connecticut, for support and encouragement throughout this project, for help in obtaining funding, for accompanying us in the field on several occasions, for her editorial expertise, and for keeping the senior author scientifically grounded.

Methods. For the majority of the summer and fall of 2016 and then less frequently in 2017 and 2018 we visited all accessible outcrops, recording their location and the lithologies found, measuring structural information using the right-hand rule, and collecting samples. Attention was paid to joint orientation and abundance. Some areas of outcrop or near surface rocks shown on older maps (Porter, 1960; Sanders, 1972a) were no longer accessible for a number of different reasons. Some were simply not accessible because of dense vegetative cover, some were on private property to which we were not granted access, some had been covered by colluvium, and some had been destroyed by development.

Field mapping was done on hill-shaded DEM base maps derived from LiDAR data. Based on our observations local area maps were constructed at scales ranging from 1:1000 up to 1:5000 depending on the size of the area[1]. These maps were then transferred to a topographic base and compiled at 1:12000. The map (Plate I) is electronic and hence a user can zoom any area to any scale and see more detail than can be seen at a scale of 1:12,000. Figure 29, illustrating the distribution of a narrow lamprophyre dike, is an example.

1. Local areas and detailed local area maps may be found in Appendix I.

On our cross section (Plate I) we have shown faults with a dip near 70°. This is an inference because most faults and not exposed and are mapped based on the interpreted offset of various rock bodies. In addition, we have shown dikes with a near vertical attitude. Most dike contacts with country rock are not exposed. We have seen only four (Figures 10A, 12A, 13C, and 15A), all steeply dipping. We have no data pertinent to the orientation of any dike with increasing depth.

Samples were collected for petrographic thin sections and basalt/diabase samples were collected for geochemical analyses. Basalt/diabase samples were broken to smaller sub-samples which were thoroughly scrubbed and placed in an ultrasonic bath to remove loose material. The sub-samples were sent to GeoAnalytical Laboratories at Washington State University. Analytical procedures followed by GeoAnalytical can be found on their websites[2].

Few contacts between lithologic units were seen in the field. Intrusive contacts with the host rock were seen in only a few locations and those contacts were invariably close to the outcrop area of the igneous rock. Hence, our drawing of contact lines, particularly at the margins of the intrusive rocks, is based on that experience: the inferred contacts are placed high on the slopes close to existing outcrops and are presumed covered by talus along the remaining area. The contacts between layered units are not generally exposed and a certain amount of conjecture exists about their exact placement.

Likewise, very few fault planes were seen in the field. Most of the faults that are exposed involve small amounts of displacement and cannot be traced beyond the outcrop. Most of the faults that we mapped were done so by observing offsets in the basalt and diabase ridges in the Wallingford quadrangle and also the Durham quadrangle (Simpson, 1969). In the northeastern corner of the Wallingford quadrangle offsets in the Holyoke ridge to the east were matched to displaced stratigraphic layering (see Appendix I, Figure I-57) compiled from interpretation of water-well completion reports (Appendix VI).

Geologic Setting. The Wallingford quadrangle is located in south-central Connecticut entirely within the Mesozoic Hartford Basin (Figure 1), a rift basin formed during the breakup of Pangaea. Non-marine sedimentation began in the Hartford Basin during Late Triassic in fluvial depositional environments and continued into the Early Jurassic (Sinemurian) Period. Near the beginning of the Jurassic period, CAMP volcanism began (see McHone, 2000; Blackburn and others, 2013) which lasted almost 610,000 years (Olsen and Fedosh, 1988; Olsen and others, 2003), resulting in eruption of three flood basalt sheets. Intrusive and extrusive volcanic rocks associated with the two oldest sheets are present in the Wallingford quadrangle. The oldest basalt (Talcott Basalt) typically is pillowed, suggesting the presence of at least local lacustrine environments, but also is composed of volcaniclastic layers. After eruption of the Talcott Basalt, widespread cyclical lacustrine/fluvial deposition commenced and lasted well after eruption of the final lavas in the basin (Olsen and others, 2005).

---

2. www.cahnrs.wsu.edu/soe/facilities/geolab/technotes/xrf_method
www.cahnrs.wsu.edu/soe/facilities/geolab/labequipment/

Accommodation space resulting from down-dropping of the basin floor and/or uplift of adjacent headlands resulted in the accumulation of more than 5 km of sedimentary and volcanic rocks along with associated intrusive igneous rocks. The lower half of the sedimentary and volcanic section is exposed within the Wallingford quadrangle. Faulting continued well into the Cretaceous Period (Roden-Tice and Wintsch, 2002) and resulted in local repetition of the stratigraphy (see Davis, 1898 for an eloquent description). Deformation and the fact that the sedimentary rocks do not crop out well create uncertainty in the thickness estimates of some of the strata. In addition, glacial till and post-glacial sand and gravel deposits cover large areas of bedrock (Porter, 1960; Stone and others, 2005).

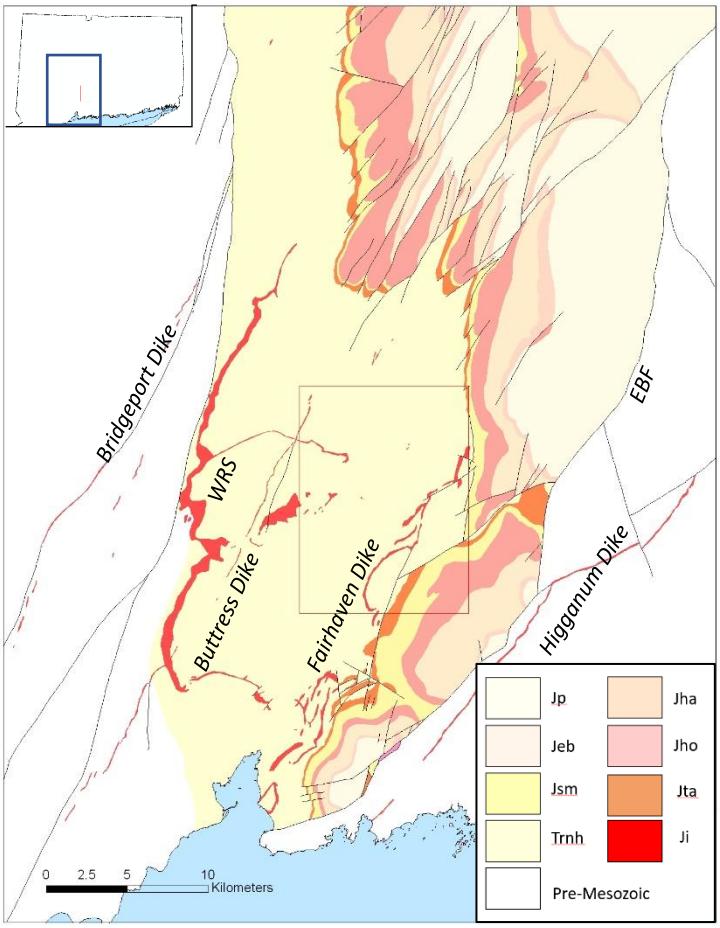

Figure 1. Geologic map of southern part of Mesozoic Hartford Basin in Connecticut (after Rogers, 1985) showing location of Wallingford quadrangle. Four diabase dikes are thought to have fed the three major lava flows in the Hartford Basin: the Fairhaven-Higganum dikes supplied the Talcott Basalt, the Buttress dike fed the Holyoke Basalt, and the Bridgeport dike fed the Hampton Basalt. Only the Holyoke and Talcott basalt crop out in the Wallingford quadrangle. Abbreviations: Jp, Portland Arkose; Jha, Hampton Basalt; Jeb, East Berlin Formation; Jho, Holyoke Basalt; Jsm, Shuttle Meadow Formation, Jta, Talcott Basalt, Trnh, New Haven Arkose; Ji, Jurassic intrusives. WRS, West Rock Sill; EBF, Eastern Border Fault.

Previous work. Although the spatial distribution of the various rocks in Connecticut has been known with some accuracy since the time of Percival (1842), the interpretation of the origin and structural configuration of the Mesozoic rocks did not progress until the time of Davis (summarized in Davis, 1898). Davis recognized that the igneous rocks in the Mesozoic basin, formed both as intrusive dikes and sills, and as lava flows, provided a stratigraphy from which to decipher the structural history of the basin. Prior to Davis, the prevailing thought was that all the Mesozoic igneous rocks were, like East Rock and West Rock in New Haven, intrusive in nature.

> "Davis's structural diagrams of the Meriden district…showing numerous faults that offset the extrusive trap ridges and subdivide the region into distinct structural blocks… demonstrated that the present structure of the Valley resulted from tilting, warping, and block-faulting of an originally horizontal mass of strata," (McDonald, 1996, p.29).

Davis gave names to the structural blocks, but did not give names to the normal faults that bounded each block. Instead, he referred to faults as the "line" between adjacent (named) blocks, such as "the Paug-Totoket line". Today, some authors still refer to specific faults by reference to Davis' informal "block" terminology, such as the "North Lamentation Mountain fault" or "South Lamentation Mountain fault" (Wintsch and others, 2011).

In the late 1930s Krynine (1936) constructed a geologic map of southern Connecticut showing most of the important faults originally mapped by Davis. Our mapping confirms the Davis and Krynine interpretations.

A very different structural interpretation was presented by Sanders and his students (Sanders and others, 1963; Sanders, 1970; 1972a; and 1977). They interpreted complexly faulted diabase outcrops in the Branford quadrangle (immediately south of the Wallingford quadrangle) to be Talcott "Formation" (see discussion about Talcott stratigraphy below) rather than intrusive dikes and sills interpreted by previous workers. In the village of Foxon they mapped the Talcott "Formation" lying adjacent to the Rabbit Rock intrusive sheet and inferred it must be a fault contact. Hence, they mapped the Foxon Fault, a down-to-the-southeast fault (antithetic to the Eastern Border Fault). The Foxon Fault forms the western border to a large graben structure, the Gaillard Graben, which includes two broad synclinal warps, the Saltonstall and Totoket synclines. Sanders, in 1972, prepared a preliminary map of the Wallingford quadrangle that projects the Sanders and others, (1963) interpreted Foxon Fault and Talcott Formation into the southern portion of the Wallingford quadrangle. As will be discussed below, we can find no supporting evidence for these structures in the Wallingford quadrangle. Rather, our mapping, like Krynine's, confirms Davis's original work.

Sanders (1962, 1972b) presented a different stratigraphic description of the Talcott Basalt in the Branford quadrangle than we are able to recognize in the Wallingford quadrangle. The Talcott Basalt was renamed the Talcott "Formation" in an abstract (Sanders, 1962), but the nomenclature was not formally changed by appropriate publication. Hence, Rodgers (1985) continued the usage of Talcott Basalt for the state map and this is the accepted nomenclature used in the National Geologic Map Database (www.ngmdb.usgs.gov/). Sanders thought that, in the Branford quadrangle (immediately south of the Wallingford quadrangle), the Talcott "Formation" is divided into four volcanic units (Figure 2) with three intervening sedimentary

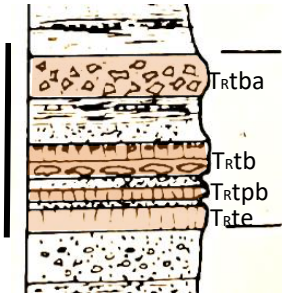

Figure 2. Stratigraphy of Talcott "Formation" as presented by Sanders (1963, Fig. 2, p.4; 1970, Table 1, p2). Black bar left subdivides 1000 feet of section. Four volcanic units (tan color on diagram) are separated by sedimentary beds that are indistinguishable from New Haven Arkose. Trtba = Fine-grained extrusive basalt, locally brecciated and amygdaloidal; Trte = Fine-grained extrusive basalt; well-developed columnar joints; Trtpb = Pillowed basalt overlain by breccia sheet; and Trtb = massive basalt breccia with arkosic matrix.

units of considerable thickness (Sanders, 1962; 1963, p.4; 1970, p.2; he reported [Sanders, 1968] that the intervening sedimentary layers are107m thick).

STRATIGRAPHY

The Wallingford quadrangle is underlain by typical rocks of the Mesozoic Hartford Basin. Although 2-3 kilometers of section may be encountered in the quadrangle, the exact thickness is difficult to determine because of poor exposure and numerous faults, most of which are not well exposed or are inferred. The only rocks well exposed within the quadrangle are the intrusive and some of the extrusive igneous rocks. The sedimentary rocks, for the most part, are poorly cemented and not well indurated and, in at least one place, were difficult to distinguish from glacial outwash.

Stratigraphic nomenclature historically relied on recognition of three basalt sheets, which for years were referred to as anterior trap, main trap and posterior trap (Davis, 1898), then later upper, middle and lower lava flows (Krynine, 1950). Emerson (1898) introduced the geographic names, Talcott, Holyoke, and Hampden, for the lava flows in Massachusetts, but that terminology was not applied in Connecticut until the late 1950's. The sedimentary layers were named and described relative to the basalts. In 1941 Krynine introduced geographic names for the stratigraphic layers: the New Haven Arkose underlies the basalt flows, the Portland Arkose overlies the basalt flows, and the Meriden Formation includes the basalt flows and intervening sedimentary layers. Lehmann (1959) proposed the names Shuttle Meadow Formation for the sedimentary layer between the Talcott Basalt and the Holyoke Basalt and East Berlin Formation for the sedimentary layer between the Holyoke and Hampden basalts. He discontinued usage of the term Meriden Formation. Lehmann's nomenclature, used in this report and in all modern-day geologic literature, was adopted into the U.S.G.S. Lexicon for Geologic Names in the National Geological Map Database (https://ngmdb.usgs.gov/Geolex/search).

The source of sediments that filled the rift basin is thought to be derived mainly from eastern areas. Early mappers noted that pebbles in the conglomerates on the eastern side of the basin consist of rock types that can be found cropping out a few kilometers east of the border fault. Indeed, Krynine (1950) thought that the sediments were derived exclusively from the Eastern Highlands and more particularly from a belt "3 to 10 miles" (5-16 km) wide east of the

border fault. This view has received support from Wintsch and his colleagues (Blevins-Walker and others, 2001; Wintsch and others, 2003; Blevins-Walker, 2008) who correlated metamorphic cooling ages from detrital white-mica in the basin with the cooling age of the Bronson Hill Terrane, a 10-20 km wide belt immediately east of the border fault. They concluded that essentially all the sediments in the Hartford Basin were derived from the Bronson Hill Terrane

Alternatively, LeTourneau (2003) and LeTourneau and others, (2015) summarize a paleogeographic model developed from studies of facies analysis, paleocurrents, sediment provenance, lithosome geometry, and basalt flow directions. That model predicts that appreciable sediment on the western margin of the Hartford Basin was derived from a western provenance. Burton and others (2005) identified clasts from conglomerates in the Pomperaug Basin (~20 km west of the Hartford Basin) that were derived from metamorphic highlands located between the Hartford and Pomperaug basins. Exposed metamorphic terrane shedding detritus into the Pomperaug Basin certainly could have shed detritus eastward into the Hartford Basin as well. Indeed, Wizevich and his students have found detrital zircons with Laurentian age cores in sediments of the Hartford Basin and concluded that some sediments had a western provenance (Giblin and others, 2017).

TRIASSIC FORMATION

New Haven Arkose

The New Haven Arkose in the Wallingford quadrangle consists of a coarser-grained facies and a finer-grained facies. The coarser-grained facies consists of gray and pinkish-gray conglomerate, conglomeratic sandstone, and coarse-grained arkosic sandstone that are ridge forming in the eastern side of the quadrangle. The finer-grained facies consists of brick-red and reddish brown coarse- to fine-grained sandstone and siltstone that are found in stream valleys and artificial highway cuts in the central and western side of the quadrangle. Because of the general eastward dip of the basin stratigraphy, the finer-grained rocks are generally older than the coarser-grained rocks; but rather than stratigraphically below the coarser-grained rocks, we interpret that the finer and coarser grained rocks are facies equivalents.

Although the New Haven Arkose underlies most of the quadrangle (Plate I), exposures of more than 5 meters of stratigraphic thickness are found in only a few places: coarse-grained facies is exposed at an unnamed hill east of Old Post Road in North Branford (local area 123 in Appendix I[3]). Considerable exposure (although not continuous) of New Haven Arkose can be found just west of Northford village (local area 103), in and adjacent to Marcus Cooke Memorial Park (local area 138), where possibly 200 m of sandstones are discontinuously exposed. The New Haven Arkose underlies several prominent ridges in the northeastern part of the quadrangle (local areas 142, 132S). The finer-grained facies can be found in Wharton Brook (local area 110), where almost 30 m of brick red arkosic sandstone and pebbly arkosic sandstone are

3. Numbers in parentheses refer to local areas that were mapped in detail. Preliminary maps of all local areas can be found in Appendix I.

exposed; in an unnamed tributary to Muddy River along the eastern part of the Tyler Mill Preserve (local area 109); in an unnamed brook that flows northward from Ashlar Village (133); and in the Spruce Glenn area (141). New Haven Arkose reportedly is exposed on private property in an unnamed tributary to Pine Brook on the western border of the quadrangle just south of Sleeping Giant (Porter, 1960). We were unable to access this outcrop. Faulting and a lack of distinctive beds make uncertain the exact stratigraphy and thickness of the New Haven Arkose.

The coarse-grained facies of the New Haven Arkose consists predominantly of gray to pinkish-gray pebbly sandstone with cobble-bearing conglomeratic lenses that grade upward to pebbly sandstone (Figure 3). Very few fine- or medium-grained beds were observed. Where adjacent to igneous intrusive rocks, the sandstones are locally gray to dark gray. The darker colored sandstones result from thermal metamorphism and hydrothermal alteration that reduces

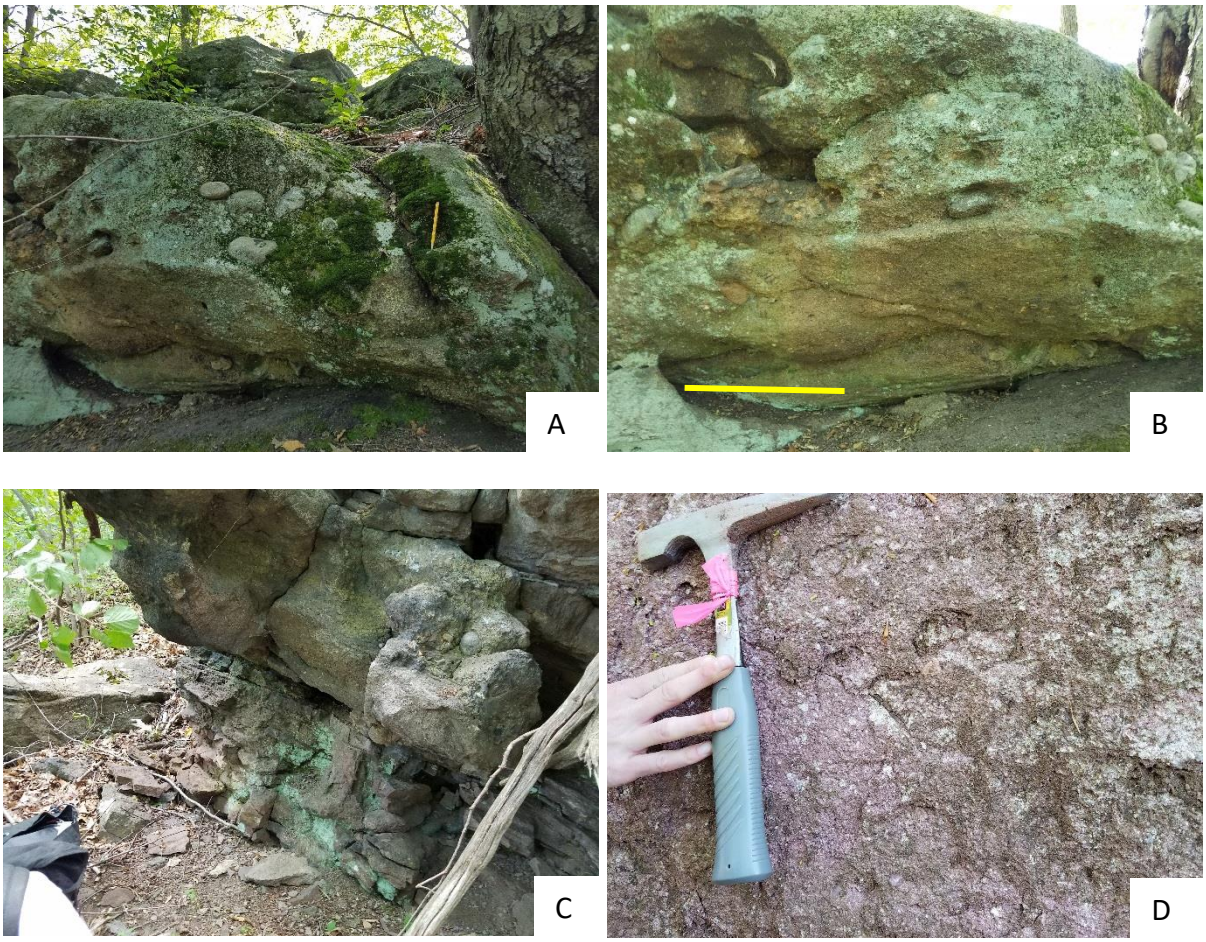

Figure 3. Coarse-grained conglomeratic lenses of the New Haven Arkose. A. Pinkish-gray to tan conglomeratic arkose, fines upward to coarse-grained sandstone. A. and B, from local area 123. Pencil is ~15 cm in length. B. Lenses of conglomeratic sandstone and coarse-grained sandstone with erosional bases and coarser material concentrated along the base. Scale bar ~25 cm. C. Parallel bedded conglomeratic sandstone overlying medium- to coarse-grained sandstone. Medium- to coarse-grained sandstone bed at lower part of outcrop is approximately 30 cm thick. Local area 116. D. Pinkish gray pebbly sandstone typical of New Haven Arkose in Wallingford quadrangle. Note poor sorting and lack of defined bedding planes. Local area 110.

the hematitic cements to magnetite/ilmenite. Locally the gray beds may be partially melted (noted also by Philpotts and Asher, 1993, in the Branford quadrangle) as evidenced by embayment in quartz and feldspar grains, matrix that lacks muscovite and contains devitrified glass masses, and quartz wisps that extend into fractures in the matrix and adjacent grains. Most of the outcrops are either parallel-bedded or massive. Weathering has obscured the original bedding in some places. Some beds are lenticular and have well developed lower bounding surfaces that cross-cut layering of the underlying material in channel-like form (see also Hubert and others, 1978, p.42). Some of the lenticular beds contain tabular cross-bedding. The few current indicators we have seen suggest streams flowed west to southwest, similar to the interpretation of Hubert and others (1978). Pebbly arkosic sandstone that may contain large cobbles is ubiquitous. The largest cobbles found are 35 cm. More abundant and larger cobbles are found farther to the east (documented quantitatively by Hubert and others, 1978, Fig. 22; LeTourneau and McDonald, 1985, Fig. 4; Mikami and Digman, 1957, pl.3). Most large clasts are well rounded, but in many places angular sandy material may be present.

The fine-grained facies is more predominant in the western portion of the quadrangle. It is composed predominantly of fine- to coarse-grained sandstone (some of which is pebbly) and siltstone. Some beds are channel-like in cross section with erosional bases that may be conglomeratic (Figure 4B). Mudrocks are likely part of the formation also, but are so poorly exposed that we did not observe any in the field. Most of the sedimentary rocks of the fine-grained facies are bedded. Most are brick-red, reddish brown, and reddish-gray; a few are tan. The finer-grained facies is composed of fining-up sequences of coarse-grained sandstone interbedded with sandy siltstone and fine-grained sandstone. The coarse-grained beds typically have erosional bases and both trough and tabular crossbedding (Figure 4C, E). The fine-grained sandstones typically are thin-bedded and ripple-laminated or plane-bedded (Figure 4D). Some of the siltstones contain pale greenish reduction spots. Light-gray caliche nodules are rare but present locally. This facies is similar to flood-plain sequences in the New Haven Arkose, reported by other investigators (Krynine, 1950, Hubert and others, 1978).

Krynine (1936; 1950, p. 41-43) recognized distinctions in the New Haven Arkose based on heavy mineral abundances: the lower part of the formation (that he mapped as lower division in1936 but referred to as “lower member” in 1950) has a relatively low abundance of garnet (<30%) in the heavy mineral separates whereas the upper part has a high abundance of garnet (~70%). He also noted that the New Haven Arkose in western Meriden and Cheshire area consists of “brick-red”, fine- to medium-grained sandstone and siltstone (“Redstone” facies of Krynine, 1936; flood-plain facies) but in eastern Meriden the New Haven Arkose is pebbly sandstone (braided channel belt of Hubert and others, 1978). Hanshaw (1968) and Hubert and others (1978) substantiated Krynine’s observation. In the Mount Carmel Quadrangle, Fritts (1963) subdivided the New Haven Arkose into upper and lower members. The lower member is predominantly grayish-orange-pink to very pale orange and dark reddish brown coarse-grained sandstones. The upper member consists of pink and reddish coarse-grained sandstones containing spherical reduction spots. The boundary between the two members that Fritts

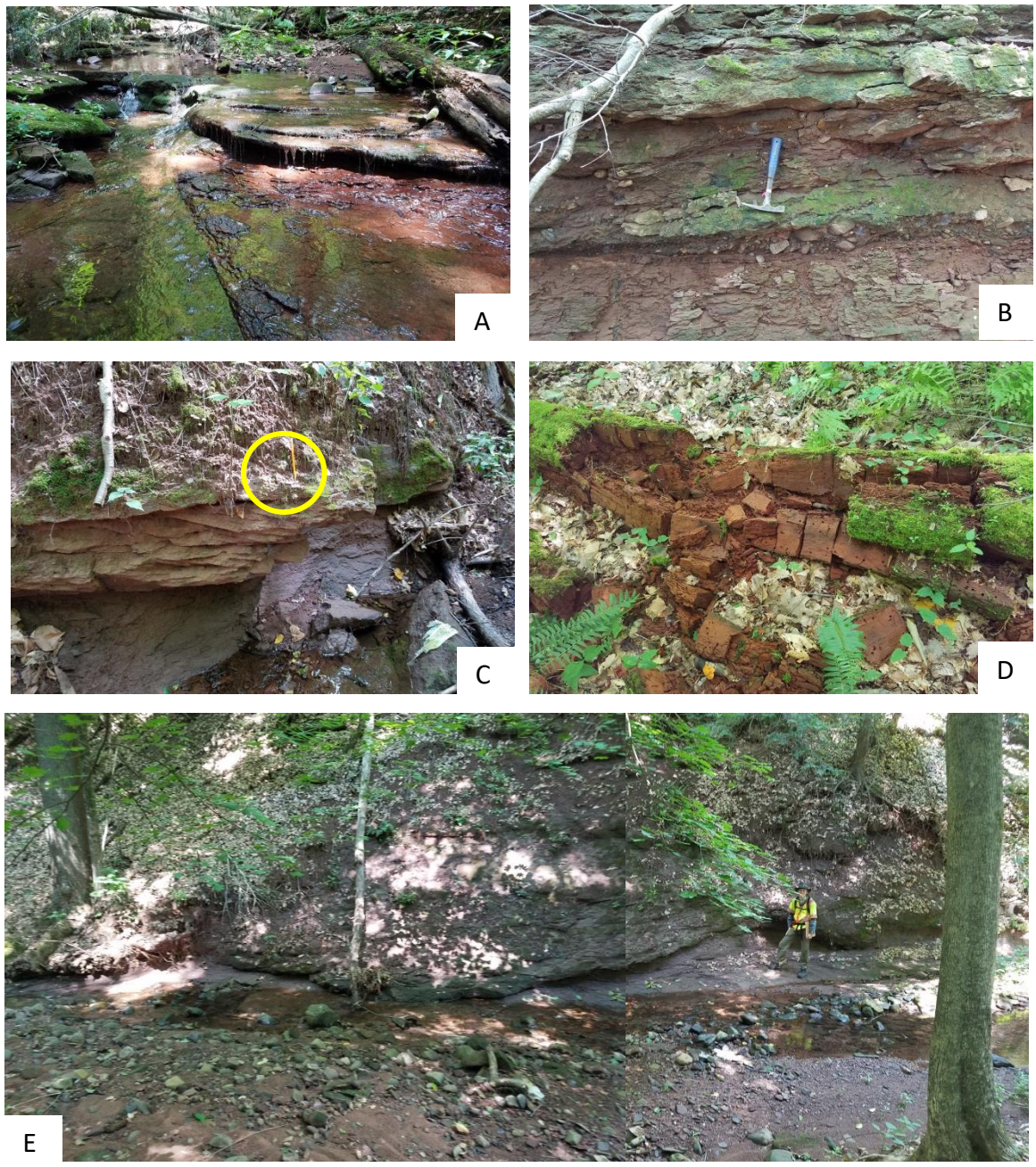

Figure 4. A. Typical stream bottom exposure of fine-grained facies of the New Haven Arkose. More resistant layers are fine- to medium-grained sandstone. B. Fining-upward sequences of sandstone, some of which is conglomeratic, and sandy siltstone. Hammer ~25 cm. C. Tabular cross-bedding in red fine-grained sandstone. Pencil (yellow circle) is 7 cm. D. Brick-red parallel-laminated fine-grained sandstone beds with unusual tubular borings. Beds approximately 3 cm thick. E. Channel sandstone is fine-medium-grained. Geologist on right side of channel ~1.8 m in height. A., D., and E.: local area 141. B. and C.: local area 135.

recognized is close to but slightly west (stratigraphically lower) of where Krynine mapped the boundary between rocks containing different heavy mineral suites.

Regional dip of the sedimentary layering is toward the east, layers farther west are generally stratigraphically lower (older) than layers farther east. The distribution of coarser grained sediments, however, is a function of being closer to the sediment source. The coarser-grained facies is interpreted as braided stream deposits on or near the distal portion of alluvial fans formed near the margin of the rift basin. The finer-grained facies was deposited farther from the basin margin in braided and meandering stream environments.

JURASSIC FORMATIONS

Talcott Basalt

The Talcott Basalt crops-out poorly in the Wallingford quadrangle, in part because of its composition, in part because of local hydrothermal alteration (Steinen and others, 2017), and possibly in part because of structural deformation. It is composed of basalt and volcaniclastic breccia. Some of the basalt is pillowed. The Talcott Basalt is exposed in four areas of the quadrangle. In the extreme northeastern corner of the quadrangle the Talcott occurs as low north-south aligned cliffs of massive basalt (local area 142). Just north of Totoket Mountain in the eastern central part of the quadrangle ephemeral outcrops of volcaniclastic agglomerate were uncovered during construction of a subdivision (local area 126). A knob of volcaniclastic debris may also be found at Northford Village (local area 125). Finally, a fault block affords an isolated exposure of pillowed basalt in an erosional depression, covered by bedded volcaniclastic debris along Village Road on the southern border of the quadrangle (local area 103). None of the outcrops expose the top of the formation and most do not expose the base. For that reason, exact formation boundaries are difficult to locate on the geological map.

The formation thickness is likewise difficult to estimate. Information derived from water-well drilling completion-reports[4] (see Appendix VI) suggests that in the northeastern corner of the quadrangle the Talcott consists of two flows separated by sediment and/or a weathered zone up to 15 m thick. The upper flow may be greater than 45 m (133 ft) thick and the lower flow almost 30 m (85 ft) thick. One driller reported that greater than 114 m (341 ft) "traprock" was penetrated in one well. In the southern part of the quadrangle only one flow was reported. Greater than 160 m (395 ft) of "traprock" was penetrated in one well. Our estimate for the thickness of the Talcott Basalt in the Wallingford quadrangle, approximately 140 m, is measured from our cross section (see Plate I). Hanshaw (1968) reported 61 m (200 ft) in the adjacent Meriden quadrangle to the north and Sanders (1972b) reported greater than 300 m (1000 ft) in the adjacent Branford quadrangle to the south.

In the Wallingford quadrangle, the contact of the basalt with the New Haven Arkose is seen in only one outcrop along the southern border of the quadrangle southwest of the village at

---

4. Drilling reports vary in their accuracy based partly on the record-keeping habit of the drillers and the timeliness of the report-filing. As examples, in an area surrounded by wells that penetrated "traprock" , some drillers reported "bedrock", "redrock", and even "granite". Many such vague reports were filed weeks after completion of the wells, suggesting that the filer of the report (not necessarily the driller) did not have records at the time of filing.

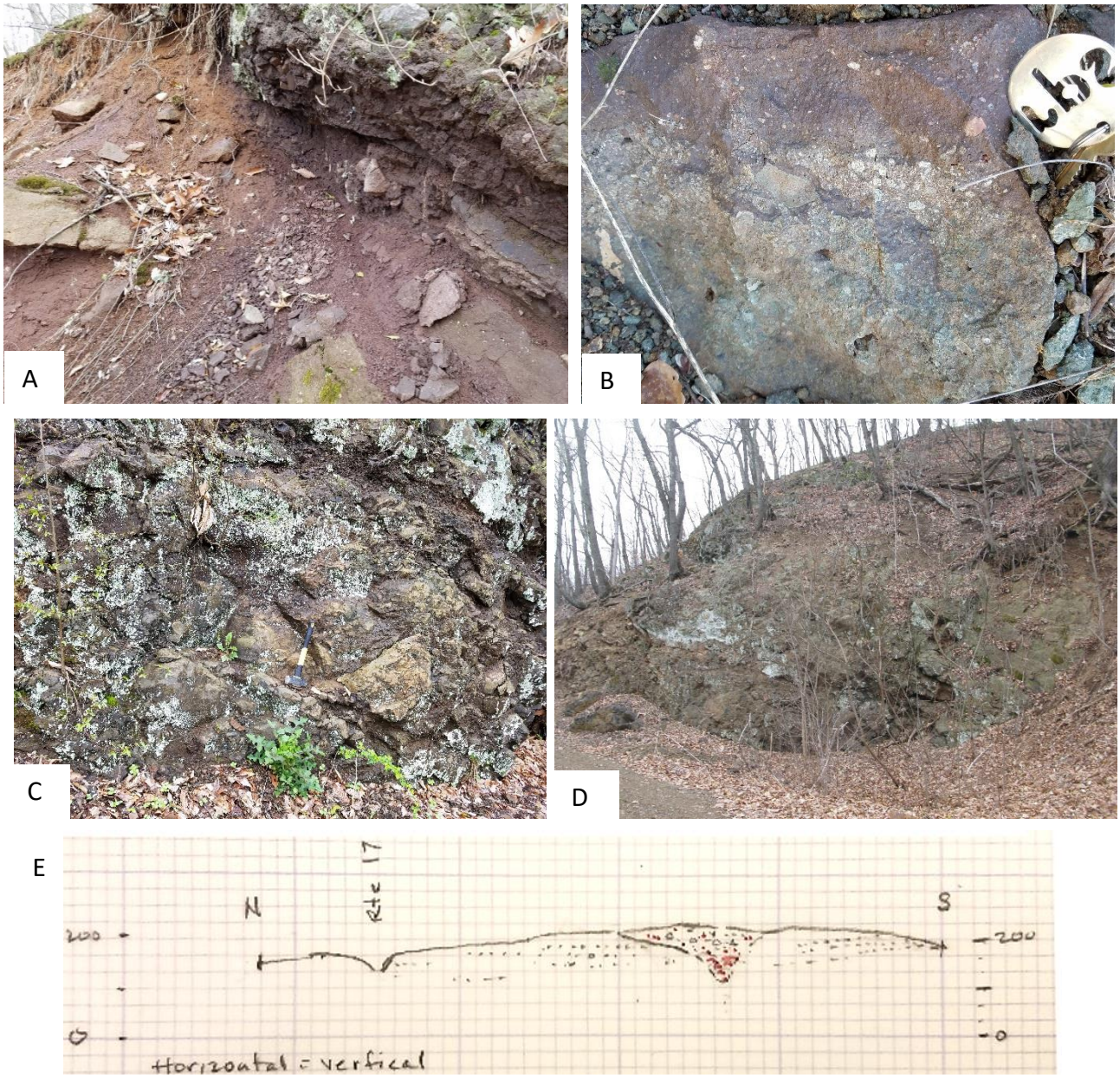

Figure 5. Details of gully-filling Talcott Basalt (local area 103; see map Appendix Figure I-7). A. Volcaniclastic breccia forms the upper part of the outcrop (Figure 5A and B) and pillow basalt forms the lower part of the outcrop (Figure 5C, D). Both cross-cut the New Haven Arkose. A. At top of the outcrop, volcaniclastic breccia on right and tan-colored bedded arkose on left. Contact dips about 20° toward east-southeast. Arkose dips 14° east. Note that bedding in the volcaniclastic breccia is conformable with the contact while the contact cross-cuts bedding in the sandstone. Width of view ~ 3m. B. Purplish-brown arkose and greenish-gray volcaniclastic breccia in loose fragment at base of mid-level outcrop. Bedding in arkose is not obvious in this fragment, but is at an angle 38° to the contact in the adjacent outcrop. Note that arkose does not contain volcanic fragments. Silt-laden fluids seeped into cracks in the volcaniclastic unit after its deposition and apparent cooling. Disc is 2 cm. C. Basalt at base of outcrop is pillowed. Southern edge of basalt just off right side of image in near vertical contact with sandstone. Contact at northern edge of basalt also near vertical and off left side of image. Height of outcrop 10-12 m. D. Detail at far-left side of outcrop in D showing lumpy pillows. Note intraflow contact in upper right. Hammer ~30 cm. E. Interpretive N-S stratigraphic section showing river-channel (gully) cross-section filled with pillow basalt at base and volcaniclastic material above. Wine-glass cross section suggests rapid erosion, possibly caused by base-level lowering that we suggest was caused by faulting (compare with Figure 33). Elevation in meters. Horizontal and vertical scales equal.

Northford (local area 103). There, pillowed basalt is laterally confined by what we interpret is a channel in the New Haven Arkose. The outcrop is local and mapped as a fault-bounded block of Talcott by Sanders (1972a). We mapped the body as somewhat elongate in an east-west direction (Figure 5). Pillowed basalt forms the base of the outcrop and volcaniclastic breccia forms the upper portions. The contact of the volcanic rocks with the New Haven Arkose is only exposed in the upper reaches of the outcrop where bedded sandstone is in contact with locally unbedded or crudely bedded volcaniclastic breccia. Sandstone at the contact is not metamorphosed and the contact appears disconformable rather than faulted (Figure 5A, C). The contact near the top of the body dips 20^{o} east-southeast, but that steepens to 38^{o} toward the southeast. At the base of the body the contact between basalt pillows and sandstone is covered by excavated debris but appears to steepen significantly on the north side and may be almost vertical on the south side (Figure 5F). Basalt pillows range from 20 cm in diameter to greater than 1 m. Although they lack radial pipe vesicles common at other Talcott outcrops (see for instance, Hubert and others, 1978, p.50; Philpotts and Lewis, 1987; Philpotts and Asher, 1992), many are vesicular. Broken selvages that formed around the pillows fill interstices between the pillows. The origin of this basalt and breccia body is enigmatic. The pillows are certainly a surface flow in contact with water and the geochemistry is consistent with this being an outcrop of the Talcott Basalt (Puffer and others, 1981a, b; Puffer and Philpotts, 1988). The pillowed basalt and overlying volcaniclastic breccia occupy a restricted volume, possibly bounded on the south by a fault or a steep erosional contact and lie next to an erosional contact to the north. The pillowed basalt and overlying breccia appear to fill an incised river channel. The depth (greater than 40 m [>130 feet]) and steepness of the proposed river banks are of concern, however. The top of the deposit is about 90 m in width. Although possible, such dimensions of river channels have not been reported in Newark basin sediments. See additional discussion on p. 52-53.

An isolated outcrop of diabase (basalt?) can be found immediately south of Route 17 at the North Branford/North Haven town line. It is massive, fine-grained, and columnar-jointed and contains surface parallel east-dipping joints. Although the top of the diabase is not exposed, we initially interpreted this to be a basalt flow close to a source fissure, rather than a dike or sill. Chemically, however, this rock more resembles an intrusive diabase than the average Talcott Basalt (see section on chemistry below). This rock body is interpreted as an intrusive body (Jb) on the state map by Rodgers (1985) and we are inclined to agree that it is an intrusive body, based on geochemistry. The geochemistry is, however, similar to the West Rock Diabase (Jwr) and not the Buttress Diabase (Jb).

Outcrops at Northford Village and extending northeast to the area between Paug Mountain and Totoket Mountain expose what is probably a continuous sheet of agglomerate or volcaniclastic breccia. The rock is composed of greenish-gray volcaniclastic layers that are crudely bedded (Figure 6A). They contain angular to rounded fragments of very fine-grained basalt (Figure 6B, C), rounded clasts of yellowish-green tuff (?) or altered scoria, clasts of scoria and cinders, clasts that resemble melted sediment, and rare clasts of coarse-grained sandstone, granitic gneiss and vein quartz. Some of the basalt clasts appear to have been plastic when

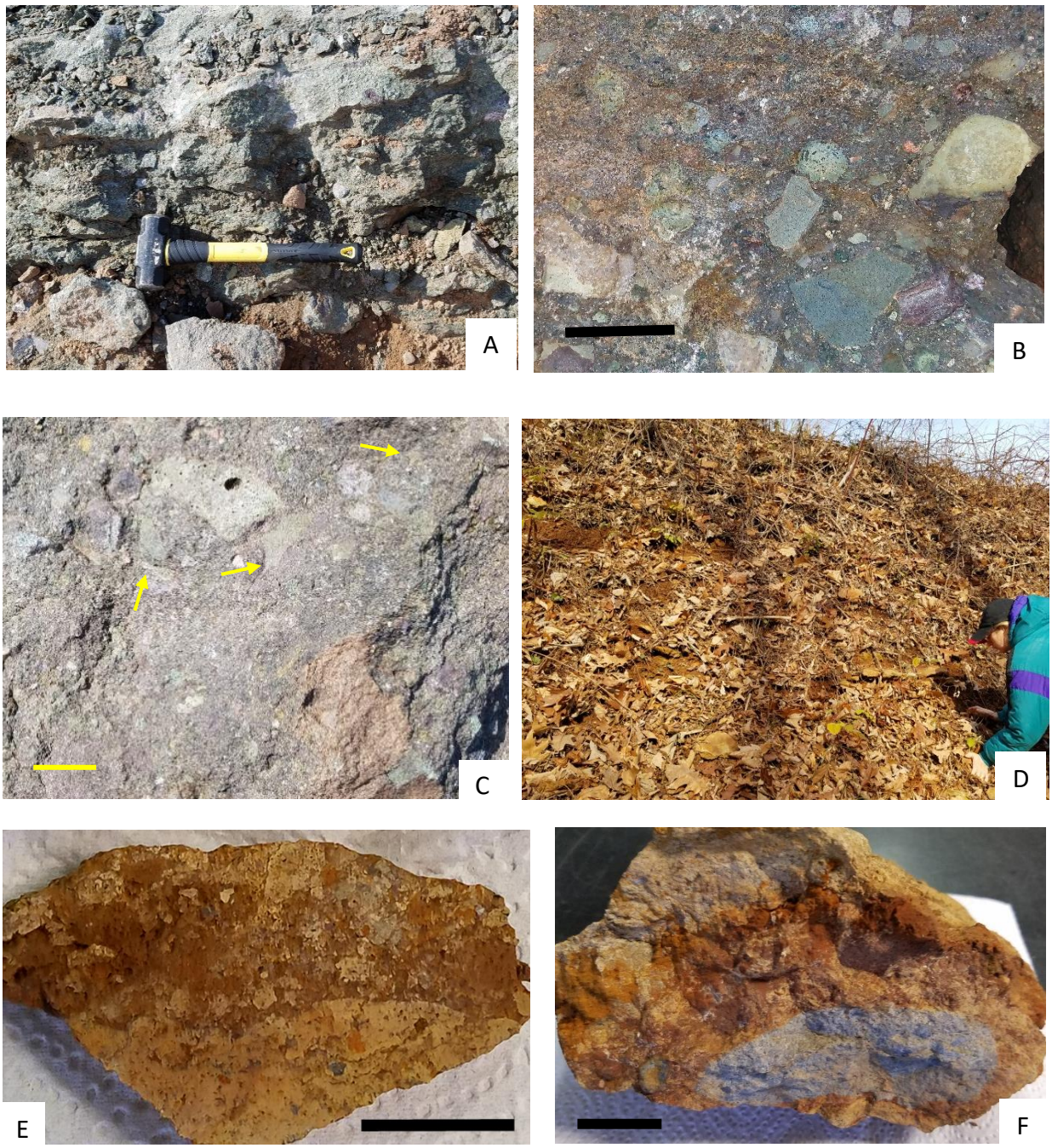

Figure 6. Volcaniclastic rocks of the Talcott Basalt. A., B., and C. from Local area 126. A. Crudely bedded greenish-gray volcaniclastic breccia. Hammer in A ~30 cm. B. Angular basalt clasts, some of which are vesicular, showing differing degrees of alteration by different color. Scale bar ~ 10 cm. C. Angular clasts with sharp protruding points (arrows) suggesting rapid deposition and little transport. Large gray clast in upper center is vesicular basalt. Numerous smaller light gray clasts may be scoria fragments. Scale bar = 3 cm. D., E., and F. Altered volcaniclastic breccia outcrop just east of Wallingford quadrangle boundry. D. Poorly exposed highly altered volcaniclastic breccia. Geologist is 1.5 m in height. E. Altered volcaniclastic breccia. Alteration products are various hydrated (?) iron oxides and ferroan calcite/dolomite. Scale bar = 2 cm. F. Altered volcaniclastic breccia. Note that basalt clasts are not as highly altered as those in E. Scale bar = 2 cm.

deposited (Figure 6C). The matrix contains devitrified glass shards and other fine-grained altered volcanic material, and detrital clastic material, mostly sand-sized, but also rare pebbles and cobbles. Locally the breccia may contain partially melted sediment, as evidenced by large embayments and reaction rims on quartz grains where they contact K-feldspar and/or lithic fragments. We have mapped this unit as Jtab on Plate I. These deposits are inferred to haveformed as the result of basalt lava explosively interacting with wet, water-saturated sediment (Priest and others, 2001, 2003; Lee-Gorishti and others, 2003; Coron, 2009). The volcaniclastic debris sporadically crops out in a belt eastward from Northford well into the Durham quadrangle (Mikami and Digman, 1957, p.65) and southward into the Branford quadrangle (Sanders, 1977). It may overlie basalt flows in places; Davis (1898, p.62) reported ash-like trap associated with the top of the lower (Talcott) lava flow in many locations in Connecticut.

Field observations indicate the volcaniclastic sheets and any basalt rock are intensely altered just north of Totoket Mountain in the eastern part of the Wallingford quadrangle and the western part of the Durham quadrangle (Steinen and others, 2017). We have indicated the altered basalt as Jtaa on Plate I (a map, presented later as Figure 35 to show the extension into the Wallingford quadrangle of faults mapped in the Durham quadrangle, also shows extent of altered Talcott Basalt). Locally, all of the basaltic material is replaced by a combination of various iron-oxides and ferroan-calcite/dolomite forming a spongy textured rock that weathers easily. One sample collected in the adjacent Durham quadrangle, inferred to be Talcott Basalt, was altered to ferroan-dolomite with pseudomorphic crystals of olivine (A. R. Philpotts, personal comm.). The alteration appears to be most intense in the area surrounding the former Coe's Quarry in North Branford, an inferred hot spring (Steinen and others, 1987). Sanders (1968, p.292) reported alteration of basalt clasts to carbonate in a volcaniclastic unit which he interpreted as the result of basalt erupting into cold lake water. Because the altered material erodes easily, it crops out poorly; hence few outcrops are found along the belt mapped as Jtaa on Plate I.

In thin section[5], the pillowed basalt is hypocrystalline and vitrophyric, with a matrix composed of glass and plagioclase and augite microlites. Phenocrysts are whole or broken and consist of plagioclase and pyroxne. Possible relict olivine crystals are replaced by iddingsite and a carbonate phase. Glomerocrysts consist of two populations. In basaltic rocks, glomerocrysts are fine-grained and composed of plagioclase laths with lesser clinopyroxene. In the coarser grained basaltic rocks, glomerocrysts are medium-grained and composed of clinopyroxene with small amounts of plagioclase. The basalt is moderately altered and partly replaced by a carbonate. Vesicles are filled with calcite or zeolites.

5. Illustrated petrographic descriptions may be found in Appendix V.

Shuttle Meadow Formation.

The Jurassic Shuttle Meadow Formation is poorly exposed in the mapped area. It crops out immediately below the Holyoke Basalt in three stream valleys (Plate 1 and Figure 7). The Holyoke/Shuttle Meadow contact is not exposed. The exposed Shuttle Meadow Formation consists of fine-grained sandstone with rare medium- and coarse-grained sandstone overlying scour surfaces. The sandstones grade upward to fine-grained sandstone. The Shuttle Meadow Formation is finer-grained than the New Haven Arkose and does not contain pebbly or conglomeratic material where exposed within the mapped area. It is thin-bedded for the most part and contains ripple stratification typical of all the Mesozoic basin-center sediments other

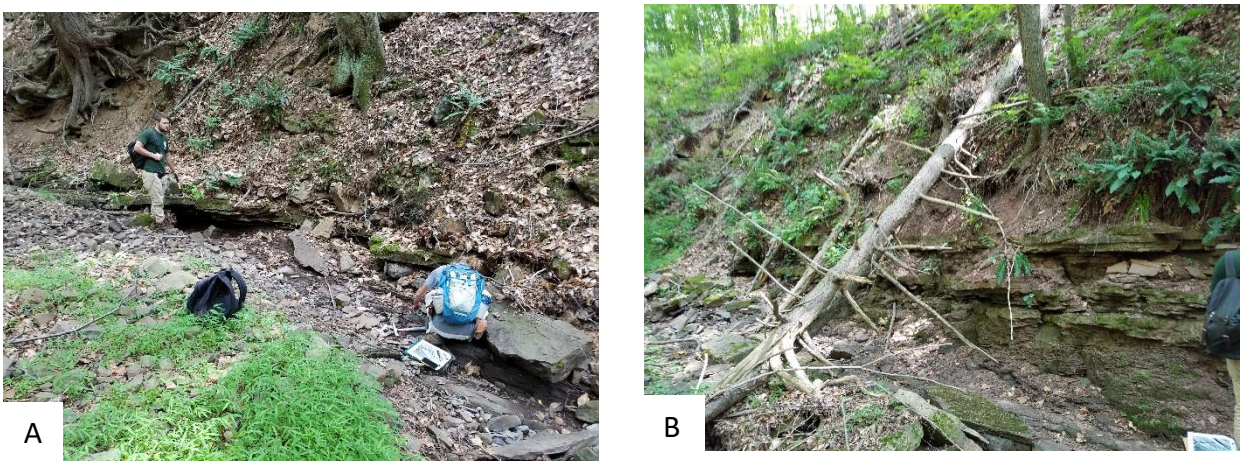

Figure 7. Shuttle Meadow Formation in Gulf Brook on Totoket Mountain Local are 121. A. Thicker beds consist of medium-grained light-brown to pale reddish-brown sandstone with local scoured bases. The sandstone grades upward to thin-bedded, fine-grained sandstone. Geologist ~1.6m in height. B. Alternating sandstone and siltstone of Shuttle Meadow formation in Gulf Brook (backpack of geologist, ~30 cm, visible on right side of image.

than the New Haven Arkose. Based on width of outcrop just north and east of Totoket Mountain, the thickness of the Shuttle Meadow Formation is estimated to be 140 m. Sanders (1972b) estimated the thickness around 900 ft (280 m) in the Branford quadrangle and Hanshaw (1968) estimated the thickness to be 250-325 ft (<100 m) in the Meriden quadrange.

Holyoke Basalt. The Holyoke Basalt occupies the southeastern corner of the Wallingford quadrangle (Figure 8, Plate I). Although two separate flows can be distinguished in the Holyoke at some locations to the north (Davis, 1898; Hanshaw, 1968; Simpson, 1969; Gray, 1982), it appears to be a single flow in the Wallingford quadrangle and to the south (Philpotts, 2010). The Holyoke has a uniform texture of medium- to coarse-grained basalt with glomero-porphryritic pyroxene. Local segregation sheets of ferro-diorite are present in the lower part of the flow (see petrographic descriptions in Appendix IV). Plagioclase phenocrysts are locally present near the upper part of the flow. The basalt is well jointed (Figure 9) and fractured. Many cooling joints megascopically appear mineralized (Figure 9A, B). Low-angle joints mimic

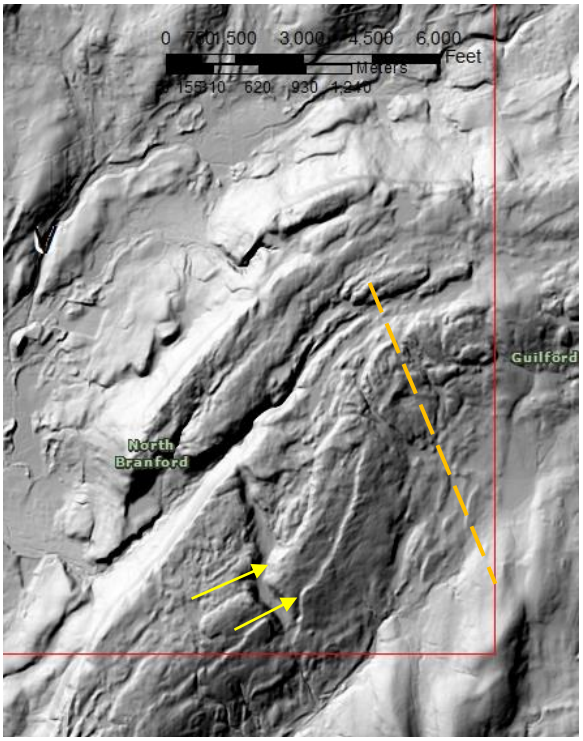

Figure 8. Hillshade digital elevation model of Totoket Mountain in southeastern corner of Wallingford quadrangle (quadrangle boundary shown in red). Holyoke Basalt forms a prominent ridge that is cut by northeast/southwest faults and fractures. Gulf Brook, the major southwest flowing stream in the center of the image, exposes Shuttle Meadow sandstones below the Holyoke. The East Berlin Formation is covered by till (southeastern corner). Bright northwesterly facing cliffs in center of flow (yellow arrows) are areas where cooling joints are mineralized and hence more resistant (see Figures 9A and B.). The surface in south central area appears flatter and is interpreted to reflect flexing of strata (see Fig. 9D) in that area. Orange dashed line is axis of synclinal warp.

the strike and dip of nearby sedimentary rocks. We interpret those to be exfoliation joints that reflect the original top surface of the lava flow (Figure 9C., D.)

Neither the top nor the base of the Holyoke Basalt is exposed in the Wallingford quadrangle. The Holyoke Basalt is about 200 m thick at the Tilcon quarry ~2 km to the south (in the Branford quadrangle) where both contacts are exposed (Philpotts, 2010). We assume the 200 m thickness for our cross section although the width of outcrop is greater than expected for a 200 m thick unit. We interpret that to be caused by structural offsets and folding. Sanders noted an apparent eastward thinning to the Holyoke Basalt that he attributed to faulting but did not report a thickness for the basalt. Previously, Longwell (1937) interpreted the eastward Holyoke thinning as stratigraphic wedging against alluvial fans associated with the border fault. Hanshaw (1968) reports the basalt is up to 500 ft (~150 m) in the Meriden quadrangle.

Figure 9. Some features of Holyoke Basalt. A. Northwest facing cliff face in which the joints in the upper part (above geologist's hand) are mineralized and in the lower part are not. Well-mineralized joint in middle top of image. Local are 115. B. Mineral deposit remaining attached to cooling joint. C. Low angle joints dipping in the direction of the basalt sheet and mimicking regional strike and dip of sedimentary beds. Local area 114 D. Exfoliation joints inferred to be parallel to the cooling surface of the Holyoke sheet are nearly horizontal at many locations in the central part of the outcrop belt. Local area 113?

East Berlin Formation

The East Berlin Formation does not crop out in the Wallingford quadrangle. Sanders (1977) mapped the East Berlin in the Branford quadrangle (immediately south) and showed the East Berlin/Holyoke contact extending into the southeast corner of the Wallingford quadrangle. Simpson (1969) mapped the East Berlin/Holyoke contact in the Durham quadrangle (immediately east) and likewise extended the contact into the southeastern corner of the Wallingford quadrangle. The two extensions, however, do not line up. We map the position of the contact indicated by Sanders based on our observations of outcrops in the Branford quadrangle.

JURASSIC INTRUSIVE IGNEOUS ROCKS

Numerous dikes and irregular shaped bodies (in plan-view) intrude the New Haven Arkose, mostly on the eastern half of the mapped area, but also in the area immediately north and east of the Sleeping Giant body and in the northwestern corner of the quadrangle. The apparent lack of dikes in the central portion of the mapped area may be because Pleistocene sediments cover large areas in that region (Porter, 1960). Aeromagnetic anomalies in the Wallingford quadrangle (USGS, 1973) are present where intrusive bodies are mapped, although no anomaly mimics any particular intrusive body. The presence of anomalies in areas covered by Pleistocene sediments suggests that intrusive rocks may underlie the unconsolidated material in some areas.

The preponderance of intrusive igneous rocks in the Wallingford quadrangle are composed of diabase; a lamprophyre dike, however, has been mapped in the northeastern part of the quadrangle (Taylor and others, 2019). Most of the intrusive rocks form relatively narrow dikes, intruded at a high-angle and thin sill-like bodies. Individual dikes may extend over several, even several tens of kilometers. Most were mapped by Percival (1842) and described by Davis (1898). Some of the dikes in Connecticut have been given informal names related to their geographic location. In the Branford quadrangle a group of irregular dikes were referred to informally as the Fairhaven dikes by Davis (1898, p. 45-46). Diabase of similar composition that intrude metamorphic rocks to the east and northeast are referred to as the Higganum dikes. In the Wallingford quadrangle, Davis (1898) referred to the Clintonville and the East Wallingford dikes. In the west-central part of the Wallingford quadrangle and in the Mount Carmel quadrangle de Boer (1968) referred to the Cross-Rocks Dike. The set of dikes in the northwestern part of the Wallingford quadrangle extends southwestward into the Mount Carmel quadrangle where it cross-cuts the West Rock sill. Dana (1891) referred to this dike as the Buttress Dike because of its morphology at West Rock.

The rocks comprising the dikes, however, are given stratigraphic designation (Charney and others, 2018) based on their chemical composition. The Fairhaven/Higganum dikes, the Clintonville Dike, the East Wallingford Dike and the Cross-Rocks Dike have a similar composition and are referred to as West Rock Diabase, following the nomenclature of Fritts (1963). The rocks comprising the set of Buttress Dike have a different chemical composition and were termed the Buttress Diabase by Fritts (1963).

The intrusive igneous bodies follow three general map trends in the Wallingford quadrangle. First, a series of massive dikes and sill-like bodies (including the Clintonville and East Wallingford dikes) extends in roughly north-south orientation from the Branford quadrangle into the eastern side of the Wallingford quadrangle. These we refer collectively to as the Fairhaven/Higganum dikes. Second, a younger set of dikes characterized by well-developed columnar jointing extends in roughly and east-west orientation across the central part of the quadrangle east and north of the Sleeping Giant body. In at least two locations in the Wallingford quadrangle the columnar-jointed rocks intrude into the Fairhaven/Higganum dike rocks and in other nearby locations they appear to cross-cut them. Rocks from both dike sets are composed of West Rock Diabase and are petrographically and chemically indistinguishable.

They are similar to rocks of the Fairhaven/Higganum dikes described by Philpotts and Martello (1986) and associated with the Talcott Basalt. Third, a group of en echelon dikes found in the northwestern quadrangle area cross-cut the Fairhaven/Higganum dikes and are composed of Buttress Diabase. These are chemically correlated to the Holyoke Basalt.

The larger dikes and intrusive bodies stand in relief forming the numerous steep-sided hills and ridges that adorn the topography of the area. Although forming topographic structures on the ground, they rarely have more than 30 m relief. Smaller dikes are associated with only a meter or so of relief; nonetheless they can be spotted on hillshaded-DEM images, and, because of that, can be accurately mapped. Davis (1898, p. 45-46) reported the dikes range from "50 to 200 feet" wide (~15-65 m). The preliminary maps of Sanders (1972b) show the dikes as wide (up to 150 m), curved structures. In fact, we find the dikes mostly to be narrow, rarely greater than 50 m in width. Where contacts are seen they usually indicate that the dike is not much wider than the basalt outcrop area at the top of the ridge. The dikes are straight segments that may be broken by faults in a fashion that causes the dike to appear curved on a map, especially at a scale of 1:24,000 and smaller. The dike at Clintonville in North Haven and Wallingford (local areas 112, 117-119) is broken into more than 15 straight segments over its three-plus kilometer length. Local outcrop patterns (see Plate I) suggest that magma intruded (1) into fractures that in part were arranged en-echelon in two orientations (006-186^{o} which seems to be associated with partially melted sediment; and 030-210^{o}), (2) as irregularly shaped masses (which contain breccia bodies; i.e., local area106 in the Tyler Mill Preserve and local area 107 near the Woodhouse Field recreation area in Wallingford), (3) along fault traces oriented 340^{o} (local area 104, the dike at Patten Road, North Haven), and (4) along a nearly east-west trend (younger dikes and sills, referred to as the Cross-Rocks Dike in the Wallingford quadrangle and other local names in the Branford and New Haven quadrangles). Most of the linear ridges appear to be offset by faulting after intrusion. Preferred fault orientations appear to be 050-070^{o} and 310-349^{o}.

Fairhaven/Higganum dikes. The dikes were formed by at least two intrusive events. The older dikes are composed of fine- to medium-grained West Rock Diabase that is mostly massive and structureless. The diabase contains plagioclase phenocrysts (~ 1 mm in length) and pyroxene aggregate phenocrysts (~ 6 mm in length). Diabase at the chilled margins in places contains phenocrysts of olivine. Diabase-sandstone contacts, in most places where they are exposed, are at a steep angle (Figure 10A). At several locations, however, the magma apparently intruded along bedding planes or at other low angles, forming sills and sill-like structures (Figure 10B, see discussion below). At other locations dikes are observed to flatten into sill-like bodies (see discussion below). At several locations the dikes appear to die out vertically (see discussion below) and may contain melted and partially melted sandstone contaminant (Fig. 10C). At numerous locations the dikes consist of or contain significant areas of diabase breccia (Figure 11). In most of the breccia, diabase clasts are set in a matrix that contains abundant detrital

Figure 10. Features of the West Rock Diabase at Clintonville (local area 112). A. Near vertical contact along east side of dike at the south end of 16-112 (Clintonville dike). Gray, lichen-covered pebbly sandstone on right is baked (contact metamorphism) but not fused. Dip of sandstone was not apparent at this location. Diabase on left is fine- to medium-grained. Note lack of columnar joints in this rock. Pencil ~ 15 cm. B. Diabase overlies sandstone at this location. Contact on lower part of slope is near vertical (see 10A), but here the igneous body spread out laterally over the sandstone becoming sill like. Sandstone dips very shallowly toward the east (left). Pencil (circle) is ~15 cm. in length. Near south end of local area 112 ridge. C. Irregular bodies of arkosic sandstone along top of 112 ridge. Mass in lower center (arrow) partially melted. Compass ~ 6 cm in width.

sedimentary grains. At numerous local areas the dikes have locally brecciated diabase at the contact with sandstone. The local breccias generally extend only a few meters or less along the contact.

Figure 11. Diabase breccia at local area 107. A. Contact (arrow) between massive diabase (foreground) with diabase breccia beyond arrow. Breccia consists of fragments of fine-grained diabase in a diabase matrix. Breccia is interpreted as backflow. B. Breccia detail, althoughheavily covered by lichen contain srounded and angular clasts. Keys ~ 5 cm. local area 107. C. Cut sample from above outcrop (Figure 10A). Amygdaloidal clasts embedded in fine-grained diabasic matrix. D. Diabase breccia at local area 106. Most of clasts are angular and fine- to medium-grained. Martrix is also fine- to medium-grained. Hammer head ~25 cm.

The dikes contain evidence for multiple intrusions at only a few places. Where the two intrusions are seen in contact in the Wallingford quadrangle, the younger intrusion has well developed columnar joints whereas the older intrusion either lacks or has very poorly developed columnar joints (Figure 12). At one location an amygdaloidal, columnar-jointed diabase intruded into an older, massive diabase dike (Figure 12A, B). The younger intrusion has well-developed chilled margin. At that location, initial intrusion is along a fault and the diabase is itself faulted by continued activity on the fault (Figure 12C). The two dikes however, have the same petrology and chemical composition (see data in Appendix III). The same jointing phenomenon is seen where two intrusive events are recognizable in the Higganum Dike (Philpotts and Asher, 1992, p.78; Philpotts and Philpotts, 2008, Fig. 2, p.68), *i.e.*, the younger (inner) dike contains well developed columnar joints whereas the older dike does not.

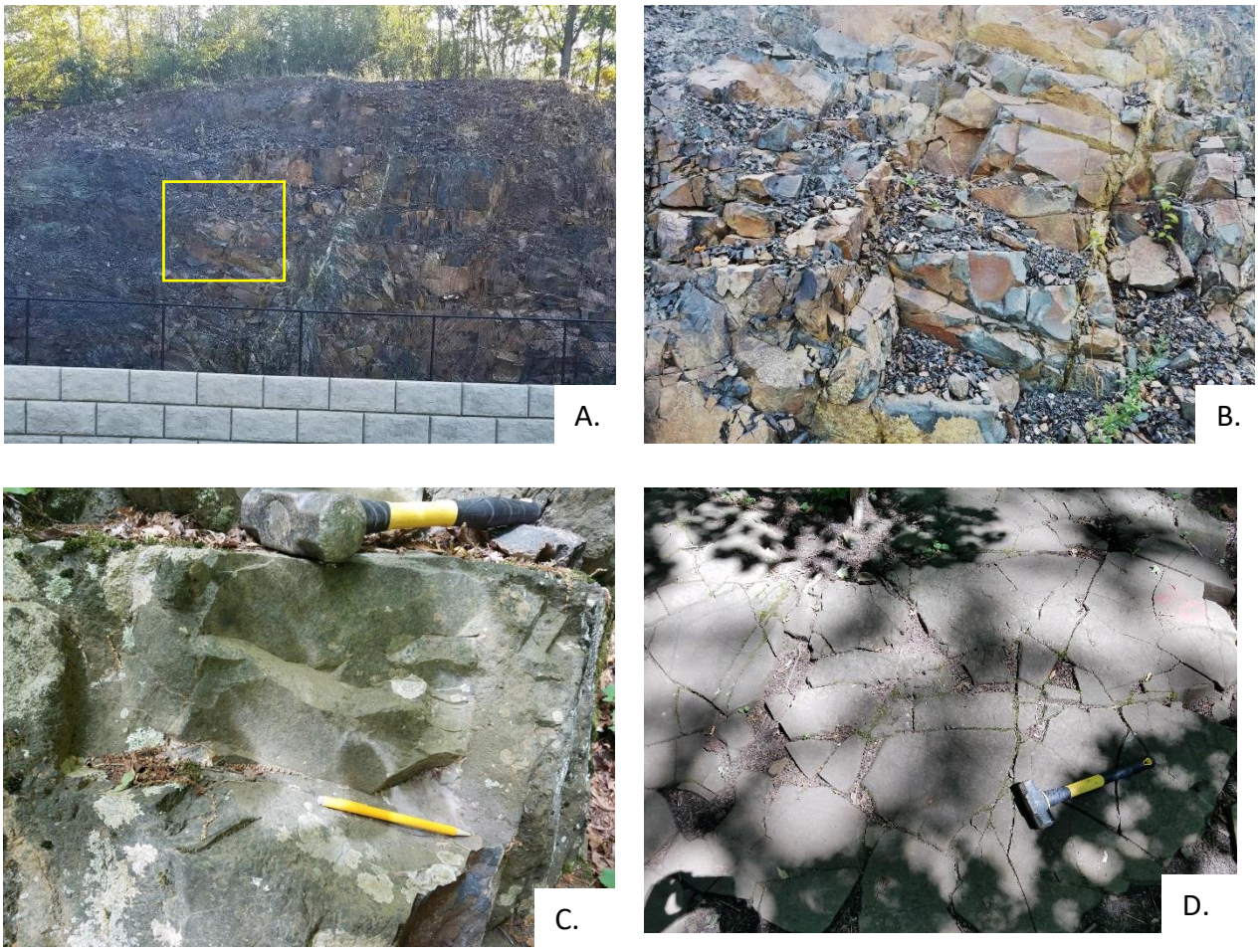

Figure 12. West Rock Diabase. A. Patten road (local area 104): Inner dike has columnar joints, outer does not. Yellow box shows approximate area of B. B. Detail of A showing inner dike. C. Contact of columnar jointed dike with older diabase (at pencil point), presumably equivalent to the outer dike of 12A, west of MacKenzie Reservoir (local area 100). Pencil ~ 7 cm. D. Columnar jointing seen on surface of sill-like body at Lufbery Park (local area 131). Note abundance of Y and T junctions. Hammer ~ 40 cm.

A long dike in the Mount Carmel quadrangle, popularly referred to as the Cross Rocks Dike, was mapped by Fritts (1963) as West Rock Diabase extending from Cheshire westward to the West Rock sill. We mapped the dike eastward into the northern half of the Wallingford quadrangle (Figure 13) and confirmed that the dike is composed of West Rock Diabase (see Appendix III). Large diameter (some greater than 1 m in maximum diameter) cooling columns are found in that diabase at all locations. Because well-developed cooling columns seem to be a physical characteristic of the younger pulse of the Talcott event, we tentatively infer that dikes with well-developed columnar joints correlate to the younger intrusion during Talcott time.

Figure 13. Columnar jointed diabase, local area 131. A. Montoweese Trail in Wallingford. Cooling joints (yellow arrows) plunge northward about 50°. This view looks westward. B. Shallow dipping contact (dashed yellow line) of arkosic sandstone with diabase. Pencil (red arrow) is 15 cm in length. Cheshire Road just east of entrance to Lufbery Park in Wallingford. C. Steeply dipping contact (red dashed line) of large sill-like (dome topped) intrusion at the northeasernt part of Lufbery Park. Scale bar ~ 15 cm. About a meter away from the contact the joints become near vertical. Compare with Figure 10A, which shows the contact of the West Rock diabase lacking columnar jointing (presumably the older intrusion of the West Rock diabase) with sandstone. Additional illustration in Appendix VII. D. Large near vertical cooling columns in diabase along southeast facing cliffs at Lufbery Park. Large poison ivy leaves (~15 cm) for scale.

The columnar jointing of the younger diabase contrasts to the outcrop style of most Fairhaven dikes, previously described, in the Wallingford and Branford quadrangles, which we infer to be the initial (older) intrusive pulse of the Talcott event. Compare Figure 10A, the contact of older diabase with host sandstone, with Figure 13 B-D, which shows the contact of younger diabase with host rocks. These older dikes tend to have been intruded along steeply dipping fractures and faults and tend to be 10-20 m or less in width in the Wallingford quadrangle, but may be 20 m or more wide in the Branford quadrangle. Some balloon into local sills, several 10's of m in preserved width, that mimic the attitude of the enclosing sediments (Figure 10B). The older diabase has poorly developed cooling columns and as a result has a much more irregular pattern of breakage, forming irregular blocks of diabase at the base of outcrops. Except where the younger diabase was identified or inferred, well-developed cooling columns were not observed in the Fairhaven dikes in the Wallingford quadrangle, even where they formed small sills.

Some segments (perhaps many) of the Fairhaven dikes apparently did not reach the ground surface as evidenced by contact metamorphosed sandstone overlying the dike segments and absence of vesicles within most of the dikes. The dike segments along Tyler Mill Road (see local areas 102, 108b and

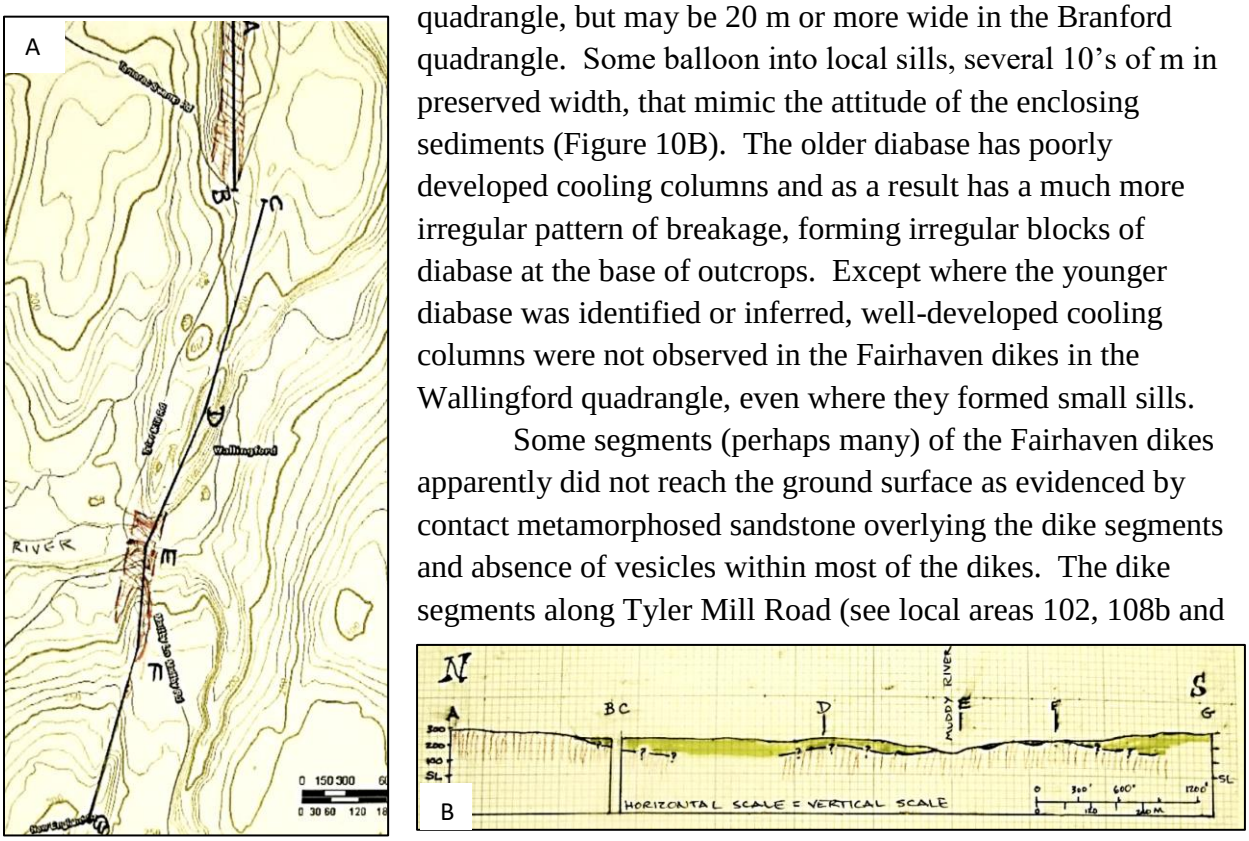

Figure 14 Map and longitudinal-section of dike at Tyler Mill Preserve (local areas 102, 108 and 108b). A. Map showing location of N-S stratigraphic cross section A-G along the southern portion of the dike (red cross-hatching) at Tyler Mill (GPS locations of points A-G in Appendix VIII. B. Stratigraphic cross section illustrating portions of dike (red cross-hatching) overlain by baked and partially fused sedimentary rock (yellow green color).

108 in Appendix I) are an example (Figure 14). The well- defined ridge (segment AB of Figure 14) held up by the diabase dike gradually diminishes southward to a gentle hill. Diabase outcrops disappear and instead gray, contact-metamorphosed sandstone is found (segment C-D of Figure 14). In places the sandstone appears to be partially melted and, in some places the melted sandstone is difficult to distinguish from diabase. The channel of the Muddy River at Tyler Mill (point E of Figure 14) exposes diabase that appears to be a continuation of the same dike to the north. It is overlain by contact metamorphosed sandstone. The dike crops out on the south side of the Muddy River but farther to the south is again covered by more gray metamorphosed sandstone (segments E-F-G of Figure 14). Chilled margins are found where the diabase contacts the enclosing sedimentary rocks (see Appendix IV, samples 108b and 108b1).

Segments of this dike did not make it to the surface at this location. Instead, the dike intruded to some depth below the surface into what was poorly lithified conglomeratic sandstone or more likely sand and gravel. The Fairhaven dike at Clintonville also has local areas where sandstone covers the top of the dike. The dike may not have reached the surface there either. This confirms the same observations and conclusion made by Davis (1898, p.43-45) in the Wallingford area. Hanshaw (1968) made similar observation on parts of the Buttress dike in the Meriden quadrangle.

The dikes at Clintonville and Tyler Mill as well as numerous small unnamed dike segments are overlain by partially melted sediments. The dikes must have been conduits to multiple pulses of flow (Lister and Kerr, 1991), some of it lateral, to provide heat sufficient to cause partial melting of the wall-rock. The partial melting is the main evidence for pulsating intrusion; we find few or no internal contacts in most of the intrusive units on the quadrangle (also see Philpotts and Asher, 1992).

Buttress Dike. The Buttress Dike crops out from Milford northeastward to Meriden, and extends across the northwestern corner of the Wallingford quadrangle. It is composed of Buttress Diabase, the chemical composition of which corresponds to that of the Holyoke Basalt (Philpotts and Martello, 1986) and, indeed, the Buttress Dike is thought to be the feeder to the Holyoke basalt flows. The dike is relatively simple at its northeastern and southwestern extremities, but in the middle, where the dike leaves the Mount Carmel quadrangle and enters the Wallingford quadrangle it is a complex mix of diabase/basalt/sandstone breccia and massive steeply-dipping diabase dikes (Figure 15). Several pulses of diabase intrusion and back-flow can

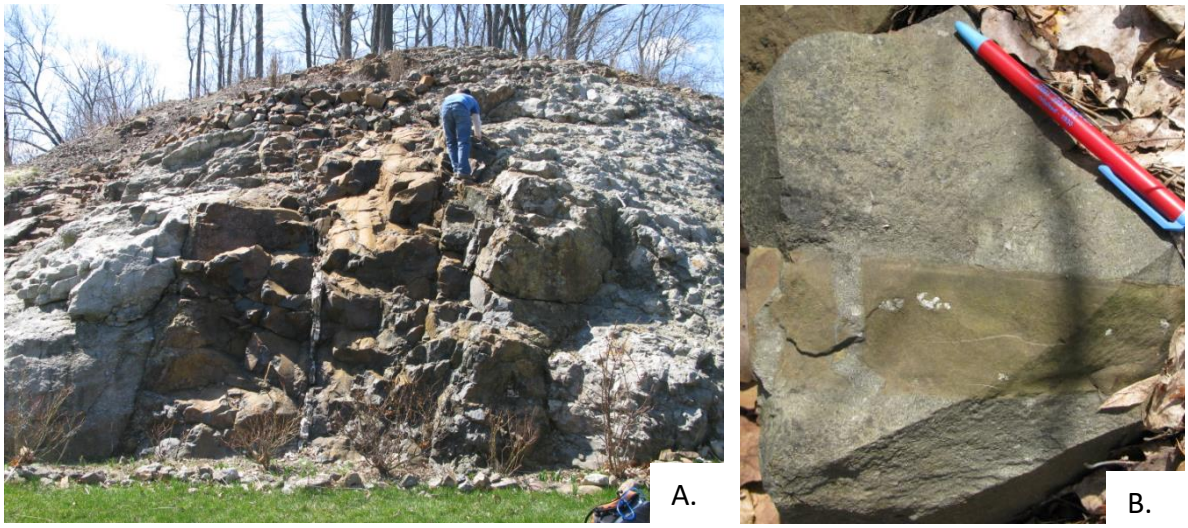

Figure 15. Massive diabase dikes range in width from meters to centimeters (local area 129S.) A. 4 m wide diabase dike intruded into bedded arkose on left and unbedded breccia on right: chilled margins on the diabase demonstrate chronology. Quartz filled fault in center of massive diabase. Geologist for scale. B. 5 cm wide dike intruded into sandstone that was unlithified or only weakly so at time of intrusion. Diabase fractured upon cooling and unconsolidated sand filled the fracture.

be documented forming autobreccia (Philpotts and Martello, 1986) at many locations. The clasts in the autobreccia are described as diabase but some, perhaps many, may have been initially extruded and hence are basalt.

Diabase forms dikes that are as much as 4 meters in width (Figure 15A), but more commonly are measured in terms of decimeters. The diabase consists of dark-gray compact rock (Figure 16). Plagioclase feldspar phenocrysts up to 1 mm long may be seen in a darker groundmass composed of pyroxene and smaller crystals of plagioclase.

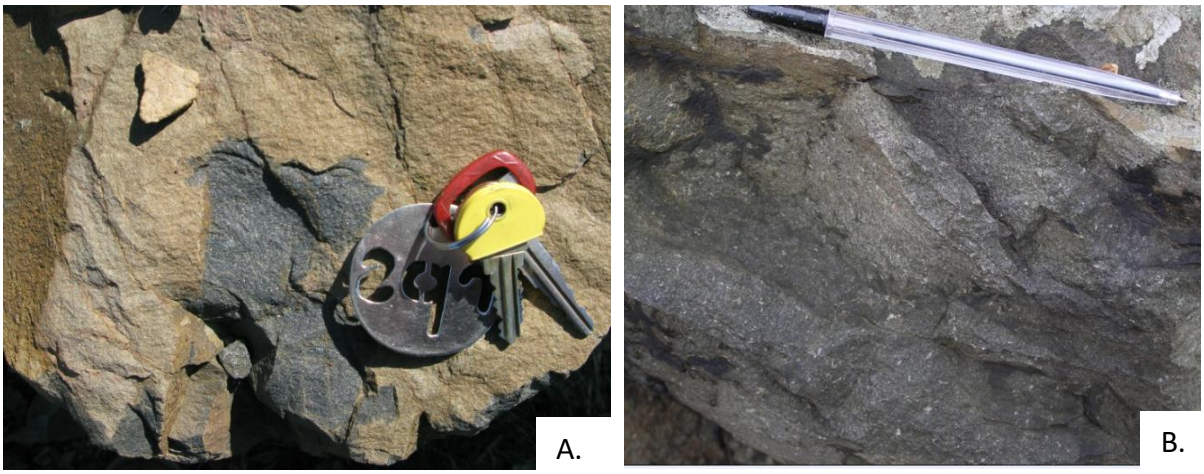

Figure 16. A. Fine-grained diabase shows typical tea-brown weathering surface (disc with keys is 5 cm diameter). Diabase is unaltered, which is unusual for Mesozoic intrusive rocks in the Hartford Basin. B. Most diabase has mm- sized plagioclase phenocrysts that are not always apparent macroscopically. Pen is 14 cm long. Local area 129S or Boulder Knoll Town Park, Cheshire, CT.

We refer to the diabase as massive in character to distinguish it from diabase breccia. The diabase dikes, however, may have internal chilled-margin contacts and/or flow structure and are not strictly massive (structureless). They are fractured/jointed in most places. Cooling joints are prominent in some exposures. Some of the diabase contains irregular areas that weather rusty giving the rock a splotchy appearance on the outcrop.

Diabase dikes in contact with bedded sediment typically oozed into the close interstices rather than breaking sedimentary grains (Figure 15B, 17). The basalt always has a chilled margin where it contacts the rock into which it intruded. In some places, partial melting of the sediment occurred at the contact, producing a dark gray to black glassy rock with numerous rounded sediment clasts that did not melt (Figure 18B). In many locations, however, the sediment shows little effect from the intrusion other than lack of strong pigmentation[6] (Figure 15A and 17). Diabase dikes in many locations are in contact with previously emplaced diabase

6. We have not determined that the lack of pigmentation was due to bleaching of an originally pigmented sediment. Perhaps the iron-bearing minerals in the sediment that would later weather to form the pigmenting minerals were altered in the baked zone. Possibly the dike restricted ground water flow that later resulted in pigmentation of the sediments distal to the dike. Sediments in some septa, however, are fused (Figure 18a).

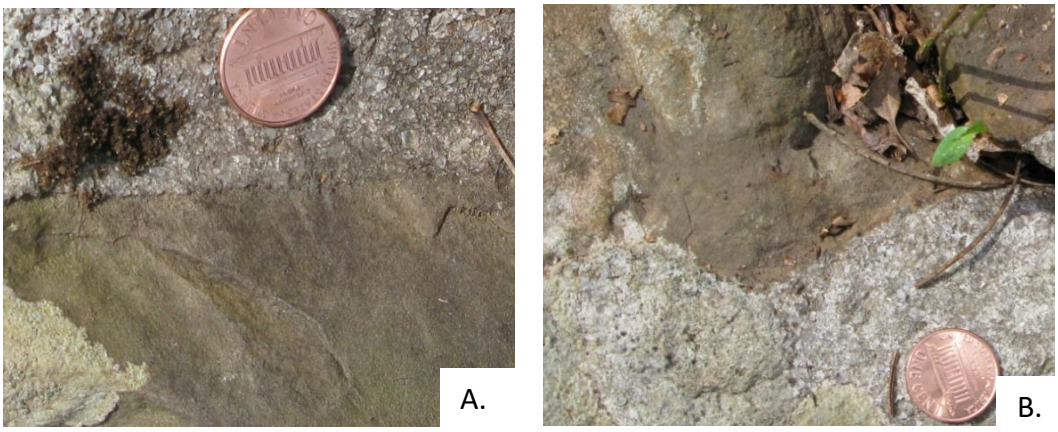

Figure 17. Contact of diabase dike with weakly-cemented or uncemented arkosic sandstone where basalt fills sediment grain interstices rather than breaking sediment grains, indicating that the sandstone was not cemented, or was poorly cemented, at the time of intrusion. Local area 129S.

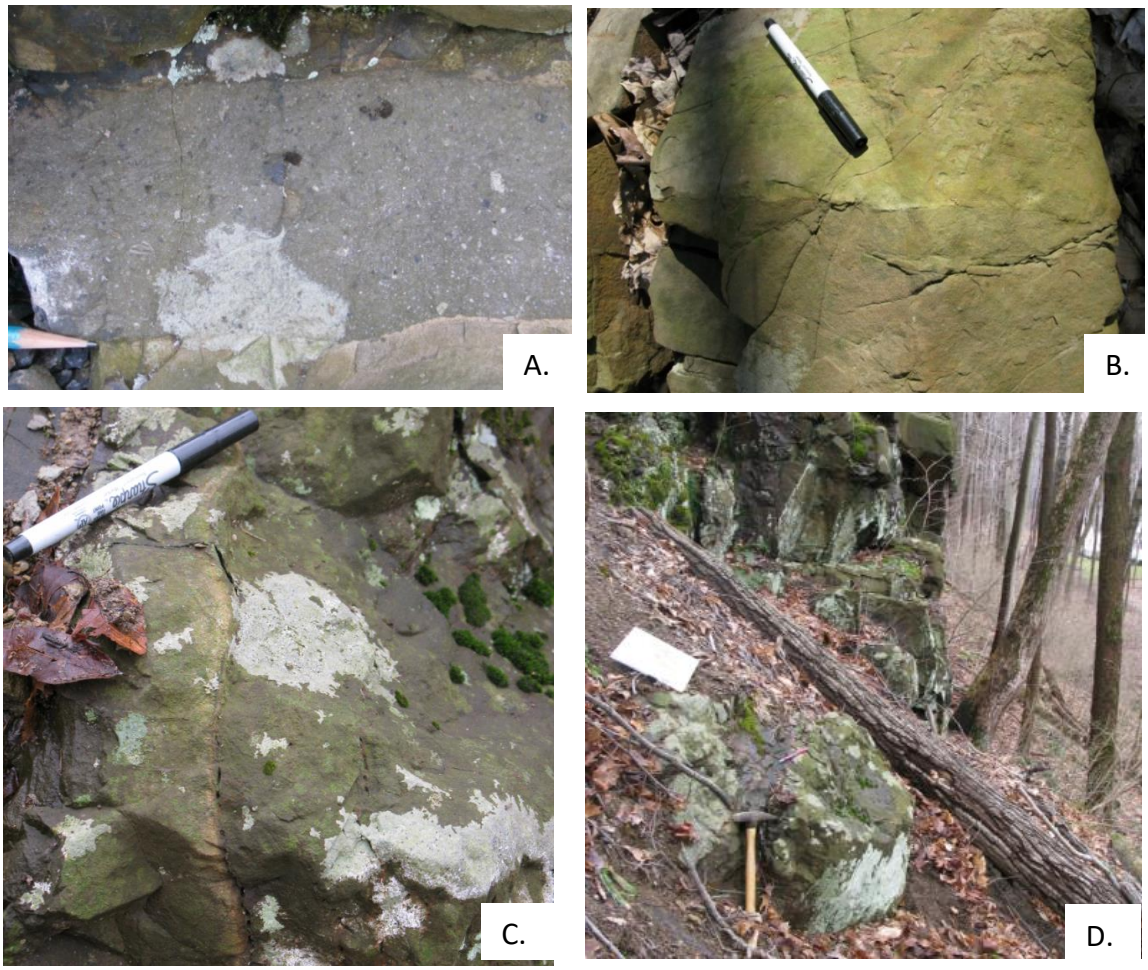

Figure 18. A. Partially fused sandstone septa between diabase breccia (top) and massive diabase (bottom) with chilled margin. Unfused clasts in sandstone are sedimentary grains composed of feldspar and of phyllite. B. Internal contact in diabase dike. Fine-grained chilled diabase (top) against coarser grained diabase. C, D. Internal contact along west side of dike. Diabase with chilled margin to the east of older diabase. Both are fine-grained. Contact in D. is behind hammer head and can be followed across base of outcrop. Local area 129S or Boulder Knoll Town Park, Cheshire, CT.

dikes (Figure 18B-D). At these locations the younger diabase shows a chilled margin up against the older coarser grained diabase. Many of the dikes are "sheeted" (Figure 19) and are a complex of several pulses of intrusion separated by time sufficient to result in cooling of the older rock.

Diabase in contact with breccia is usually coarse-grained (Fig. 20A); a chilled margin, however, has been observed only in a few locations. In some cases (Fig. 20B) the contact is indistinct, that is, massive diabase becomes brecciated across an indistinct contact and the brecciated diabase contains increasing amounts of sand matrix with increasing distance from the indistinct contact.

Breccia is a prominent component of the Buttress Dike. Two breccia varieties are found. The more abundant is diabase breccia with variable amounts of detrital sand and gravel in the matrix. Diabase and perhaps even basalt clasts range in abundance from almost 100% of the rock, particularly near the margin of the dike where they fit together, to almost 0% (i.e. they are absent), but generally they form about 60% of the rock. Diabase clasts are generally rounded when in contact with a sedimentary matrix, but many are angular. Clasts range in size from a few millimeters to almost a meter; most are 2-4 cm. Some of the clasts contain delicate appendages (Fig. 21C, E) that suggest that they were plastic and had molten interiors at the time of incorporation into the breccia. Clasts of sedimentary rock are also found in many locations. Most sandstone clasts are rounded; some are subrounded (Figure 21B). They are up to 10 cm in diameter except for one location that contains clasts of subrounded sandstone up to 60 cm in diameter (Fig. 21D). Most breccia with sedimentary matrix does not contain any diabase matrix.

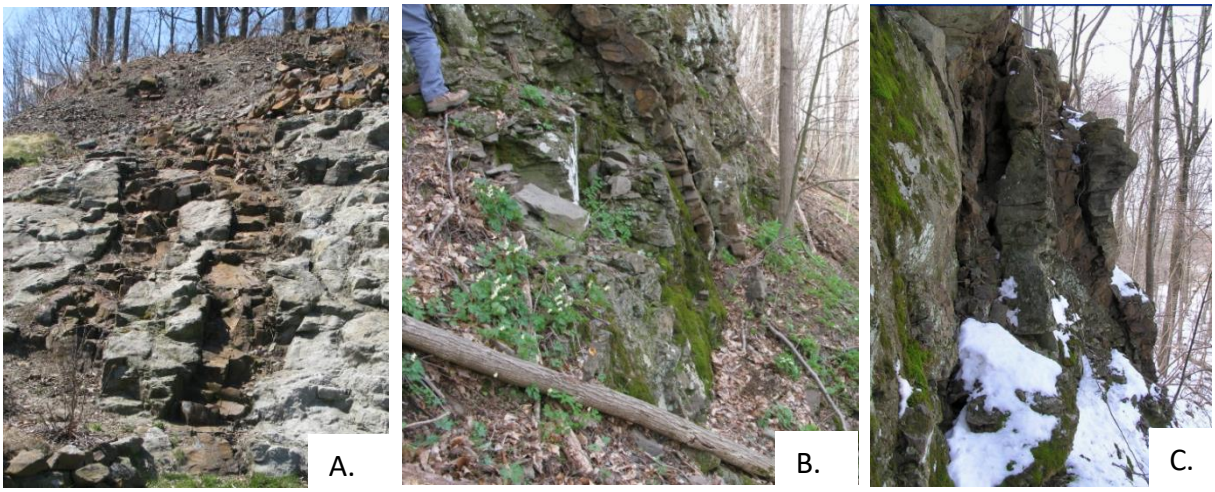

Figure 19. A. "Sheeted" dike on east side of ridge with fragment of sandstone septa caught up in middle. Sandstone is cut off at top where it is partially fused. Both dike halves contain one or more internal contacts indicating multiple pulses of intrusion. An internal contact can be seen in middle of dike on right. These are most easterly dikes diagrammatically illustrated in Figure 23. Local area 129S. B. Sheeted dikes on west side of ridge near where Buttress Dike exits the quadrangle. B. and C from Boulder Knoll Town Park, Cheshire, CT. C. Multiple dikes on west side of ridge. Sandstone septa, with irregular or wavy contacts separate two sheeted complexes that contain one or more internal contacts.

In several locations, most notably near the western border of the quadrangle, diabase forms the matrix in the breccia (Figure 22). In these locations angular clasts are all diabase, or perhaps basalt. Clasts range in size up to 25 cm. Some clasts show a spheriodal fabric that resembles weathering rinds, perhaps a selvage caused by cooling or baking. The diabase matrix is all fine-grained but still shows chilled margins against the clasts. In many places the matrix displays flow banding.

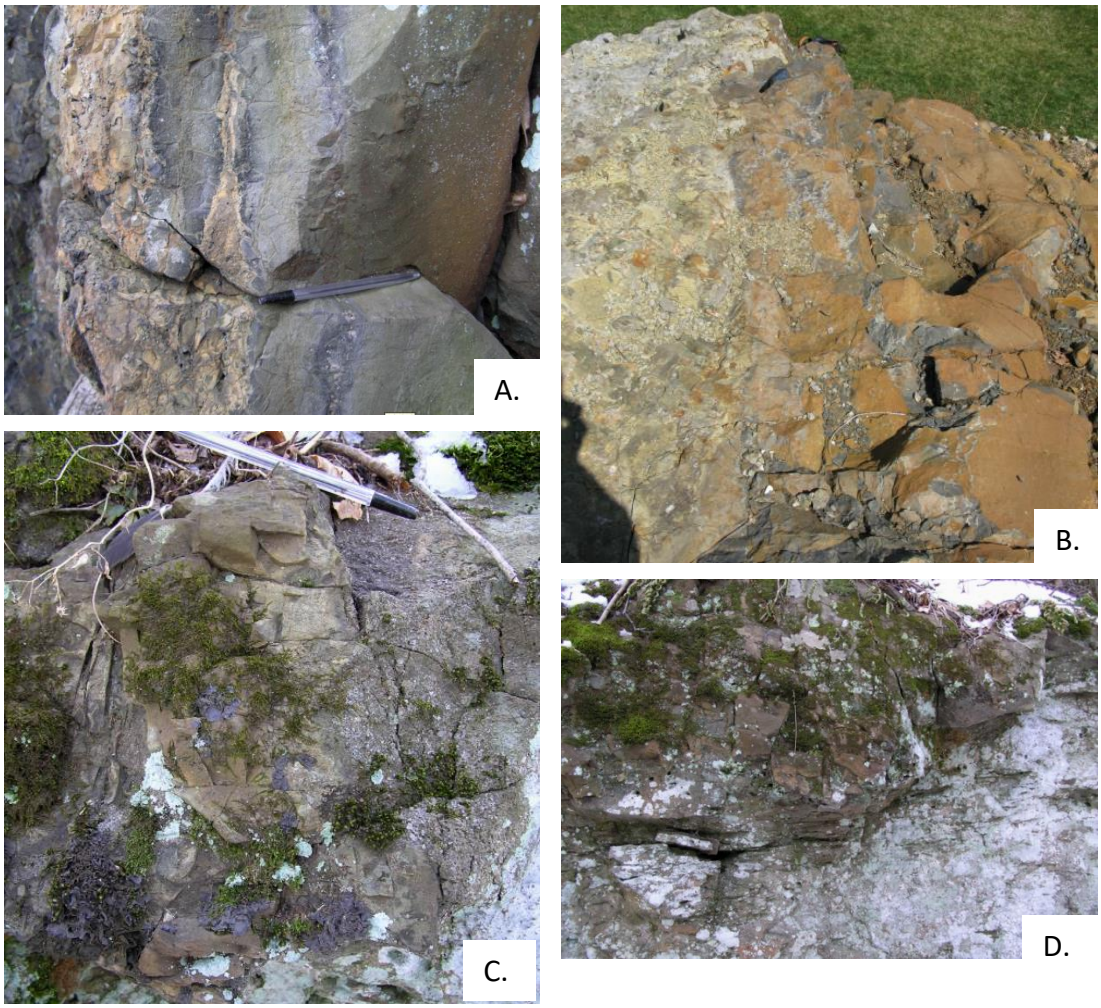

Figure 20. Diabase contacts. A. Fine-grained, brecciated diabase with chilled margin (center) in contact with massive diabase (right). B. Massive diabase (far right) gradually becoming breccia with sand matrix (left). Sand matrix is in part fused close to the massive diabase. Elsewhere in outcrop (behind photographer), massive diabase has a chilled margin against the breccia. C. Diabase breccia in contact with bedded sandstone septa. Sandstone dips away from viewer. D. View of diabase/sandstone contact, looking north parallel to the ridge trend. Note that fracture along which breccia intruded "zig-zagged" across and along sandstone bedding planes. Bedding dips toward the east at about 10°. Local area 129S (Figure 20B or Boulder Knoll Town Park, Cheshire, CT (Figures 20A, C, D).

A.

B.

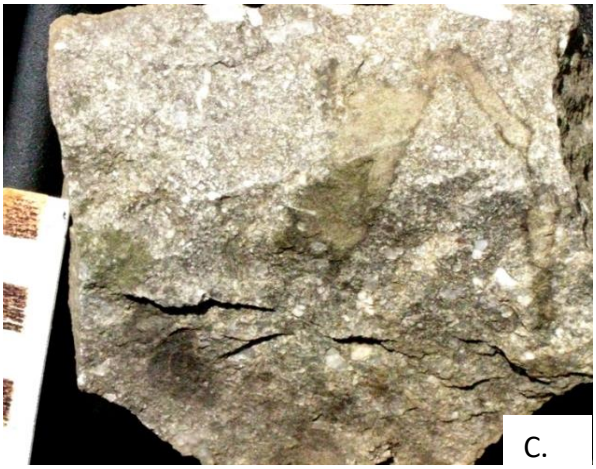

C.

Figure 21. Breccia with sand matrix (Boulder Knoll Town Park, Cheshire, CT). A. Breccia with angular diabase clasts in a sand matrix (light areas). Sand has penetrated into fractures between large clasts in center part of image. B. Large rounded sandstone clast with rounded diabase clasts. Somewhat rounded diabase clasts fit tightly together with little matrix, suggesting they were plastic at the time of their formation. C. Diabase clast with a delicate tail, suggesting that some of diabase clasts were plastic or even molten at time of formation. Scale on left with cm squares. D. Breccia with large clasts of sandstone and diabase in a sandy matrix. Pencil is 8 cm. E. Breccia that retains porosity into which a diabase clast leaked its molten interior.

.

D.

E.

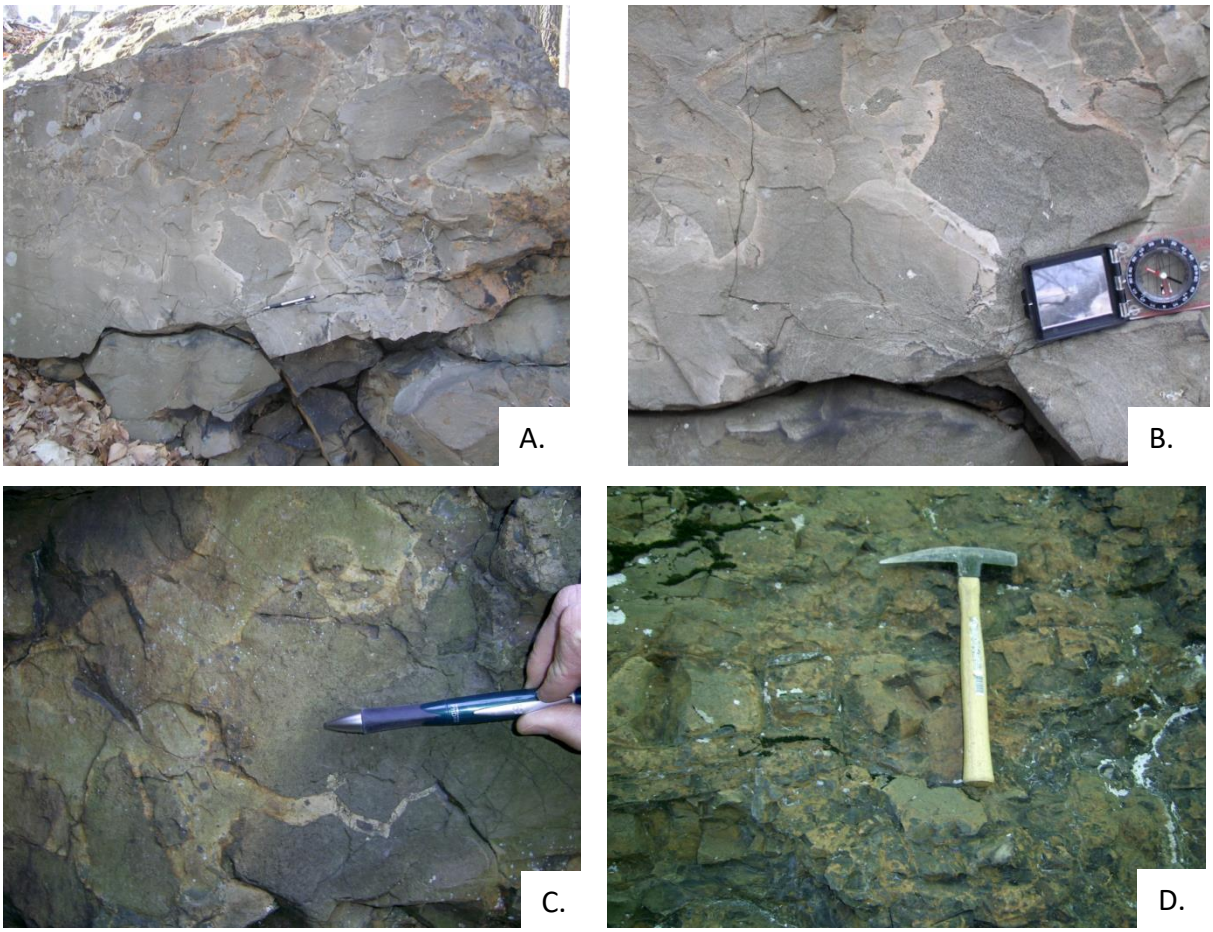

Figure 22. Breccia with diabase matrix. (Boulder Knoll Town Park, Cheshire, CT.) A. Diabase clasts are angular with some small clasts apparently broken from adjacent larger clasts. Note chilled margin on diabase matrix and fresh appearance of both clasts and matrix. B. Detail of A. showing flow banding in matrix (below and to left of compass). Clast above compass is diabase. Compass ~ 10 cm wide. C. Diabase matrix intruded into small fractures in diabase clast. D. In some areas breccia with diabase matrix has rusty patina on weathered surface.

Instructive cross sections. Because individual dikes, breccia bodies, and sandstone septa are too narrow to be shown on maps of the complex part of the Buttress dike, we here describe two cross sections that aid interpretation of the history of the dike.

Cross section at Wallingford Road. One cross section (Figure 23), at the northern end of the ridge at Wallingford Road, is *on private property.* The main feature of complex dike at this location is a 4-m-wide dike of massive diabase that occurs in the middle of the outcrop (Figure 15A). The eastern contact of this dike with bedded sandstone displays a baked and brecciated zone that is about 10 cm wide. Diabase at the contact grades toward the center and west side of the dike into massive, more coarsely crystalline diabase. The western side of the dike abruptly grades into diabase breccia (Figure 20B) with large irregular clasts. Although most of the exposed contact of diabase lacks a chilled margin with the breccia, at one area near the top of the outcrop the diabase has an apparent (anomalous) chilled margin. The breccia contains increasing

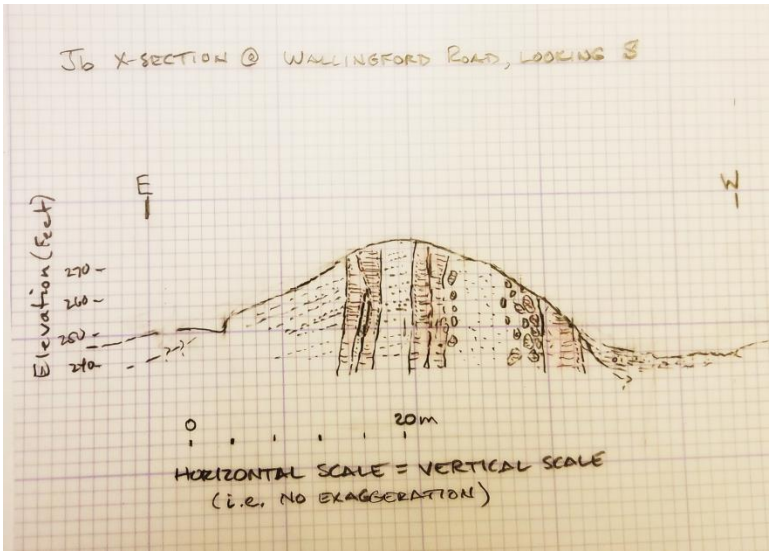

Figure 23. Cross section of Buttress Dike at Wallingford Road in Cheshire (local area 129S). Buttress Dike consists of at least two and possibly three separate intrusions. Two sheeted dikes, approximately a meter wide, are farthest to the east, both with chilled margins against New Haven Arkose. A thin septa of sandstone separates the dikes at the base of the outcrop, but pinches out upward. Both dikes are chilled against the septa. At the sandstone-septa pinch-out, the in-board dike is chilled against the outer and therefore older dike. In the middle of the Buttress complex is a 3-4 m wide dike with a fault in its middle. The fault is mineralized with quartz. This dike has a chilled eastern margin against bedded sandstone. Its western margin grades into diabase breccia with sand matrix. Many diabase clasts in the breccia have chilled margins and the diabase dike in a few places is chilled against the sandstone matrix. The diabase clasts are larger and more abundant near the contact with the diabase dike. The middle of the breccia consists of greater than 95% unbedded arkosic sandstone. A diabase dike is found on the western side of the Buttress and abruptly grades into the diabase breccia on its eastern side. It is relatively coarse-grained at the contact with the breccia but is fine-grained where the outcrop ends, suggesting that it has a chilled western margin. The diabase breccia has abundant large clasts near its contact with the diabase dike, but clasts become smaller and less abundant toward the middle of the breccia body. The two dikes bordering the breccia have chilled outer margins, but generally are not chilled or are only locally chilled against the breccia. Thus, the dike and breccia appear to be the result of the same event. The relation of this intrusive event with the other two dikes is uncertain.

amounts of light-gray to white sand matrix with increasing distance from the diabase contact. About 3 m from the contact, diabase clasts completely die out and massive, *unbedded* white sandstone remains (see right side of Fig. 15A). Toward the western side of the breccia, diabase clasts become increasingly more abundant. A poorly exposed contact with a diabase dike on the western side of the complex lacks a chilled zone.

To the east of the massive diabase, conglomeratic sandstone shows distinct bedding (350^{o}/15E) but lacks pigmentation: it is light gray to white (Figure 15A). It is cut on the east by sheeted dikes (Fig. 19A) that show distinct chilled margins. Thin veins of glassy diabase extend into the sandstone. The thin sheets pinch or swell on the outcrop. Some die out. Thin sheet dikes in the sandstone on the east side of the dike complex can be traced some distance to the south. The contact of the diabase against the sandstone does not break across individual sand grains, but, rather, the diabase intruded into the sand interstices forming a microscopically jagged contact. This indicates that the sand lacked pore-filling cement at the time of intrusion.

Interstices in the breccia adjacent to the western side of the massive diabase are filled with a succession of hydrothermally precipitated minerals (Figure 24). Quartz was the initial precipitate in many of the open pore spaces. This was followed by precipitation of ankerite or siderite in some pores and finally calcite and/or dolomite. At other places along the ridge, barite precipitated after the calcite/dolomite. Only a few pores contain all phases of the succession.

Most lack the quartz and some lack the ankerite. The sequence of precipitation here is the same as that observed farther west at Jinny Hill (Fritts,1962; Ryan, 1986).

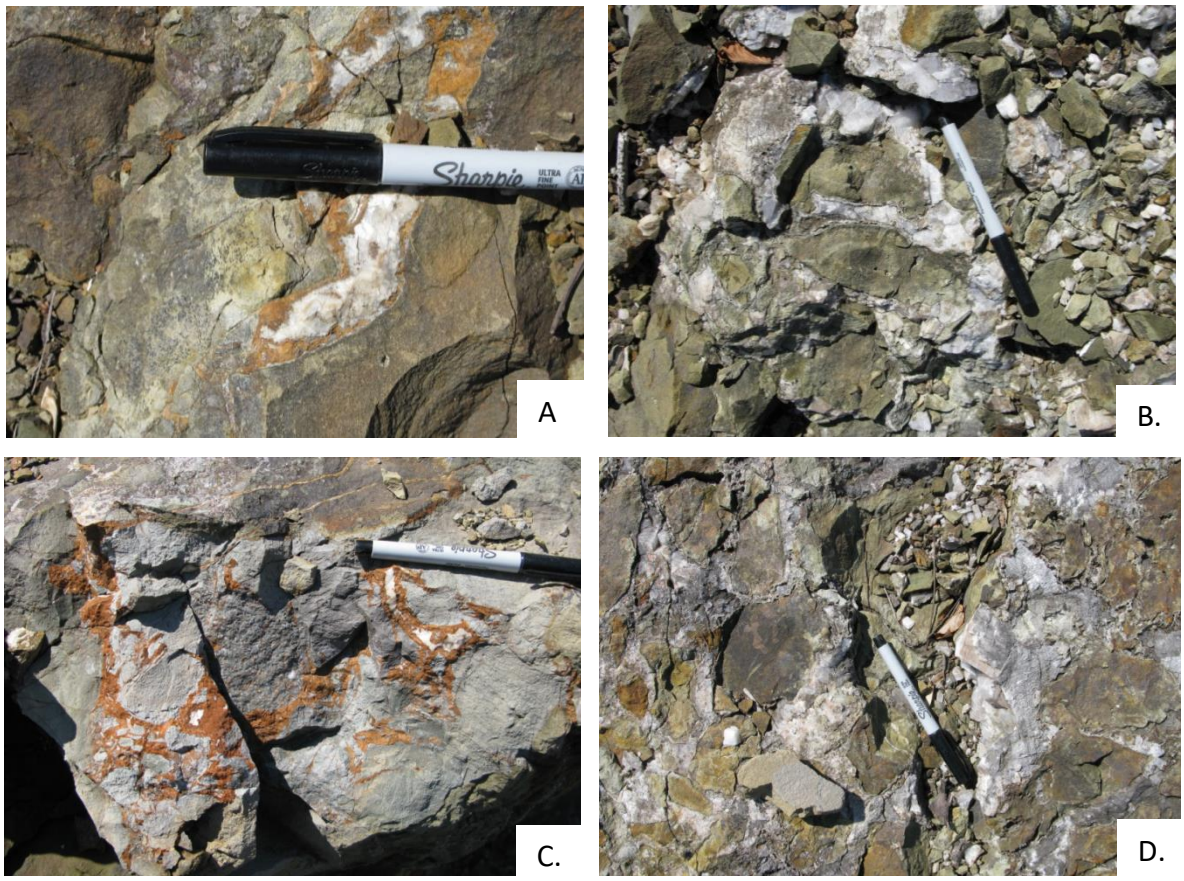

Figure 24. Mineralization into what were open pores interstitial to diabase clasts in breccia at Wallingford Road cross section (local area 129S). A. Complete sequence of initial lining of quartz crystals, followed by ankerite and/or siderite, and pore-filling calcite and/or dolomite. Pen is ~20 cm. B. Pore margin is rimmed by quartz crystals, upon which calcite and/or dolomite precipitated. Ankerite is absent. C. Locally, ankerite and white carbonate fill interstitial pores. Quartz is absent. D. Some interstitial pores in the breccia are filled only by white carbonate minerals. Both quartz and ankerite are absent.

Quartz mineralization is found at the outcrop on Wallingford Road (Figure 15A). A 5-10 cm wide fault, oriented 210°/80W, in the middle of a 4-m-wide diabase dike is mineralized (Figure 25). Quartz was deposited within the fault zone and numerous internal contacts along with broken fragments of diabase suggest several fault-mineralization episodes. Euhedral calcite crystal molds within the quartz indicate co-precipitation during at least one of the episodes.

Figure 25. Quartz deposition along fault (local area 129S, see Fig. 15A). Holes in quartz seen to left of marking pen are euhedral molds after calcite or dolomite.

Normal movement is indicated on this fault. Similar quartz, along with quartz fibers and slickensided surfaces are found several hundred meters south in the massive diabase. Presumably the diabase, the fault, and its quartz precipitate are continuous, although not continuously exposed, over that distance.

Interpretation of cross section. We cannot distinguish the age relation between the 4-m-wide massive dike and the narrower sheeted dikes immediately to its east. They are probably not coeval: the sheeted dikes may have intruded into fractures prior to intrusion of the wider dike, for reasons we will argue below. We infer that the 4-m-wide dike was wider during its intrusion, but split apart immediately after its emplacement. The dike west of the breccia is the other half to the 4- m dike. The split may have occurred when the driving force behind the rising basaltic magma was exhausted which may have been accompanied by rapid release (explosive) of exsolved gas and steam (de Boer, 1968). The sudden release of pressure resulted in collapse of unconsolidated sand that formed the fissure wall closer to the surface and allowed an episode of return flow, first of partially congealed brecciated diabase and perhaps basalt (autobreccia of Philpotts and Martello, 1986, p.108) followed by increasing amounts of collapsed sand and gravel. This suggests close proximity to the ground surface at the time. In any case, diabase breccia is found on both sides of the breccia dike adjacent to the massive diabase, which for the most part lacks chilled margins. The influx of collapsed sand then filled the center of the dike forming unbedded sandstone. The split diabase dike was still hot enough to locally fuse some of the collapsed sand.

The two dikes (sheeted dikes on east and split massive dike on west) were probably not coeval because the eastern set shows no indication of backflow and the western, larger dike shows no evidence of multiple pulses of magma emplacement (*i.e.*, that produced nested dikes on the east).

Magma flow through the western (split) dike probably intruded after the eastern sheeted dikes had cooled and congealed rather than the reverse. This interpretation is based on the expectation that the sheeted dikes would have taken advantage of the poorly consolidated (therefore weak) breccia to ascend to the surface *had the breccia been there*. By this reasoning, the breccia did not exist at the time the sheeted dikes were formed.

Cross section at western edge of Wallingford quadrangle. The Buttress Dike at the western boundary of the Wallingford quadrangle (and at northern boundary of Cheshire's Boulder Knoll town park) is bounded on both east and west sides by massive dikes (Figure 26). Breccia is poorly exposed but apparently occupies all the volume between. The eastern side is made up of two or more sheeted dikes. Internal chilled contacts and a chilled margin at the eastern contact with sandstone have been observed. A contact with the breccia was not seen. The breccia apparently consists of two end-member types: the breccia on the east has a sandstone (unbedded) matrix with diabase clasts. Breccia farther west has diabase matrix

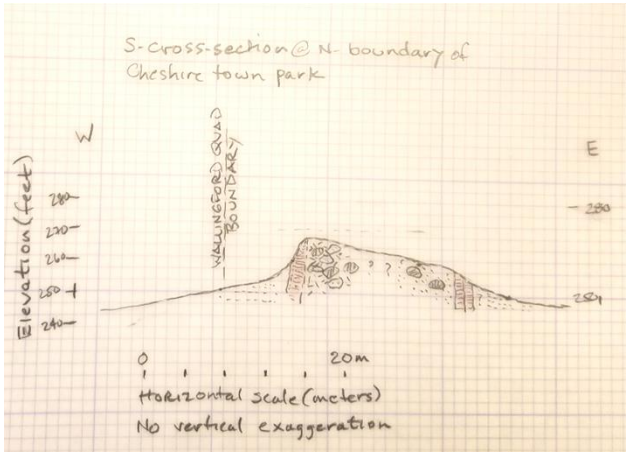

Figure 26. Cross section of Buttress Dike at western boundary of Wallingford quadrangle, looking north (local area 129S).

with both sandstone and diabase clasts. The two end-members most likely grade into each other, but outcrops showing such were not observed. A 2-4 m wide massive diabase dike is found on the western edge of the complex. Neither chilled margins nor internal contacts were observed in this dike. In places it appears brecciated and may grade on its inboard side into breccia.

The segment of the Buttress dike farthest north in the Wallingford quadrangle (near, but just south of Connecticut Rte. 68; local area 129N) also displays two dikes at its eastern and western boundaries. Light-gray sandstone fragments were found between outcrops of the two dikes. The sandstone appears non-bedded and may have been collapsed into the dike after intrusion.

19th century barite /copper mining. During the mid 1800's mining and extraction of the mineral barite was a lively industry at the Jinny Hill mines in Cheshire (Fritts, 1962) about 2 km west of the Buttress Dike ridge in Cheshire. The mineral is white and was used to pigment paint. In addition to barite, small amounts of copper minerals were found (see also Moritz and references therein: https://www.mindat.org/loc-10340.html). The main barite mines are along three east –west fracture and fault zones in New Haven Arkose south and west of the Buttress Dike outcrop belt in the Wallingford quadrangle (Fritts, 1962; 1963).

Along the ridge formed by the Buttress Dike in the Wallingford quadrangle, prospect pits were dug and several adits and other underground workings were driven (see Figure 27). Fritts suggests that copper rather than barite was the object of these prospects. Although few ore minerals were seen on the surface, it is possible that some could be found in the waste piles adjacent to the prospect trenches. Reports of loose ore fragments at Cross-Rocks Dike bearing evidence of derivation from a smelter-site (de Boer, 1968), perhaps support the suggestion (Fritts, 1962) that the prospects were dug and "salted" to promote investment. However, at the northern site shown on Figure 27, a square foundation was found around which abundant slag fragments were littered (Figure 28). A recent study by University of Connecticut graduate student (Fellows and Ouimet, 2019) found evidence of former charcoal pits just east of this site, suggesting possible attempts to smelt (on site) the ore recovered from the underground workings.

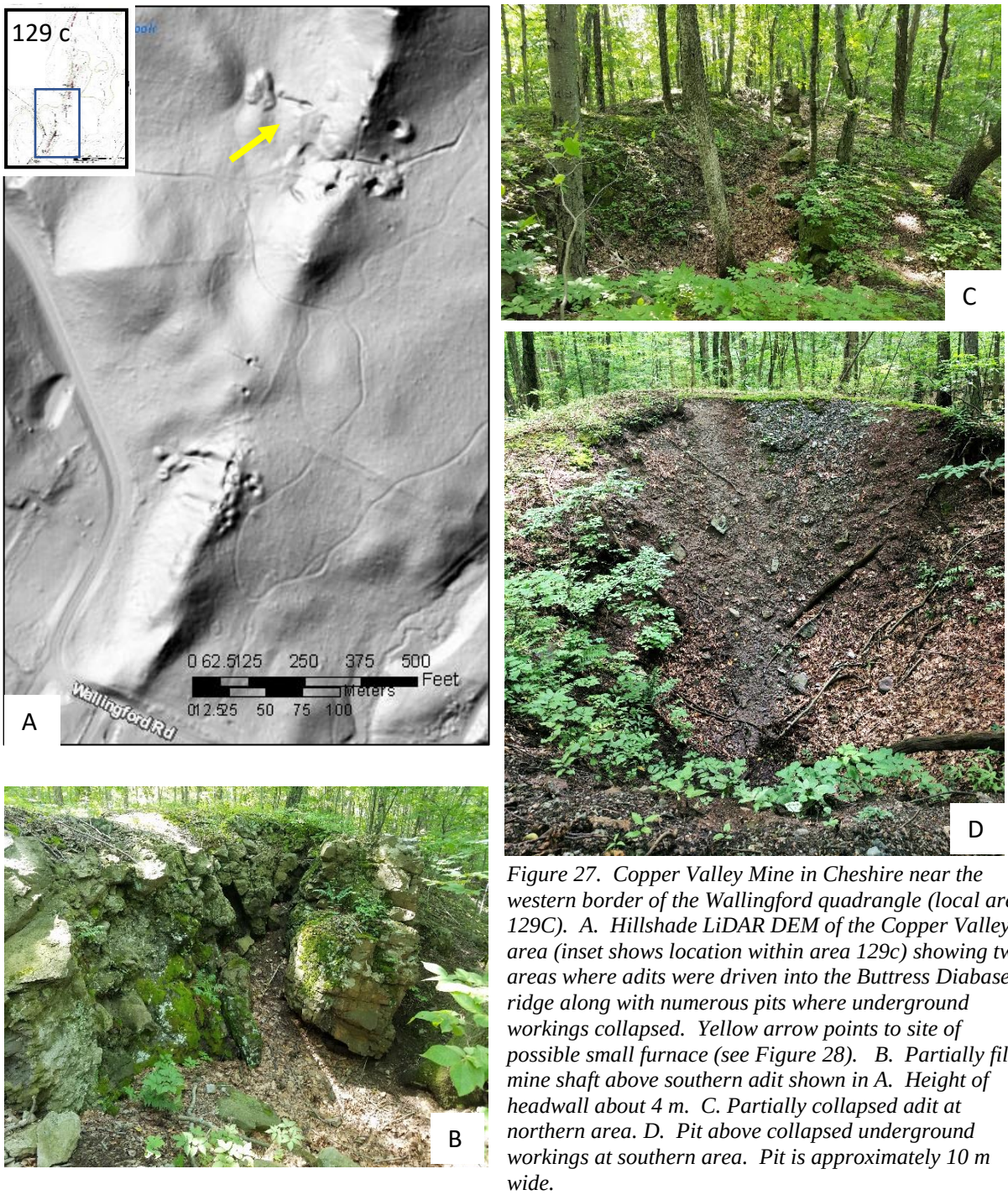

Figure 27. Copper Valley Mine in Cheshire near the western border of the Wallingford quadrangle (local area 129C). A. Hillshade LiDAR DEM of the Copper Valley area (inset shows location within area 129c) showing two areas where adits were driven into the Buttress Diabase ridge along with numerous pits where underground workings collapsed. Yellow arrow points to site of possible small furnace (see Figure 28). B. Partially filled mine shaft above southern adit shown in A. Height of headwall about 4 m. C. Partially collapsed adit at northern area. D. Pit above collapsed underground workings at southern area. Pit is approximately 10 m wide.

East-west fractures are mineralized at Jinny Hill and other locations in west and north-central Cheshire. East-west fractures cut the Buttress Dike and mineralization appears in the breccia of the Buttress Dike (Figure 24). This suggests that fracturing of the rock and deposition of the barite and copper minerals post-dates the emplacement of the Buttress Dike.

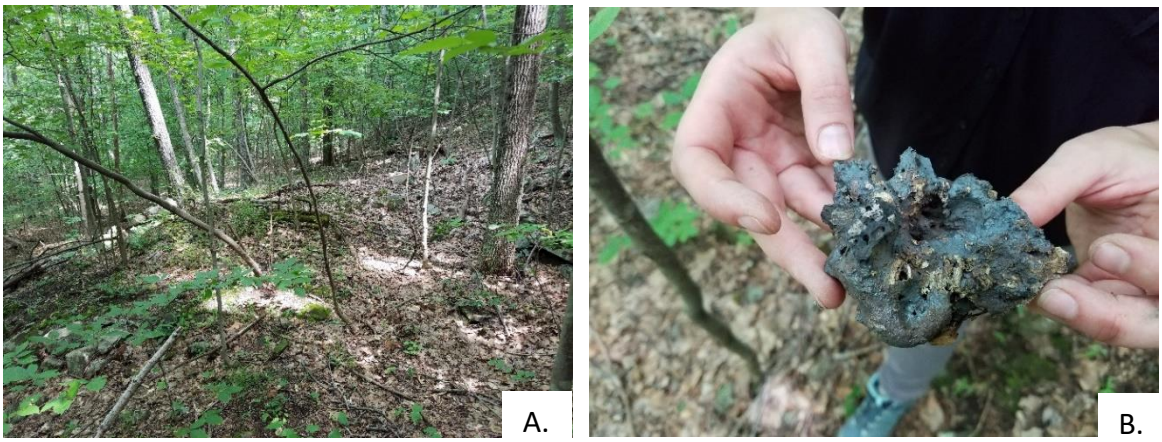

Figure 28. Possible smelter site at Copper Valley mine. Flat area (A) near northernmost workings where abundant slag (B) litters the ground.

Lamprophyre.[7] A 500 m long lamprophyre dike previously described by Eppler (1999), intrudes a Talcott Basalt-aged diabase dike in local area 132 (Figure 29; Appendix I, Figure I-45). The dike in Wallingford is one of several camptonite dikes first reported by Russell (1923). The lamprophyre has a fine-grained chilled contact with diabase indicting intrusion of the lamprophyre postdated cooling of the diabase. Armstrong and Besancon (1970) and Armstrong and Stump (1971) report K-Ar ages of 152 + 3 Ma and 169 + 2 Ma for the dike in Wallingford.

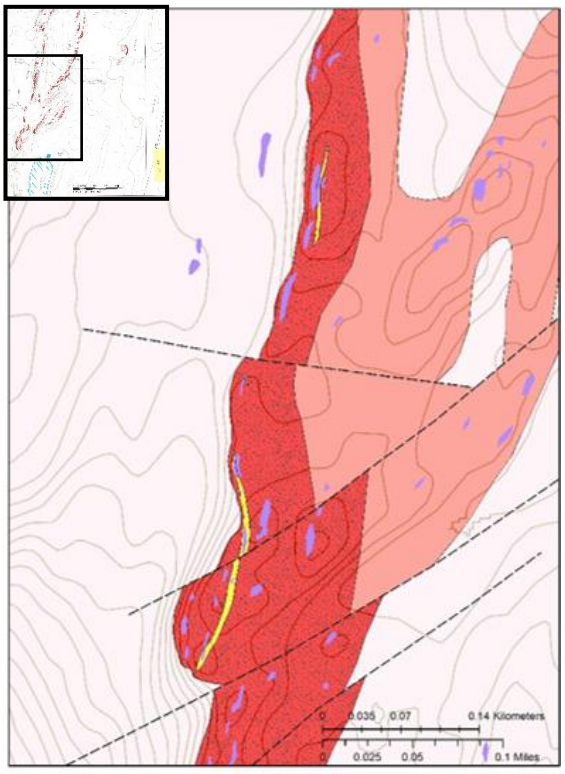

The dike is composed of several *en echelon* segments that trend roughly N-S. The dike is ~1.5 m wide, but tapers to ~0.5 m wide at segment ends where exposures are poor and crumbly. At the northernmost extent, the lamprophyre is 0.3 m wide and cross obliquely across the diabase at an attitude of 356°. At the southernmost extent, the lamprophyre consists of

Figure 29. Local map of area 132 (shown as 132W in Appendix I; inset shows location of Figure 29 within local area 132W). Lamprophyre is shown in yellow and intruded into West Rock Diabase with columnar jointing (dark red with stipple). Area underlain by New Haven Arkose is uncolored, pink area underlain by West Rock Diabase. Outcrop shown in purple. Eppler (1999) includes a map showing lamprophyre dikes having a much greater (longer) extent than we were able to document.

7. Based on Taylor and others, 2019, and an unpublished report by Taylor.

numerous, irregularly emplaced dikelets ranging from 1 to a few cm wide. We interpret this as the southern termination of the dike. Due to the lack of outcrop, we do not know if the northernmost exposure is a segment end or overall dike termination. Because the dikes are narrow, they form poor outcrops and are only seen where intruded into resistant diabase or basalt.

The dike is composed of several zones, each differing in grain size and abundance of phenocrysts and vesicles wide (Figure 30). The chilled margins range from ~0.5 to ~1.3 cm and are composed of extremely fine grains with few phenocrysts. Inwards, a zone approximately 10 - 20 cm wide is composed of a fine-grained groundmass, abundant mafic phenocrysts, with or without vesicles. The center of the dike is ~100 cm wide and is composed of a fine-grained groundmass with abundant mafic phenocrysts and elongated vesicles, up to 2 cm long.

Figure 30. Photograph of the south end of the lamprophyre dike exhibiting flow differentiation. Exposed width of dike ~0.5m. Local area 132W.

Mineralogy and Petrology. Lamprophyres are characteristically silica undersaturated and contain abundant, exceptionally large, mafic phenocrysts and vesicles. The lamprophyre groundmass (Figure 31) is composed of generally euhedral grains of kaersutite (ferric amphibole), titanaugite, albite and opaque phases of magnetite and ulvospinel. Feldspar is restricted to interstices of the mafic phases. It is anhedral and exhibits complex compositional

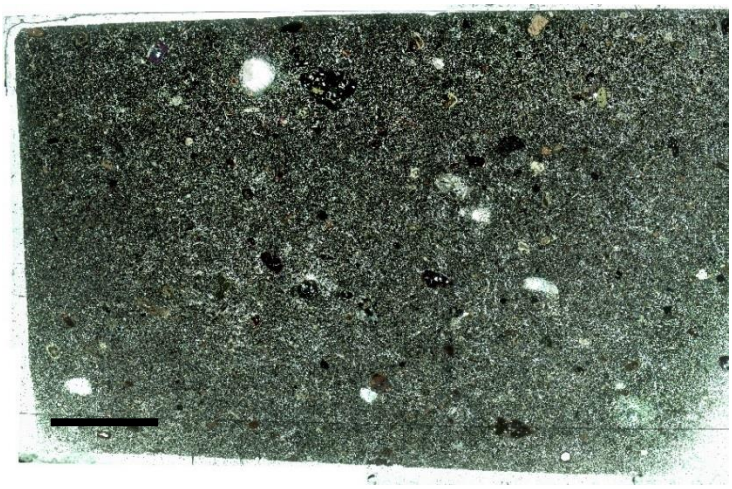

Figure 31. Photograph of sample WL-4 thin section showing clinopyroxene and kaersutite phenocrysts and calcite vugs (amygdules?) set in a fine- to medium-grained groundmass of magnetite, clinopyroxene, hornblende, and plagioclase. Plane light. Scale bar ~ 5 mm.

zoning. The feldspar ranges in composition from albite to orthoclase, as well as mixed variations of the two. The groundmass contains the accessory mineral apatite along with minor amounts of pyrite and ilmenite. Lamprophyres with this mineral assemblage may be classified as camptonite. Phenocrysts are composed mainly of kaersutite with lesser amounts of titanaugite, omphacite, spinel, and opaques, and range in size from 0.5 cm to 1.8 cm. Phenocrysts exhibit a variety of disequilibrium textures (Figure 32). Some are euhedral with only a small, normally zoned rim. Others are subhedral to euhedral and contain a reversely zoned rim. Numerous phenocrysts contain large embayments, interpreted as resorbtion/overgrowth textures. Cores of kaersutite are rimmed by ulvospinel and clinopyroxene.

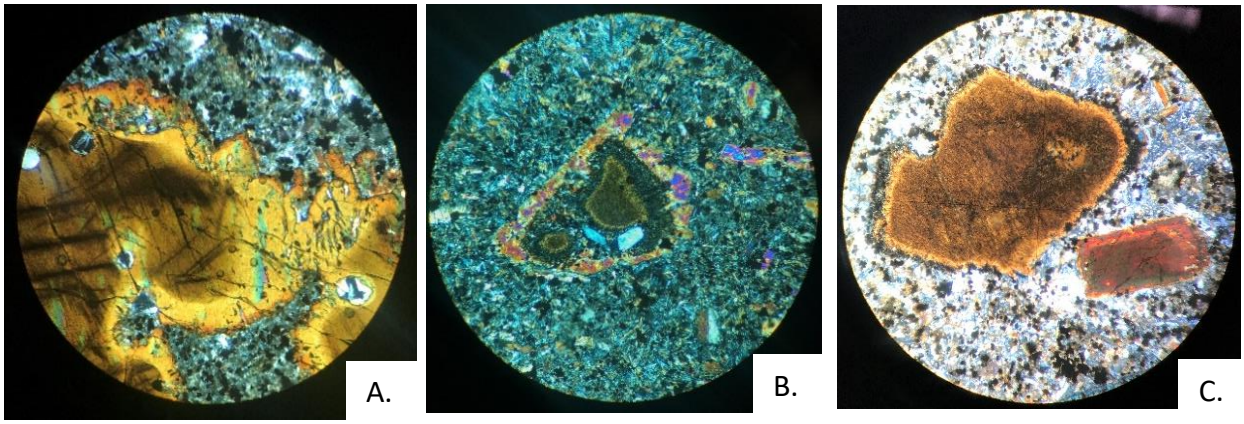

Figure 32. Photomicrographs of kaersutite phenocrysts of varying levels of alteration. A. Large phenocryst showing reaction rims, embayment and compositional changes exhibited by darker areas. Width of view is 2mm. B. Phenocryst is nearly resorbed and contains a clinopyroxene rim. Width of view is 2mm. C. Subhedral phenocryst with an opacite rim and a euhedral titanaugite phenocryst. Width of view is 5mm.

CHEMICAL ANALYSES

During the course of this project, major and minor element concentrations were determined for approximately 50 samples. The objectives of the chemical studies were several. First was to determine the chemical classification of the samples in the Wallingford quadrangle. Second was to confirm the distinction of previous workers that the lava flows (two of which are exposed in the quadrangle) have distinct chemical signatures and that two sets of dikes have chemical compositions that match the flows. Third, and important to our study, was to determine with which lava flow each the various dikes and sills that intrude the New Haven Arkose in the Wallingford quadrangle is associated.

Analyses reported in this section are from only the least weathered (chemically altered) samples based on LOI and alkali concentrations8. Analyses were performed on 6 lamprophyre samples (2 from our collection and 4 from Taylor and others, 2019), 3 Talcott Basalt samples, 7 Holyoke Basalt samples and 16 samples from the diabase localities, most of which were mapped

8. Sample locations are reported in Appendix II. Chemical analyses on all samples are reported in Appendix III.

as Buttress Diabase by Rodgers (1985), but are considered West Rock Diabase (with or without columnar joints) by this study.

On a total alkali-silica diagram, basalt flows and diabase intrusions of the Talcott and Holyoke events plot within the basalt and basaltic-andesite field (Figure 33); lamprophyre, which contains less than 10% modal olivine, plots near the tephrite field. Analyses within the trachy-basalt and basaltic trachy-andesite were reported by previous authors (Puffer and others, 1981a, 1981b; Philpotts and Martello, 1986; Puffer and Philpotts, 1988, Snelling, 2012) to have

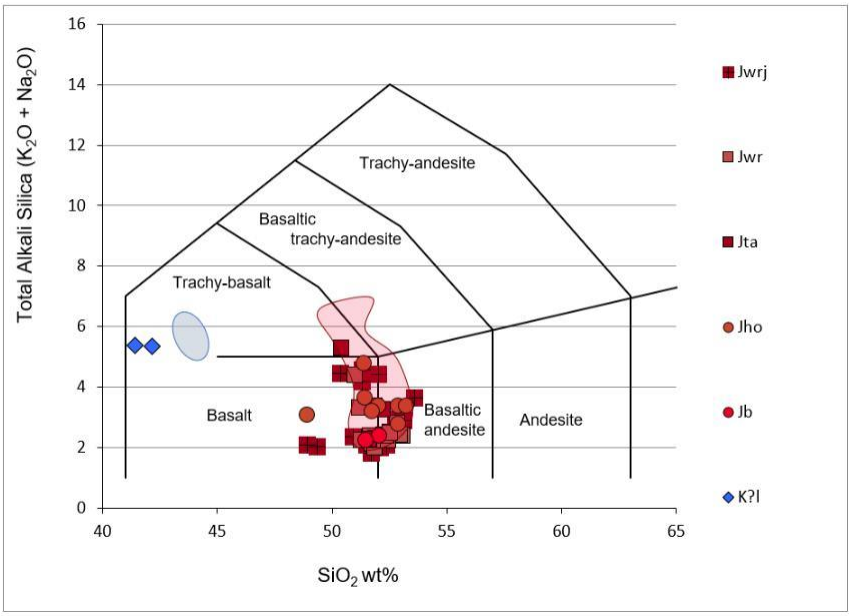

Figure 33. Total Na2O+K2O/SiO2 (wt. %) bivariate plot showing the classification of lamprophyre, basalt and diabase within the Wallingford quadrangle. (Classification of the International Union of Geological Sciences in 1972, LeBas and Streckeisen, 1991). The shaded areas on the diagram represent the range of reported values from the same formations by the previous authors (see text references above).

been altered. Because we removed the altered samples from this discussion, we report only one analysis within those fields.

The major and minor element trends of the Holyoke and Talcott suites are plotted on bivariate element diagrams (Figure 34A-D). We chose MgO (as previous authors have done) instead of SiO_2 as the abscissa on these diagrams because MgO is useful to track the fractionation of a basalt-type melt. The MgO concentrations of all samples fall between 5.1 and 9.28 wt. %. The Talcott Basalt has higher MgO concentration (6.83-8.28 wt. %) than the Holyoke Basalt (5.5-6.1 wt. %). The West Rock Diabase (intrusive equivalent of the Talcott Basalt) shows more scatter (6.0-9.3 wt. %)[9]; the Buttress Diabase (intrusive equivalent of the Holyoke), however, has MgO content that overlaps the West Rock diabase (the TiO_2 content of the Buttress Diabase is less, allowing the chemical distinction of the two). MgO vs major element bivariate plots consistently show that the values for Holyoke forms a single trend that is separate from Talcott Basalt and its intrusive equivalents (see

9. One outlier, a sample from Sleeping Giant laccolith (122-3), has a relatively low MgO concentration of 5.19 wt. % (a similar value from the Sleeping Giant laccolith was determined by Schnabel, 1968).

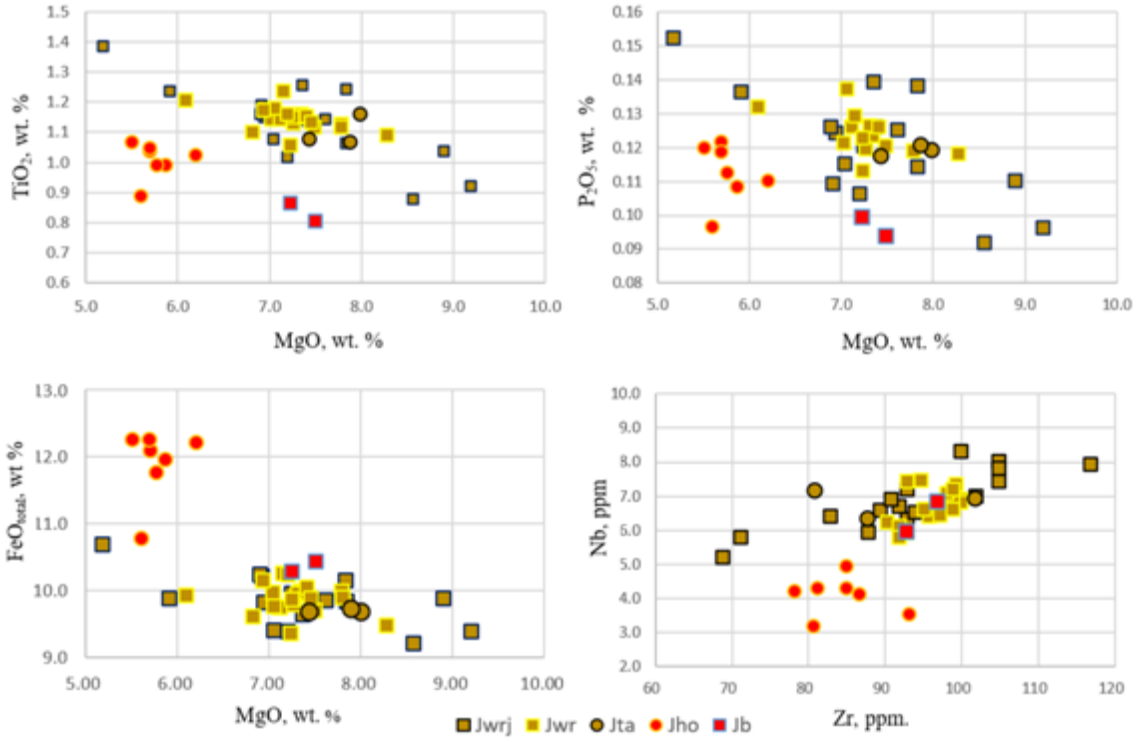

Figure 34. Bivariate plots of several cations vs. MgO (A-C) and Nb vs Zr (D). Most plots show chemical distinction between the two flows, but dikes associated with the two flows tend to show overlapping values. The dikes from the two flow events can be distinguished on the TiO2 vs MgO and on some trace element plots. Note that Jwr and Jwrj overlap and cannot be distinguished chemically. Note that symbol colors have been changed (compared to Figure 33) so that different sample populations could be more easily distinguished.

particularly Fig. 34A). The two trends do not overlap. The major and minor element trends of the Talcott and its related intrusive units are consistent with the variation produced by crystal fractionation of major phases from a primitive, MORB-like magma (Philpotts and Martello, 1986; Philpotts, 1997).

Our data show that the basaltic igneous rocks exposed in the Wallingford quadrangle may be chemically classified as basalt and basaltic andesite. The Talcott and Holyoke magmas can be distinguished chemically; they have separate chemical trends and thus it is unlikely that the younger one (Holyoke) is the derivative of the older one. At least two pulses occurred during emplacement of the Talcott Basalt and its related diabase. Although they may be distinguishable by field evidence, they are not chemically distinct: the West Rock Diabase has the same chemical composition during its entire history of emplacement. Although cooling was sufficient to produce a chilled margin on the younger Jwr intrusion, insufficient time occurred to affect differentiation of the magma. Some of the intrusive samples have slightly elevated K_2O

concentrations, suggesting they may be contaminated by assimilation of wall rocks (see Philpotts and Asher, 1993).

Early mapping of southern Hartford Basin did not have the guidance of chemistry to distinguish between the various dikes, and hence the dikes in the Branford and Wallingford quadrangles were mapped as Buttress equivalents (Rodgers, 1985). Our data (Appendix III and Steinen and others, 2017) corroborate the findings of Philpotts and Martello (1986) and show that the dikes of the Wallingford quadrangle, except for the Buttress Dike in the northwest corner, are all formed of West Rock Diabase. Recently Dyer and Fleming (2019) have further reinforced that correlation.

STRUCTURE

Deciphering the structure of this area is difficult because Pleistocene sediments (glacial till and diverse meltwater deposits; see Stone and others, 2005) cover large areas of the quadrangle, perhaps as much as 40%. In addition, the sedimentary layers that make up the New Haven Arkose and the Shuttle Meadow Formation are not well consolidated and crop out poorly. The Mesozoic sedimentary rocks are not well enough exposed to display their stratigraphy. Thus, distinctive sedimentary beds could not be used to interpret faults and folds. The basalt lava flows have been used instead. This condition is common throughout the Hartford Basin; historically, faults and folds have only been interpreted where basalt ridges are displaced or warped (Davis, 1898; Krynine, 1950).

FAULTS

Major faults can be interpreted in the Wallingford quadrangle from displacement of the Holyoke Basalt, which is well exposed in the southeastern part of the quadrangle and in the abutting Durham quadrangle to the east. Faults that are interpreted based on displacement of the Holyoke Basalt ridge in the Durham quadrangle (Simpson, 1969; Sanders, 1977) are easily identified on hillshaded-DEM models and can be extended reliably into the eastern part of the Wallingford quadrangle (Figure 35). Southwestward extension of those faults for more than 1-2 km, however, becomes problematic because of the lack of displaced marker horizons. It is likely that many faults remain unmapped in the quadrangle because of poor exposure and the lack of identified marker horizons. We extended the interpreted length of several faults southwestward based on cursory dip-domain analysis (Wise, 1992) although the boundary between dip domains may not be one continuous fault

What appear to be large displacements of the Holyoke ridges in the Durham quadrangle dissipate in the Wallingford quadrangle. The displacement may become widely distributed in the poorly consolidated New Haven Arkose. Thus, our extension of any particular fault into the basin is not the only possible hypothesis. The strain may have been accommodated by several dispersing faults.

Most of the mapped faults have down-to-the-northwest sense of movement and are presumed to be normal faults. Several faults in the northeastern corner of the Wallingford

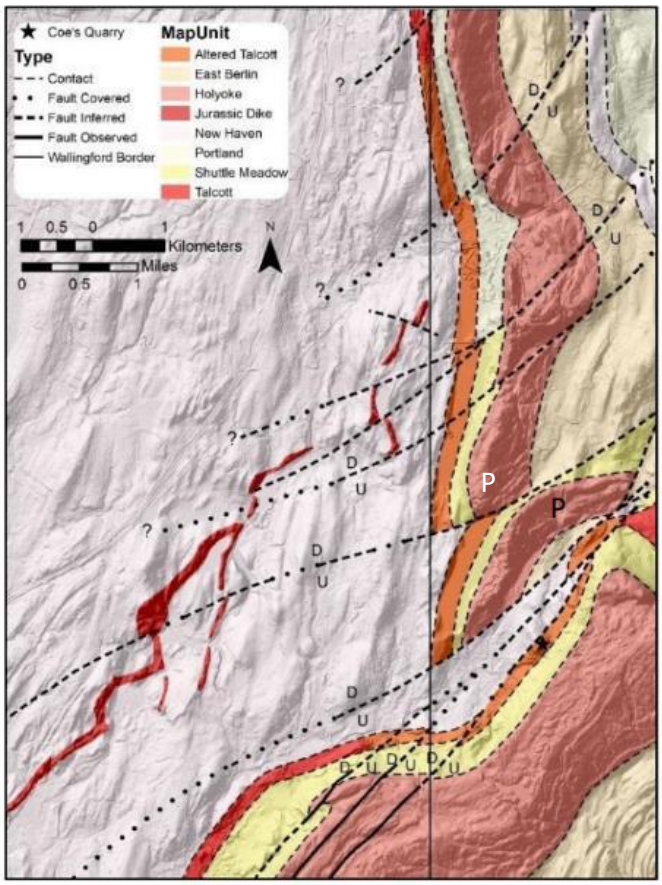

Figure 35. Hillshade-DEM model of parts of the Durham and Wallingford quadrangles with geology superposed (from Steinen and others, 2017, Figure 5). Faults in the Durham quadrangle (after Simpson, 1969) are readily identifiable from offsets of the basalt ridges and the resulting topographic anomalies. Note that this map also shows the interpreted extent of the previously discussed Talcott Basalt (see p.17) and the location of the Coe's Quarry hot spring deposit (dark blue star). The northern boundary of this map is just south of the northern boundary of the Wallingford and Durham quadrangles.

Feature labeled "P" is Paug Mountain (see discussion on p.51).

Quadrangle where mapping was aided by interpretation of water-well drilling reports (see Appendix I, Figure I-57) have down-to-the-southeast movement. Apparent sense of displacement along the faults in the northeastern corner can be traced to similar apparent displacements of the Holyole basalt ridge in the Durham quadrangle as observed on hillshaded DEM models (Figure 35 and Appendix I). Some (or all) faults also may have a strike-slip component of movement.

Fault planes are rarely seen. One is illustrated in Figure 12 where the dike at Patten Road (local area 104) apparently intruded along a fault plane (inferred from deformation of sandstone beds on opposite sides of the dike), but then was itself faulted. Although a fault plane is not exposed, a fault is interpreted in sandstone outcrops southwest of Northford Village (Figure 36; local area 103B). There the arkose has been deformed by normal drag on opposite sides of the fault. A fault-line escarpment is found along portions of this fault (Figure 36B). Several small prospect pits were dug along the fault just north of illustration of Figure 36B in the hopes of finding copper or barite mineralization as was found farther to the west (Fritts, 1962).

Figure 36. Fault (yellow dashed line) ~ 1.5 km west of Northford Village. A. Fault looking south. West dipping sandstone beds (red line) on the up-thrown side of the fault are interpreted as caused by normal drag against the down-thrown side of fault. Tree to right of fault approximately 15 cm in diameter. B. Fault looking north. Down-thrown side on west (left). Sandstone beds dip steeply west as a result of drag along the fault. Geologist in distance left (circle) is ~1.6 m in height.

Most of the faults are oriented ~030^{o} and 220-245^{o} (Figure 37). Less evident are northwest-southeast oriented faults (Figure 37B). The northwest-southeast faults appear offset by the northeast-southwest striking faults. Outcrops at many locations adjacent to suspected faults at ridge offsets have well-defined joint sets that appear to parallel to the faults that produced the ridge-offset. The dike of West Rock Diabase in the Clintonville area is segmented. The segments are offset in a number of places by steeply dipping faults that are identified by ridge offset and joint sets presumed parallel to the fault.

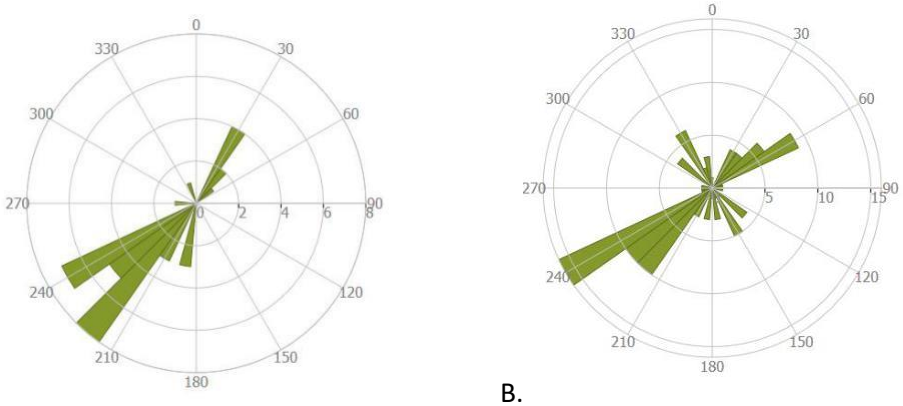

Figure 37. A. Rose diagram for azimuths of faults of known or inferred sense of movement, measured from Plate I and in the field (n=35). B. Rose diagram for all faults, including inferred faults with unknown sense of movement, measured from Plate I and in the field (n=69).

Fault trend distributions are partially controlled by which rocks are exposed and how the faults are manifest in those exposures. The rose diagram (Figure 37B) was constructed from faults measured both in the field and from the map (Plate I). This rose diagram is dominated by small displacement faults in the northeastern part of the map where faults interpreted from water-well data were matched to corresponding displacements observed on DEMs in the Holyoke Basalt ridge in the Durham quadrangle.

Many fracture surfaces in the basalt/diabase outcrops contain faint slickenlines, which have varying orientations and multiple directions of indicated slippage. These fractures and their slickenlines show no preferred orientations (contrast this with Crespi and others 2015, p. 91 and p. 103). We do not interpret major fault movement from these features, but rather consider the slickenlines to be minor adjustments of the basalt or diabase sheet to the changing conditions it experienced.

The Quinnipiac River Valley is deep (up to 65 m depth to bedrock surface: Mazaferro, 1973) and remarkably straight. Topography rises abruptly along its western border. We interpret these observations to suggest structural control of the topography and propose that a major fault along the western side of the valley is responsible. This feature is shown on Plate I as a covered fault that is queried. To the west of the queried fault, topography rises abruptly 20-40 m to a rather animated topography; east of the fault the topography is relatively subdued. West of the Quinnipiac River Valley the sedimentary units have a relatively uniform attitude whereas sedimentary attitudes east of the valley can be subdivided into several dip-domains separated by inferred faults. Additional support for this concept is provided by Chang (1968) who proposed a buried fault near the middle of the basin, from New Haven to near Meriden, to explain his gravity data. Eaton and Rosenfeld (1960) similarly, while interpreting gravity data, proposed that the deepest part of the Hartford basin is near Middletown, suggesting one or more "step-down" basin-ward faults. Wenk (1984) and Ellefsen and others, (1990) came to the same conclusion using seismic and gravity data respectively.

JOINTS

Most joints were mapped within the basalt and diabase units in the Wallingford quadrangle because they are better exposed, but also because joints are more widely spaced in the sedimentary units compared with the igneous units. Although more than 800 joint orientations were measured (employing right-hand rule; see Appendix V), fewer than 75 were measured in the sedimentary units. Cooling joints (columnar joints) were not included in the dataset.

Although there is much scatter to the data (Figure 38), dominant joint trends were observed: joints that strike 345-360^{o} dip northeast to east (using right-hand convention); joints striking 315-330^{o} dip northeast; joints striking 240-255^{o} dip northwest; and those striking 75-90^{o} dip southeast to south. These joint trends compared well with regional Hartford Basin stress data collected from fault slip analysis and joint measurements (Weitz 1972; Piepul, 1975;

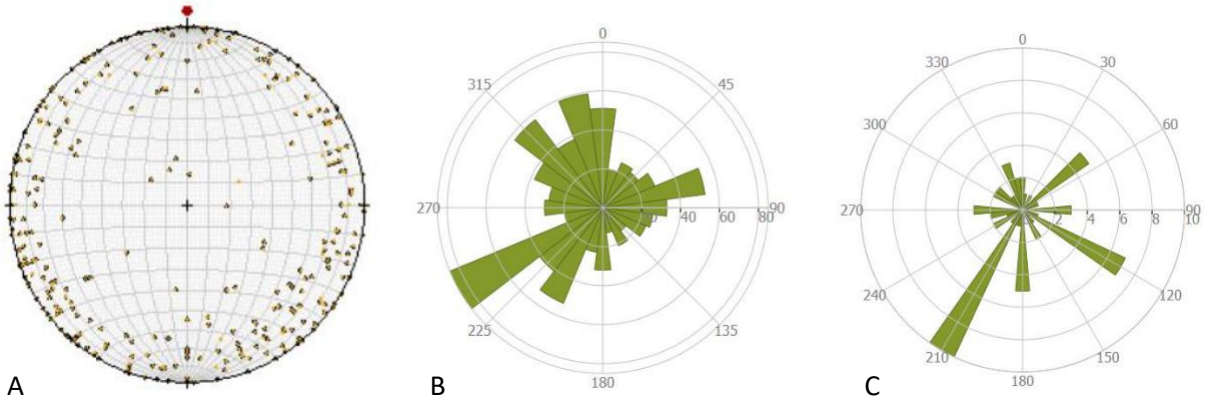

Figure 38. Stereonet (A) and corresponding rose-diagram (B) for all joints within the Wallingford quadrangle; n=837. C. Rose diagram for joints in sedimentary units only; n=69. Petals are binned in 15° azimuth intervals for B. but are binned in 10º intervals in C. Petal length corresponds to number of measurements. Note B. and C. have different scales for petal length.

Drzewiecki and others, 2012; Farrell, 2015). The 245^{o} joint trend corresponds well with a NE-SW joint trend observed in the Hartford South quadrangle (Drzewiecki and others, 2012). Note that the joints in sedimentary rocks are but a small subset of the total population and have slightly different trends than the total population.

The 240^{o} joints along with the 340^{o} joints correlate with basin inversion phases 2a and 2b of Crespi and others (2015), where the dominant extension direction is NW-SE and E-W. Phase 2a and 2b are considered to evolve contemporaneously during the drainage of the CAMP magmatic reservoirs related to synrift NE-SW compression (Crespi and others, 2015; Farrell, 2015). The 360^{o} joint trend reflects the contemporary stress state, phase 4, of the Hartford Rift Basin, where compression is oriented E-W (Crespi and others, 2015; Farrell, 2015). This stress state developed as a response to seafloor spreading of the Atlantic Mid-Ocean Ridge (Zoback, 1992; Hurd and Zoback, 2012; Farrell, 2015).

In the Wallingford quadrangle, joints in sedimentary rocks typically are more widely spaced than in the igneous rocks, a feature noted by Lehmann (1959) in the Middletown quadrangle. This, along with fewer exposures of the sedimentary rocks, resulted in an order-of-magnitude fewer joint measurements in sedimentary rocks. In addition to there being fewer measurements in the sedimentary rock units, those that were measured have different orientations than those measured in igneous rocks (Figure 38C). Sediments in the Wallingford quadrangle are neither well cemented nor indurated. Stress that formed joints in the brittle igneous rocks may have been accommodated by irregular fractures or intergranular adjustments in the sedimentary rocks.

Comparison with fault orientations. Most larger displacement regional faults share a northeast-southwest orientation and likely have an important strike-slip component to their displacement. This corresponds to the strong 240^{o} trend in the joint data although joints are

extensional features. We interpret that joints, once formed in an entensional stress field, were used later to accommodate the stress that changed to a compressional regime.

Comparison with other regions. We find limited correspondence of the joint and fault orientation. Piepul (1975), and Mikami and Digman (1957) found that that joints and faults appear unrelated in southern Connecticut. Farther north however, Drzewiecki and others (2012) found greater correspondence between fault and joint orientations in the Hartford South quadrangle.

Most previous joint analyses have attempted to distinguish joint patterns in pre-Mesozoic rocks from Mesozoic basin rocks and to relate measured joints and faults in the area. Piepul (1975), for instance, measured more than 2500 joints around the southern end of the Eastern Border Fault, including some of the Wallingford quadrangle. He found variation between different areas in the pre-Mesozoic terrane with 030^{o} and 349^{o} being dominant directions.

Joints in rocks of the Mesozoic basin clustered in the $020\text{-}040^{o}$ range and 350^{o}, similar to those in pre-Mesozoic rocks. Faults and joints appeared unrelated in the both the pre-Mesozoic area and the Mesozoic Basin.

Mikami and Digman (1957) measured more than 1000 joints in the Guilford 15 min. quadrangle in both Mesozoic strata and pre-Mesozoic rocks. They found a wide range of strike directions in both sectors and could not distinguish between the two sectors. They also found that joint directions were unrelated to observed fault orientations in either sector.

In the Middletown quadrangle, Lehmann (1959) found jointing better developed in the finer-grained rocks than in coarser-grained rocks. He noted persistence of joints striking $035\text{-}215^{o}$ but, although noting a general parallelism of the joints and faults in the quadrangle, declined to attribute the joint orientation to a producing stress.

Burton (in Burton and others, 2005) measured more than 2000 joints in the Mesozoic Pomperaug Basin and surrounding pre-Mesozoic rocks in western Connecticut. He found joint trends in in the pre-Mesozoic rocks were essentially the same as those on the Mesozoic Basin and concluded that the joints in both were created during a Mesozoic extensional regime.

In 1971, Weitz (in Drzewiecki and others, 2012, Fig. 30) measured more than 450 joints in the Hartford South quadrangle and found a strong NE-SW trend (both 030^{o}+/- and 210^{o}+/-), a moderate $290\text{-}310^{o}$ trend, and a 070^{o} trend. These trends mimicked the fault trends mapped by Drzewiecki and others, 2012.

FOLDS

In the southern part of the Hartford Basin, Mesozoic strata have been warped into two broad synclines whose axes lie roughly perpendicular to the Eastern Border fault. These are named the Totoket and Saltonstall synclines (Davis, 1898). The northwestern portion of the Totoket syncline lies in the southeastern corner of the Wallingford quadrangle. The synclinal folding does not appear to have affected the northeast-southwest faults that cut the Holyoke basalt. We infer that the folding pre-dated most faulting within the basin.

Both synclines have secondary anticlinal and synclinal warps whose axes may or may not be perpendicular to the border fault. A secondary syncline, interpreted from a hillshade-DEM model, warps the Totoket syncline in the Wallingford quadrangle (Figure 8). Its axis is at an oblique angle to the border fault.

The broad width of the Holyoke Basalt outcrop belt on Totoket Mountain suggests that either numerous small displacement faults or slight warping of the basalt must exist. Indeed we have mapped (see Plate I) several small displacement faults that we interpret have down to the west displacement. We do not think the total offsets are sufficient to account for the exaggerated width of the basalt outcrop. In addition we have observed locations where the basalt that has near horizontal to slightly west-dipping exfoliation joints (Figure 9D) that normally are oriented close to the regional orientation of the sedimentary rocks (Figures 4A and 9C). This observation suggests to us that the basalt sheet is also warped parallel to the major faults that cut the basalt. Sanders (1972b, p.86) also described a flattening of the axis of the Totoket syncline that he associated with the northeast-southwest faults.

DISCUSSION

Our observations in the Wallingford quadrangle have been unable to confirm either Sanders' (1970; 1972a) description of the Talcott "Formation" (see Figure 2) or his mapped extent of Talcott rocks (see Appendix Figure VII-8). Rather, we have determined that much of the outcrop area of the Talcott Basalt shown on Sanders' maps (dated 1968-1972) and on the State Map (Rodgers, 1985) is composed of coarse-grained pebbly arkosic sandstone that lacks any megascopic volcanic material and should more properly be considered New Haven Arkose. We have mapped a volcaniclastic sheet as Talcott Basalt extending through the village at Northford (local area 125). The sheet then bends around to the east (local area 126), following the structure indicated by the Holyoke Basalt outcrop belt on Totoket Mountain, into the Durham quadrangle. Alteration of the volcaniclastic sheet becomes pronounced ~1 km west of the Wallingford/ Durham quadrangle boundary and it crops out in only two places (Figure 6D-F). The altered material is described in completion-reports for water-wells as "redrock". Using our field observations supplemented by drilling reports we can map the altered material into the Durham quadrangle (Steinen and others, 2017). Sanders inferred a down-to-the-southeast fault that cross-cuts the Talcott Basalt and brought New Haven Arkose into contact with Shuttle Meadow Formation. The fault heads directly toward the gap between Pistapaug and Totoket mountains where a down-to-the-northwest fault exists (Simpson, 1969). Our data supports Simpson's interpretation.

Sanders and others, (1963) interpreted a graben structure in the Branford quadrangle they named the Gaillard Graben. The east side of the graben is bounded by the Mesozoic Eastern Border Fault, a down-to-the-west normal fault. The west side of the graben is bounded by an interpreted down-to-the-east normal fault that they named the Foxon Fault. The Foxon Fault is antithetic to the Eastern Border Fault. The Foxon Fault is shown to extend into the Wallingford

quadrangle (Sanders and others, 1963; Sanders, 1972a; 1977) and northward where, after some abrupt bends, it cuts out the Talcott Basalt west of Pistapaug Mountain ("P" on Figure 35). We have not been able to confirm the structure as Sanders presents it. Instead, we interpret down-to-the-west and northwest faults in the area that are typical in the Hartford Basin elsewhere. Rather than being missing due to faulting, the Talcott Basalt has been altered in this area (Steinen and others, 2017) by hydrothermal fluids that also deposited travertine at Coe's Quarry (Steinen and others, 1984).

Sanders (1972b, p. 67) inferred that the Holyoke Basalt in the Branford quadrangle consists of two flows, based on textures. Vesicularity, brecciation, and weathering profiles are commonly used to identify the top of a lava flow (numerous publications by W.M. Davis). Gray (1982) used those criteria to suggest two flow events in the Holyoke in the New Britain area. (Hubert et al used similar criteria to interpret two flow events in the Talcott Basalt in Meriden.) A vesicular top and a weathering profile were found at the top of the Holyoke in the southeastern corner of the quadrangle. None were observed, however, below the top of the Holyoke in the Wallingford quadrangle. Hence, we cannot confirm Sanders' (1972b) interpretation. In addition, Longwell (1937), who searched for "evidence for a composite flow" in the New Haven Water Company tunnel at the north end of Lake Saltonstall (in the Branford quadrangle), found only one flow. Sanders (1972b) conceded, however, that the outcrop of the Holyoke at "the Connecticut Turnpike" (currently Interstate-95) in the Branford quadrangle has evidence for only one flow.

Our map confirms the structural interpretations of numerous geologists since Davis (1898), with the exception of Sanders (1972a; 1977). It will necessitate some changes to the state map (Rodgers, 1985). Our work, and also the recent work of Dyer and Fleming (2019), confirms the work of Philpotts and Martello (1986), requiring that the intrusive dikes and sills be reclassified on the state map, from Buttress Diabase (Jb) to West Rock Diabase (Jwr) based on the similarity of their geochemistry to the Talcott Basalt. In addition, the areal extent of the Talcott Basalt needs modification on the state map. The previous work of Sanders (1972b; 1977) in the Branford quadrangle likewise may need reinterpretation.

The interpretation at area 103 of pillow basalt and volcaniclastic breccia filling a channel greater than 30 m in depth (Figure 5A, F) has interesting implications. Such a channel eroded into the New Haven Arkose should not occur on distal portions of an alluvial fan or on a flood plain by normal channel migration and erosion or fan progradation. Rather gully-producing erosion likely occurred as a result of an abrupt change in base level. We argue that the base level change near the eastern margin of the Mesozoic Hartford Basin most likely occurred because of fault activity connected to either ongoing rift-tectonism or to incipient or pending volcanic activity. A fault-produced scarp could, in a short period of time, be excavated to a deep, steep-sided, wine-glass shaped gully into which the lava would flow. Lava entering the channel from the west likely would dam the river, even if intermittent, creating a local reservoir of water in which the lava could form pillows (Figure 39). The exact location of the fault responsible for

creating such an escarpment is not known at this time but likely is west of the outcrop but east of the possible Fairhaven feeder dikes. We have placed a queried fault in this location on Plate I.

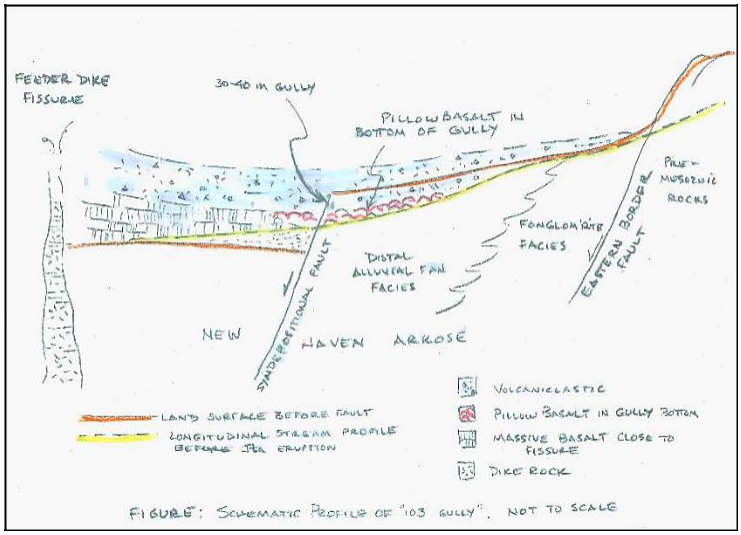

Figure 39. Sketch (not to scale) of longitudinal profile of intermittent stream issuing from the eastern highlands and flowing across the syndepositional fault scarp hypothesized for 16-103. Incision of the fault scarp could produce a 30-40 m deep gully into which lava would flow during an eruption.

Our interpretation suggests the channel into which the basalt flowed was produced by syndepositional faulting. It is generally accepted based on inferential evidence that rift tectonism occurred throughout the sedimentation history of the Hartford Basin. Dip angles generally increase toward the border fault and seem greater in older sediments. Formation thicknesses in general increase toward the east side of the basin (reported by many, but best documented by LeTourneau and McDonald, 1985, Fig. 7). In addition, relief must have been continuously renewed to provide a source for coarse detritus throughout the history of the basin. Our interpretation adds additional inferential evidence for syn-depositional tectonism in the Hartford Basin.

The roughly east-west Cross-Rocks Dike is composed of West Rock Diabase and apparently originates near the northern end of the West Rock Sill (see Figure 1). The sill was intruded near the base of the New Haven Arkose at or near the time of eruption of the Talcott Basalt, and the Cross Rocks Dike was intruded at or near the same time. Western exposures of the Cross Rocks Dike intrude the older layers of the New Haven Arkose and therefore, at the time of intrusion, were deeper than eastern exposures of the dike. Columnar joints in the dike plunge about 45^{o} generally toward the north (Figure 13A). The roughly east-west dike therefore dips about 45^{o} to the south. Farther east, the dike, at some shallower depth, flattened into a narrow sill-like body and broke up into narrower digits (see detailed map for local area 131 in Appendix II). Columnar joints at the eastern end of the dike are vertical or steeply dipping (Figure 13 B, D) suggesting tabular digitate sheets.

Near the New Haven/Hamden town boundary, other dikes (Mill Rock Dike, East Rock Dike) also flatten into sill like bodies (*i.e.*, Peters Rock in North Haven) suggesting this is a general phenomenon, possibly a function of closeness to the surface at the time of intrusion. We suggest that the flattening of dikes of West Rock Diabase occurs near the hypothesized

Quinnipiac Valley Fault because the displacement on the fault downdropped the New Haven/Talcott contact and that the sill-like bodies were close to the surface.

On the east side of the Wallingford and Branford quadrangles, sills and sill-like bodies of West Rock diabase are found close to the Talcott outcrop belt and, therefore, were close to the surface at the time of their intrusion. This suggests that the intrusive pulse lacked sufficient buoyancy to reach the surface at those locations.

We suggest that the sills near the Quinnipiac Valley Fault were also close to the surface because of a similar lack of buoyance of the intruding magma and that the sills (and overlying stratigraphy) were down-dropped by the Quinnipiac Valley Fault (Figure 40). If there are no faults on the east side of the Quinnipiac Valley (none are exposed), the Quinnipiac Valley Fault may have had as much as 1.5-1.8 km of displacement (approximately equal to the thickness of the New Haven arkose). If more faults exist than are exposed (which is not unlikely), cumulative displacement on all the faults will approximate 1.8 km and inferred the displacement on the Quinnipiac Valley fault will be less. Displacement of that magnitude was predicted by Ellefsen and others (1990) and inferred by Wenk (1984).

Abundant dikes and sills of Talcott age are present only in the southern portion of the Hartford Basin, more or less coincident with the extent of the West Rock Sill. Perhaps deflation of the West Rock Sill caused the collapse and fracturing of the sediments and sedimentary rocks above it similar to caldera collapse. Many of the smaller dikes (Figure 14) and sills did not have the buoyancy to reach the surface. This might be explained if most of the dissolved gases in the sill magma exsolved during the Talcott eruptions prior to collapse.

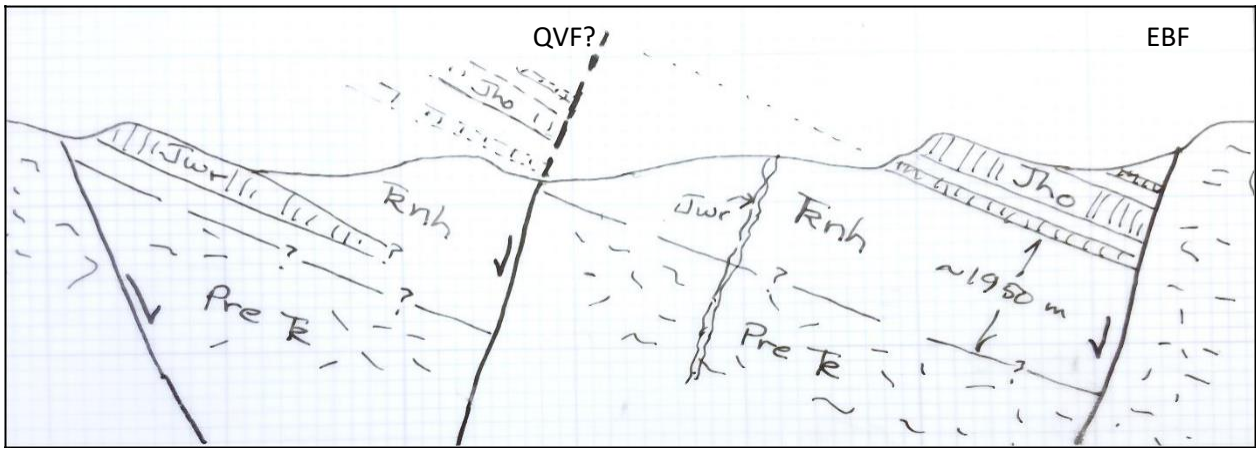

Figure 40. Cross section sketch (not to scale) from Eastern Border fault (EBF) on east to West Rock Sill on west, showing maximum possible displacementt on hypothesized Quinnipiac Valley Fault that repeat some thickness of the New Haven Arkose. The arkose is thought to be about 1950 m thick (Krynine, 1950; Hubert and others, 1978).

REFERENCES CITED

Armstrong, R.L., and Besancon, J., 1970, A Triassic time scale dilemma: K-Ar dating of Upper Triassic mafic igneous rocks, eastern U.S.A. and Canada and post-upper Triassic plutons, western Idaho, U.S.A.: Eclogae Geol. Helvetiae, 63:15-28.

Armstrong, R.L., and Stump. E., 1971, Additional K-Ar dates, White Mountain Magma Series, New England. Amer. Journ. Sci. 270:331-333.

Blackburn, T.J., Olsen, P.E., Bowring, S.A., McLean, N.M., Kent, D.V., Puffer, J., McHone, J.G., Rasbury, E.T., and Et-Touhami, M., 2013, Zircon U-Pb geochronology links the end-Triassic extinction with central Atlantic magmatic province. Science 340:941-945.

Blevins-Walker, J., 2008, An eastern Provenance for the New Haven and Portland Formations of the Hartford and Pomperaug Basins. Indiana University, unpub. M.S. thesis, 163 pp.

Blevins-Walker, J., Kunk, M.J., and Wintsch, R.P., 2001, An eastern provenance for the New Haven Arkose and the Portland Formation of the Hartford and Pomperaug basins: Broad terrane revisited. Geol. Soc. Am., Abstracts with program, NE Section, v.33, #1, p.81.

Burton, W.C., Huber, P., McHone, J.G., and LeTourneau, P.M., 2005, A new look at the structure and stratigraphy of the early Mesozoic Ponperaug Basin, southwestern Connecticut. 97th New England Intercollegiate Geology Conference, State Geological and Natural History Survey of Connecticut Guidebook #8, p. 251-294.

Chang, C. C., 1968, A gravity study of the Triassic valley in southern Connecticut. unpub. M. A. thesis, Wesleyan Univ., Middletown, CT., 108p.

Charney, A.B., and Philpotts, A.R., 2004, Upward and downward flow in a camptonite dike. Geological Society of America, *Abstracts with Programs*, Vol.36(2), pp.136

Charney, Allison B, Steinen, Randolph P., and Thomas, Margaret A., 2018, Mesozoic dike nomenclature in Connecticut. Geological Society of America *Abstracts with Programs*. V. 50, No. 2. doi: 10.1130/abs/2018NE-311153

Coron, C.R., 2009, Volcanic debris flows in a Talcott-Shuttle Meadow transition lake sequence, Connecticut. Geol. Soc. Amer. Abstracts with Prog. 41:

Crespi, J.M., Farrell, J.A., Evans, M.A., Smith, M.R., and Pirovane, N.D., 2015, Faulting in the Hartford Basin and its relation to magmatic activity, intrabasinal fluid flow, and mineralization. Guidebook for Field Trips, 107th Ann. Mtg., New Eng. Intercoll. Geol. Conf., p87-106.

Dana, J.D., 1891, *On the Four Rocks of the New Haven Region: Wast Rock, West Rock, Pine Rock and Mill Rock.* Tuttle, Morehouse and Taylor, New Haven Connecticut, 120p.

Davis, W.M., 1896, The quarries in the lava beds at Meriden, Connecticut. American Journal of Science, Ser. 4, 1:1-13.

Davis, W.M., 1898, The Triassic formation of Connecticut. U.S. Geol. Surv. Ann. Rpt. 18, pt. 2, pp. 1-192.

de Boer, Jelle, 1968, Late Triassic volcanism in the Connecticut Valley and related structure. Guidebook for Field Trips, 60th Ann. Mtg., New Eng. Intercoll. Geol. Conf., C5, p.1-12.

Drzewiecki, P.A., Schroeder, T., Steinen, R.P., and Thomas, M.A., 2012, *The Bedrock Geology of the Hartford South Quadrangle, Connecticut, with Map and Cross-sections.* State Geological and Natural History Survey Quad. Report #40, 39p.

Dyer, M.P., and T.H. Fleming, 2019, Chemical composition of intrusive rocks from the Fair Haven Heights and Foxon regions, Hartford Basin, Connecticut. Geological Society of America Abstracts with Programs. Vol. 51, No. 1, ISSN 0016-7592. doi: 10.1130/abs/2019NE-328601

Eaton, G.P., and Rosenfeld, J.L., 1960, Gravimetric and structural investigations in central Connecticut. 21st Internat. Geol. Congress, Copenhagen, Report pt. 2:168-178.

Ellefsen, K.J., Simmons, G., Dowling, J.J., Dehlinger, P., and Gray, N.H., 1990, Gravity modeling of a normal fault in the Hartford Basin. Northeastern Geology 12:231-237.

Emerson, B.K., 1898, Description of the Holyoke Quadrangle, Massachusetts. U.S. Geol. Surv., Geological Atlas, Folio 50.

Eppler, D.R., 1999, The relationship between mineralogic and textural features of a camptonite dike with fO_2 and fH_2O. University of Connecticut, Storrs, Unpub. MSc thesis, 52p.

Farrell, J.A., 2015, Paleostress States and tectonic evolution of the Early Mesozoic Hartford Basin: Unpub. M.Sci. Thesis, University of Connecticut. 82p.

Fellows, B.E., and Oiumet, William, 2019, What the hearth is going on? Mapping relict charcoal hearths in southern New England to better understand regional patterns of historical deforestation and charcoal production. Univ. Connecticut Center for Integrative Geosciences, Geoscience Day Research Presentations, May 2019.

Fritts, C.E., 1962, The barite mines of Cheshire. Cheshire Historical Society, 36p.

Fritts, C.E., 1963, Bedrock Geology of the Mount Carmel Quadrangle, Connecticut. U.S. Geol. Surv. Map GQ-199.

Giblin, J., Wizevich, M.C., and Luna, M., 2017, Provenance analysis of sedimentary strata in the Mesozoic rift basins in Connecticut using detrital zircon geochronology. Geol. Soc. Amer. *Abstracts with Prog.* V. 49, #2. doi:10.1130/abst/2017NE-291480.

Gray, N.H., 1982, Mesozoic volcanism in north central Connecticut. State Geol. Nat. Hist. Surv. of Connecticut, Guidebook #5, p.173-194.

Hanshaw, P.M., 1968, Bedrock geologic map of the Meriden quadrangle, New Haven, Hartford, and Middlesex counties, Connecticut. U.S. Geol. Surv. Map, GQ-738. 4p.

Hubert, J.F., Reed, A.A., Dowdall, W.L., and Gilchrist, J.M., 1978, *Guide to the Mesozoic Redbeds of Central Connecticut*. State Geological and Natural History Survey of Connecticut, Guidebook #4, 129p.

Hurd, O., and Zoback, M. D., 2012, Intraplate earthquakes, regional stress and fault mechanics in the Central and Eastern US and Southeastern Canada: Tectonophysics 581:182-192.

Krynine, P. D., 1936, Triassic sedimentary rocks of southern Connecticut: Ph.D. Dissert. Yale Univ., New Haven, CT, 260p.

Krynine, P.D., 1941, Triassic sediments of Connecticut (abstract). Geol. Soc. Am. Bull. 52:1919.

Krynine, P.D., 1950, *Petrology, Stratigraphy, and Origin of the Triassic Sedimentary Rocks of Connecticut.* State Geological and Natural History Survey of Connecticut, Bull. 73, 247p.

LeBas, M.J., and Streckeisen, A.C., 1991, The IUGS systematics of igneous rocks. Journ. Geol. Soc. London 148:825-833.

Lee-Gorishti, Y, Coron, C.R., Cooper, J, and Fleming, T., 2003, Characterization of flows and dikes in Northford, CT. Geol. Soc. Amer. Abstracts with Prog. 35(3).

Lehmann, E.P., 1959, The Bedrock Geology of the Middletown Quadrangle. State Geological and Natural History Survey of Connecticut, Quadrangle Reptort #8, 40p.

LeTourneau, P.M., 2003. Tectonic and climatic controls on the stratigraphic architecture of the Late Triassic Taylorsville Basin, Virginia and Maryland, USA. In: P.M. LeTourneau and P.E. Olsen, (eds.), The Great Rift Valleys of Pangea in Eastern North America, Volume II, p. 12-58. New York, Columbia University Press

LeTourneau, P.M., and McDonald, N.G., 1985, The sedimentology, stratigraphy, and paleontology of the Lower Jurassic Portland formation, Hartford Basin, central Connecticut. State Geology and Natural History Survey of Connecticut, Guidebook 6:353-391.

LeTourneau, P.M., McDonald, N.G., Olsen, P.E., Ku, T.C., and Getty, P.R., 2015, Fossils and facies of the Connecticut Valley Lowland: Ecosystem structure, and sedimentary dynamics along the footwall of an active rift. Guidebook for field trips 107th Ann. Mtg., New Eng. Intercoll. Geol. Conf., p107-151.

Longwell, C.R., 1937, Sedimentation in relation to faulting. Geological Society of America Bull. 48:433-442.

Mazaferro, D.L, 1973, Hydrologic data for the Quinnipiac River basin, Connecticut. Connecticut Water Resource Bulletin 26, 54p.

McDonald, N.G., 1996, The Connecticut Valley in the Age of Dinosaurs: A Guide to the Geologic Literature, 1681-1995. State Geological and Natural History Survey of Connecticut, Bulletin 116, 241p.

McHone, J.G., 2000, Non-plume magmatism and rifting during the opening of the central Atlantic Ocean: Tectonophysics 316:287-296.

Mikami, H.M., and Digman, R.E., 1957, The bedrock geology of the Guilford 15-minute quadrangle and a portion of the New Haven quadrangle. State Geological and Natural History Survey of Connecticut, Bull. 86, 99p.

Olsen, P.E. and Fedosh, M.S., 1988, Duration of the early Mesozoic extrusive igneous episode in eastern North America determined by use of Milankovitch-type lake cycles: Geol. Soc. Am. Abstracts with Prog. 20:59.

Olsen, P.E., Kent, D.V., Et-Touhami, M., and Puffer, J.H., 2003, Cyclo-, magneto-, and bio-stratigraphic constraints on the duration of the CAMP event and its relationship to the Triassic-Jurassic boundary. *In:* W.E. Hames and others, The Central Atlantic Magmatic Province: Insights from Fragments of Pangaea. AGU Geophysical Monograph 136:7-32.

Olsen, P.E., Whiteside, J.H., LeTourneau, P.M, and Huber, P., 2005, Jurassic cyclostratiography and paleontology of the Hartford Basin, Guidebook for Field Trips, 97th Ann. Mtg., New Eng. Intercoll. Geol. Conf., p55-105.

Percival, J.G., 1842, Report on the geology of the State of Connecticut; New Haven, published by the State, 495p.

Philpotts, A.R., 2010, The Holyoke Basalt at the Tilcon Quarry, North Branford: the geology, petrology, and history of one of the worlds largest flood-basalt eruptions. *in* Geological Society of Connecticut Field Trip Guidebook 1, p. 8-16.

Philpotts, A.R., and Asher, P.M., 1992, The first Mesozoic magma of the Hartford Basin: Examination of the feeder dike, a laccolith, and the Talcott lava flow. New England Intercollegiate Geology Conference Guidebook 84th annual meeting, vol. 1, p. 67-85.

Philpotts, A.R., and Asher, P.M., 1993, Wallrock melting and reaction effects along the Higganum diabase dike in Connecticut: contamination of a continental flood basalt feeder. Journ. Petrology 34:1029-1058.

Philpotts, A.R., and Lewis, C.L., 1987, Pipe vesicles - and alternate model for their origin. Geology 15:971-974.

Philpotts, A.R., and Martello, A., 1986, Diabase feeder dikes for the Mesozoic basalts in southern New England. Am. Journ., Science 286:105-126.

Piepul, R.C., 1975, Analysis of jointing and faulting at the southern end of the Eastern Border Fault, Connecticut. University of Massachusetts, unpub. M.Sc. Theses, Department of Geology Cont. 23, 109p.

Porter, S.C., 1960, *The Surficial Geology of the Wallingford Quadrangle with Map*. State Geol. Nat. Hist. Surv. of Connecticut, Quadrangle Rept. 10, 42p.

Priest, J., Coron, C.R., and Fleming, T.H., 2001, Origin of basalt breccias in the Fairhaven dike system, Wallingford, CT. Geol. Soc. Amer. Abstracts with Prog. 33:

Priest, J., Coron, C.R., and Fleming, T.H., 2003, Distribution of peperites in the Wallingford-Northford, CT, area. Geol. Soc. Amer. Abstracts with Prog. 35(3):

Puffer, J.H., Hurtubise, D.O., Geiger, F.J., and Lechler, P., 1981a, Chemical composition and stratigraphic correlation of the Mesozoic basalt units of the Newark Basin, New Jersey, and the Hartford Basin, Connecticut, Part 1. Geol. Soc. Amer. Bull. 92:155-159.

Puffer, J.H., Hurtubise, D.O., Geiger, F.J., and Lechler, P., 1981b, Chemical composition and stratigraphic correlation of the Mesozoic basalt units of the Newark Basin, New Jersey, and the Hartford Basin, Connecticut, Part 2. Geol. Soc. Amer. Bull. 92:515-553.

Puffer, J.H., and Philpotts, A.R., 1988, Eastern North American quartz tholeiites: geochemistry and petrology. in Manspeizer, W. (ed.). *Triassic-Jurassic Rifting: Continental Breakup and the Origin of the Atlantic Ocean and Passive Margins*: Amsterdam, Netherlands, Elsevier Sci. Pub. Part B, p. 579-605.

Roden-Tice, M.K., and Wintsch, R.P., 2002, Early Cretaceous normal faulting in southern New England; evidence from apatite and zircon fission-track ages. Journ. Geology 110:159-178.

Rodgers, John, 1985, *Bedrock Geological Map of Connecticut*. State Geological and Natural History Survey of Connecticut, Nat'l. Resource Atlas Series, 1:125,000, 2 sheets.

Russell, W.L., 1923, The camptonite dikes in the Connecticut Triassic. Am. Journ. Sci. Ser. 5, 5:409-416.

Ryan, S.S., 1986, Description and paragenetic interpretation of quartz-carbonate-barite veins of the Hartford Basin. Univ. Connecticut unpub. MSc thesis.

Sanders, J.E., 1962, Stratigraphy of the Talcott Formation (Upper Triassic), southern Connecticut [abstr.]; Geol. Soc. Am. Spec. Pap. 68:260.

Sanders, J.E., Guidotti, C.V., and Wilde, P., 1963, Foxon Fault and Gaillard Graben in the Triassic of Southern Connecticut. State Geol. Nat. Hist. Surv. of Connecticut, Rpt of Invest. No.2, 16p.

Sanders, J.E., 1968, Stratigraphy and primary sedimentary structures of fine-grained, well bedded strata, inferred lake deposits, Upper Triassic, central and southern Connecticut. Geol. Soc. Am. Spec. Pap. 106:265-305.

Sanders, J.E., 1970, Stratigraphy and Structure of the Triassic Strata of the Gaillard Graben, South-Central Connecticut. State Geol. Nat. Hist. Surv. of Connecticut, Guidebook #3, 15p.

Sanders, J.E., 1972a, Preliminary geologic map of the Wallingford Quadrangle. CT. Unpublished Maps and reports on file in Connecticut Geological and Natural History Survey library archives.

Sanders, J.E., 1972b, Branford Bedrock. Unpublished Maps and reports on file in Connecticut Geological and Natural History Survey library archives, 131p.

Sanders, J.E., 1977, Preliminary geologic map of the Branford Quadrangle. CT Unpublished Maps and reports on file in Connecticut Geological and Natural History Survey library archives.

Schnabel, R.W., 1968, Chemical analyses of selected samples of diabase and basalt from Connecticut. U.S. Geological Survey Open-file Rept. OF68-237, 4p.

Simpson, H.E., 1969, Preliminary bedrock geologic map of part of Durham quadrangle, Connecticut. U.S. Geol. Surv. Open File Rpt. 69-257, 3p.

Snelling, R.A., 2012, Chemical variation within the Talcott flood basalt, Connecticut. unpub. Honors thesis, Wesleyan University, Middletown, CT, 134p.

Steinen, R.P., Gray, N.H., and Mooney, J. (1987), A Mesozoic carbonate hot-spring deposit in the Hartford Basin of Connecticut. J. Sediment. Petrol. 57:319-326.

Steinen, R.P., Bogarts, James, Charney, A.B., VanderLeest, R.,and Glairon, S., 2017, A hypothesis for the disappearance of the Talcott Basalt in the vicinity of Wallingford, CT, Geological Society of America *Abstracts with Programs.* Vol. 49; doi: 10.1130/abs/2017NE-290397

Stone, J.R., Schafer, J.P., London, E.H., DiGiacomo-Cohen, M.L., Lewis, R.S., and Thompson, W.B., 2005, Quaternary Geologic Map of Connecticut and Long Island Sound Basin (1:125,000). U.S. Geol. Surv. Sci. Invest. Map # 2784.

Taylor, Kaitlin A., Charney, Allison B., and Steinen, Randolph P., 2019, Petrogenesis of lamprophyres in the Wallingford Quadrangle. Geological Society of America , *Abstracts with Programs*. ISSN 0016-7592, doi: 10.1130/abs/2019NE-328386.

U.S. Geological Survey, 1973, Aeromagnetic map of the Wallingford quadrangle, New Haven County, Connecticut: U.S. Geol. Surv. Geophys. Invest. Map, GP-865, 1:24,000.

Weitz, Joseph L., 1972, Structural Element Map of the Hartford South 7.5' Quadrangle. Unpublished Map Collection, Connecticut Geological and Natural History Survey files, Department of Energy and Environmental Protection.

Wintsch, R.P., Roden-Tice, M., Kunk, M.J., and Aleinikoff, J.N., 2003, Ductile to brittle Mesozoic overprint of Alleghanian structures, Bronson Hill terrane, Rockville area, Connecticut: in, Brady, J. B., and Cheney, J. T., Guide-book for geological field trips in the five college region. 95th Annual Meeting of the New England Intercollegiate Geological Conference, Trip A3, A1-A31.

Wintsch, R.P., Roden-Tice, M., and Kunk, M.J., 2011, Poly-metamorphism and poly-deformation of Bronson Hill rocks, Northeastern Connecticut. In Geological Soc. Connecticut Guidebook No. 2., 38p.

Wise, D.U. 1992, Dip domain method applied to the Mesozoic Connecticut Valley rift basins. Tectonics 11:1357-1368.

Zoback, M. L., 1992, Stress field constraints on intraplate seismicity in eastern North America: Journal of Geophysical Research: Solid Earth (1978–2012), 97, 11761-11782.

APPENDIX I. Index Map and Local Area Maps.

Index map showing local areas and local area outcrop maps. The local area outcrop maps show accurately the location of outcrops and structural measurements made at those outcrops. Because of scale factors, outcrop locations on the local area maps are considered more accurate that those shown on Plate I. The local area maps also may show initial interpretations that were not always our final interpretation. Interpretations on Plate I reflect our final thinking. Some local area maps have a rough legend or explanation, but many do not. Outcrops of igneous rocks shown in red (diabase and basalt) or purple (lamprophyre); outcrops of sedimentary rocks shown in other colors. Areas of numerous small outcrops or abundant rubble considered "near surface rocks" are shown with ruled pattern. Structural symbols are standard.

Figure I-1

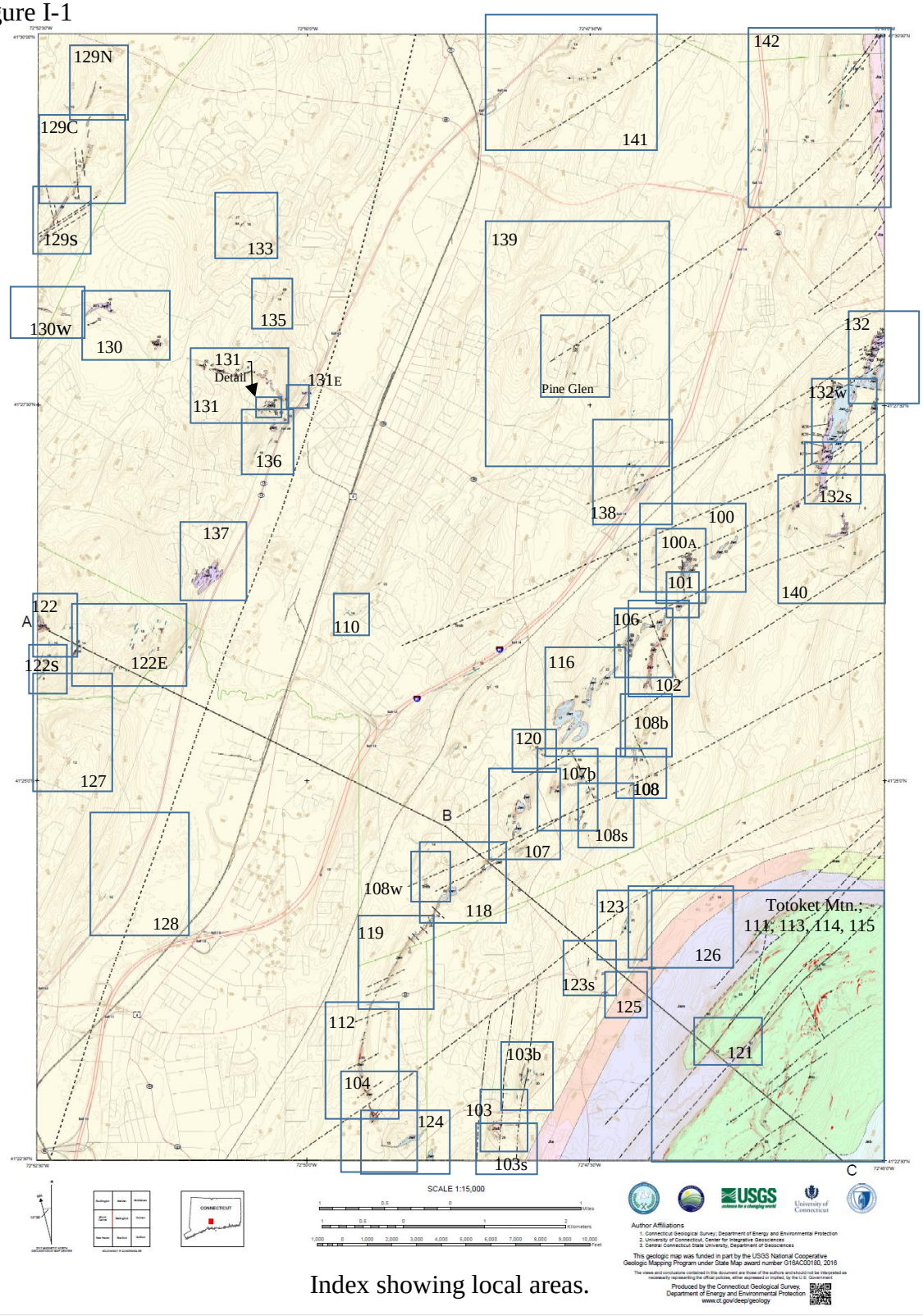

Index showing local areas.

Figure I-2. Local area 100

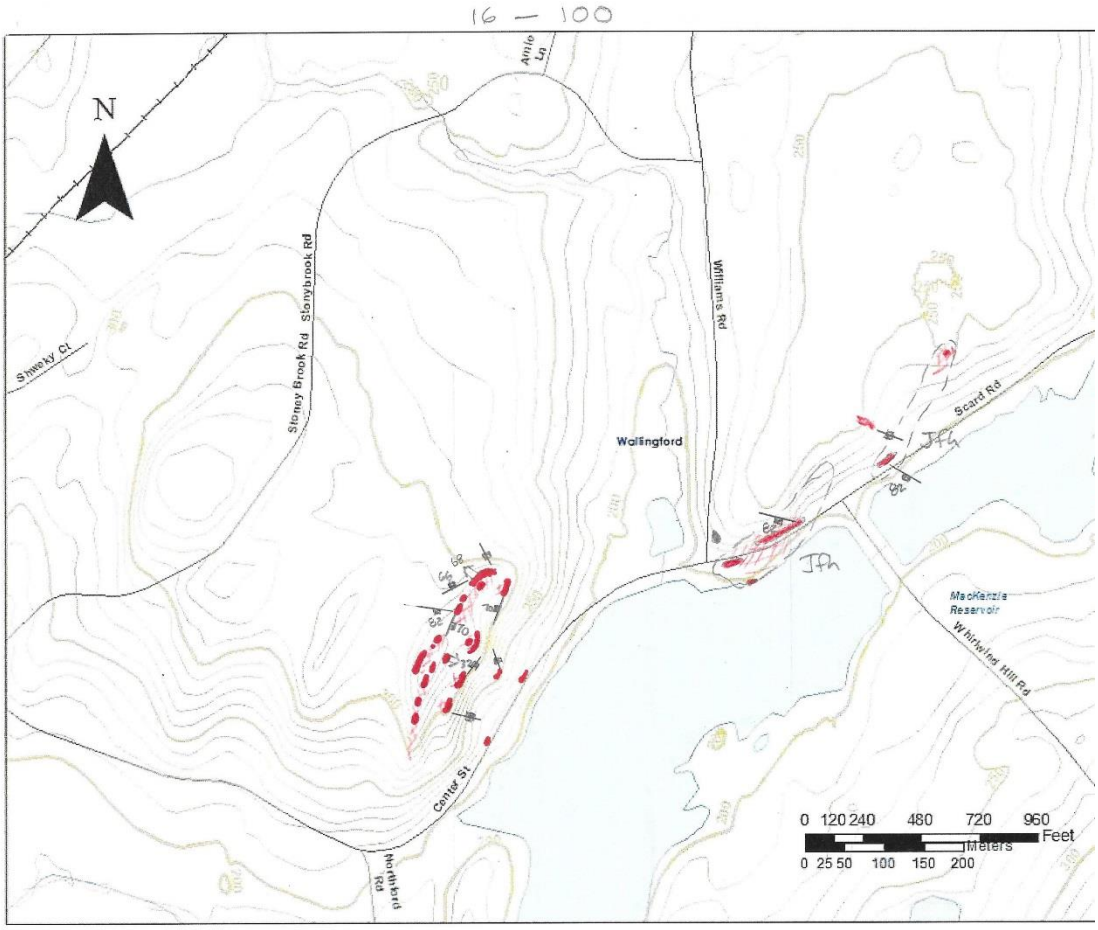

Figure I-3. Local area 100A (detail of southwestern area of local area 100.

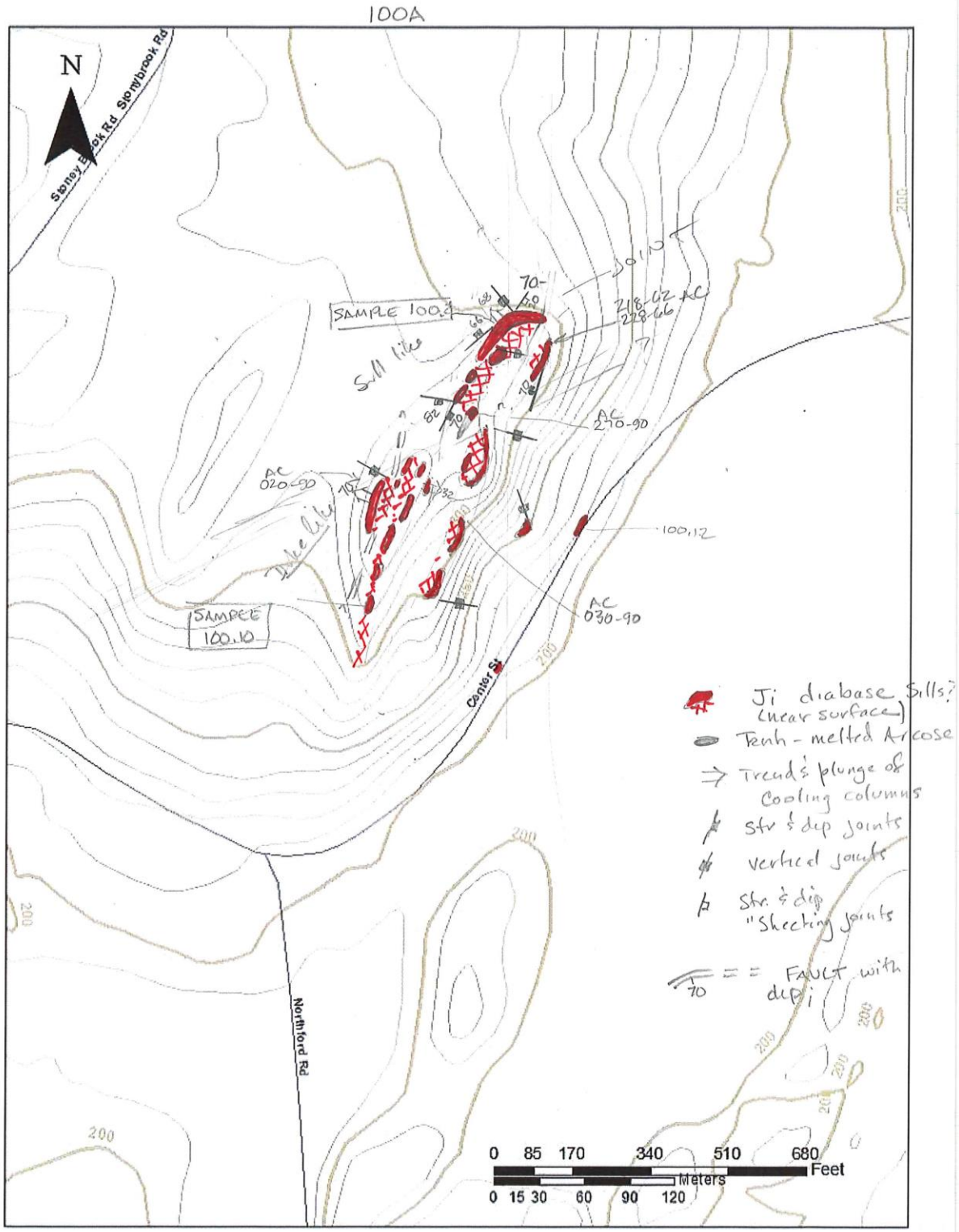

Figure I-4. Local area 101

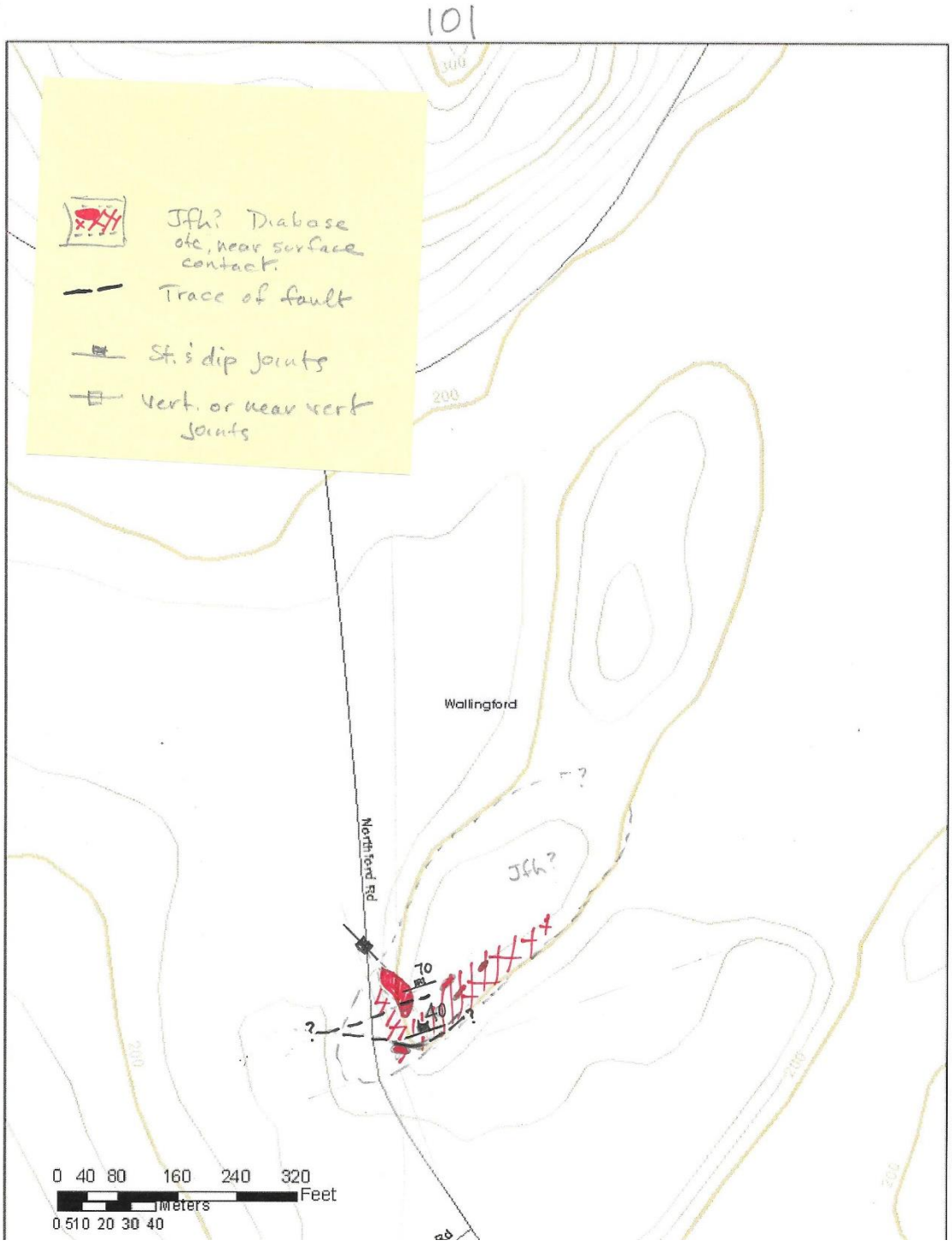

Figure I-5. Local area 102

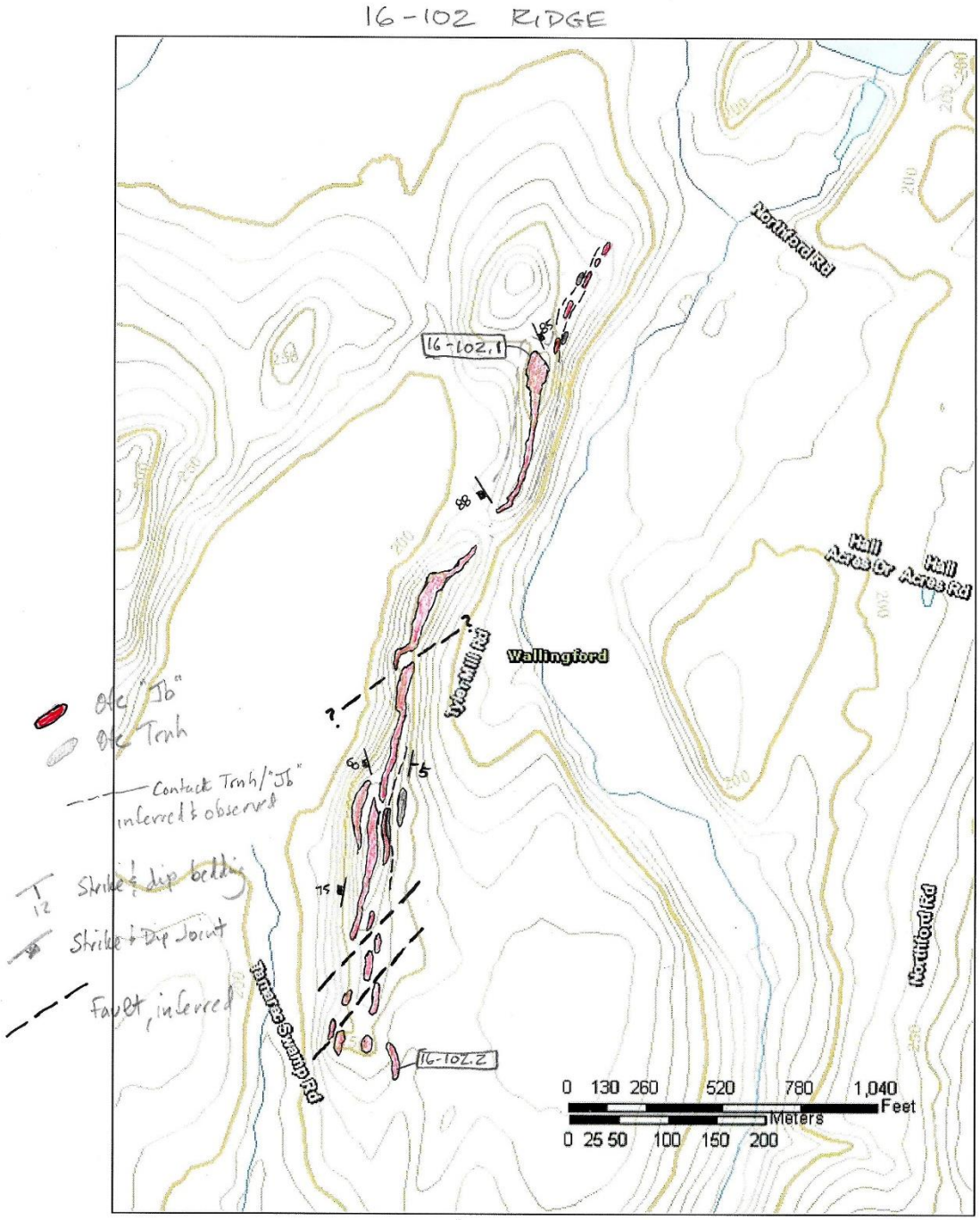

Figure I-6. Local area 103.

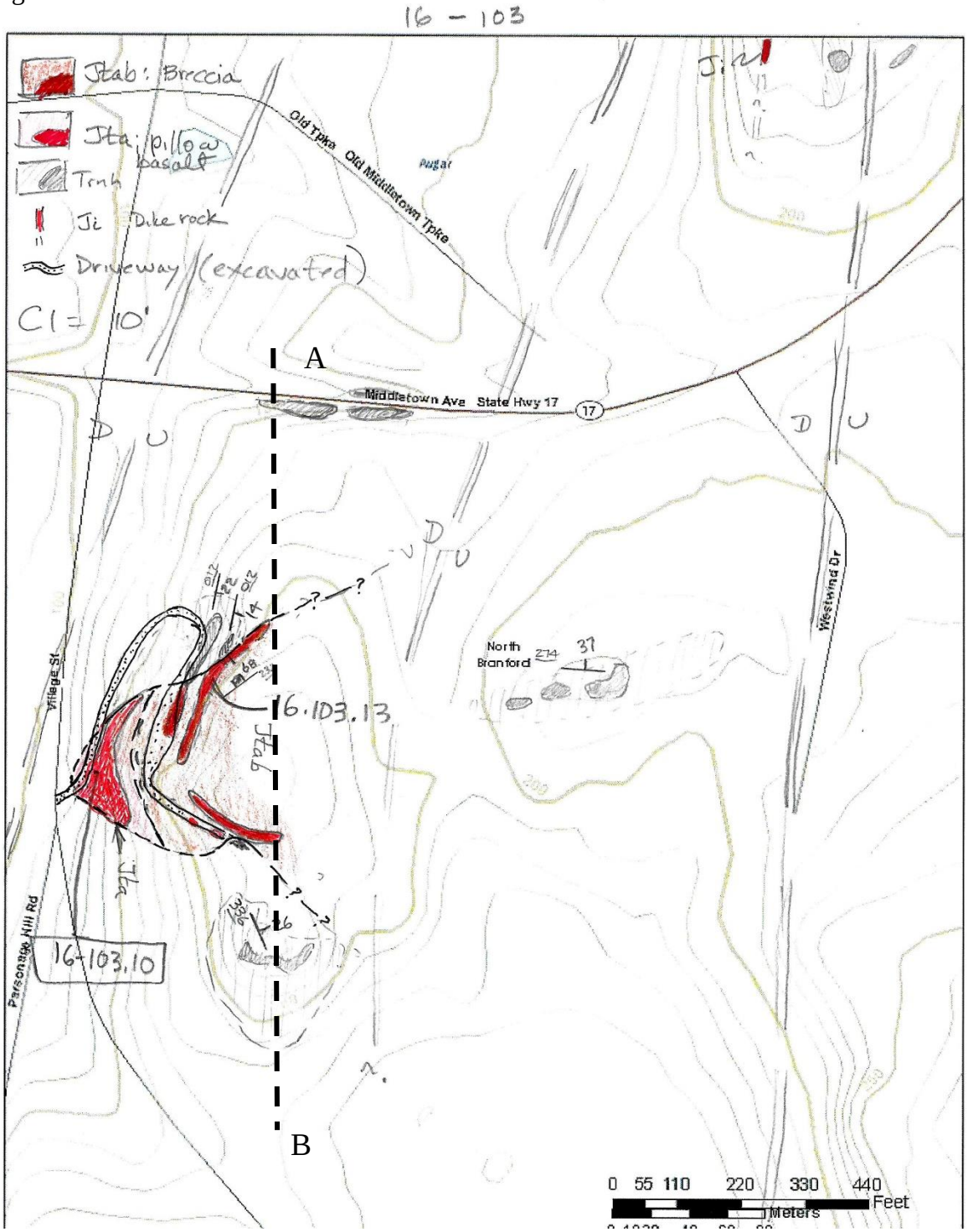

Line of cross section AB on Figure 5E.

Figure I-7. Local area 103b

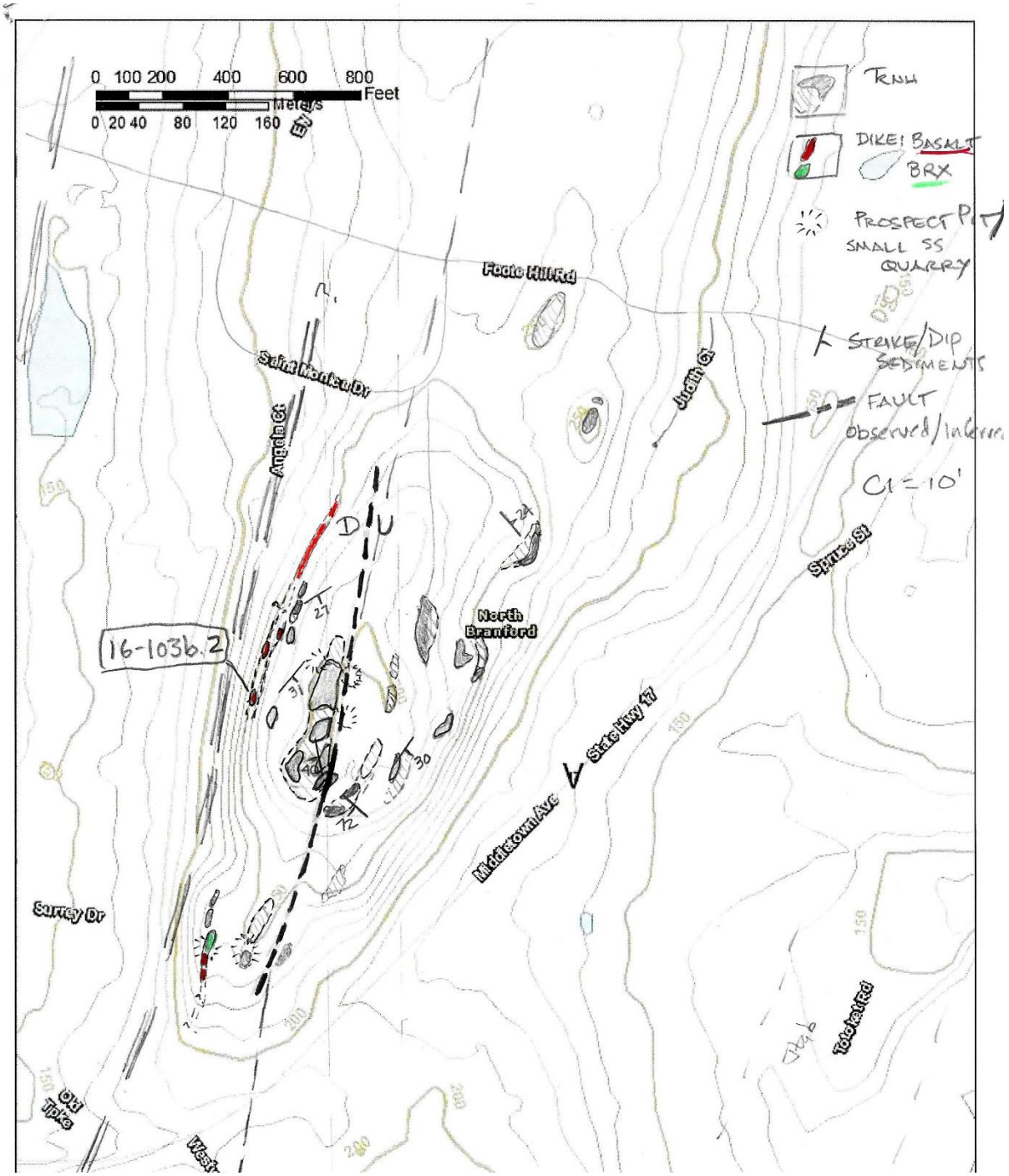

Figure I-8. Local area 103s

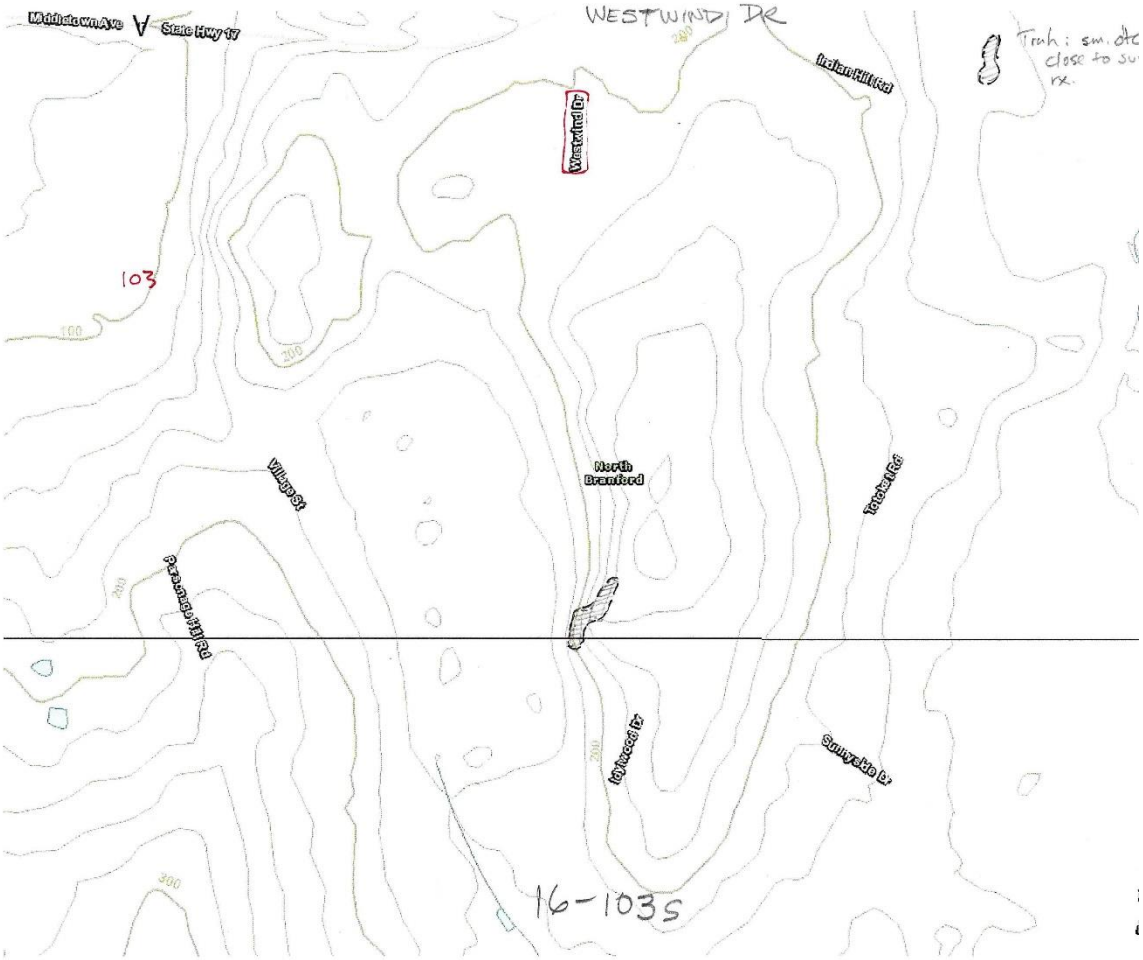

Figure I-9. Local area 104

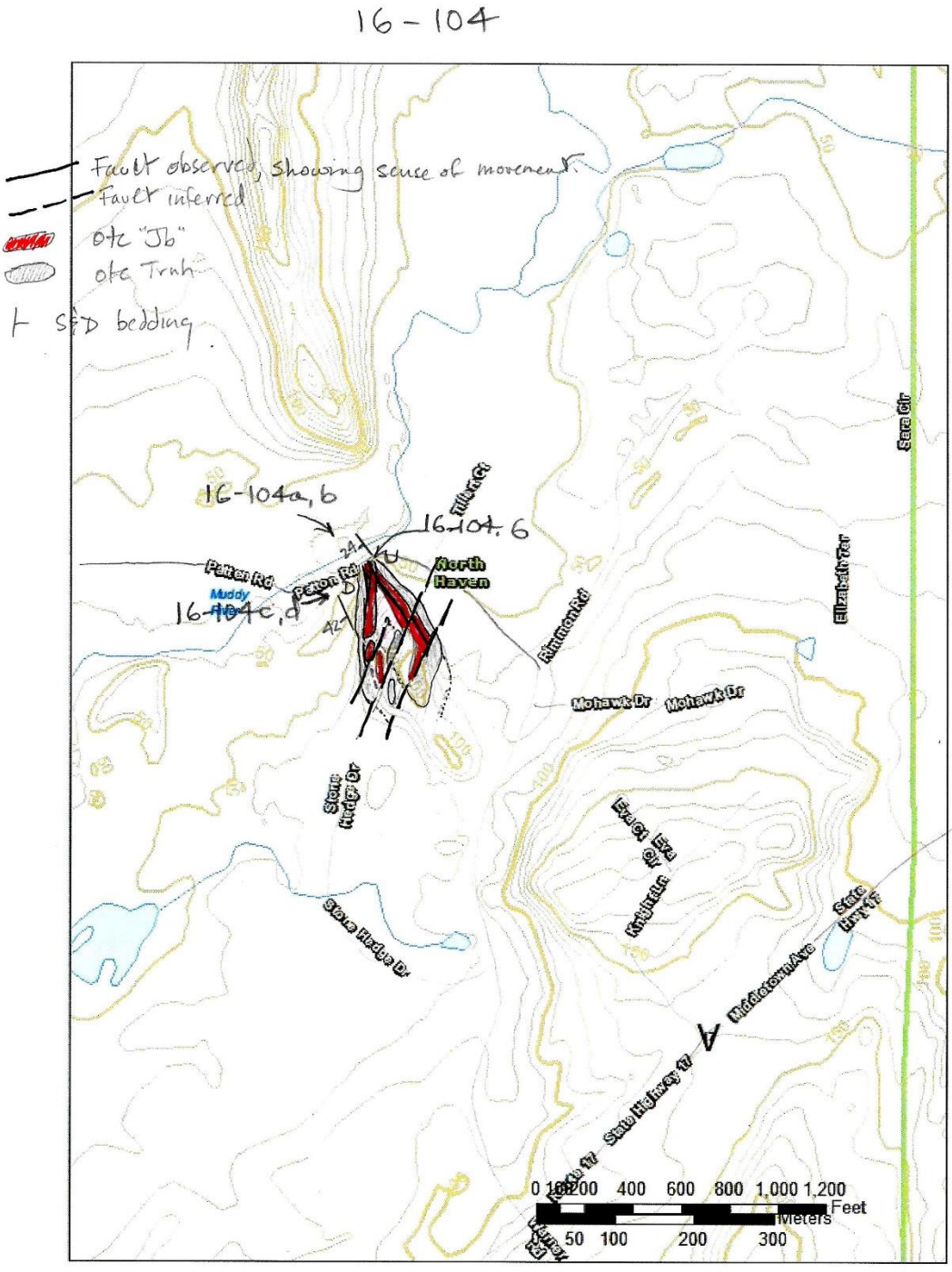

Figure I-10. Local area 106.

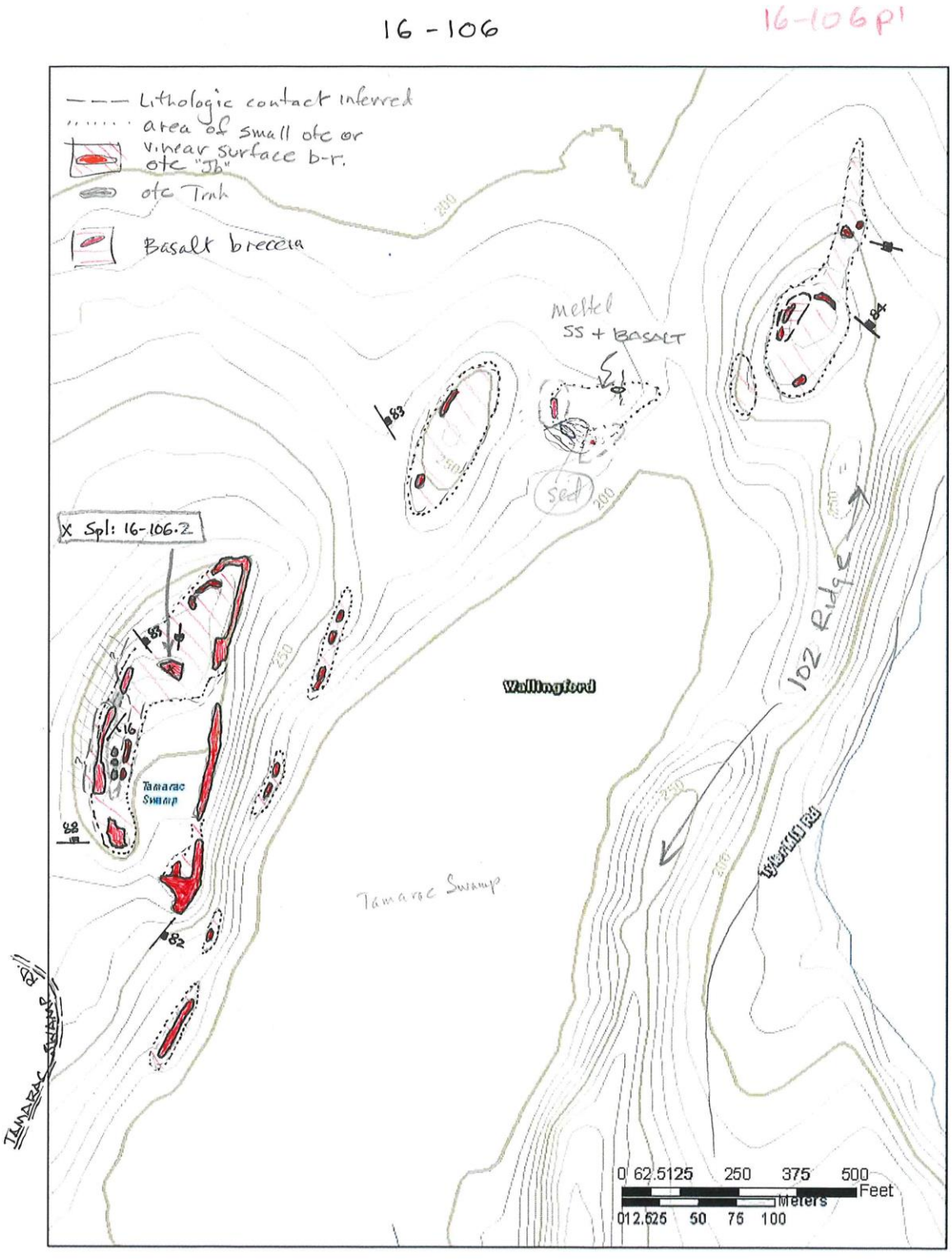

Figure I-11. Local area 107, 107b

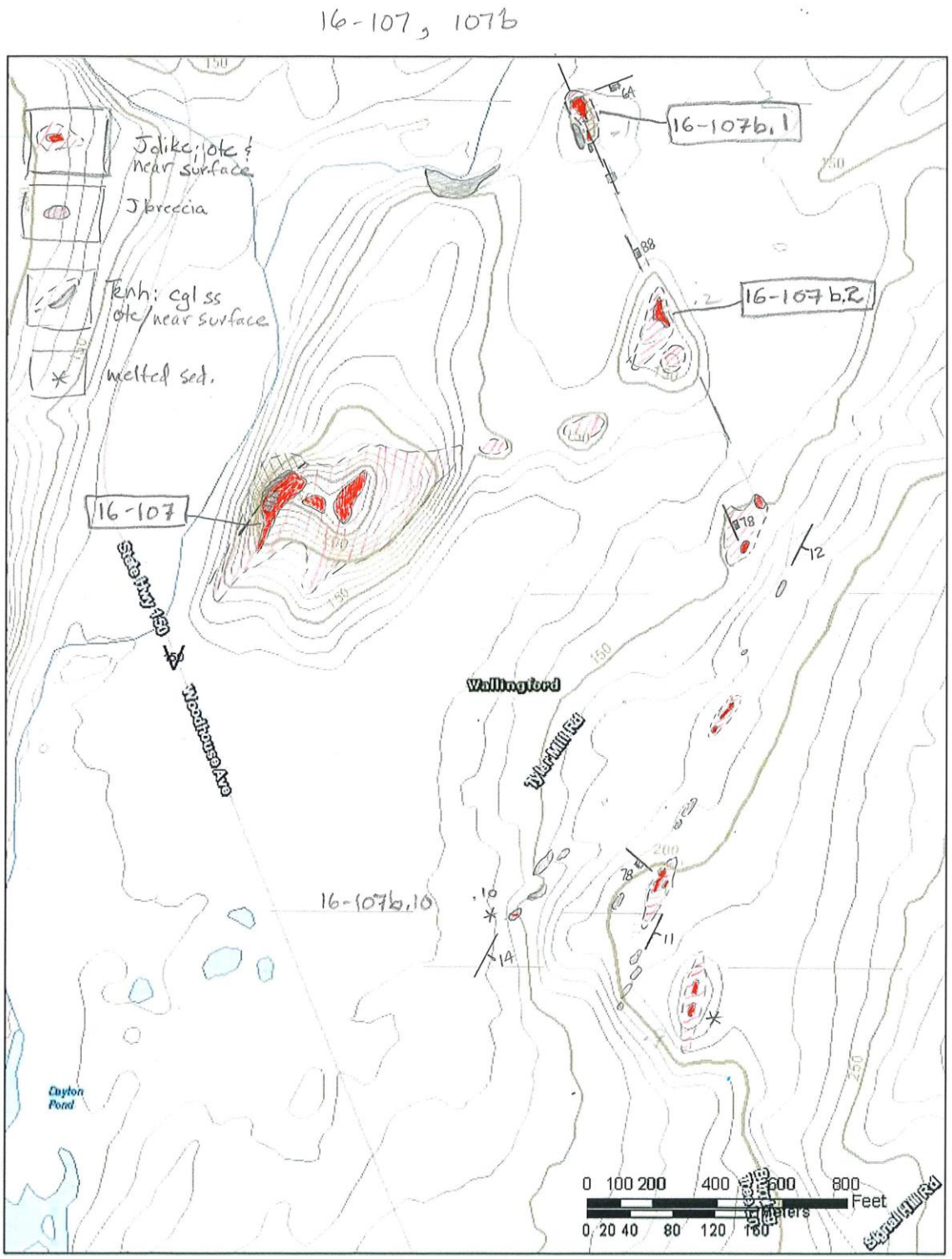

Figure I-12. Local area 108

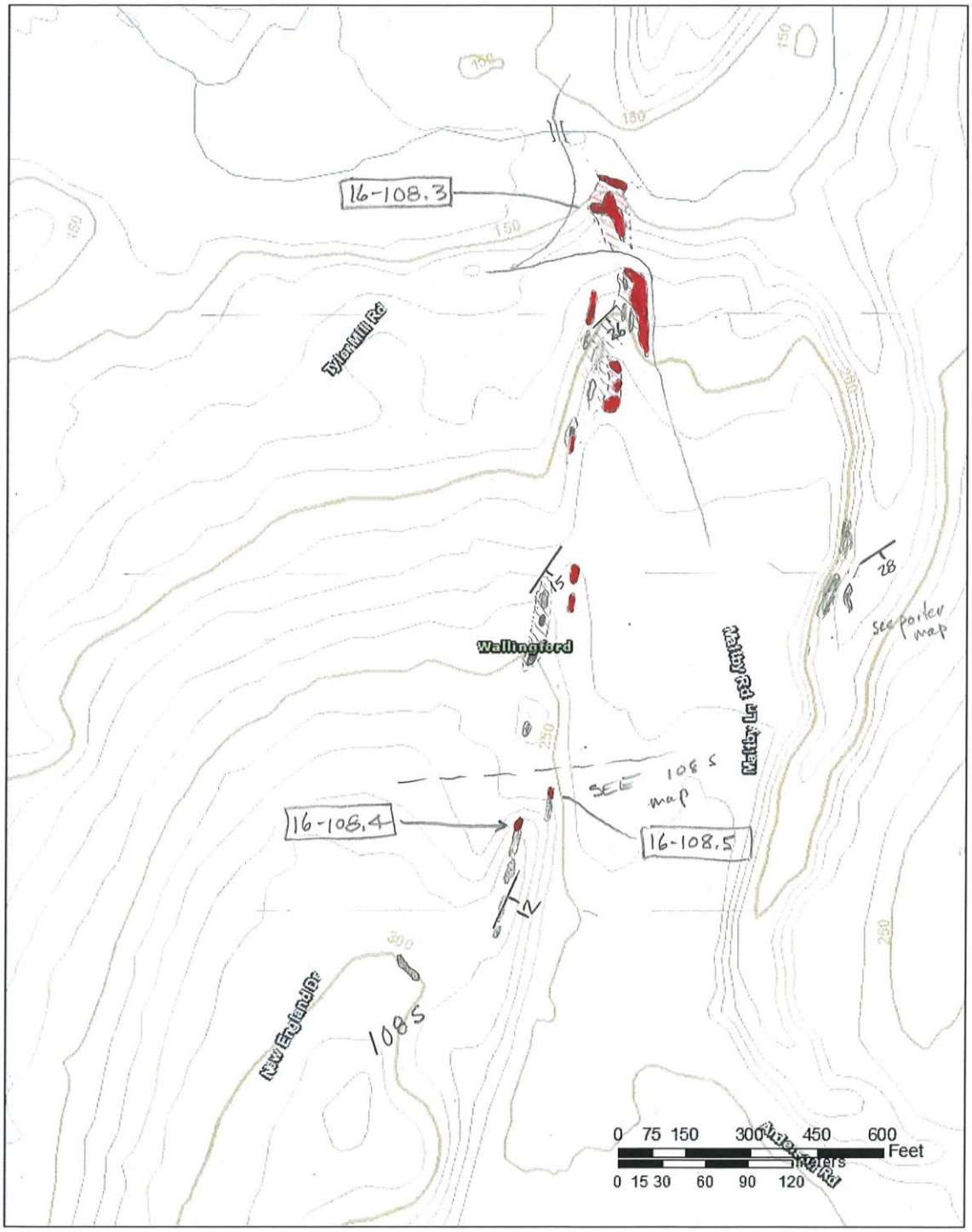

Figure I-13. Local area 108b

Figure I-14. Local area 108s

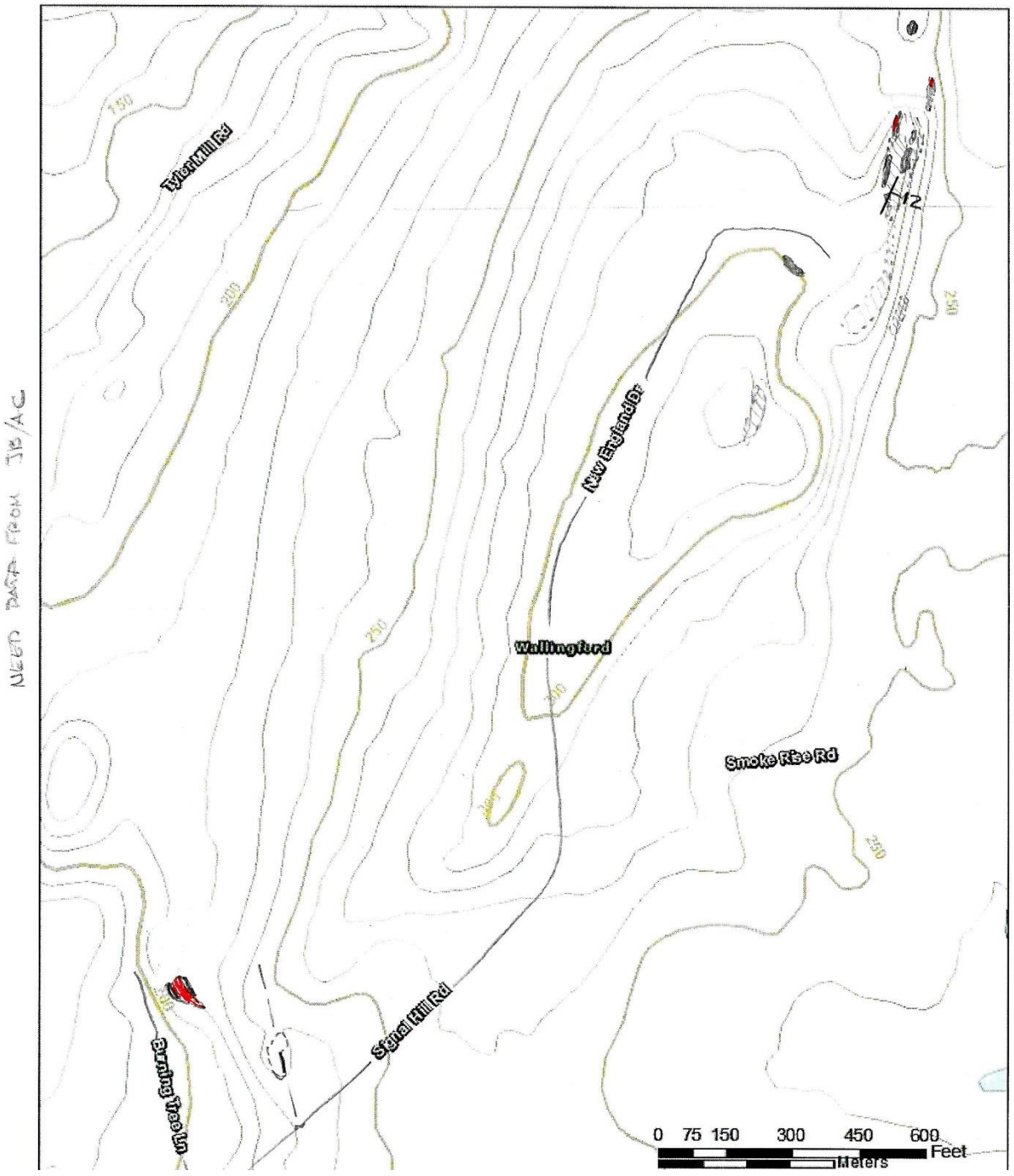

Figure I-15. Local area 110

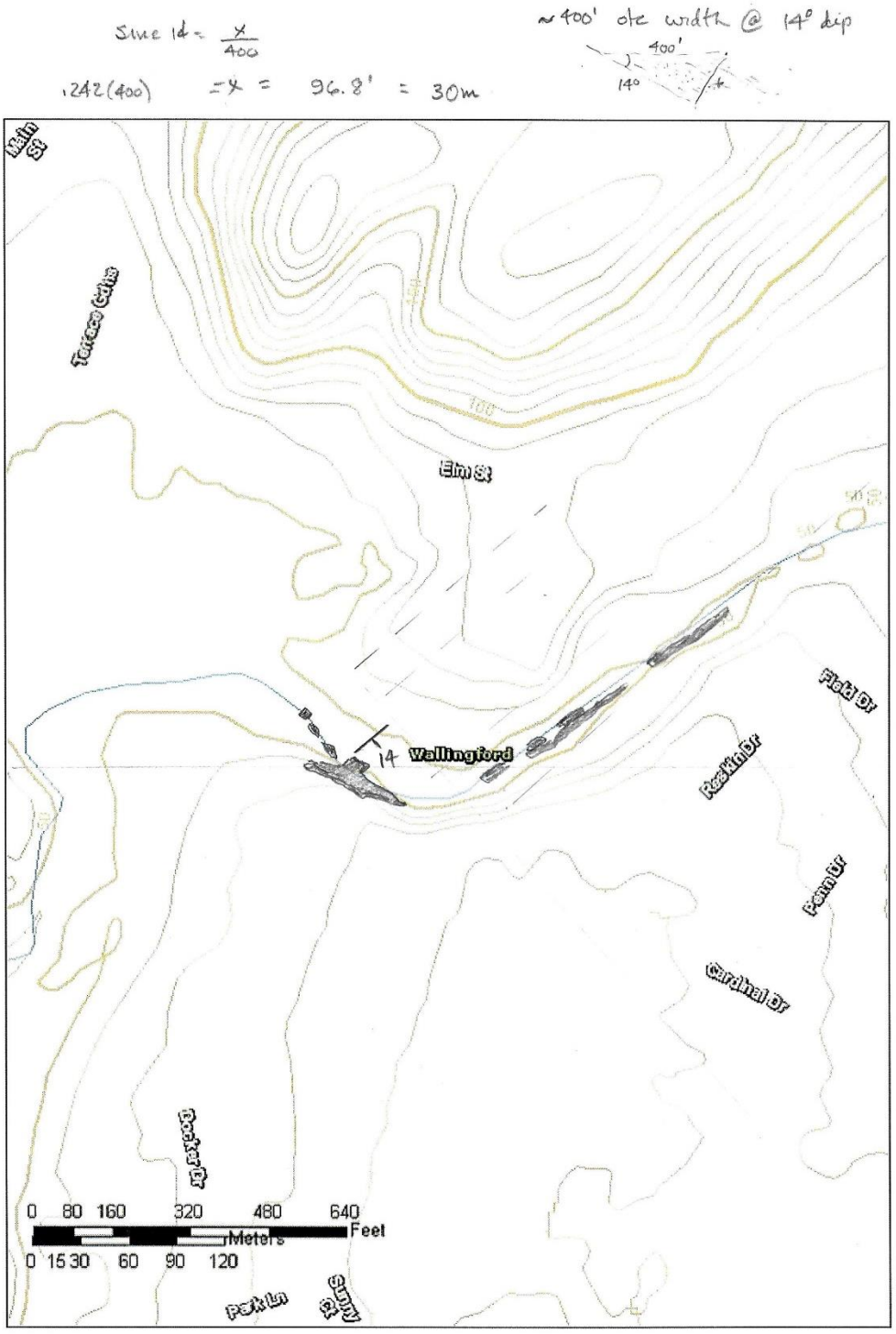

Figure I-16. Local area 112

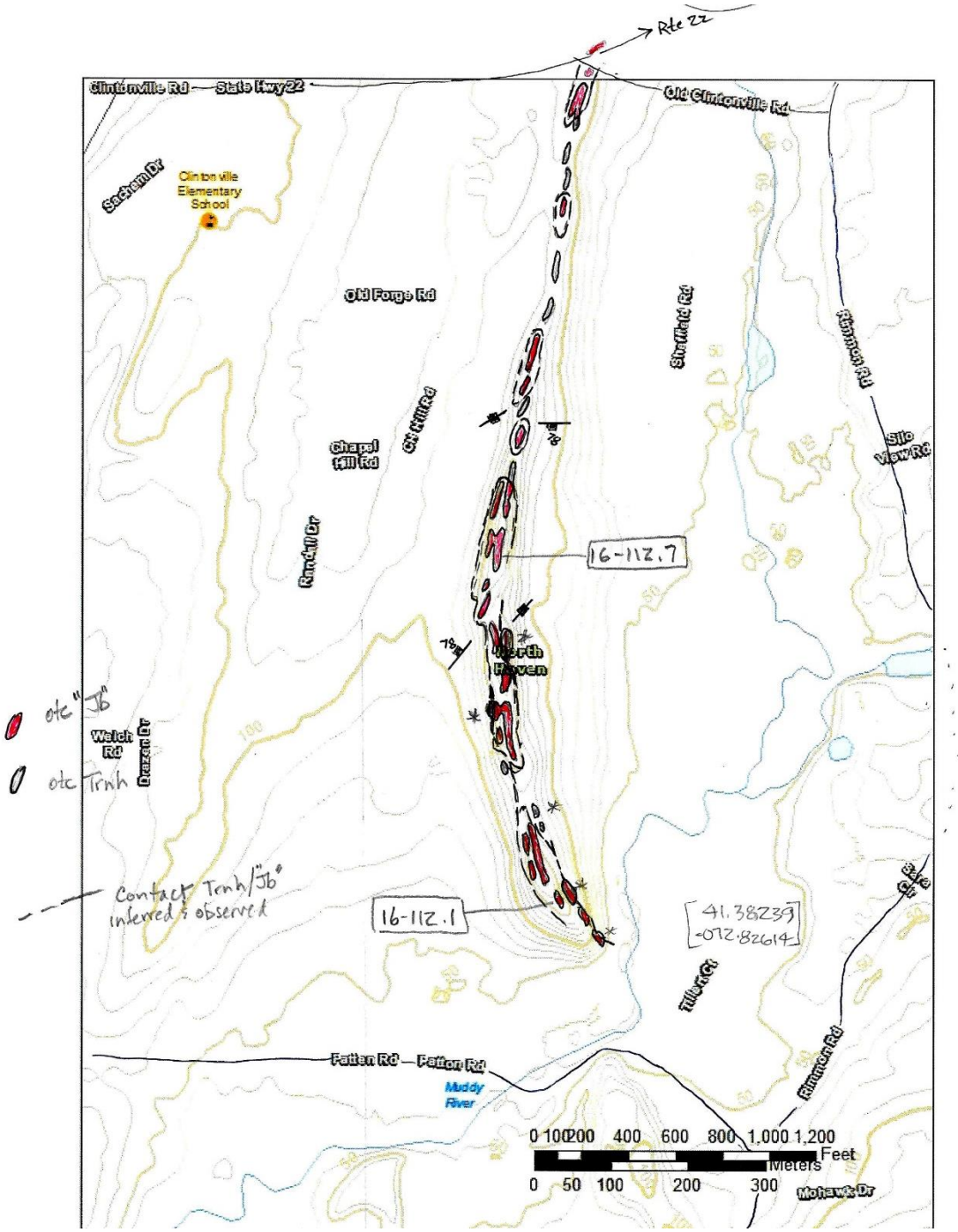

Figure I-17. Totoket Mountain, local areas 111, 113, 114 and 115.

Figure I-18. Local area 116.

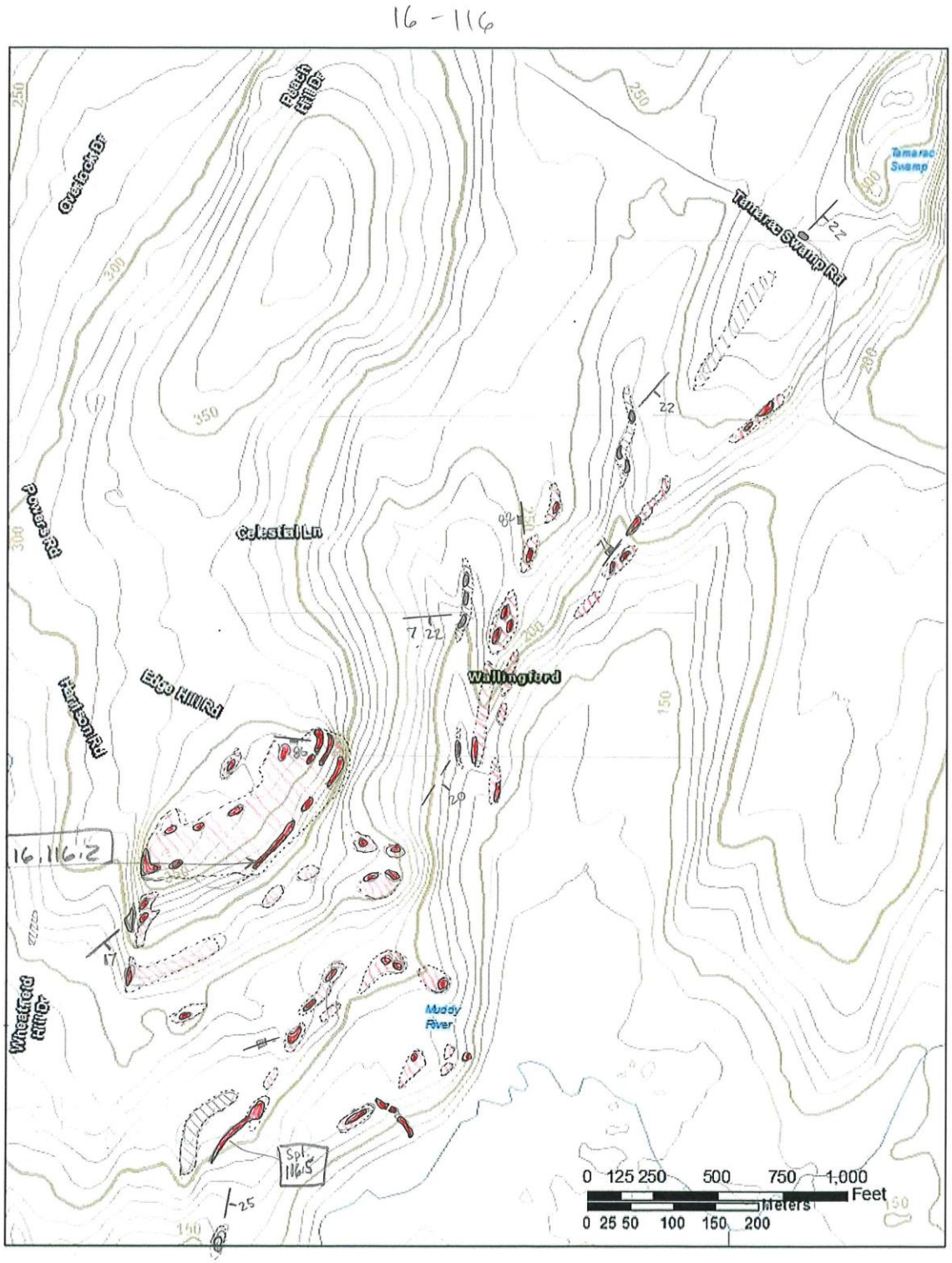

Figure I-19. Local area 117.

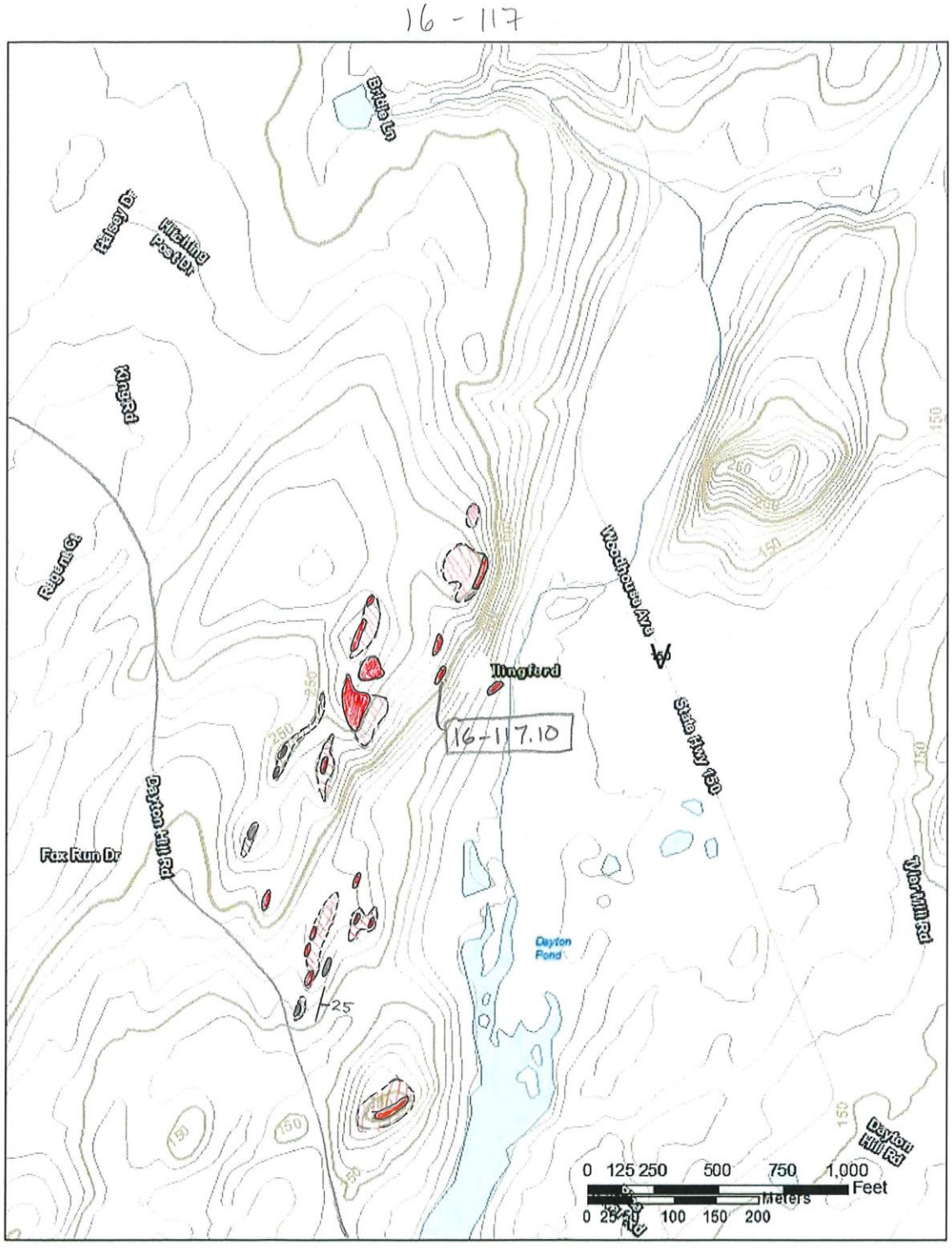

Figure I-20. Local area 118

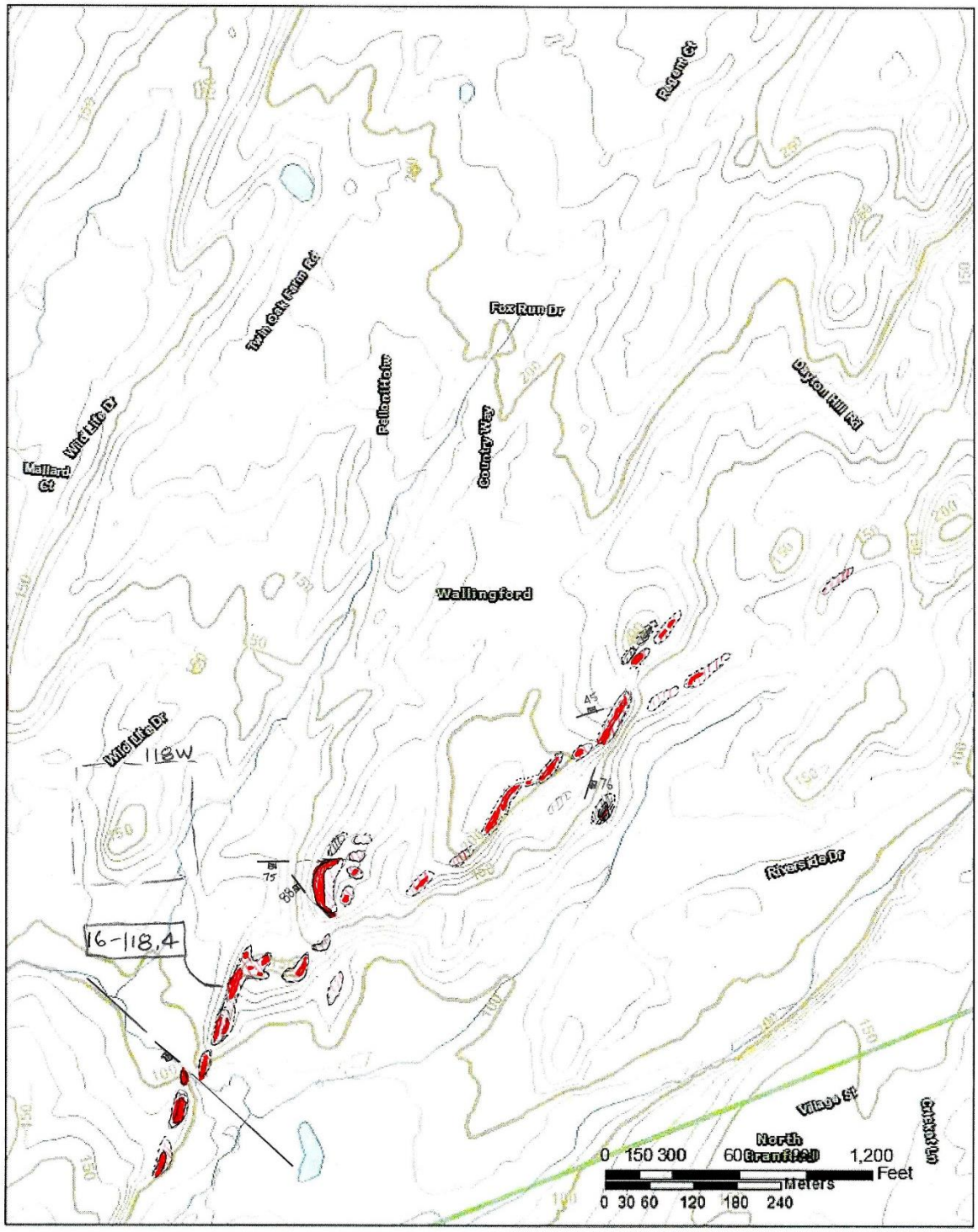

Figure I-21. Local area 118w

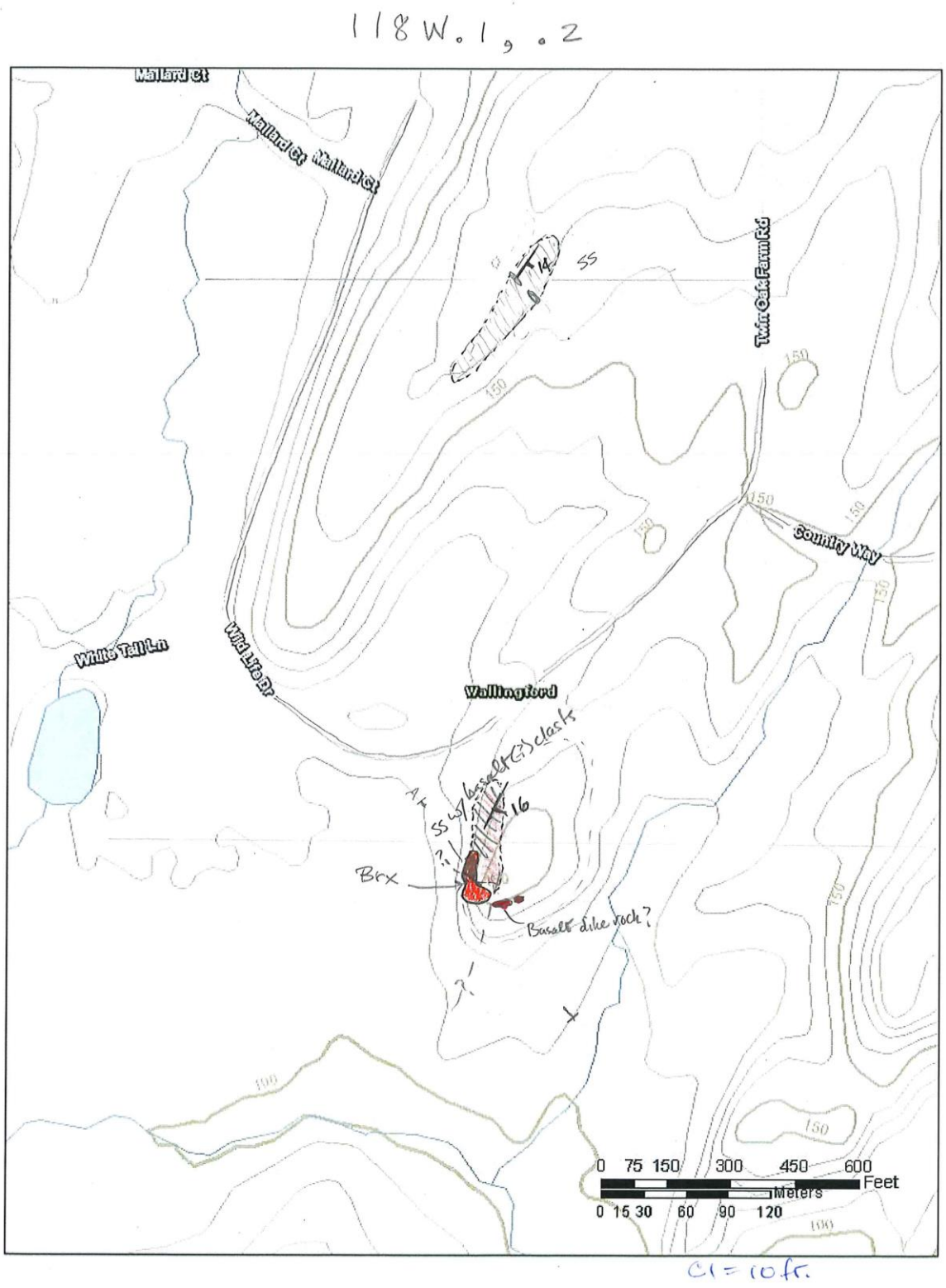

Figure I-22. Local area 118w – detail.

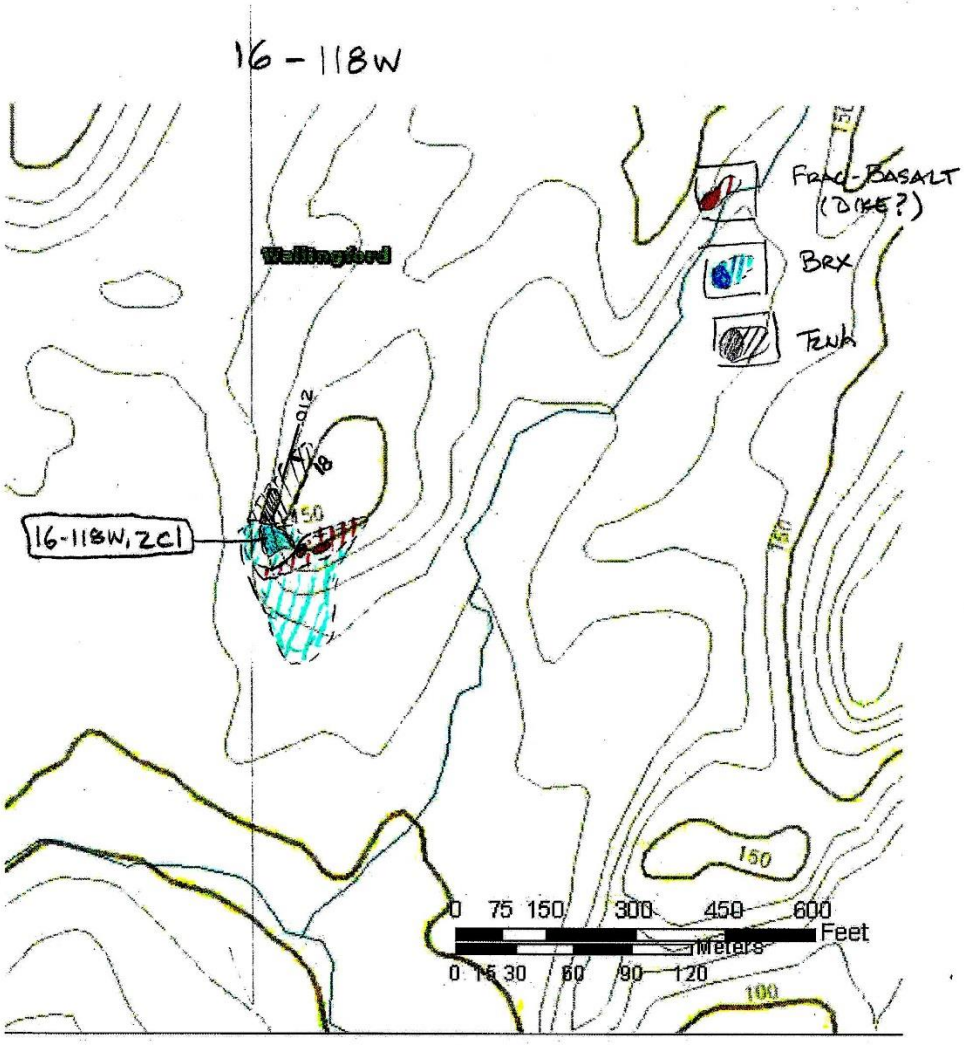

Figure I-23. Local area 119

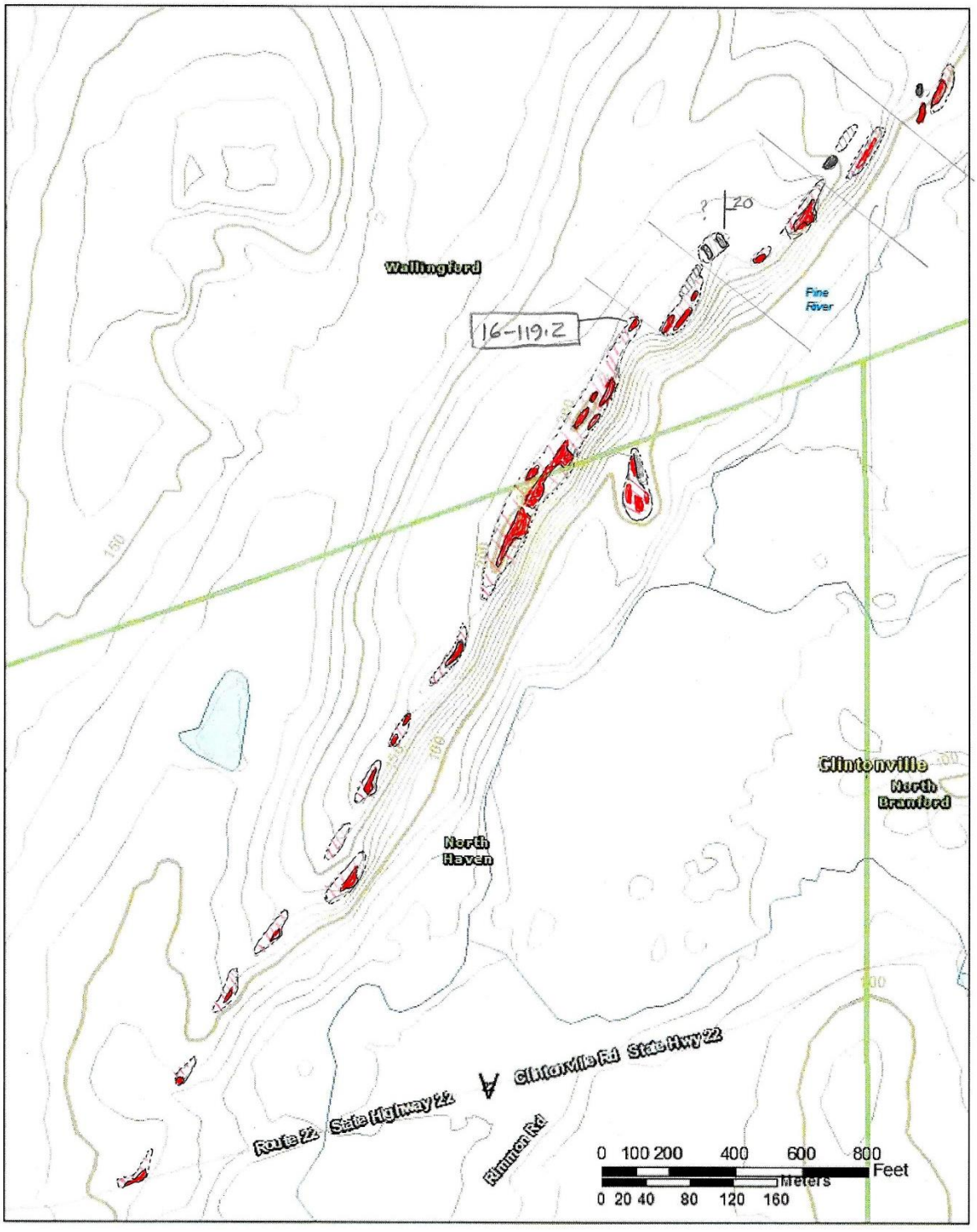

Figure I-24. Local area 120

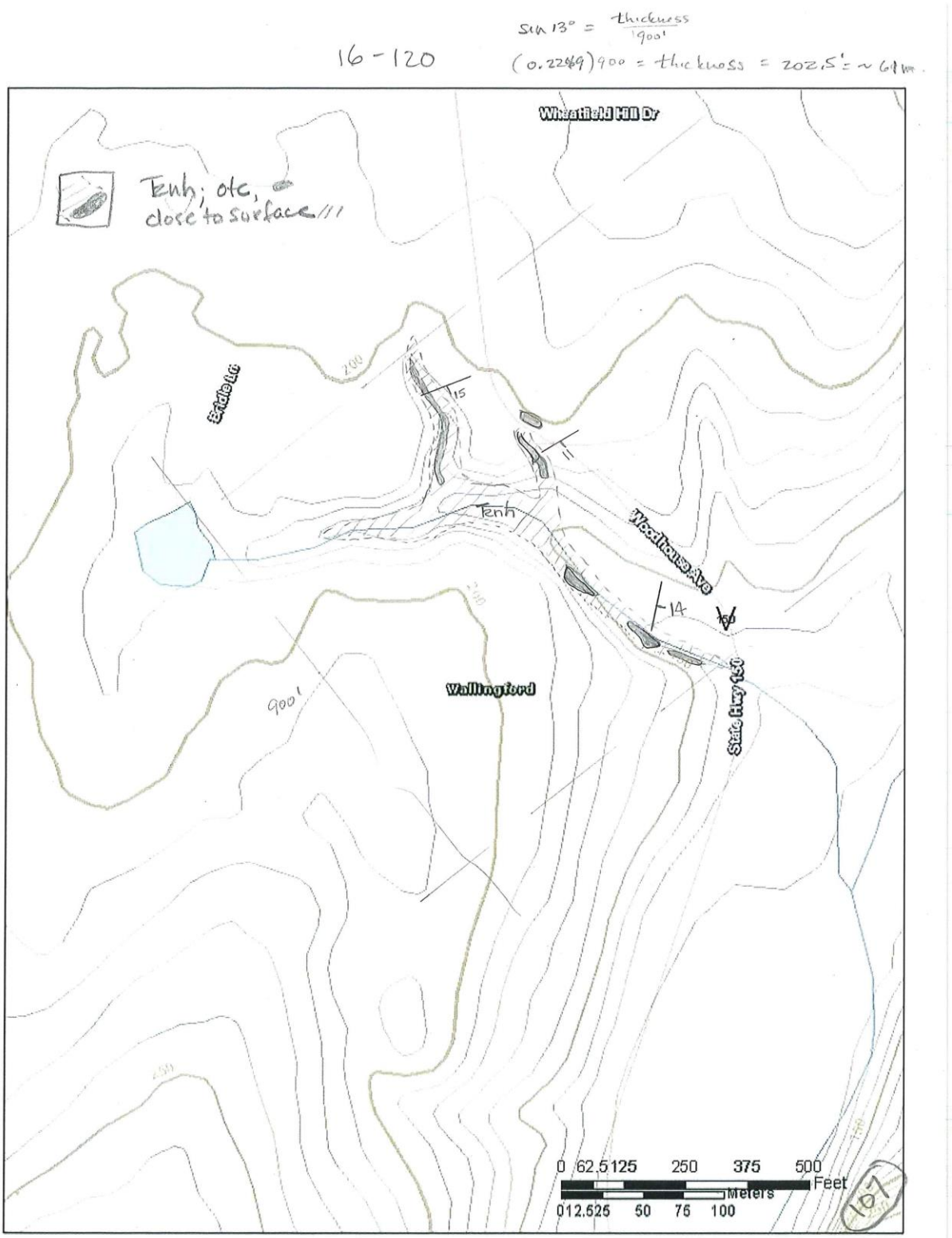

Figure I-25 Local area 121. Totoket Mountain, Jho/Jsm contact.

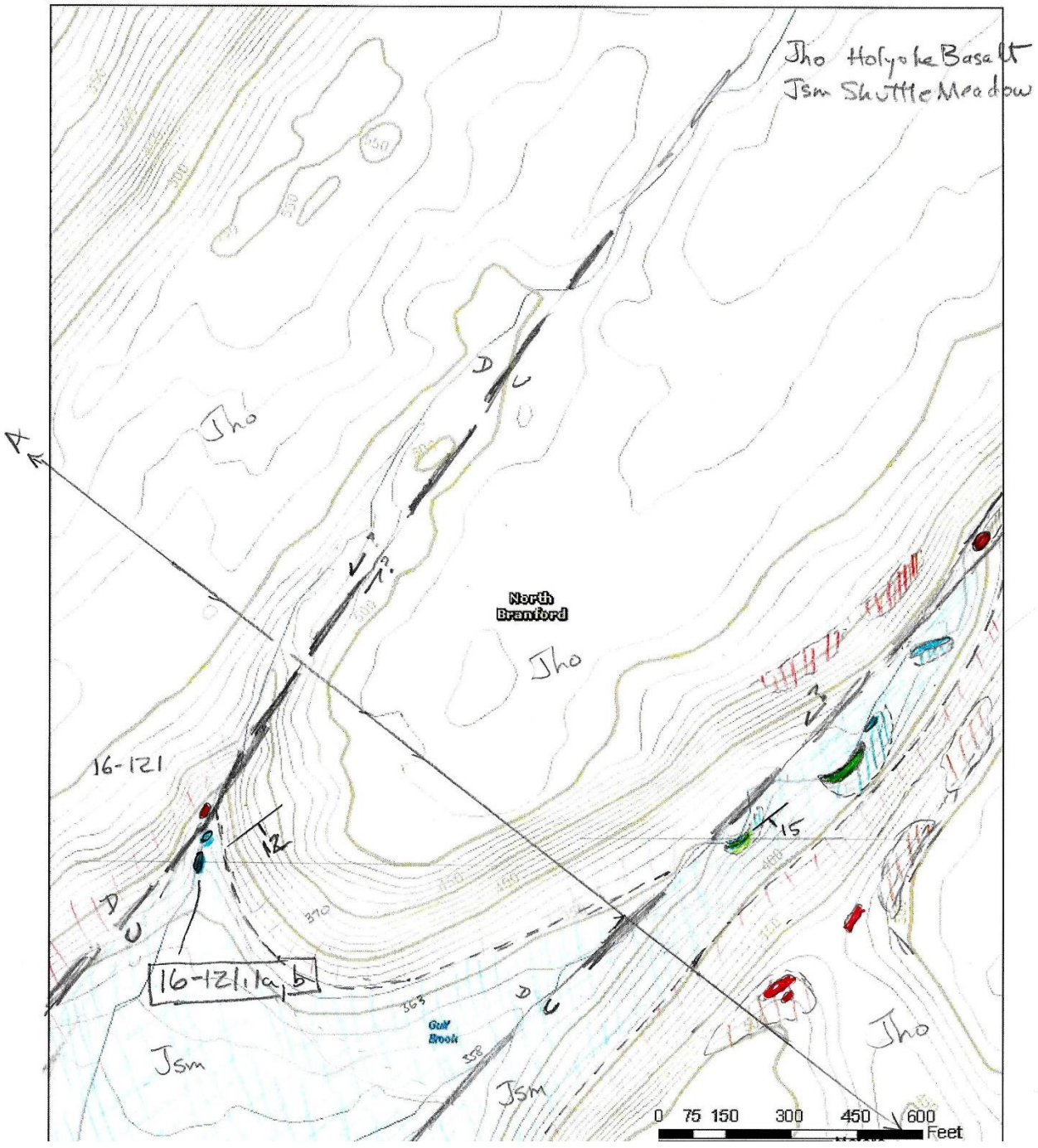

Figure I-26. Local area 122 at Sleeping Giant State Park.

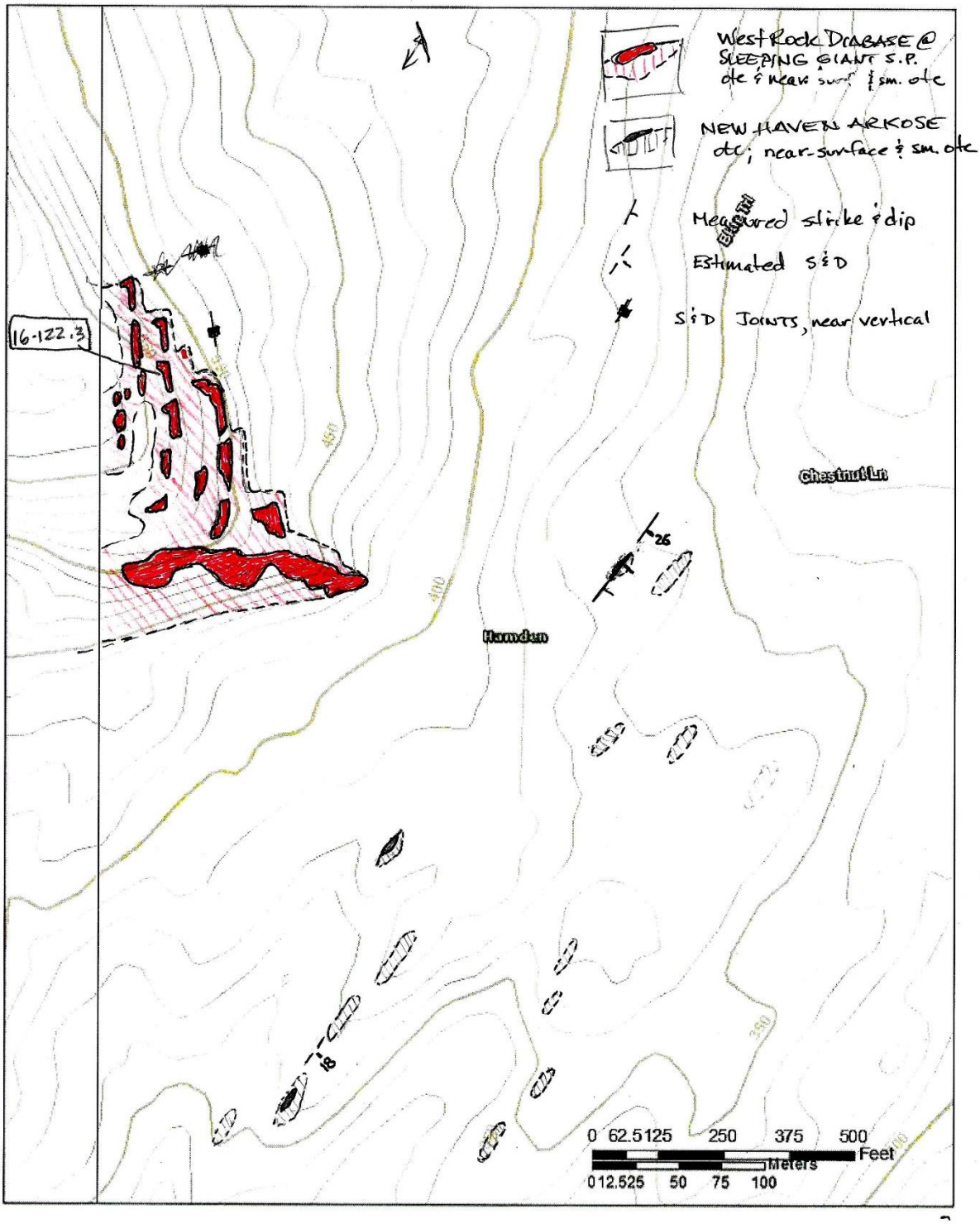

Figure I-27. Local area 122E, Sleeping Giant State Park.

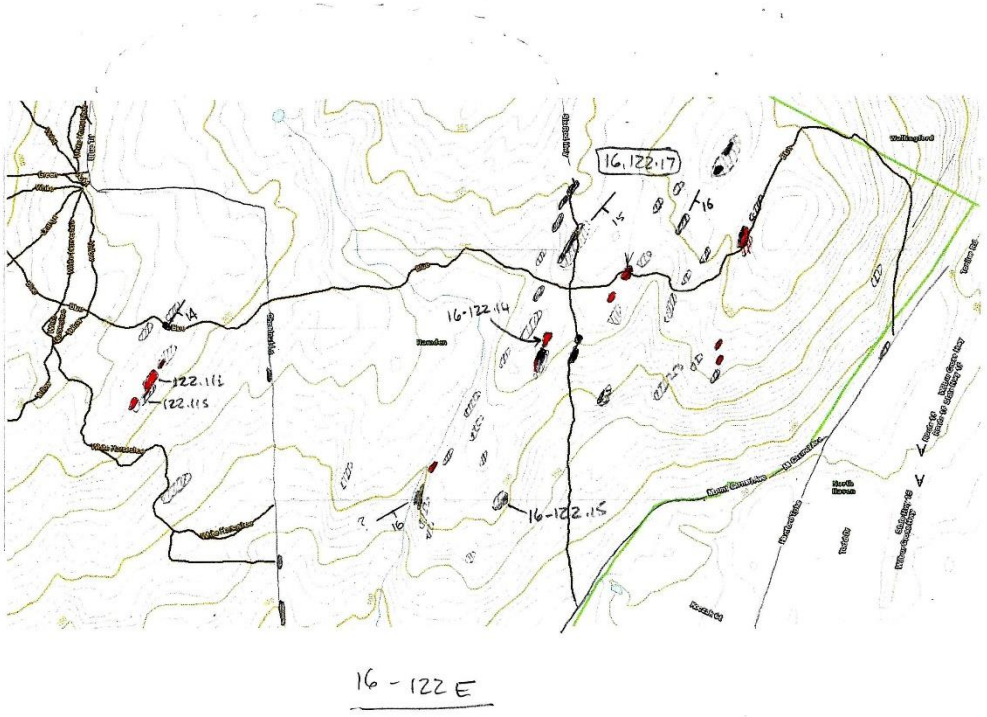

Figure I-28. Local area 122S, Sleeping Giant State Park.

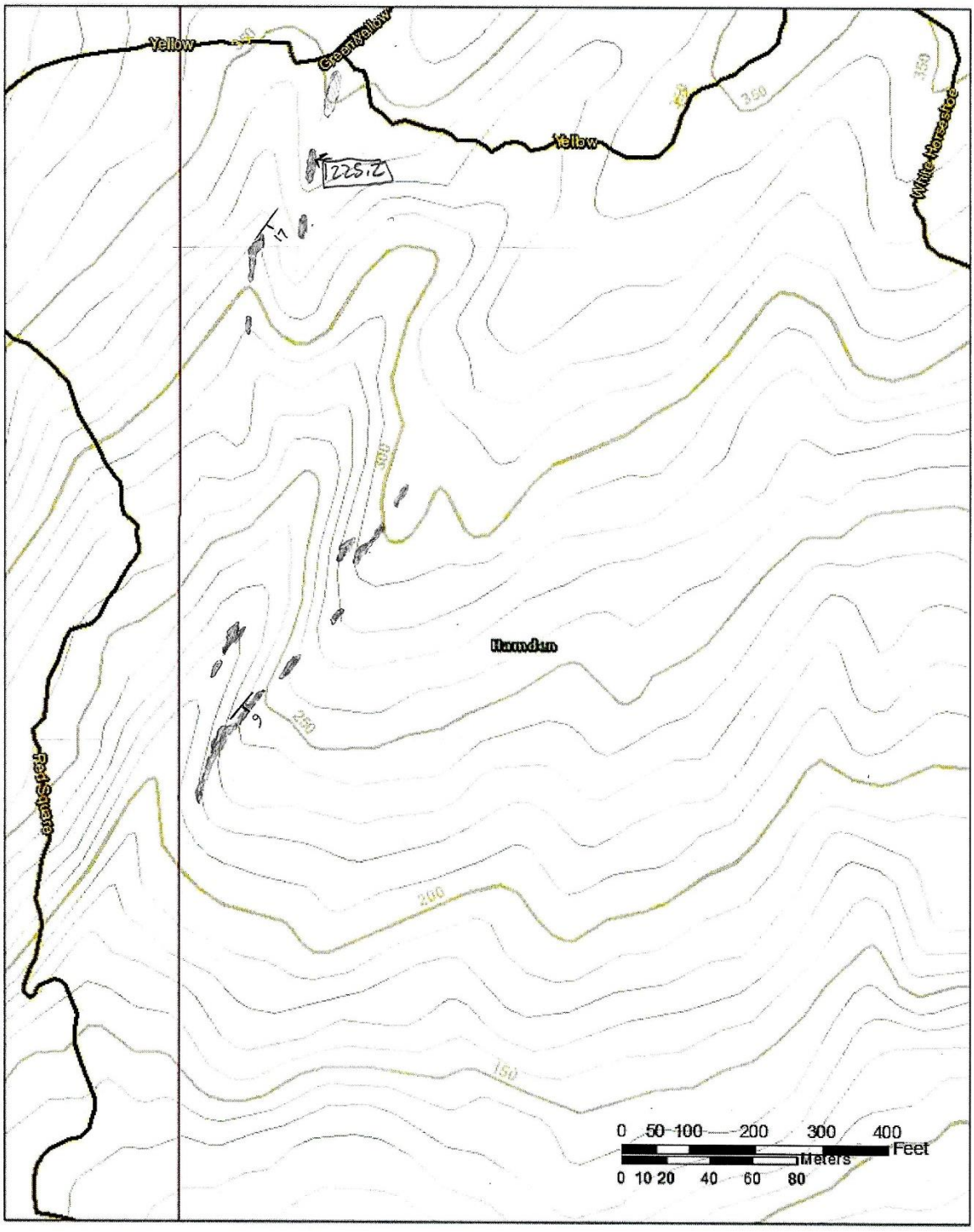

Figure I-29. Local area 123, Old Post Road.

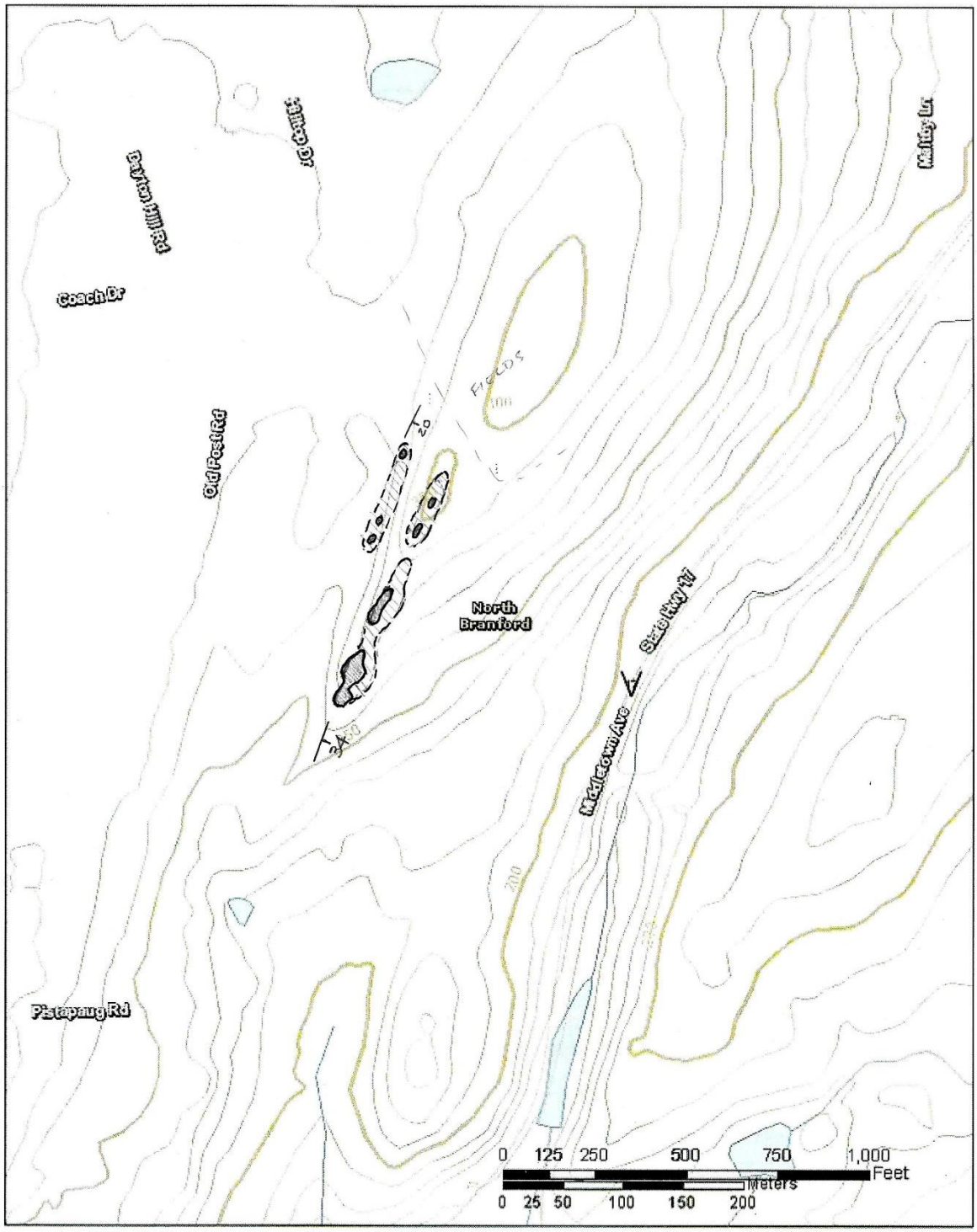

Figure I-30. Local area 123S

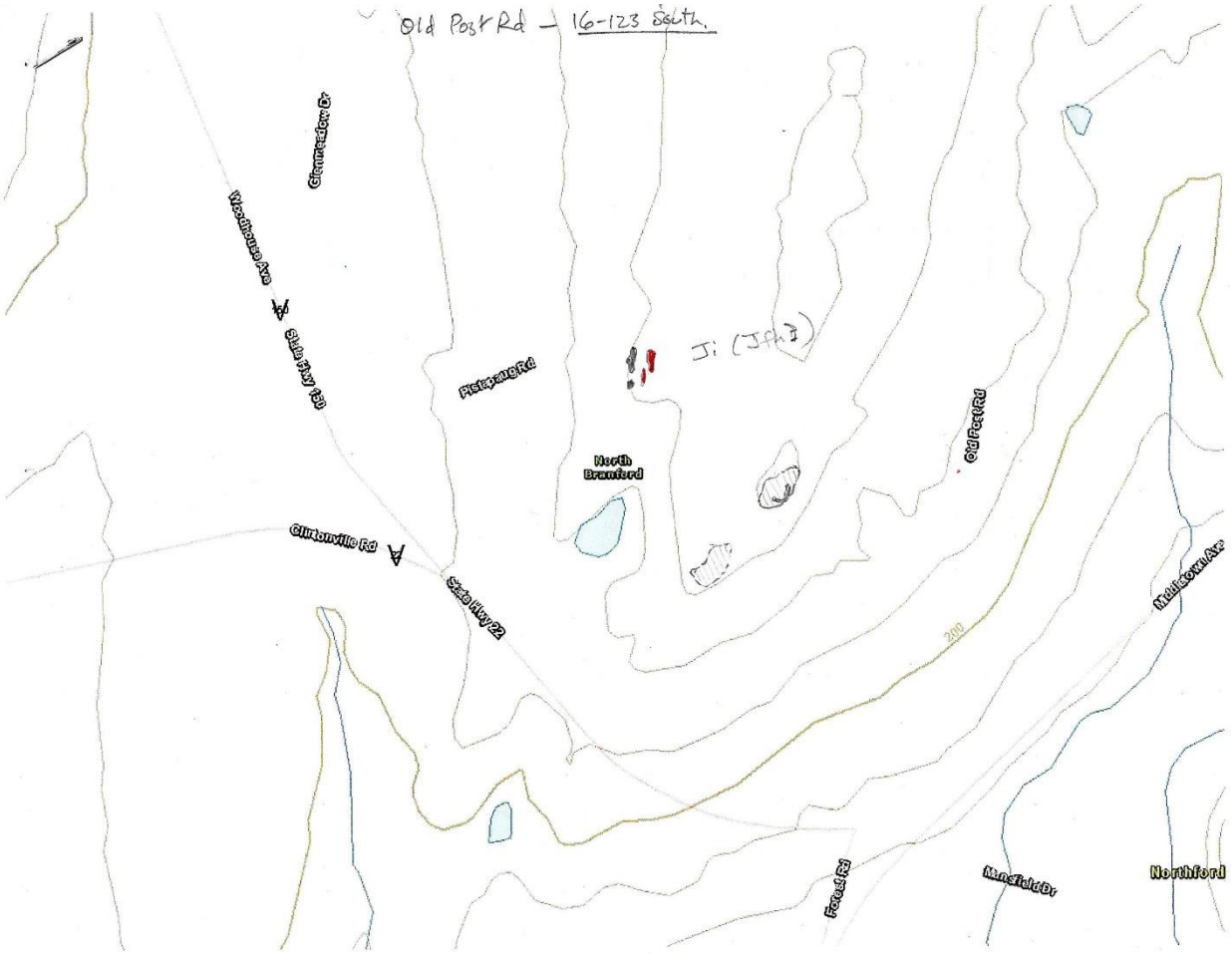

Figure I-31. Local area 124.

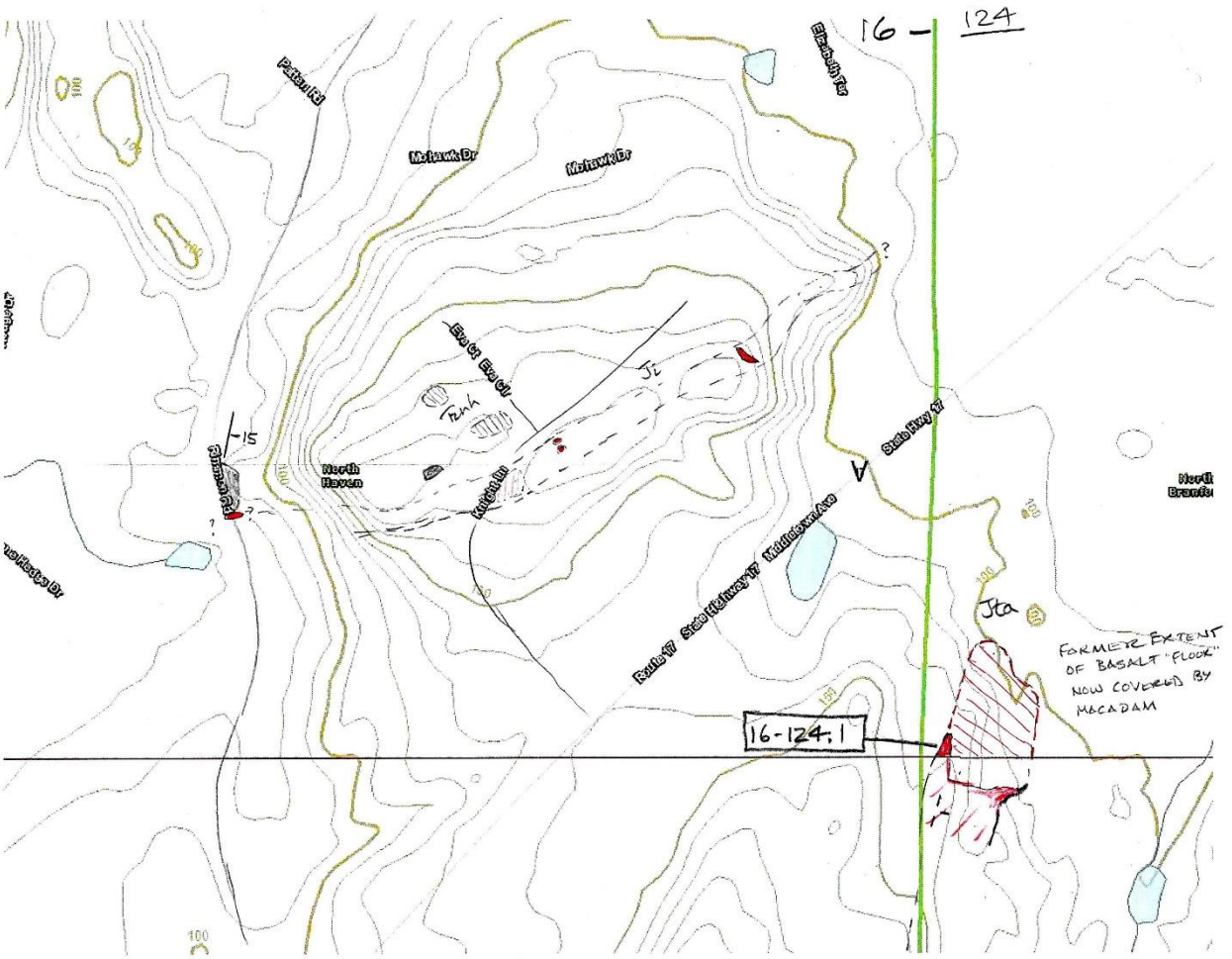

Figure I-32. Local area 125

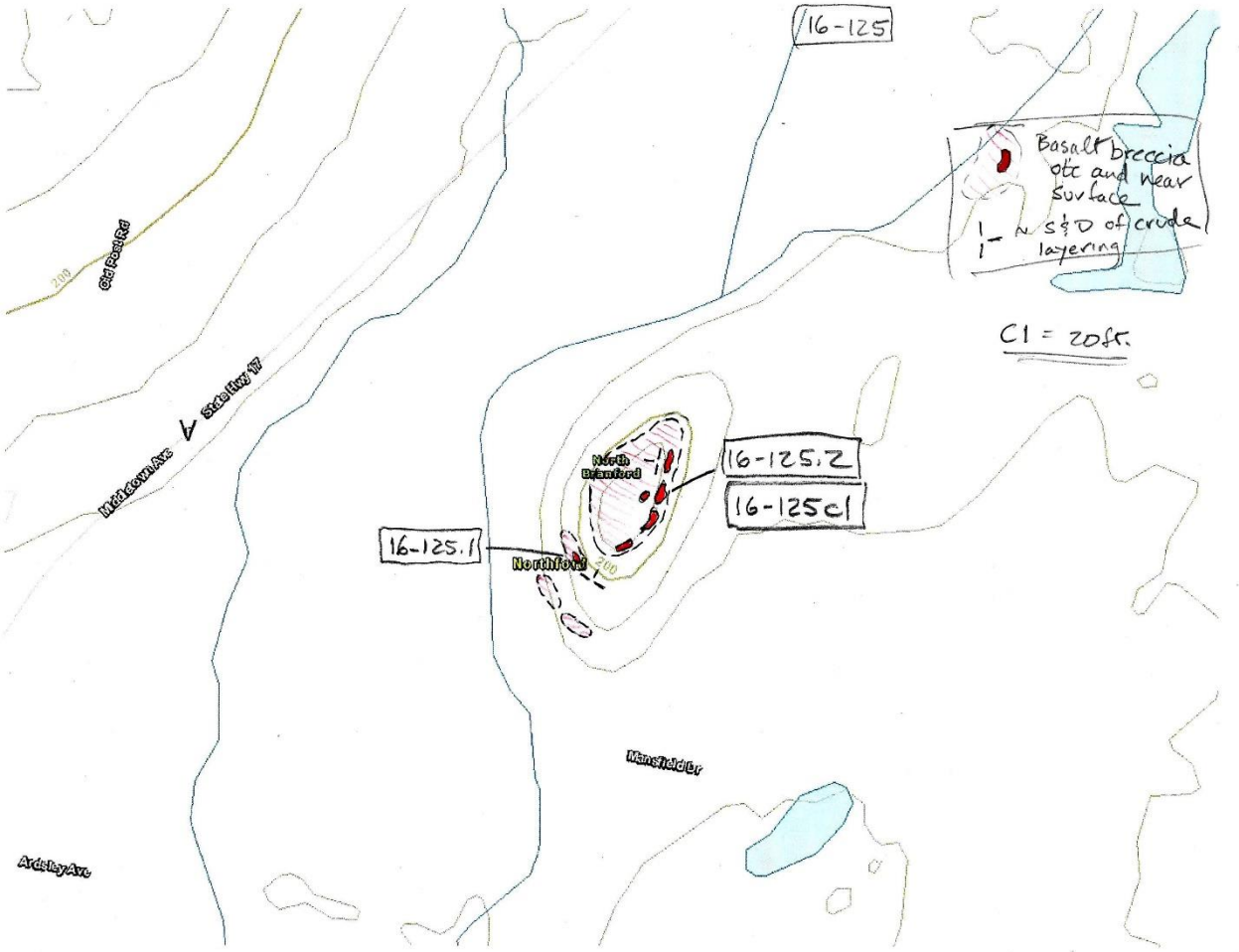

Figure I-33. Local area 126.

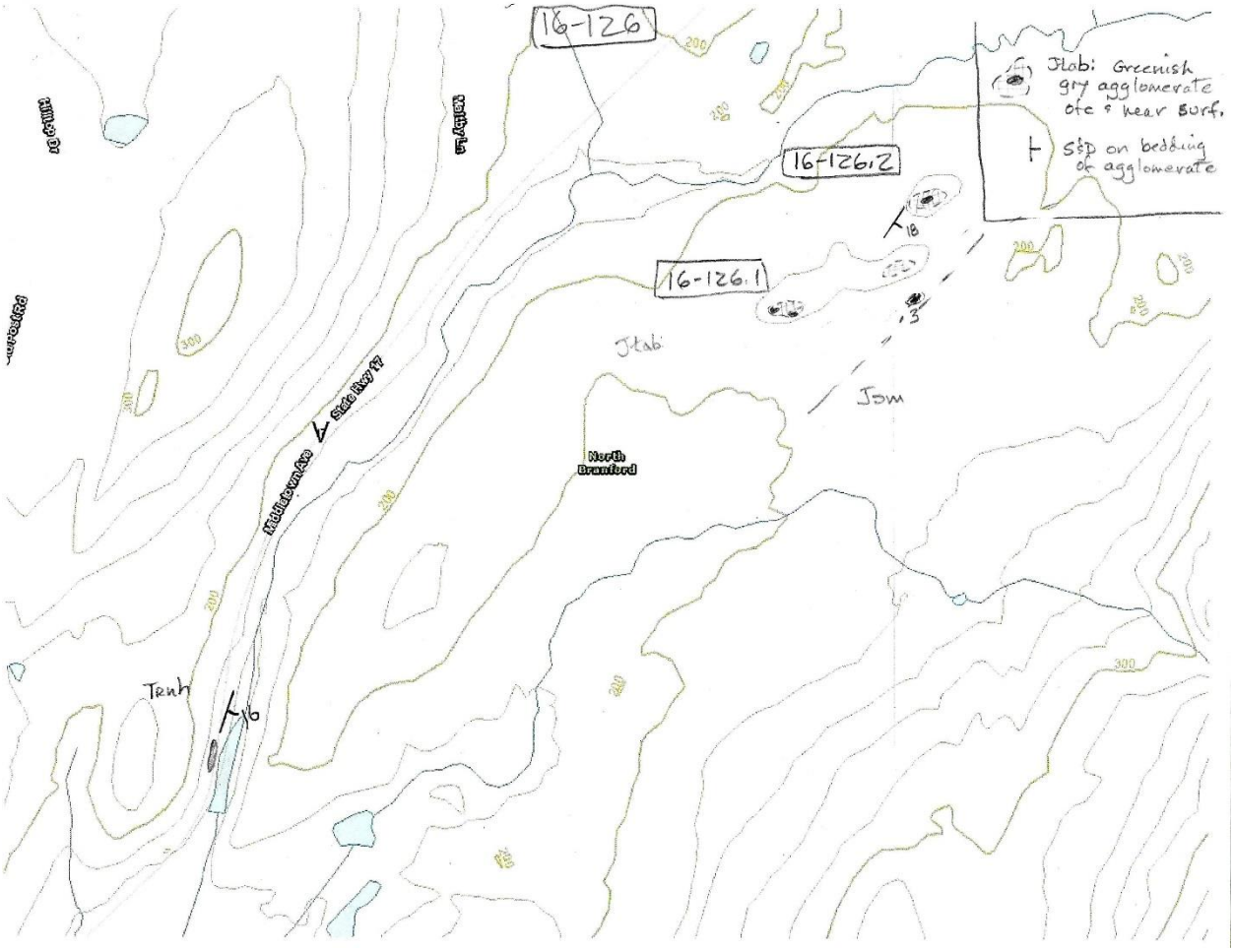

Figure I-34. Local area 127

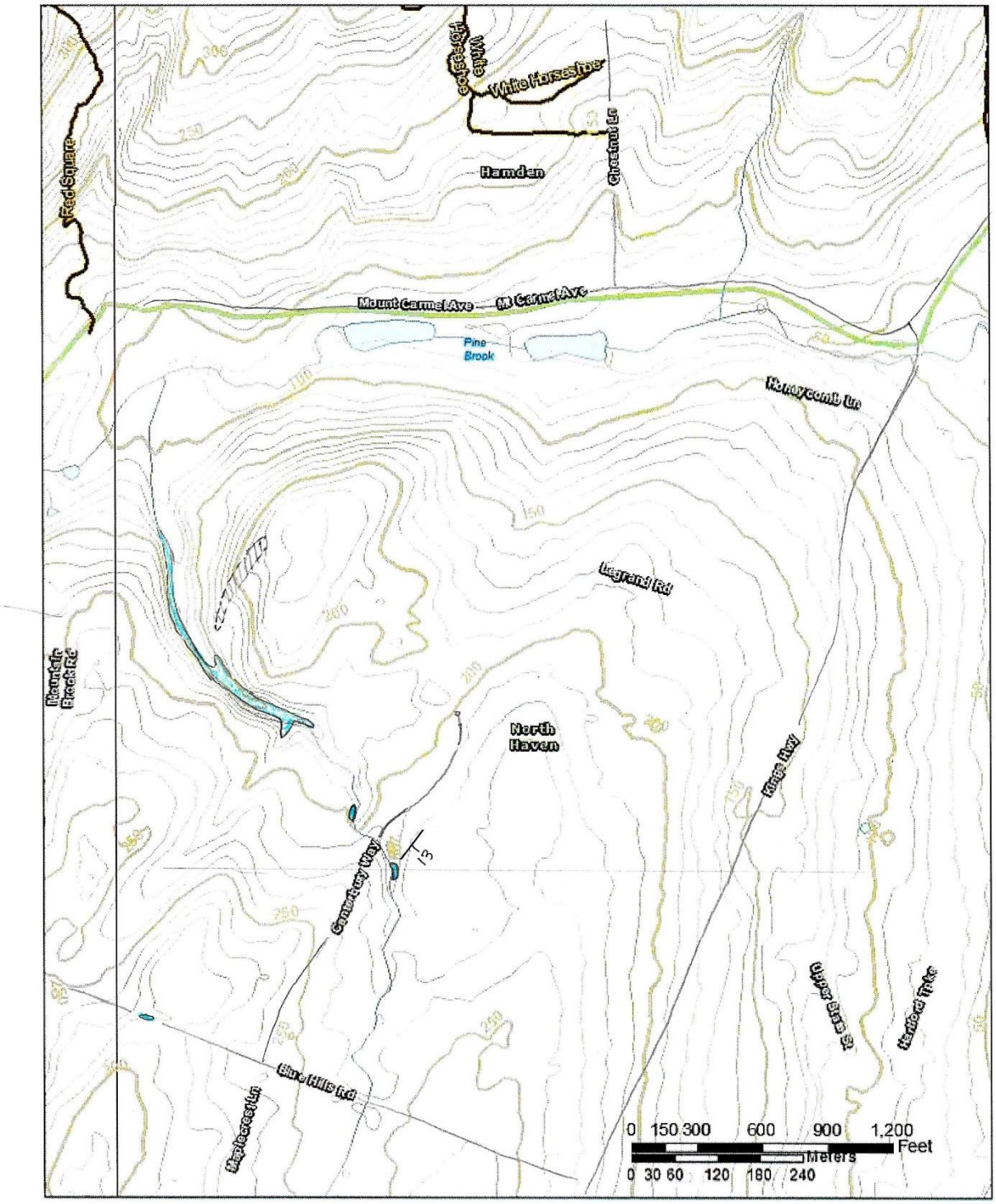

Figure I-35. Local area 128

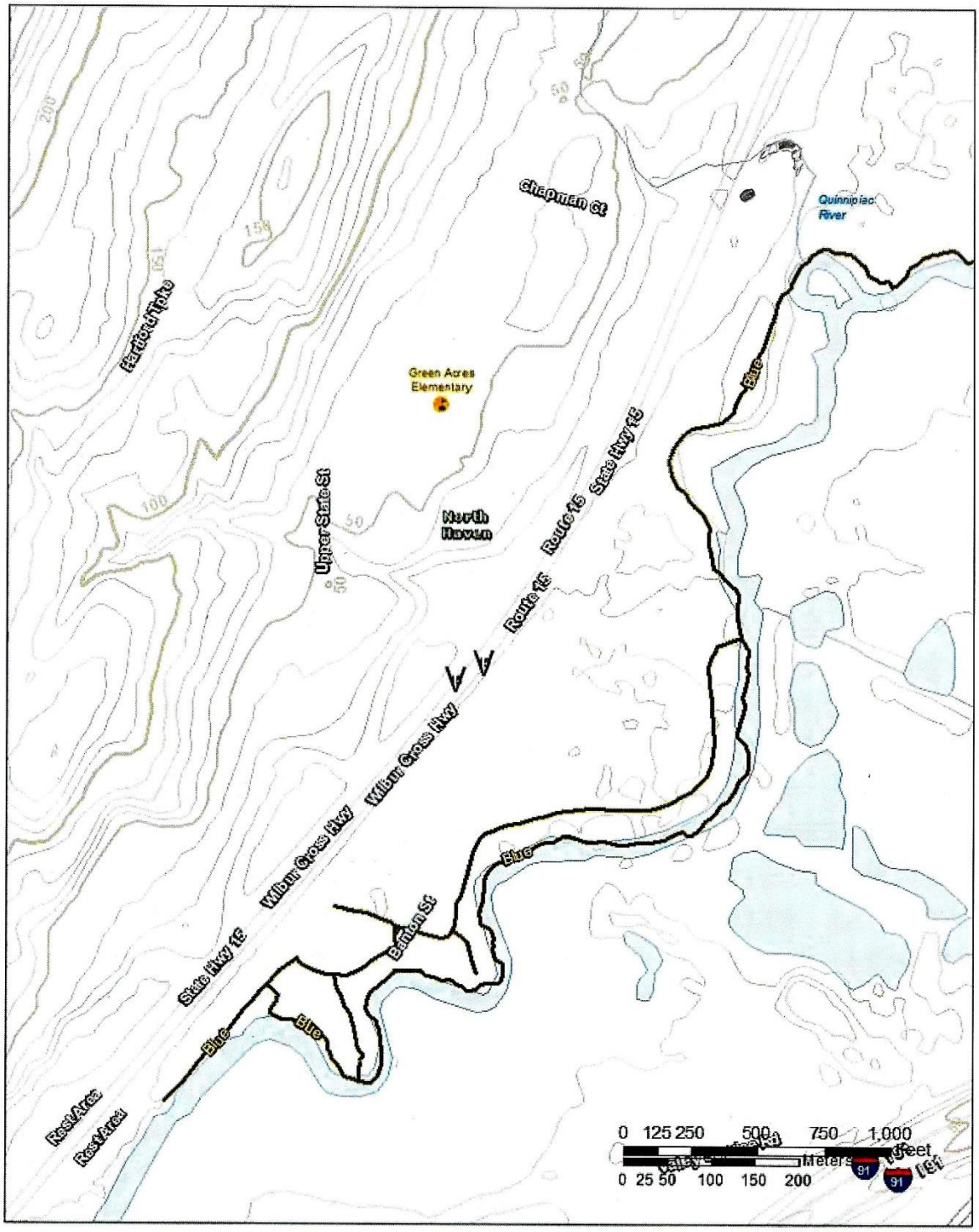

Figure I-36. Local area 129C. Rectangle is approximate area of Figure 27A

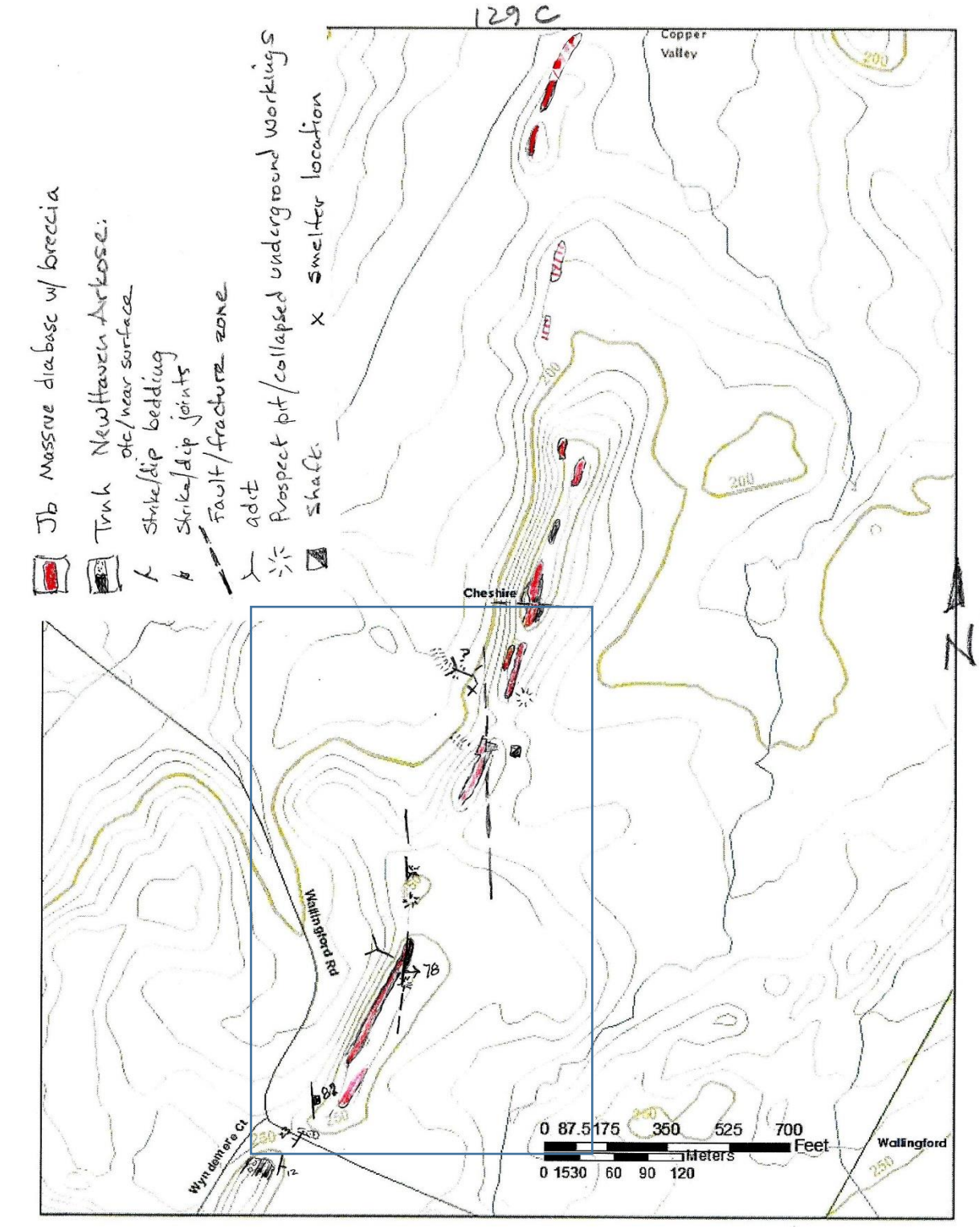

Figure I-37. Local area 129N

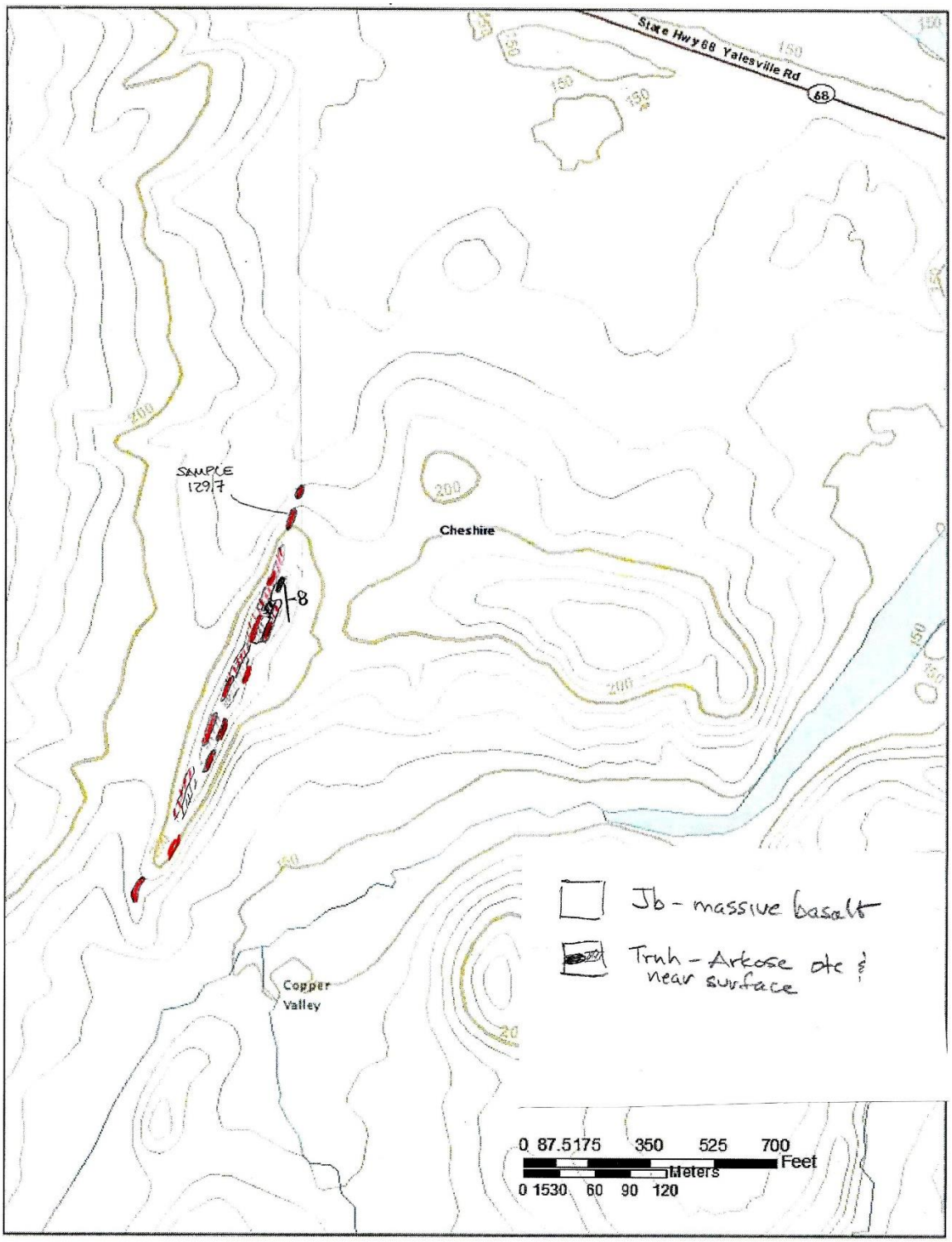

Figure I-38. Local area 129S. Blue dashed lines located cross sections shown on Figure 23 (northern) and Figure 26 (southern,)

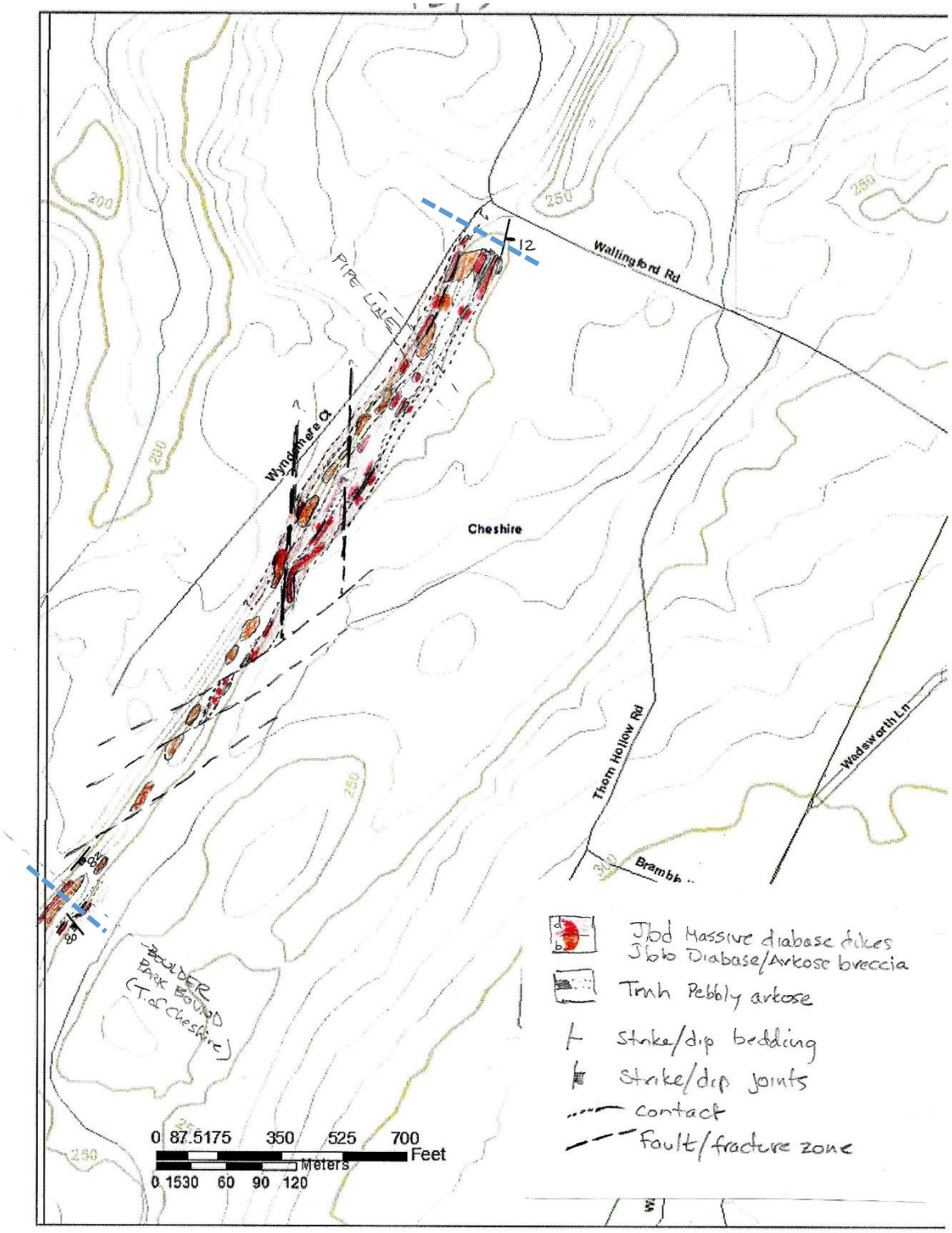

Figure I-39. Local area 130.

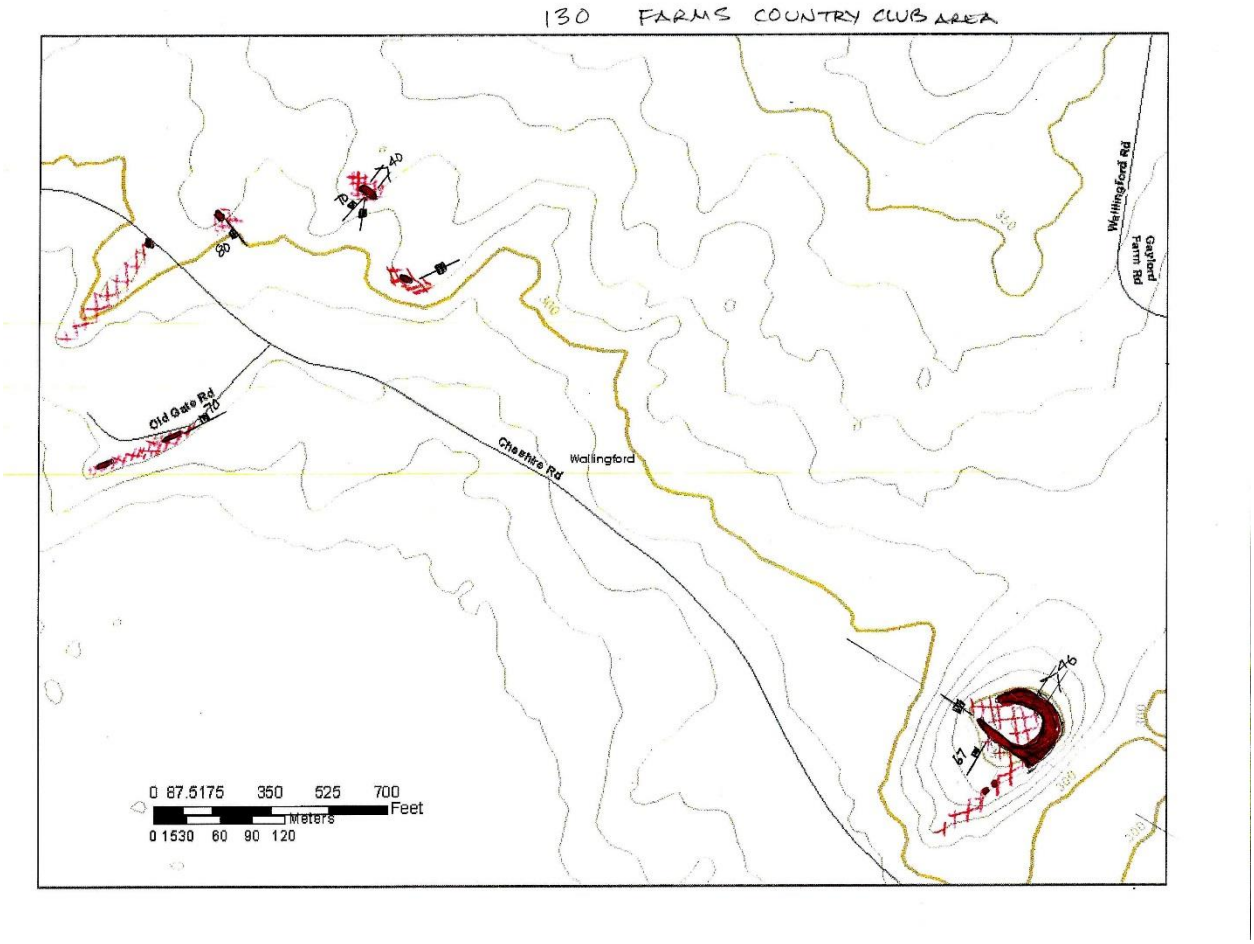

Figure I-40. Local area 130W

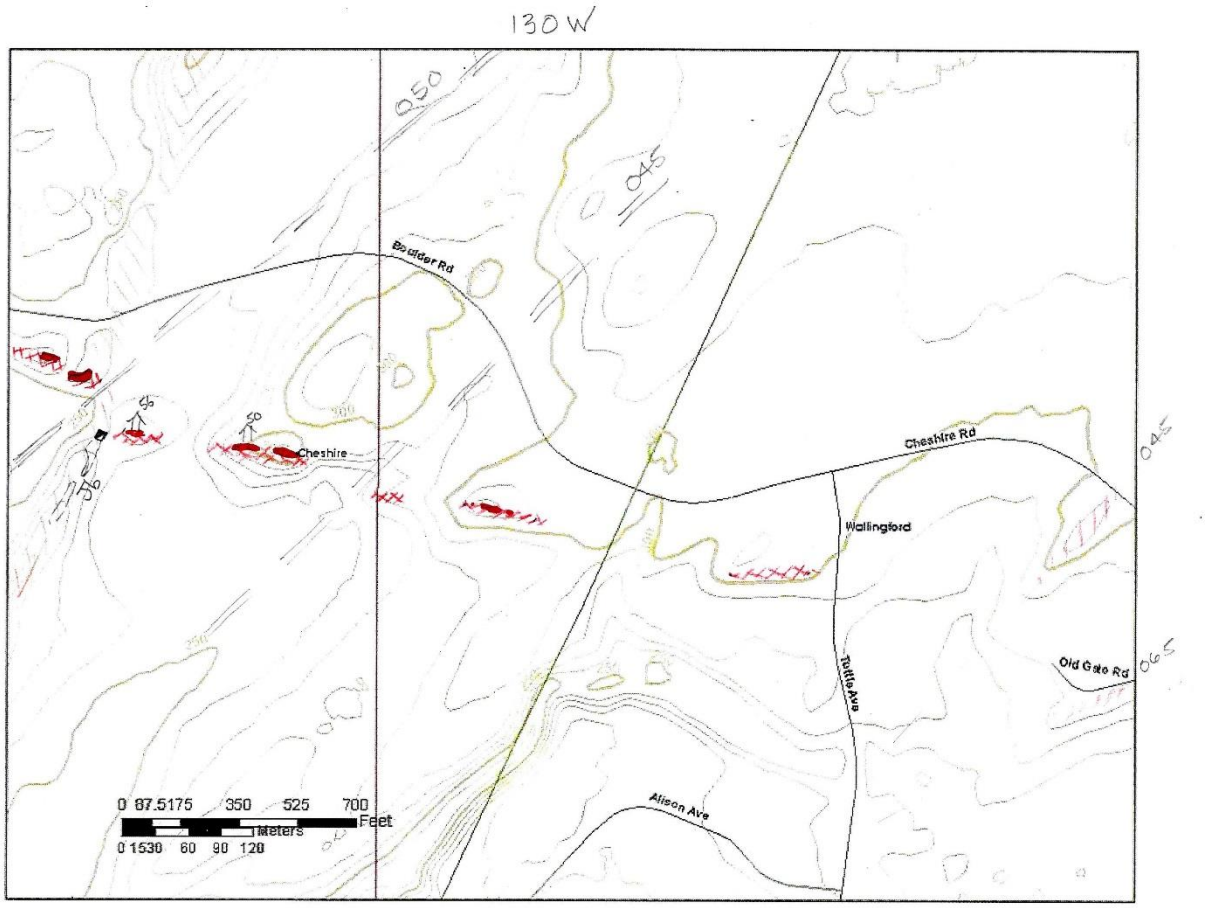

Figure I-41. Local area 131

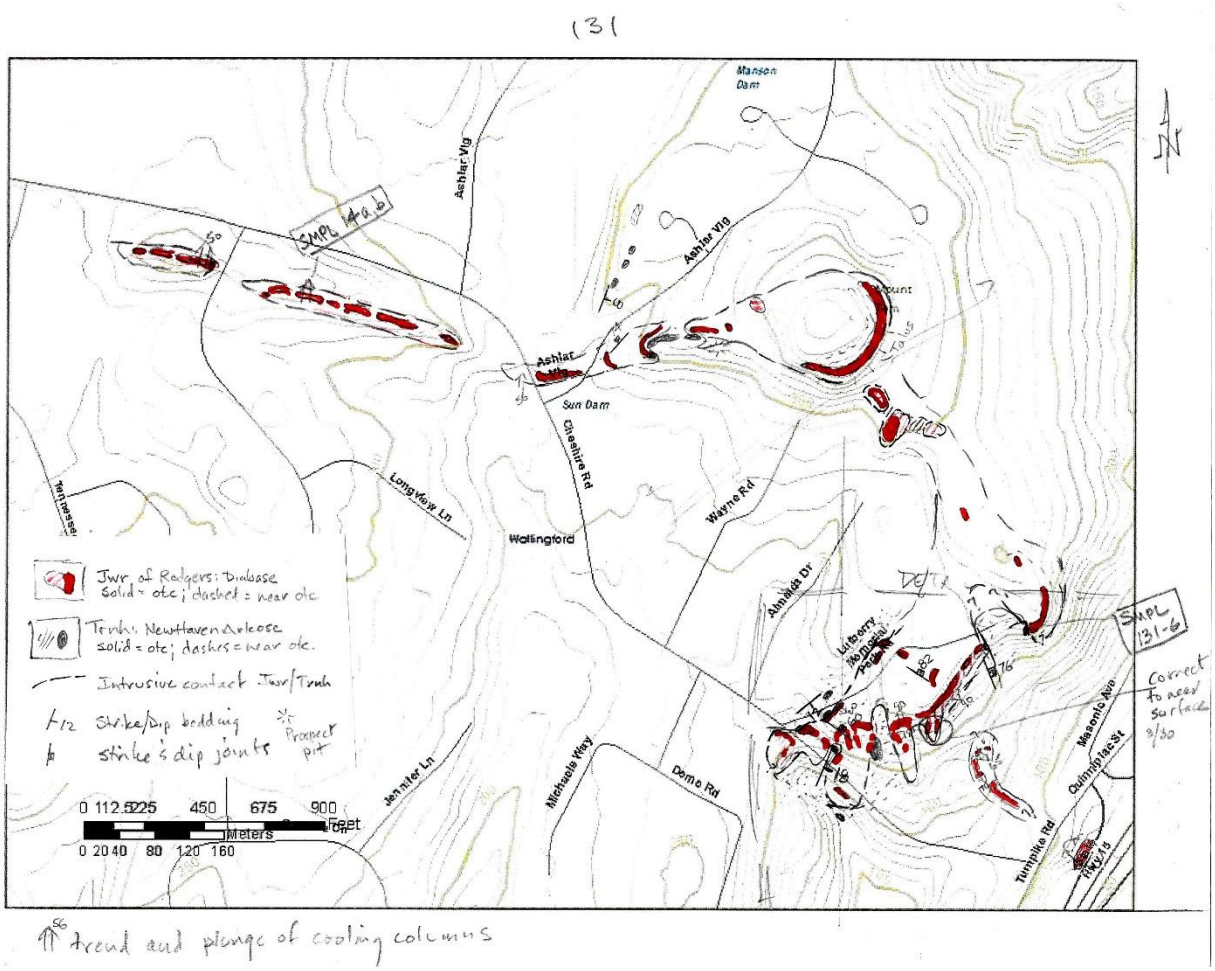

Figure I-42. Local area 131E

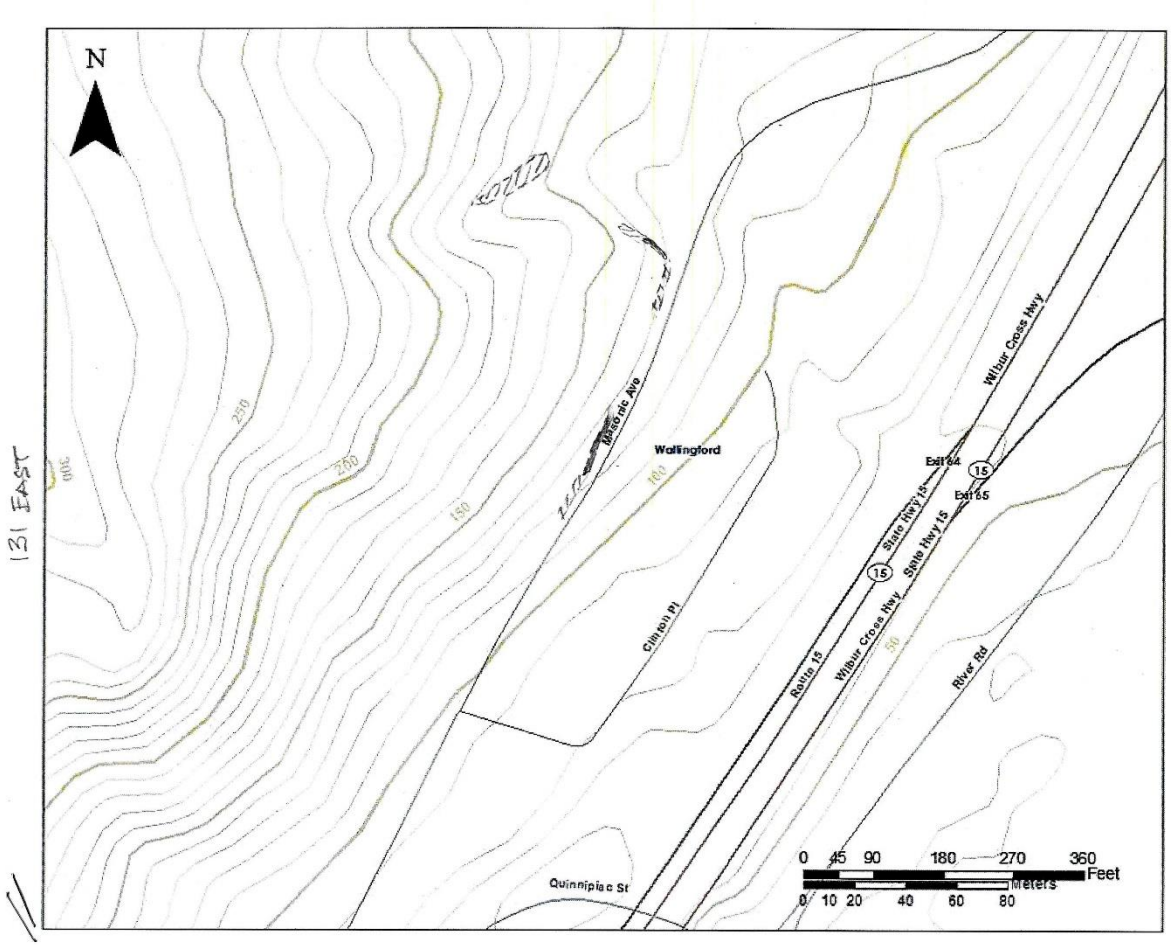

Figure I-43. Local area 131 Detail

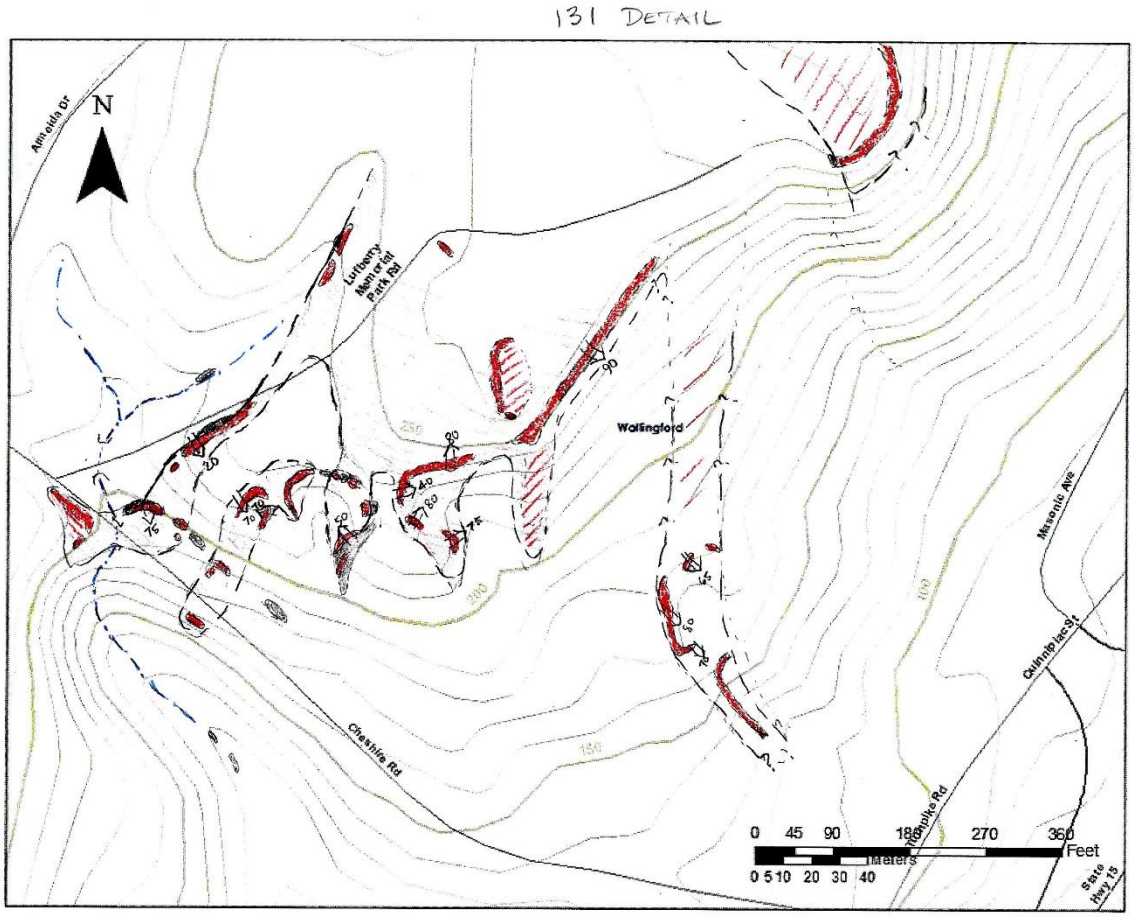

Figure I-44. Local area 132

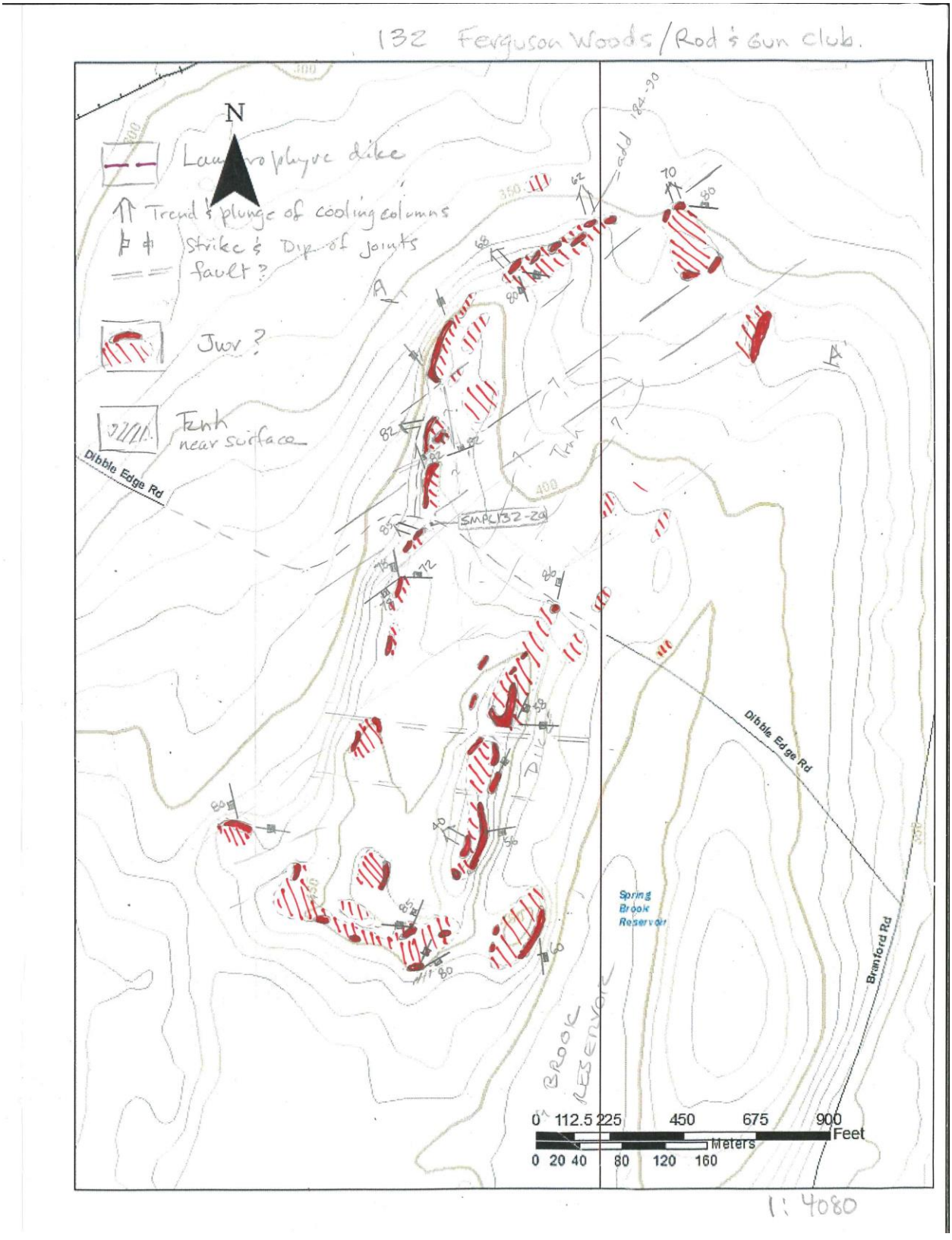

Figure I-45. Local area 132S

Figure I-46. Local area 132W. Rectangle locates approximate area of Figure 29.

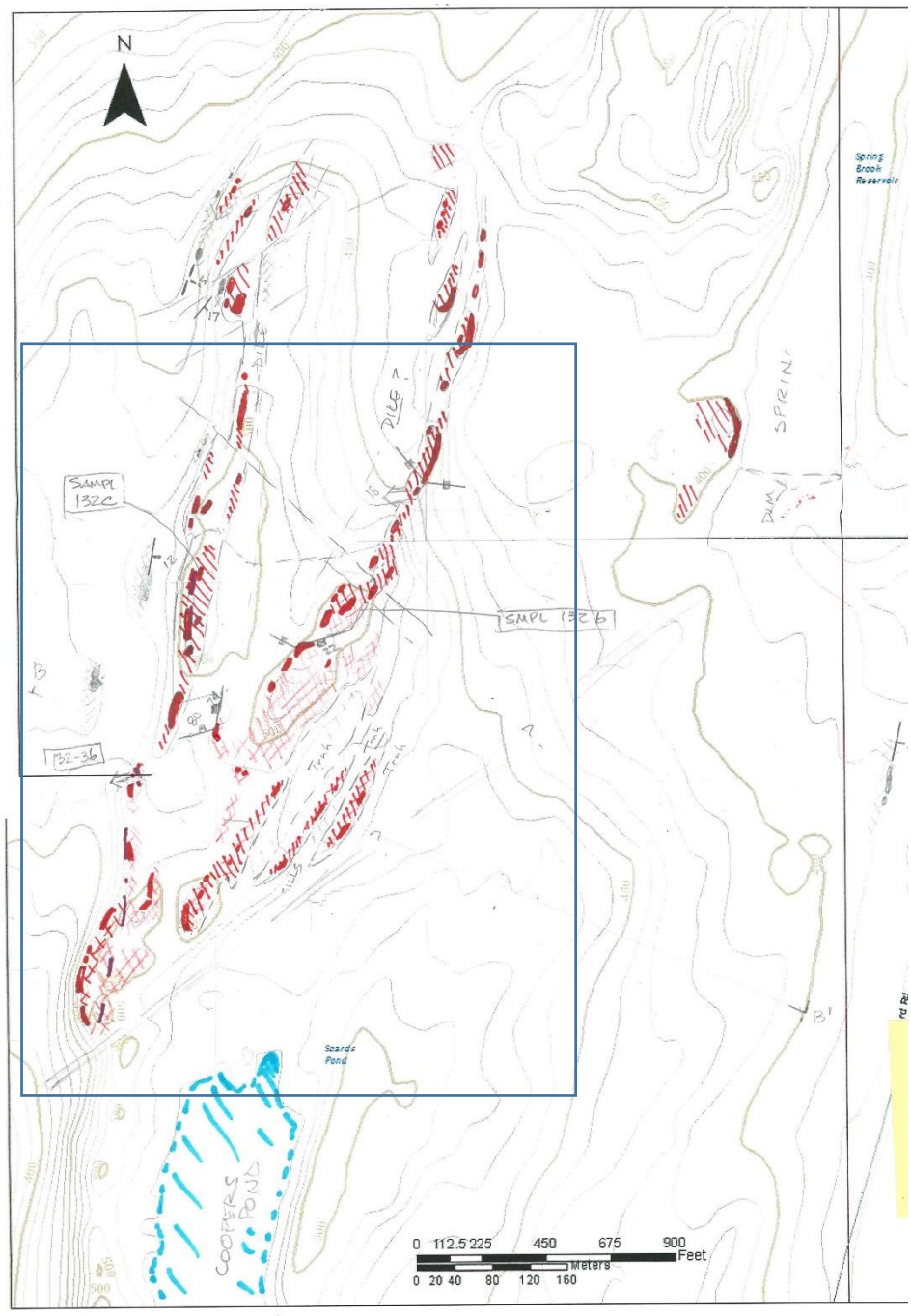

Figure I-47. Local area 133

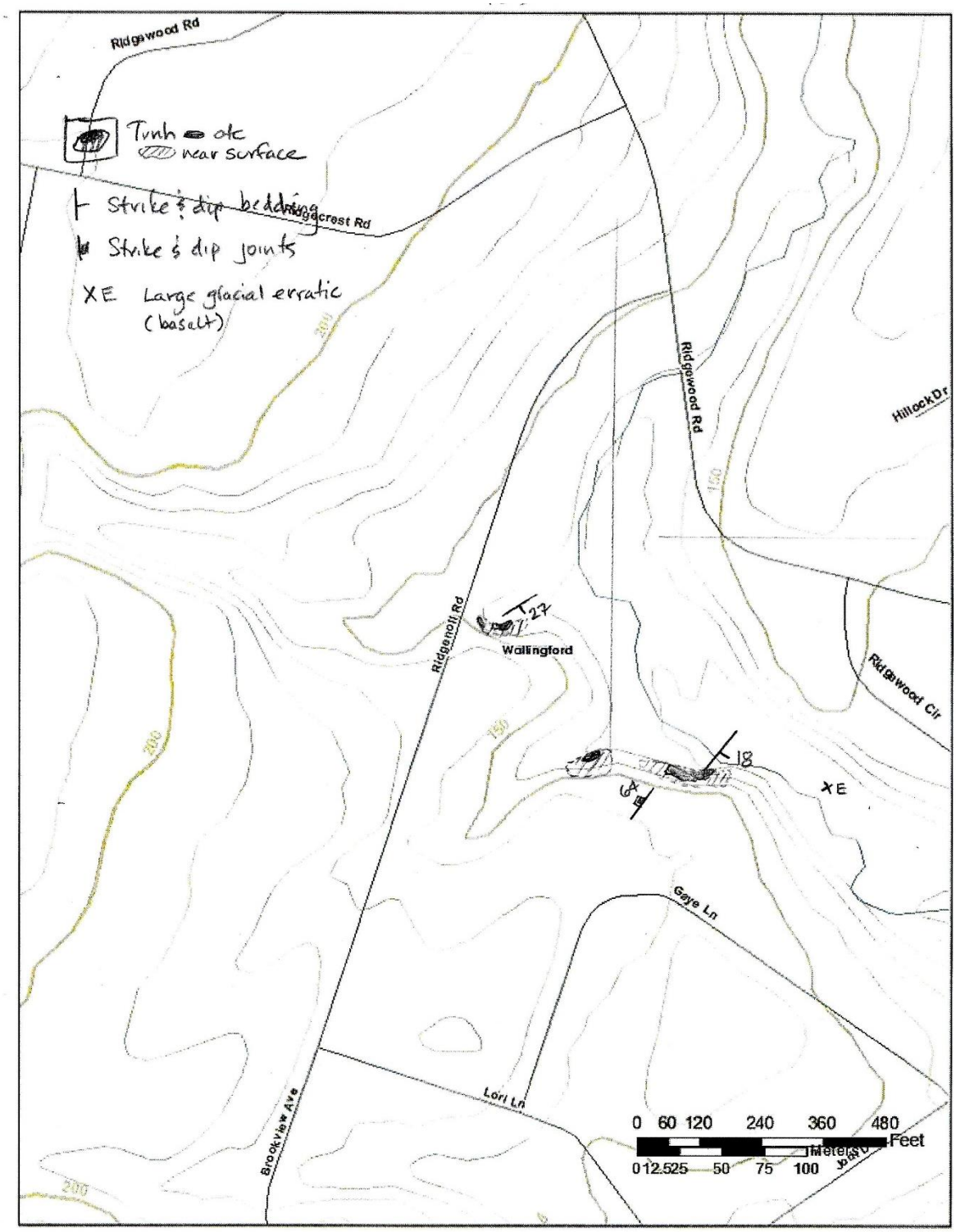

Figure I-48. Local area 135.

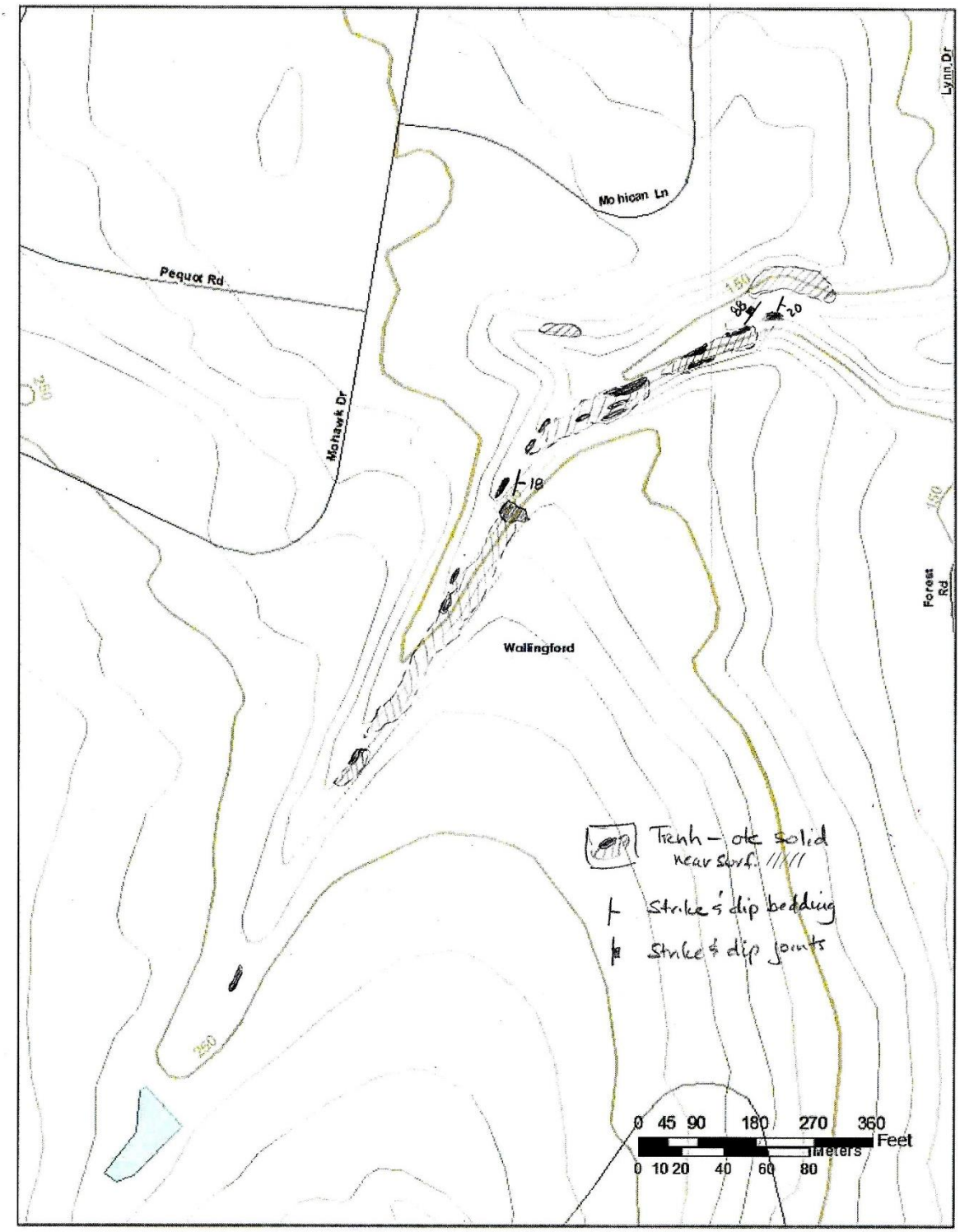

Figure I-49. Local area 136

Figure I-50. Local area 137

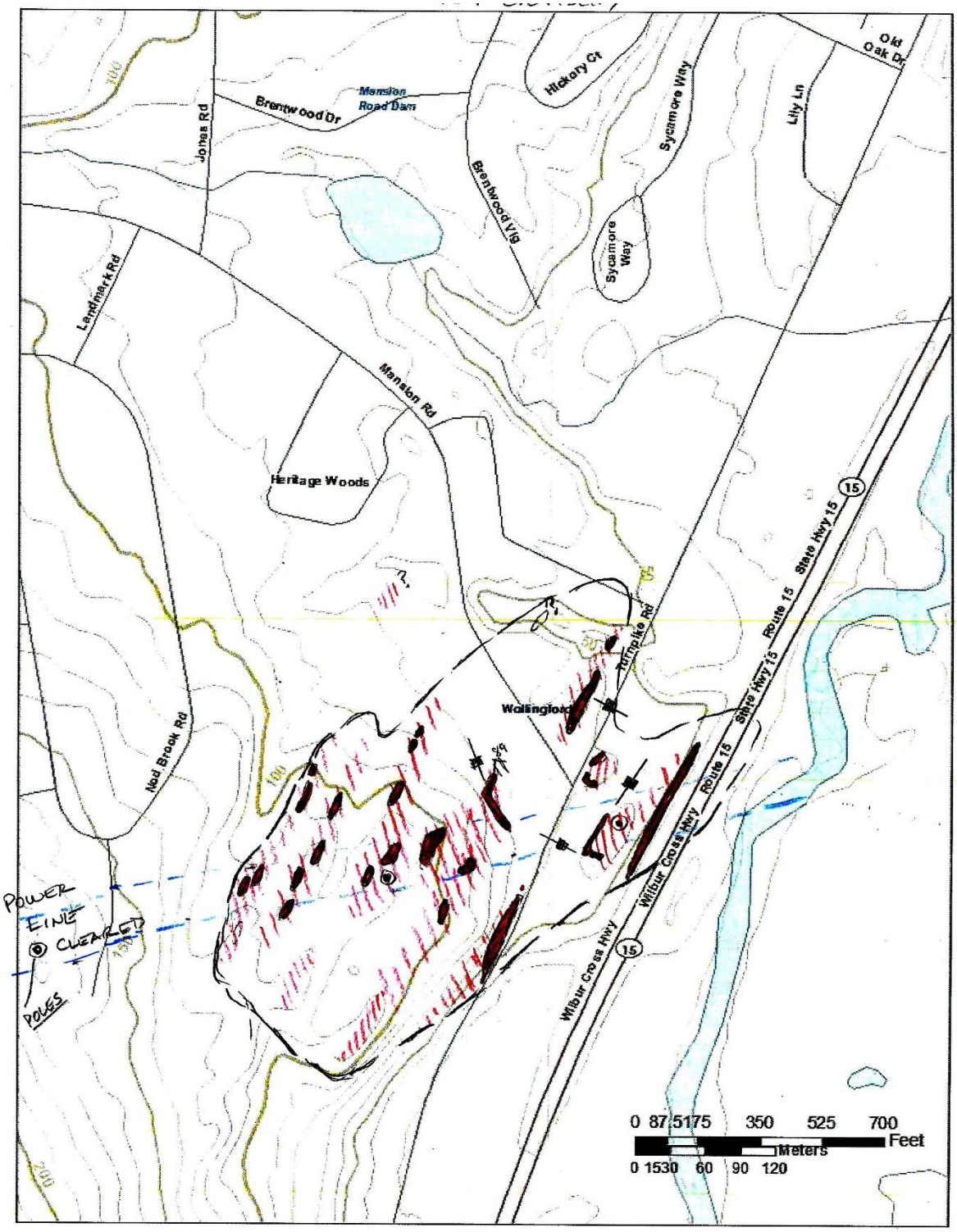

Figure I-51 Local area 138

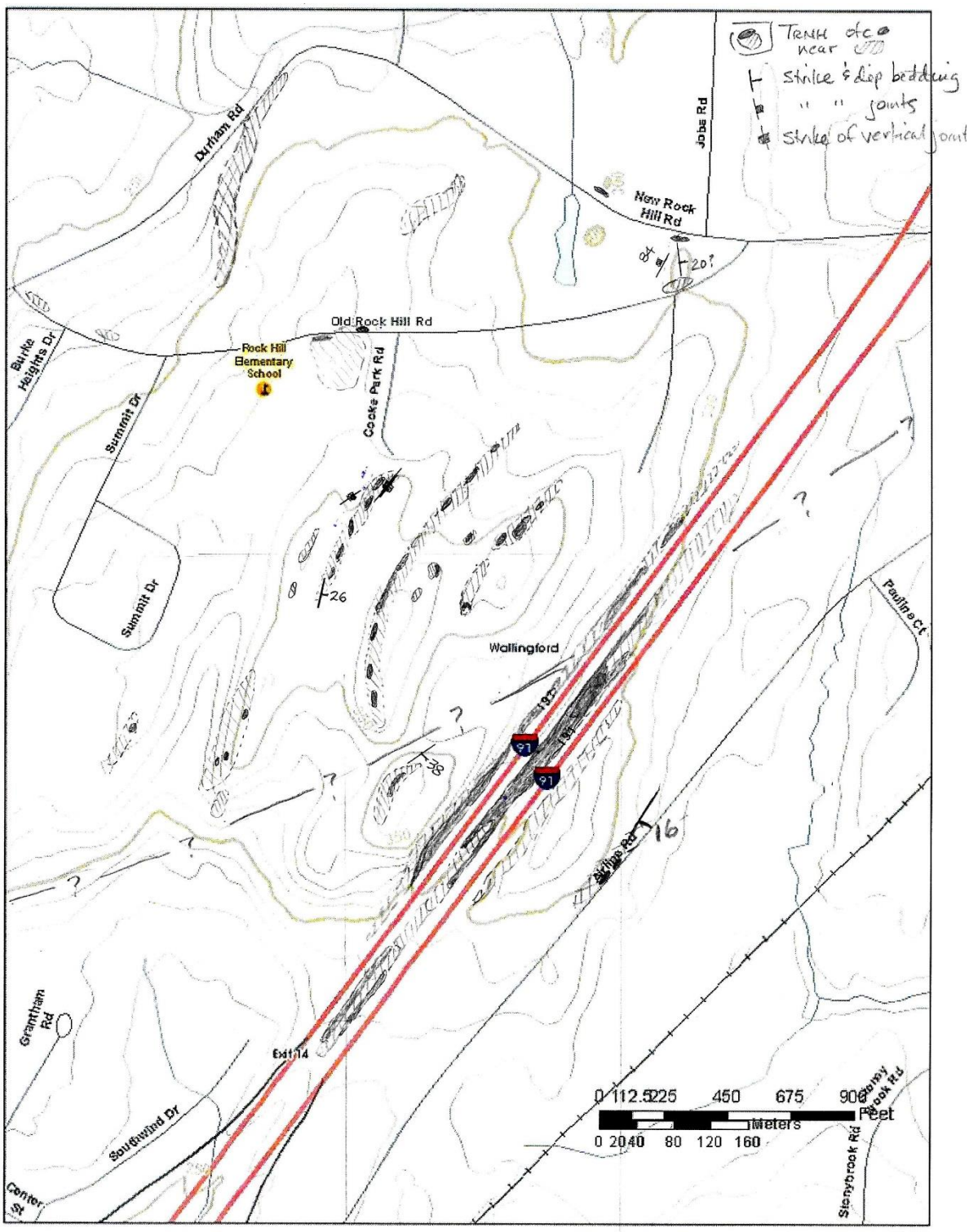

Figure I-52. Local area 139

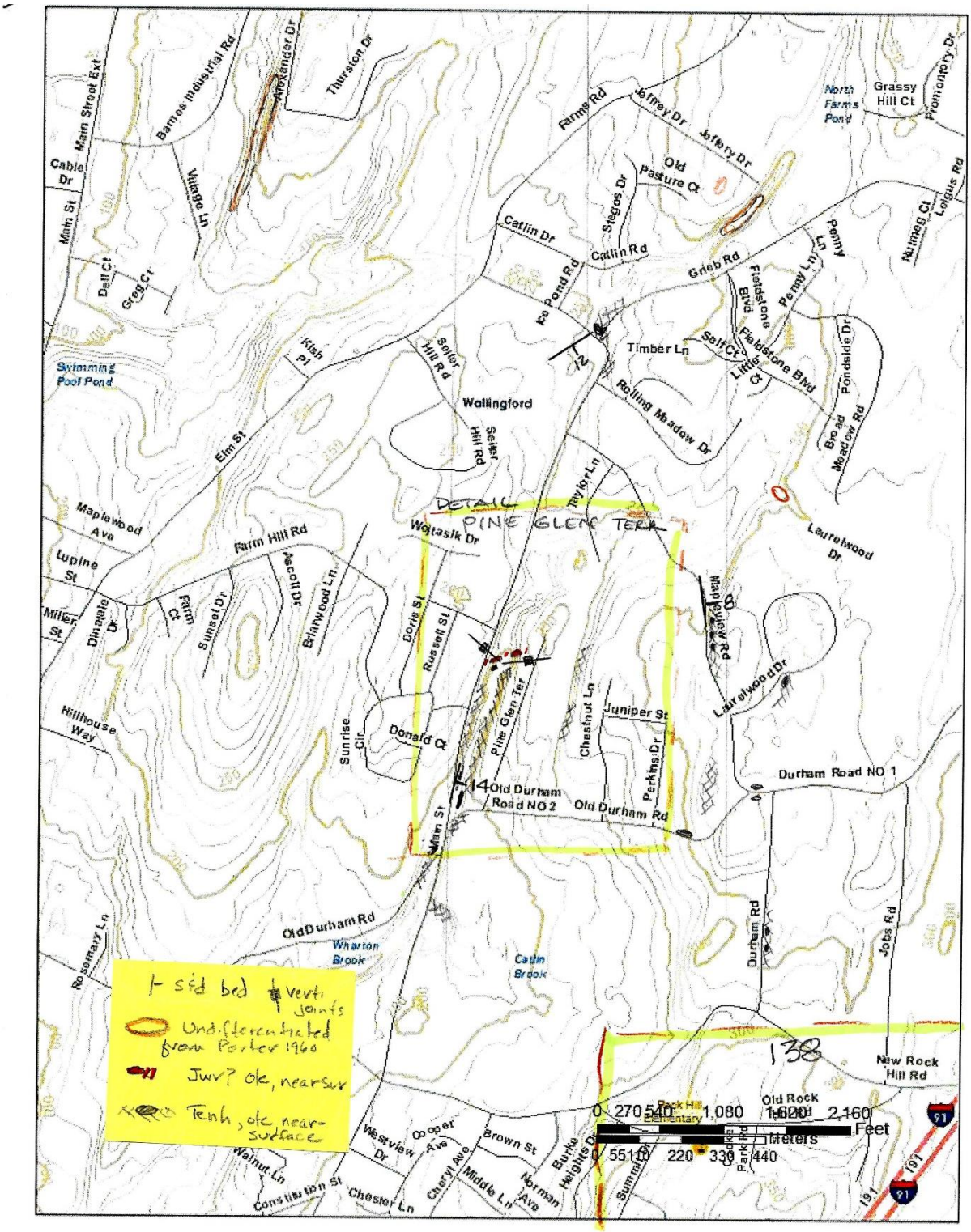

Figure I-53 139 detail: Pine Glen Terrace

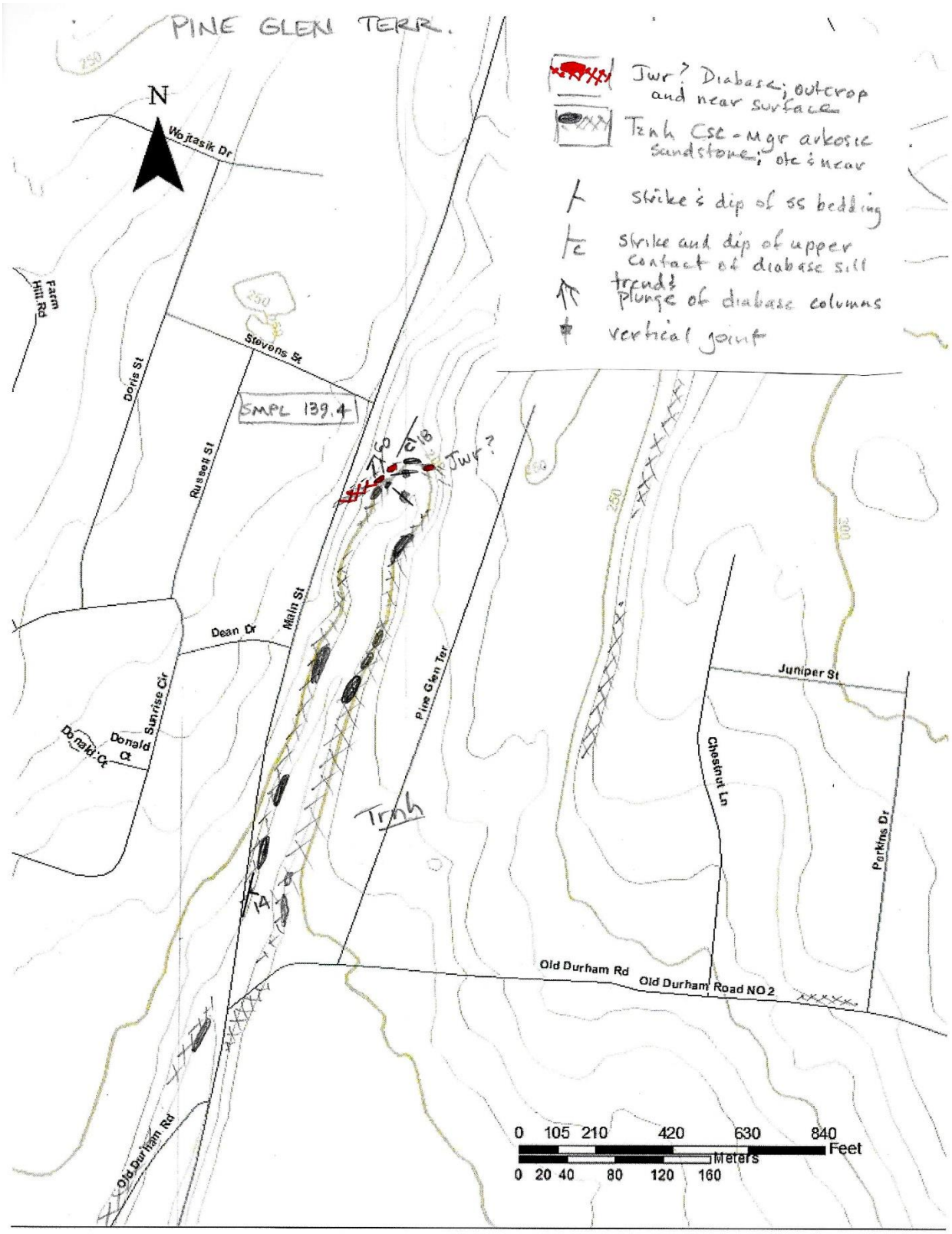

Figure I-54. Local area 140

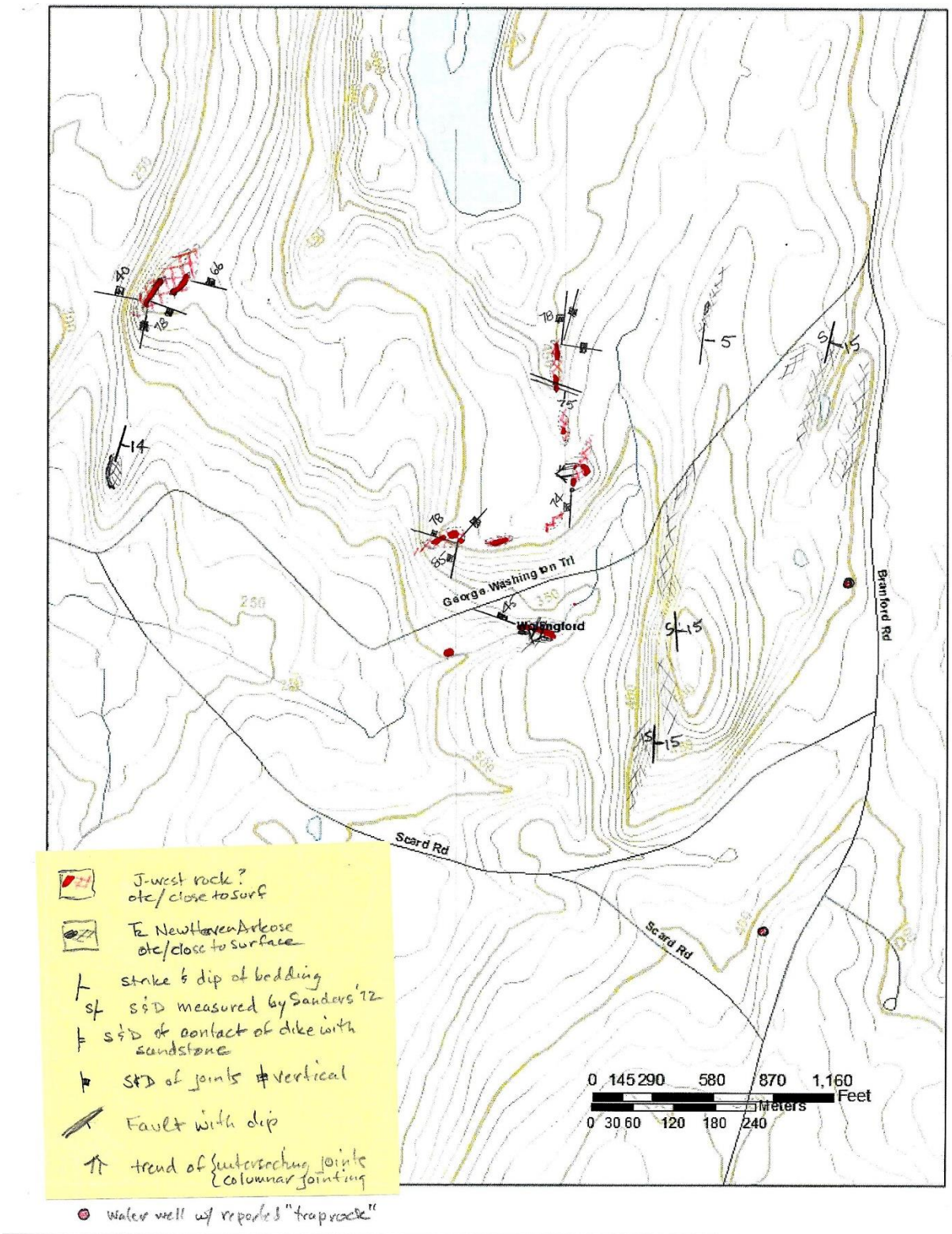

Figure I-55. Local area 141

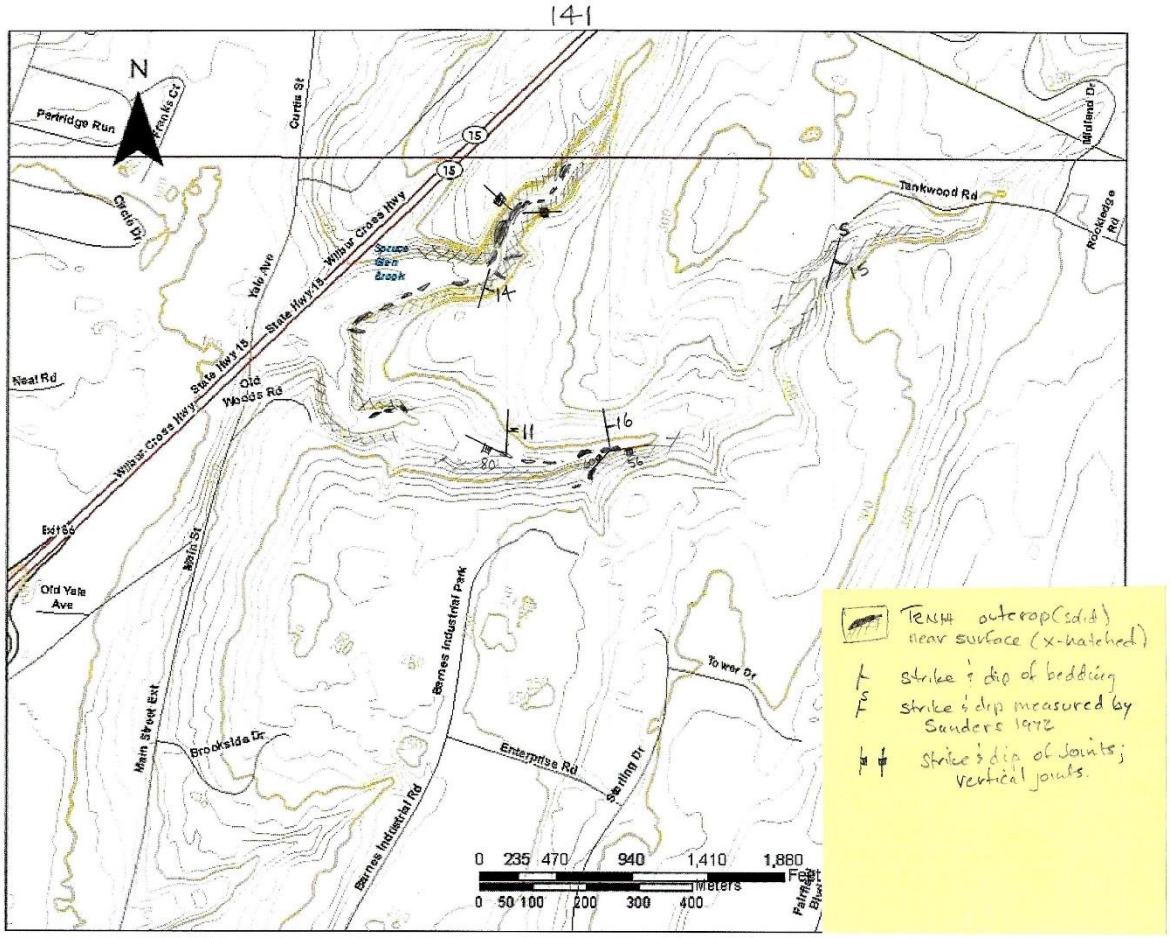

Figure I-56. Local area 142

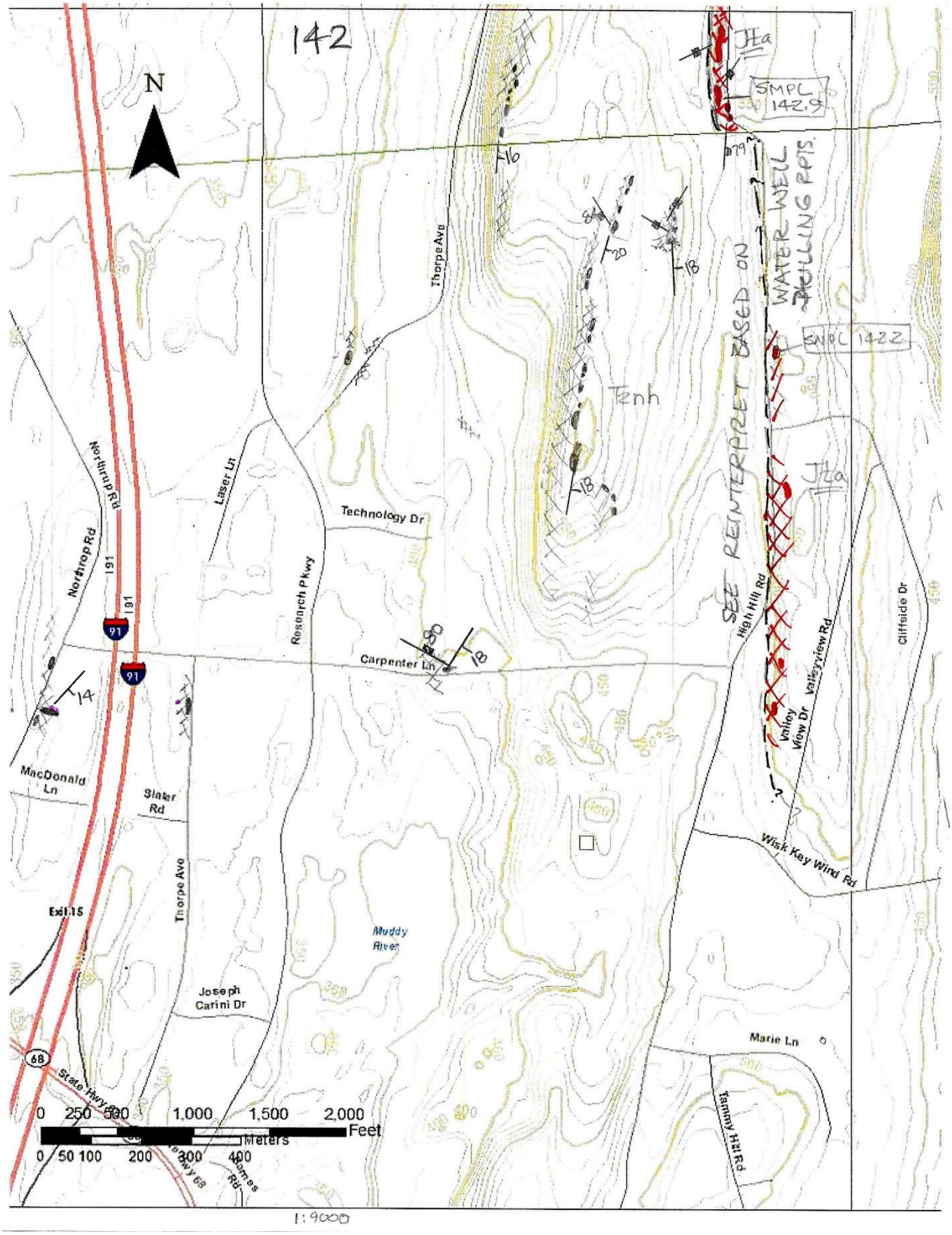

Figure I-59. Water well data, area 142 and surrounding on LiDAR DEM.

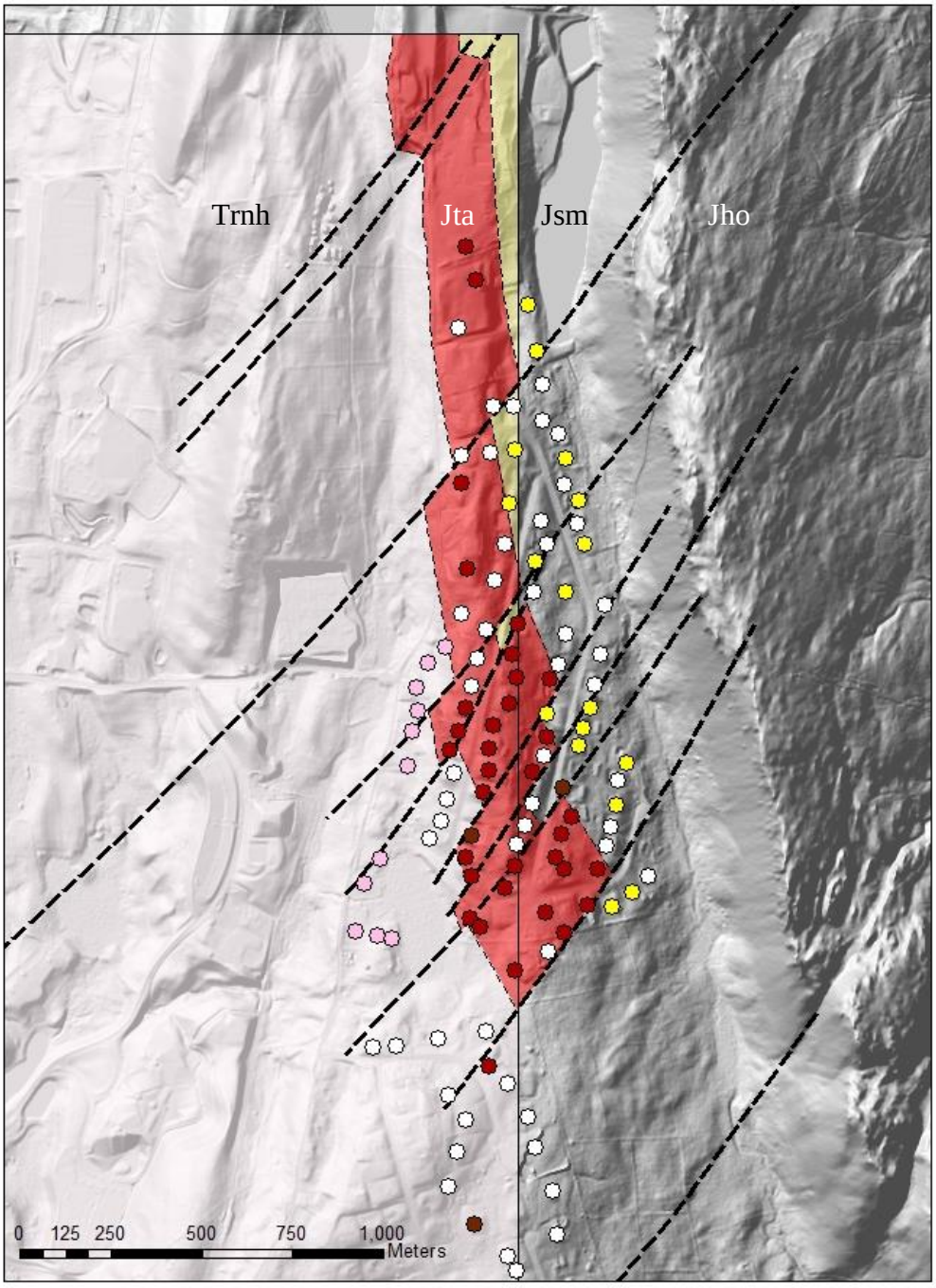

Area 142, NE corner, including part of Durham quadrangle. NE corner of Wallingford quadrangle indicated by lighter hillshaded relief. Water wells indicating interpreted formation at top of boring: pink=New Haven Arkose, red=Talcott Basalt. Yellow=Shuttle Meadow Formation, dark red=traprock of undetermined affinity, white=undetermined stratigraphy. Heavy black lines are interpreted faults.

Figure I-58. Unnamed stream north of Rte 17 and north-east of local area 126.

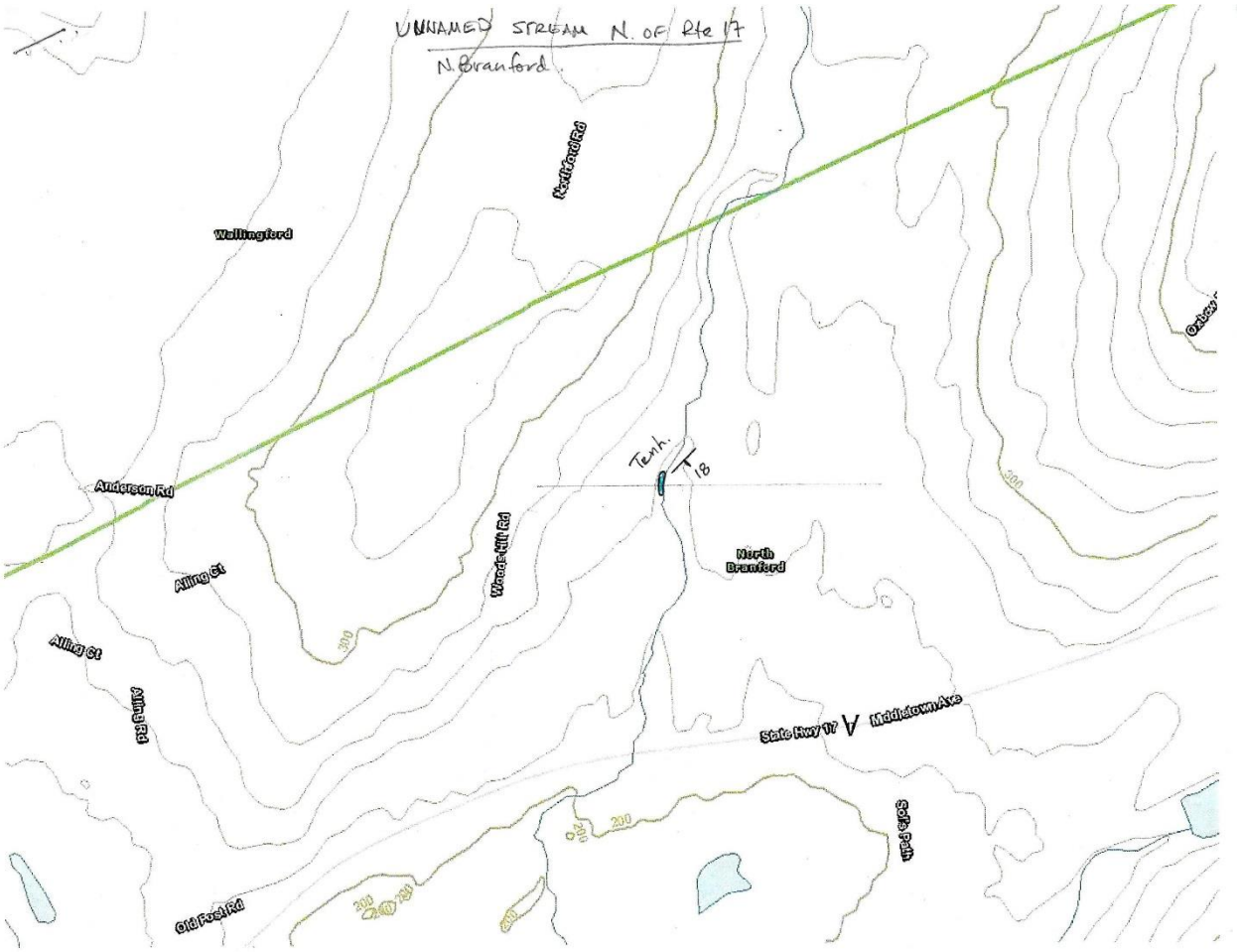

Appendix II. Sample Locations

Area	Number	Lithology	Latitude	Longitude	Rodgers 1985	Current interpretation	Use
100	100-2	Diabase	41.441804	-72.778998	Jb?	Jwrj	TS + XRF
100	100-7	Magnetic Diabase	41.4411703	-72.779104	Jb?	Jwr	ThinSect.
100	100-8	Diabase	41.440986	-72.779648	Jb?	Jwr?	ThinSect.
100	100-10	Diabase	41.440187	-72.780046	Jb?	Jwr	TS + XRF
101	101-3	Diabase	41.436466	-72.7801202	Jb?	Jwr	TS + XRF
102	102-1	Diabase	41.434186	-72.78255	Jb?	Jwr	XRF
102	102-2	Diabase	41.42757	72.784417	Jb?	Jwr	XRF
103	16-103.10	basalt	41.37875	-72.80838	Trnh	Jta	TS + XRF
103	16-103.13	agglomerate?	41.37902	-72.8078	Trnh	Jtaa	Thin section
103b	16-103b.2	Diabase	41.38467	-72.80352	Jta	Jwr	TS + XRF
104	16-104a	massive diabase, dike 1	41.3806	-72.8256	Jb	Jwr	TS + XRF
104	16-104b	Amydgal-diabase, dike 2	41.3806	-72.8256	Jb	Jwrj	TS + XRF
104	16-104c	sandstone	41.3806	-72.8256	Trnh	Trnh	TS
104	16-104d	sandstone	41.3806	-72.8256	Trnh	Trnh	TS
104	16-104.6	part-melted ss?	41.3806	-72.8256	Trnh	Trnh	TS
106	16-106.2	Diabase	41.4329	-72.7881	Jb?	Jwr	TS + XRF
107	16-107	diabase	41.4164	-72.7991	Jb	Jwr	TS + XRF
107b	16-107b-1	diabase	41.42076	-72.79493	Jb	Jwr	XRF
107b	16-107b-2	diabase	41.41795	-72.79473	Jb	Jwr	XRF
107b	16-107b.10	amygdaloidal diabase	41.41292	-72.79647	Trnh	Jwr	TS
108	108.3	diabase	41.42007	-072.78690	Jb	Jwr	TS + XRF
108	16-108.4	breccia	41.41592	-72.78778	Trnh/Jb	Trnh/Jwr	TS + XRF
108	16-108.5	diabase	41.41653	-72.7873	Jb	Jwr	TS
108	108.82	diabase			Jb	Jwr	TS
108b	16-108b	part-melted ss?	41.422	-72.786	Jb	Trnh	TS
108b	16-108b	Part-melted ss	41.422	-72.786	Jb	Trnh	TS
108b	16-108b1	ss/diabase contact	41.42063	-72.78727	Jb	Trnh/Jwr	TS
108b	16-108b2	ss/diabase contact	41.42063	-72.78727	Jb	Trnh/Jwr	TS
111	16-111	basalt	41.3903	-72.7767	Jho	Jho	TS + XRF
112	16-112.1	diabase	41.3824	-72.8262	Jb	Jwr	TS + XRF
112	112.7	diabase	41.38682	-72.82726	Jb	Jwr	TS
112	16-112?	melted sed?			Jb	Trnh	TS
113	16-113.3	basalt	41.39896	-72.77003	Jho	Jho	TS + XRF
113	16-113.4	basalt	41.4007	-72.7683	Jho	Jho	TS + XRF
113	16-113.7	basalt	41.40007	-72.7663	Jho	Jho	TS + XRF
114	16-114.2	basalt	41.3794	-72.7577	Jho	Jho	TS + XRF
113	113.16	lamprophyre	41.40058	-072.76843		K?l	TS + XRF
115	115.3	ferrodiorite	41.38138	-072.76857	Jho	Jho	TS
115	115.4	basalt			Jho	Jho	TS + XRF
115	16-115.1	basalt	41.3784	-72.7655	Jho	Jho	TS + XRF
115	16-115.2	basalt	41.3087	-72.7672	Jho	Jho	TS + XRF
116	16-116.2	diabase	41.42475	-72.79695	Jb?	Jwr	TS + XRF

Area	Number	Lithology	Latitude	Longitude	Rodgers 1985	Current interpretation	Use
116	16-116.5	diabase	41.4214	-72.7974	Trnh	Jwr	TS + XRF
117	16-117.10	diabase	41.41418	-72.80245	Jb	Jwr	TS + XRF
118	16-118.4	diabase	41.40385	-72.8157	Jb	Jwr	TS + XRF
118w	16-118w-2c	basalt clast					XRF
119	16-119.2	diabase	41.3996	-72.8201	Jb	Jwr	TS + XRF
121	16-121	basalt	41.3872	-72.7756	Jho base	Jho	TS
121	16-121.1a	f-g sandst	41.38703	-72.77653	Jho	Jsm	TS
121	16-121.1b	c-g sandst	41.38703	-72.77653	Jho	Jsm	TS
122	16-122.3	diabase	41.4349	-72.87458	Jwr	Jwrj	TS + XRF
122	16-122.11	diabase	41.43155	-72.8694	Jwr	Jwrj	TS + XRF
122	16-122.11	sandstone	41.43155	-72.8694	Jwr	Trnh	TS
122	16-122-14	diabase	41.43202	-72.85938		Jwrj	XRF
122	16-122.15	sandstone	41.42943	-72.8618	Trnh	Trnh	TS
122	16-122.17	diabase	41.43307	-72.85913	Jwr	Jwrj	TS + XRF
122s	16-122s-2	sandstone	41.43237	-72.87312		Trnh	TS
124	16-124.1	basalt (124.3)	41.3748	-72.8172	Jb	Jwr	TS + XRF
125	16-125.1	agglomerate?	41.3937	-72.7879	Jta	Jtab	TS
125	16-125.2(1)	agglomerate?	41.39373	-72.78782	Jta	Jtab	TS
125	16-125.2(2)	agglomerate?	41.39373	-72.78782	Jta	Jtab	TS
125	16-125cl	basalt clast	41.39373	-72.78782	Jta	Jtab	XRF
126	16-126.1-1	agglomerate?	41.4028	-72.77782	Jsm	Jtab	TS
126	16-126.1-3	agglomerate?meltSed?	41.4028	-72.77782	Jsm	Jtab	TS
126	16-126.2	agglomerate?	41.4041	-72.7757	Jsm	Jtab	TS
126	16-126.2	agglomerate?	41.4041	-72.7757	Jsm	Jtab	TS
129	129-7	Diabase	41.494826	-72.866284	Jb	Jb	TS + XRF
129	129-8	Fused ss	41.494482	-72.866358	Trnh	Trnh	ThinSect.
130W	130W	Diabase	41.469817	-72.876109	Jwr	Jwrj	TS + XRF
131	131-14a	Diabase	41.462796	-72.849073	Jwr	Jwrj	TS + XRF
131	131-14B	Diabase	41.462796	-72.849073	Jwr	Jwrj	TS + XRF
131	131-6	Diabase	41.459459	-72.839176	Jwr	Jwrj	TS + XRF
132	132-2a	Diabase	41.4644325	-72.7518601	Jb?	Jwrj	TS + XRF
132	132-36	Lamprophyre	41.455401	-72.759033	Jb?	K?l	XRF
132	132-36A	Lamprophyre	41.455401	-72.759033	Jb?	K?l	ThinSect.
132	132-36B	Lamprophyre	41.455401	-72.759033	Jb?	K?l	ThinSect.
132	132-43	Diabase	41.452261	-72.759438	Jb?	Jwrj	TS + XRF
132	132-43a	clastic dike	41.4521413	-72.7592931			Thin Sect.
132	132-b	Diabase	41.457099	-72.756251	Jb?	Jwr	TS + XRF
132	132-c	Diabase	41.457324	-72.7580936	Jb?	Jwrj	TS + XRF
136	136-1	Diabase	41.4562003	-72.840657	Trnh	Jwrj	TS + XRF
136	136-4	Diabase	41.457215	-72.838495	Trnh	Jwrj	TS + XRF
137	137-1	Diabase	41.440302	-72.849726	Jwr	Jwrj	TS + XRF
140	140-1	Diabase	41.445321	-72.755908	Jb	Jwrj	TS+XRF
140	140-3A	Breccia	41.446618	-72.756288	Jb?	Jwrj	ThinSect.

Area	Number	Lithology	Latitude	Longitude	Rodgers 1985	Current interpretation	Use
140	140-3B	Breccia	41.446618	-72.756288	Jb?	Jwrj	ThinSect.
142	142-2	Basalt	41.493966	-72.751837	Jta	Jta	TS + XRF
142	142-9	Basalt	41.4981875	-72.7529928	Jta	Jta	TS + XRF

Appendix III: X-ray Fluorescence Data

	100-2 Jwrj	100-10 Jwrj	101-3 Jwr	16-102.1 Jwr	16-102.2 Jwr	16-103b 2 Jwr	16-103. 10 Jta	16-104a Jwr	16-104b Jwrj
	Unnormalized Major Elements (Weight %):								
SiO2	52.09	51.26	51.66	51.76	50.99	51.85	52.21	52.62	51.32
TiO2	0.877	1.236	1.206	1.117	1.157	1.144	1.078	1.149	1.063
Al2O3	14.17	14.71	14.29	13.85	14.38	14.23	13.76	14.32	13.59
FeO*	9.22	9.89	9.93	9.70	9.99	9.98	9.69	9.96	9.84
MnO	0.174	0.176	0.158	0.192	0.175	0.179	0.178	0.180	0.163
MgO	8.57	5.92	6.10	7.50	7.35	7.04	7.44	7.32	7.84
CaO	11.34	10.51	11.28	10.71	8.67	11.29	7.34	10.80	7.92
Na2O	1.61	1.77	1.77	1.65	3.25	1.79	2.67	1.83	4.09
K2O	0.38	0.54	0.60	0.46	1.14	0.19	0.57	0.57	0.48
P2O5	0.092	0.136	0.132	0.120	0.123	0.121	0.117	0.126	0.114
Sum	98.52	96.14	97.12	97.07	97.23	97.82	95.06	98.87	96.42
LOI %	0.80	3.31	2.12	2.06	1.88	1.48	4.43	0.35	3.12
	Major elements are normalized on a volatile-free basis, with total Fe expressed as FeO.								
	Normalized Major Elements (Weight %):								
SiO2	52.87	53.32	53.19	53.33	52.44	53.01	54.93	53.22	53.23
TiO2	0.890	1.290	1.240	1.150	1.189	1.169	1.134	1.162	1.102
Al2O3	14.39	15.30	14.71	14.27	14.79	14.55	14.47	14.48	14.09
FeO*	9.36	10.28	10.22	10.00	10.27	10.20	10.19	10.07	10.20
MnO	0.180	0.180	0.160	0.198	0.180	0.183	0.187	0.182	0.169
MgO	8.70	6.15	6.28	7.73	7.56	7.20	7.83	7.40	8.13
CaO	11.51	10.93	11.61	11.04	8.92	11.55	7.73	10.92	8.21
Na2O	1.64	1.84	1.82	1.70	3.35	1.83	2.81	1.86	4.24
K2O	0.39	0.57	0.62	0.47	1.17	0.20	0.60	0.57	0.50
P2O5	0.090	0.140	0.140	0.123	0.126	0.124	0.123	0.126	0.117
Total	100.00	100.00	100.00	100.00	100.00	100.00	100.00	100.00	100.00
	Unnormalized Trace Elements (ppm):								
Ni	102	60	70	85	90	85	82	81	85
Cr	396	178	222	268	299	263	265	249	274
Sc	38	37	36	37	36	36	34	36	36
V	241	274	270	269	273	271	256	271	251
Ba	131	174	154	154	408	99	350	168	318
Rb	10	16	19	9	29	6	13	15	9
Sr	207	178	183	173	616	257	267	187	290
Zr	69	105	100	93	97	93	102	96	89
Y	17	23	24	22	23	22	24	22	21
Nb	5.2	8.0	6.9	5.9	6.8	5.9	6.9	6.4	6.5
Ga	16	17	17	17	18	16	15	16	16
Cu	86	121	120	115	118	115	112	115	106
Zn	64	83	74	73	74	73	96	77	72
Pb	4	6	8	3	5	3	11	5	2

	100-2	100-10	101-3	16-102.1	16-102.2	16-103b 2	16-103. 10	16-104a	16-104b
	Jwrj	Jwrj	Jwr	Jwr	Jwr	Jwr	Jta	Jwr	Jwrj
Unnormalized Trace Elements (ppm):									
La	8	11	8	10	9	11	10	14	8
Ce	18	27	25	25	24	25	28	28	26
Th	1	2	1	2	3	2	3	3	3
Nd	8	14	17	11	14	14	13	15	13
U	0	2	0	0	1	2	1	1	2
sum tr.	1421	1335	1353	1373	2142	1399	1690	1406	1628
in %	0.14	0.13	0.14	0.14	0.21	0.14	0.17	0.14	0.16
sum m+tr	98.67	96.28	97.26	97.20	97.45	97.96	95.23	99.01	96.58
M+Toxides	98.71	96.32	97.30	97.25	97.51	98.01	95.28	99.05	96.63
w/LOI	99.51	99.63	99.42	99.31	99.39	99.49	99.71	99.40	99.75
if Fe3+	100.54	100.72	100.52	100.39	100.50	100.59	100.79	100.51	100.84
Normalized Trace Elements (ppm):									
NiO	129.9	76.7	89.5	108.3	115.0	108.5	103.7	102.4	107.6
Cr2O3	579.4	260.6	324.3	391.5	437.6	384.0	387.9	364.2	400.6
Sc2O3	57.5	56.4	54.6	56.7	55.8	55.7	51.5	55.7	55.8
V2O3	354.8	403.5	396.9	396.2	400.9	398.4	376.6	399.3	369.5
BaO	146.4	193.9	172.2	172.1	455.1	110.3	390.8	187.2	354.9
Rb2O	11.0	17.9	20.3	10.1	31.5	6.6	14.6	16.7	10.3
SrO	244.7	210.0	216.2	204.7	728.5	303.9	315.7	221.0	343.4
ZrO2	92.9	141.2	135.3	125.8	131.2	126.3	137.2	129.7	120.8
Y2O3	22.0	28.7	30.1	27.8	29.0	27.7	30.5	28.3	26.8
Nb2O5	7.4	11.4	9.9	8.5	9.7	8.4	9.9	9.2	9.3
Ga2O3	21.0	23.4	23.0	22.3	23.9	21.9	20.5	21.9	21.6
CuO	107.5	151.1	150.5	143.7	147.5	143.5	140.0	144.5	132.5
ZnO	80.2	102.9	92.0	90.7	91.5	91.4	119.8	96.1	89.2
PbO	4.3	5.9	8.4	3.5	5.0	3.2	12.1	4.8	2.4
La2O3	8.9	13.1	9.3	11.9	10.8	12.5	11.4	16.2	9.8
CeO2	22.5	32.9	30.7	30.3	28.9	31.0	34.8	34.9	31.5
ThO2	0.7	2.2	0.9	2.6	3.4	2.5	3.7	3.2	2.8
Nd2O3	9.3	16.8	19.5	13.1	15.9	16.6	15.5	17.1	14.7
U2O3	0.4	2.3	0.0	0.2	1.2	1.8	1.3	1.1	2.0
sum tr.	**1901**	**1751**	**1783**	**1820**	**2722**	**1854**	**2178**	**1854**	**2105**
in %	**0.19**	**0.18**	**0.18**	**0.18**	**0.27**	**0.19**	**0.22**	**0.19**	**0.21**

	16-106.2	16-107	16-107b.1	16-107b.2	AC-108.3	16-108.4	16-111	16-112.1	16-113.3
	Jwr	Jwr	Jwr	Jwr	Jwr	Jwr	Jho	Jwr	Jho
	Unnormalized Major Elements (Weight %):								
SiO2	51.85	53.07	51.92	51.94	52.83	51.20	52.90	52.67	52.87
TiO2	1.124	1.128	1.143	1.088	1.054	1.178	1.023	1.152	0.991
Al2O3	13.97	14.52	14.13	13.53	14.08	14.75	13.15	14.13	14.17
FeO*	9.99	9.80	9.75	9.49	9.37	9.76	12.21	10.05	11.96
MnO	0.177	0.173	0.186	0.172	0.185	0.286	0.210	0.176	0.213
MgO	7.80	7.27	7.13	8.28	7.24	7.06	6.21	7.42	5.87
CaO	9.30	11.08	10.82	10.91	9.96	8.02	8.84	10.44	9.88
Na2O	1.90	1.82	1.77	1.72	1.89	2.49	2.78	1.97	2.27
K2O	1.47	0.56	0.54	0.50	0.92	0.81	0.58	0.47	0.50
P2O5	0.119	0.119	0.126	0.118	0.113	0.137	0.110	0.126	0.108
Sum	97.69	99.54	97.50	97.75	97.65	95.70	98.01	98.59	98.83
LOI %	1.41	0.53	1.05	1.60	1.39	3.60	1.36	1.06	0.45
	Major elements are normalized on a volatile-free basis, with total Fe expressed as FeO.								
	Normalized Major Elements (Weight %):								
SiO2	53.07	53.31	53.25	53.13	54.10	53.50	53.98	53.42	53.50
TiO2	1.151	1.134	1.172	1.113	1.080	1.231	1.044	1.168	1.002
Al2O3	14.30	14.59	14.49	13.85	14.42	15.41	13.41	14.33	14.33
FeO*	10.22	9.84	10.00	9.71	9.60	10.20	12.46	10.20	12.10
MnO	0.181	0.174	0.191	0.176	0.189	0.299	0.215	0.178	0.216
MgO	7.98	7.30	7.31	8.47	7.41	7.38	6.34	7.52	5.94
CaO	9.52	11.14	11.10	11.16	10.20	8.38	9.02	10.59	10.00
Na2O	1.94	1.83	1.81	1.76	1.94	2.60	2.83	2.00	2.30
K2O	1.51	0.56	0.55	0.51	0.94	0.85	0.59	0.48	0.50
P2O5	0.121	0.119	0.128	0.120	0.115	0.143	0.111	0.126	0.108
Total	100.00	100.00	100.00	100.00	100.00	100.00	100.00	100.00	100.00
	Unnormalized Trace Elements (ppm):								
Ni	89	71	74	106	89	77	30	85	32
Cr	297	244	242	450	324	248	26	262	24
Sc	37	38	37	36	38	38	51	38	48
V	271	273	268	266	247	276	362	275	335
Ba	377	149	150	148	206	250	139	260	125
Rb	40	17	16	15	29	27	16	9	16
Sr	259	175	172	173	174	207	136	243	134
Zr	95	92	97	90	100	99	85	98	78
Y	23	21	23	22	23	23	27	23	27
Nb	7.4	5.9	6.4	6.2	6.8	6.8	4.3	7.1	4.2
Ga	17	17	15	17	17	18	18	17	17
Cu	112	111	117	109	105	97	70	119	66
Zn	76	76	76	70	76	77	97	79	96
Pb	3	2	3	3	8	59	4	2	4

	16-106.2	16-107	16-107b.1	16-107b.2	AC-108.3	16-108.4	16-111	16-112.1	16-113.3
	Jwr	Jwr	Jwr	Jwr	Jwr	Jwr	Jho	Jwr	Jho
Unnormalized Trace Elements (ppm):									
La	10	11	10	8	14	8	8	10	6
Ce	28	23	30	21	31	27	26	24	13
Th	4	4	3	2	4	3	3	3	3
Nd	13	10	14	8	14	15	11	12	9
U	1	1	2	1	1	2	2	1	1
sum tr.	1758	1339	1356	1550	1505	1558	1114	1569	1038
in %	0.18	0.13	0.14	0.16	0.15	0.16	0.11	0.16	0.10
sum m+tr	97.87	99.68	97.64	97.91	97.80	95.86	98.12	98.75	98.93
M+Toxides	97.92	99.72	97.68	97.96	97.85	95.90	98.16	98.80	98.96
w/LOI	99.33	100.25	98.73	99.56	99.24	99.50	99.52	99.86	99.41
if Fe3+	100.44	101.34	99.81	100.61	100.28	100.59	100.87	100.98	100.74
Normalized Trace Elements (ppm):									
NiO	113.3	90.5	93.9	134.3	112.8	98.0	38.0	108.0	40.3
Cr2O3	434.2	356.4	354.0	657.1	472.8	361.9	37.6	383.3	34.9
Sc2O3	56.3	57.7	56.6	55.4	58.1	58.3	77.6	58.6	73.5
V2O3	398.3	401.7	394.6	391.2	363.4	406.3	532.3	404.7	493.0
BaO	420.8	166.0	167.6	165.0	230.1	278.8	155.3	290.7	139.5
Rb2O	43.7	18.2	17.7	16.9	32.2	29.8	17.5	10.2	17.0
SrO	306.6	206.9	203.4	204.5	205.4	244.3	161.2	287.7	158.6
ZrO2	128.0	124.4	131.3	122.1	134.9	134.2	114.9	132.5	105.8
Y2O3	29.1	27.1	29.5	27.6	28.6	29.7	34.2	28.8	34.7
Nb2O5	10.6	8.5	9.2	8.9	9.8	9.7	6.2	10.1	6.0
Ga2O3	22.6	22.8	20.8	22.3	22.3	24.3	24.3	22.7	22.3
CuO	140.0	139.0	146.3	136.3	131.2	121.7	87.6	149.2	82.5
ZnO	94.7	94.2	95.2	87.1	94.7	96.3	120.1	98.0	119.7
PbO	3.1	2.5	3.1	2.9	8.8	64.0	4.2	2.6	4.4
La2O3	11.6	12.8	11.8	9.1	16.5	9.6	9.6	11.4	6.8
CeO2	34.2	27.8	36.4	26.3	37.6	32.6	31.8	29.6	16.1
ThO2	3.9	4.2	3.4	2.4	4.8	3.6	3.2	3.4	3.3
Nd2O3	15.5	12.0	16.2	9.6	15.8	16.9	12.5	14.4	10.5
U2O3	1.1	0.7	1.8	1.1	1.5	1.8	1.9	1.6	1.0
sum tr.	**2268**	**1773**	**1793**	**2080**	**1981**	**2022**	**1470**	**2048**	**1370**
in %	**0.23**	**0.18**	**0.18**	**0.21**	**0.20**	**0.20**	**0.15**	**0.20**	**0.14**

	16-113.4 Jho	16-113.7 Jho	16-114.2 Jho	16-115.1 Jho	16-115.2 Jho	16-116.2 Jwr	16-116.5 Jwr	16-117.10 Jwr	16-118.4 Jwr
	Unnormalized Major Elements (Weight %):								
SiO2	53.25	48.92	51.38	51.42	52.03	52.97	52.53	52.26	52.44
TiO2	0.987	0.887	1.037	1.048	1.067	1.235	1.147	1.116	1.098
Al2O3	13.99	11.80	14.03	13.95	13.79	13.69	14.27	13.85	13.90
FeO*	11.77	10.79	12.10	12.25	12.26	10.26	9.87	9.90	9.62
MnO	0.207	0.186	0.208	0.223	0.220	0.178	0.175	0.180	0.168
MgO	5.78	5.61	5.71	5.70	5.51	7.16	7.25	7.80	6.83
CaO	9.49	11.29	7.83	9.48	9.61	10.42	10.67	10.86	10.91
Na2O	2.77	2.31	4.37	3.02	2.77	1.78	1.92	1.85	1.67
K2O	0.61	0.77	0.39	0.62	0.60	0.63	0.60	0.57	0.57
P2O5	0.113	0.096	0.121	0.118	0.120	0.129	0.123	0.118	0.129
Sum	98.96	92.65	97.18	97.83	97.98	98.44	98.54	98.49	97.33
LOI %	0.85	6.66	2.31	1.19	0.93	0.91	0.66	1.14	2.01
	Major elements are normalized on a volatile-free basis, with total Fe expressed as FeO.								
	Normalized Major Elements (Weight %):								
SiO2	53.81	52.79	52.88	52.56	53.11	53.82	53.30	53.06	53.88
TiO2	0.997	0.958	1.067	1.072	1.089	1.255	1.164	1.133	1.128
Al2O3	14.13	12.74	14.44	14.26	14.07	13.91	14.48	14.06	14.28
FeO*	11.89	11.64	12.45	12.53	12.51	10.42	10.01	10.05	9.88
MnO	0.210	0.200	0.214	0.228	0.224	0.180	0.178	0.182	0.172
MgO	5.84	6.05	5.87	5.83	5.63	7.27	7.35	7.92	7.02
CaO	9.59	12.18	8.06	9.69	9.81	10.58	10.83	11.03	11.21
Na2O	2.80	2.50	4.50	3.08	2.82	1.80	1.94	1.88	1.71
K2O	0.62	0.83	0.40	0.64	0.61	0.64	0.61	0.58	0.59
P2O5	0.113	0.103	0.124	0.120	0.121	0.130	0.123	0.119	0.132
Total	100.00	100.00	100.00	100.00	100.00	100.00	100.00	100.00	100.00
	Unnormalized Trace Elements (ppm):								
Ni	32	26	33	33	30	87	81	97	82
Cr	25	18	19	19	18	278	254	334	272
Sc	49	42	48	49	49	37	36	36	36
V	335	306	333	343	344	283	272	268	251
Ba	146	130	181	95	119	176	218	265	171
Rb	18	18	9	13	16	14	20	17	17
Sr	147	129	156	168	127	173	175	168	171
Zr	81	93	81	85	87	99	95	92	99
Y	28	26	30	30	29	24	22	22	24
Nb	3.2	3.5	4.3	4.9	4.1	7.3	6.6	6.1	6.6
Ga	17	16	20	18	18	17	17	15	16
Cu	66	51	73	74	69	125	115	111	112
Zn	92	90	97	98	98	80	78	75	75
Pb	3	4	4	4	3	5	3	5	4

	16-113.4	16-113.7	16-114.2	16-115.1	16-115.2	16-116.2	16-116.5	16-117.10	16-118.4
	Jho	Jho	Jho	Jho	Jho	Jwr	Jwr	Jwr	Jwr
Unnormalized Trace Elements (ppm):									
La	9	9	12	9	9	10	10	11	12
Ce	15	23	21	25	20	24	26	22	27
Th	2	3	3	3	4	3	3	2	2
Nd	11	11	11	14	11	14	13	11	14
U	0	3	2	1	2	1	2	1	2
sum tr.	1077	1002	1137	1084	1057	1458	1447	1556	1393
in %	0.11	0.10	0.11	0.11	0.11	0.15	0.14	0.16	0.14
sum m+tr	99.07	92.75	97.29	97.94	98.09	98.58	98.68	98.65	97.47
M+Toxides	99.10	92.78	97.33	97.97	98.12	98.63	98.73	98.69	97.51
w/LOI	99.95	99.45	99.64	99.16	99.05	99.54	99.39	99.83	99.52
if Fe3+	101.26	100.64	100.99	100.52	100.41	100.68	100.48	100.93	100.59
Normalized Trace Elements (ppm):									
NiO	40.8	32.7	41.4	41.7	38.8	110.5	103.5	122.8	104.5
Cr2O3	35.9	26.7	27.9	27.2	26.7	406.1	370.7	487.9	397.1
Sc2O3	74.8	65.1	74.0	75.4	75.2	56.6	54.9	55.8	54.8
V2O3	492.4	449.9	489.3	504.0	506.1	416.3	400.1	394.8	368.8
BaO	162.6	145.5	202.3	105.8	133.1	196.9	243.3	295.9	191.1
Rb2O	19.8	20.1	9.5	13.9	17.0	15.8	21.9	18.1	18.3
SrO	173.3	152.5	183.9	198.4	150.2	205.0	207.4	198.7	202.6
ZrO2	108.9	125.9	109.7	115.0	117.3	134.1	128.5	124.0	134.2
Y2O3	35.9	33.3	37.7	37.7	36.4	30.1	28.1	27.6	30.0
Nb2O5	4.6	5.0	6.1	7.0	5.9	10.5	9.4	8.7	9.4
Ga2O3	23.0	21.8	26.2	24.0	24.0	23.1	23.0	20.3	21.2
CuO	82.2	63.5	91.8	92.8	86.3	157.0	144.5	139.4	139.7
ZnO	114.2	112.0	121.1	122.1	122.0	99.3	96.7	92.9	93.0
PbO	3.2	4.0	4.3	3.8	3.6	5.0	3.3	4.8	4.1
La2O3	10.7	10.3	14.0	11.1	10.5	11.9	12.1	12.8	14.5
CeO2	19.0	27.9	26.3	30.5	25.1	29.2	32.2	26.7	33.6
ThO2	1.8	3.4	3.5	3.1	4.1	3.5	3.2	2.4	2.4
Nd2O3	12.4	12.5	13.1	16.2	12.7	15.9	14.8	12.2	16.0
U2O3	0.4	3.5	2.2	1.2	2.0	0.8	2.0	1.3	2.4
sum tr.	**1416**	**1316**	**1484**	**1431**	**1397**	**1928**	**1900**	**2047**	**1838**
in %	**0.14**	**0.13**	**0.15**	**0.14**	**0.14**	**0.19**	**0.19**	**0.20**	**0.18**

	16-118w.2cl	16-119.2 Jwr	16-122.3 Jwrj	16.122.11 Jwrj	16.122.14 Jwrj	16-122.17 Jwrj	16-124.1 Jwr	16-125cl Jtab	129-7 Jb
	Unnormalized Major Elements (Weight %):								
SiO2	46.94	52.39	53.11	51.86	53.58	52.01	52.55	76.04	51.48
TiO2	1.372	1.136	1.384	1.146	1.075	1.016	1.173	0.855	0.794
Al2O3	18.43	14.14	14.56	14.20	13.74	14.22	14.33	11.70	15.05
FeO*	7.82	9.89	10.69	9.96	9.41	9.39	10.15	2.03	10.27
MnO	0.303	0.175	0.181	0.174	0.230	0.166	0.183	0.016	0.201
MgO	7.13	7.46	5.19	7.25	7.05	7.21	6.94	0.14	7.40
CaO	5.37	10.75	10.13	10.96	7.52	8.54	10.78	1.26	10.88
Na2O	4.67	1.81	2.06	1.81	1.98	2.85	1.84	5.59	1.82
K2O	0.22	0.56	0.81	0.37	1.66	1.58	0.63	0.26	0.42
P2O5	0.145	0.119	0.152	0.120	0.115	0.106	0.126	0.101	0.092
Sum	92.40	98.43	98.28	97.85	96.36	97.08	98.69	98.00	98.40
LOI %	6.84	0.73	0.92	1.28	2.77	2.69	0.91	1.59	1.06
	Major elements are normalized on a volatile-free basis, with total Fe expressed as FeO.								
	Normalized Major Elements (Weight %):								
SiO2	50.80	53.22	54.04	53.00	55.60	53.58	53.24	77.59	52.32
TiO2	1.485	1.154	1.409	1.171	1.116	1.046	1.189	0.872	0.81
Al2O3	19.94	14.37	14.82	14.51	14.26	14.64	14.52	11.94	15.30
FeO*	8.47	10.05	10.88	10.18	9.76	9.67	10.28	2.07	10.44
MnO	0.328	0.178	0.184	0.178	0.238	0.171	0.185	0.017	0.20
MgO	7.72	7.58	5.28	7.41	7.32	7.42	7.04	0.15	7.52
CaO	5.81	10.92	10.31	11.21	7.80	8.79	10.92	1.29	11.05
Na2O	5.06	1.84	2.10	1.85	2.06	2.93	1.87	5.71	1.85
K2O	0.24	0.57	0.83	0.38	1.72	1.63	0.63	0.26	0.43
P2O5	0.157	0.121	0.155	0.123	0.119	0.110	0.128	0.103	0.09
Total	100.00	100.00	100.00	100.00	100.00	100.00	100.00	100.00	100.00
	Unnormalized Trace Elements (ppm):								
Ni	100	89	43	78	68	80	69	4	57
Cr	365	281	47	242	184	256	229	198	198
Sc	44	36	36	37	33	36	36	15	44
V	296	272	298	272	251	252	273	92	268
Ba	174	145	203	145	936	388	183	322	122
Rb	4	19	27	14	61	65	15	10	16
Sr	253	170	181	173	211	286	181	65	126
Zr	111	92	117	93	102	88	99	80	61
Y	28	22	28	23	23	21	23	10	23
Nb	9.1	5.8	7.9	6.3	7.0	5.9	7.2	6.0	3.2
Ga	19	17	18	16	16	16	17	8	16
Cu	360	117	150	122	58	118	118	216	70
Zn	96	74	87	73	151	71	77	67	80
Pb	28	4	5	4	17	7	4	9	6

	16-118w.2cl	16-119.2	16-122.3	16.122.11	16.122.14	16-122.17	16-124.1	16-125cl	129-7
		Jwr	Jwrj	Jwrj	Jwrj	Jwrj	Jwr	Jtab	Jb
Unnormalized Trace Elements (ppm):									
La	13	8	12	10	14	11	10	6	7
Ce	33	24	33	23	29	20	25	14	12
Th	3	2	4	3	3	2	3	4	2
Nd	18	15	18	11	17	11	12	10	8
U	2	2	0	0	3	1	0	1	1
sum tr.	1953	1392	1314	1346	2182	1733	1380	1136	1120
in %	0.20	0.14	0.13	0.13	0.22	0.17	0.14	0.11	0.11
sum m+tr	92.59	98.57	98.42	97.99	96.57	97.25	98.83	98.11	98.51
M+Toxides	92.65	98.62	98.45	98.03	96.62	97.30	98.88	98.14	98.55
w/LOI	99.50	99.35	99.37	99.31	99.40	99.99	99.78	99.73	99.60
if Fe3+	100.37	100.45	100.56	100.41	100.44	101.04	100.91	99.96	100.74
Normalized Trace Elements (ppm):									
NiO	127.0	112.7	54.1	99.6	86.3	101.7	87.3	4.7	72.3
Cr2O3	534.1	410.0	68.4	353.7	268.3	374.3	334.6	289.2	289.5
Sc2O3	66.9	54.8	55.4	56.4	50.6	54.6	55.2	22.4	66.7
V2O3	434.9	399.9	437.7	400.4	368.8	370.7	401.3	135.5	394.4
BaO	193.7	161.8	226.8	161.6	1044.8	432.8	204.2	359.5	136.2
Rb2O	4.1	20.4	29.2	15.1	66.4	70.6	16.6	11.1	17.3
SrO	298.6	201.4	214.5	204.8	249.1	338.2	213.7	76.9	149.1
ZrO2	149.8	124.9	158.6	125.3	137.4	119.0	133.9	108.6	82.4
Y2O3	34.9	27.7	35.3	29.2	28.6	26.9	29.2	12.3	29.3
Nb2O5	13.0	8.3	11.3	9.0	10.0	8.4	10.3	8.6	4.6
Ga2O3	25.5	22.9	24.2	22.0	21.8	21.0	22.4	10.2	21.8
CuO	450.5	146.1	187.1	152.8	72.1	147.2	148.0	270.5	88.1
ZnO	119.4	91.7	108.3	91.4	188.2	88.0	95.3	83.4	99.8
PbO	30.4	4.0	5.8	4.1	18.5	7.8	4.6	9.8	6.5
La2O3	15.2	9.0	14.5	11.6	16.2	12.7	11.4	7.3	7.9
CeO2	40.1	29.7	40.4	28.8	36.1	24.7	30.9	17.6	14.8
ThO2	3.5	2.4	4.4	3.2	3.8	2.3	3.5	4.1	1.7
Nd2O3	21.5	16.9	21.0	13.2	19.8	13.2	13.5	11.5	9.6
U2O3	1.8	2.0	0.0	0.1	3.0	0.8	0.4	1.1	1.4
sum tr.	**2565**	**1846**	**1697**	**1782**	**2690**	**2215**	**1816**	**1444**	**1493**
in %	**0.26**	**0.18**	**0.17**	**0.18**	**0.27**	**0.22**	**0.18**	**0.14**	**0.15**

	130W Jwrj	131-6 Jwrj	131-14A	131-14B	132-B Jwr	132-C Jwrj	132-2A Jwrj	132-36 K?l	132-43 Jwrj
	Unnormalized Major Elements (Weight %):								
SiO2	50.36	52.36	63.06	52.33	51.28	51.70	50.91	41.42	51.52
TiO2	0.919	1.143	0.438	0.861	1.156	1.038	1.148	4.371	1.139
Al2O3	13.25	14.12	12.18	16.49	14.26	13.38	14.21	13.68	14.36
FeO*	9.39	9.85	8.40	9.55	10.24	9.89	9.83	12.43	9.96
MnO	0.148	0.170	0.129	0.142	0.178	0.160	0.167	0.243	0.164
MgO	9.20	7.62	5.46	6.91	7.21	8.90	6.95	5.36	7.39
CaO	7.44	10.85	1.27	3.08	10.93	10.75	10.88	9.72	10.45
Na2O	3.73	1.60	0.75	1.90	1.71	1.48	1.75	2.64	1.64
K2O	0.70	0.48	3.17	2.22	0.52	0.32	0.59	2.75	0.44
P2O5	0.096	0.125	0.029	0.112	0.126	0.110	0.124	0.936	0.126
Sum	95.24	98.31	94.89	93.59	97.61	97.71	96.56	93.54	97.19
LOI %	4.32	1.22	4.38	5.80	1.90	1.92	2.98	5.69	2.56
	Major elements are normalized on a volatile-free basis, with total Fe expressed as FeO.								
	Normalized Major Elements (Weight %):								
SiO2	52.88	53.26	66.46	55.91	52.54	52.91	52.72	44.27	53.01
TiO2	0.96	1.160	0.460	0.920	1.180	1.060	1.190	4.670	1.170
Al2O3	13.91	14.36	12.84	17.62	14.61	13.69	14.71	14.62	14.78
FeO*	9.86	10.02	8.85	10.20	10.49	10.12	10.18	13.29	10.25
MnO	0.16	0.170	0.140	0.150	0.180	0.160	0.170	0.260	0.170
MgO	9.66	7.75	5.76	7.38	7.38	9.10	7.19	5.73	7.61
CaO	7.81	11.03	1.34	3.29	11.19	11.00	11.27	10.39	10.75
Na2O	3.92	1.63	0.79	2.04	1.75	1.51	1.82	2.82	1.69
K2O	0.74	0.49	3.34	2.37	0.54	0.33	0.61	2.94	0.46
P2O5	0.10	0.130	0.030	0.120	0.130	0.110	0.130	1.000	0.130
Total	100.00	100.00	100.00	100.00	100.00	100.00	100.00	100.00	100.00
	Unnormalized Trace Elements (ppm):								
Ni	106	81	19	50	81	108	76	26	71
Cr	523	283	33	123	265	482	248	11	250
Sc	38	37	14	28	36	38	36	17	38
V	240	270	90	166	267	264	270	319	269
Ba	139	196	1630	1318	166	134	151	847	144
Rb	20	12	91	80	22	8	17	87	11
Sr	184	181	123	250	230	184	184	1345	179
Zr	71	92	117	154	93	83	93	421	91
Y	19	22	16	34	24	20	23	36	22
Nb	5.8	6.7	7.5	13.9	7.4	6.4	7.2	124.5	6.9
Ga	15	15	14	19	17	16	16	25	16
Cu	79	116	5	50	112	102	116	49	113
Zn	68	77	77	78	78	73	72	184	75
Pb	3	5	17	51	4	4	4	17	4

	130W	131-6	131-14A	131-14B	132-B	132-C	132-2A	132-36	132-43
	Jwrj	Jwrj			Jwr	Jwrj	Jwrj	K?l	Jwrj
Unnormalized Trace Elements (ppm):									
La	11	11	18	31	9	14	10	88	9
Ce	20	25	32	62	25	20	29	182	25
Th	2	3	8	11	3	2	1	10	2
Nd	10	16	15	31	14	12	14	87	14
U	2	2	4	3	1	2	1	3	2
sum tr.	1553	1451	2329	2554	1454	1572	1370	3880	1342
in %	0.16	0.15	0.23	0.26	0.15	0.16	0.14	0.39	0.13
sum m+tr	95.40	98.46	95.12	93.85	97.75	97.87	96.70	93.93	97.33
M+Toxides	95.45	98.51	95.16	93.90	97.80	97.93	96.75	94.02	97.37
w/LOI	99.77	99.73	99.54	99.70	99.70	99.85	99.73	99.71	99.93
if Fe3+	100.81	100.82	100.48	100.76	100.84	100.94	100.82	101.09	101.04
Normalized Trace Elements (ppm):									
NiO	134.7	103.5	24.1	63.8	102.4	137.7	97.3	33.3	89.8
Cr2O3	763.9	413.9	47.9	180.2	386.9	705.1	362.7	15.9	365.5
Sc2O3	58.5	56.6	21.3	42.6	55.8	57.7	55.8	26.7	58.6
V2O3	352.8	397.4	132.0	244.9	392.5	388.2	397.0	469.0	395.6
BaO	155.3	218.7	1820.3	1471.6	184.8	149.3	168.3	945.6	160.4
Rb2O	22.3	13.4	99.0	87.5	24.4	9.3	18.7	95.3	11.6
SrO	217.1	213.9	145.1	295.4	271.9	218.1	217.7	1591.0	212.2
ZrO2	96.2	124.4	158.3	208.2	126.2	111.6	126.0	568.2	123.1
Y2O3	23.5	28.4	20.7	43.7	30.6	25.4	29.1	45.3	28.4
Nb2O5	8.3	9.6	10.7	19.9	10.6	9.2	10.4	178.1	9.9
Ga2O3	19.9	20.3	19.2	26.1	22.7	21.3	22.2	33.6	21.6
CuO	98.4	144.6	6.6	62.7	139.8	127.4	144.7	61.6	141.6
ZnO	84.3	95.8	95.5	96.7	97.6	91.4	89.9	229.6	93.6
PbO	2.9	5.2	17.9	54.4	4.3	4.5	4.1	18.7	4.6
La2O3	13.2	13.1	20.8	36.3	10.4	16.3	11.9	103.5	10.0
CeO2	24.0	30.5	38.7	75.7	30.1	24.2	36.0	223.1	31.2
ThO2	1.8	3.3	8.9	12.8	3.3	1.8	1.5	11.7	1.9
Nd2O3	11.7	18.3	17.7	36.7	16.8	14.1	16.1	101.5	16.6
U2O3	2.1	2.1	4.4	3.3	1.4	1.7	1.0	3.8	1.7
sum tr.	**2091**	**1913**	**2709**	**3063**	**1913**	**2114**	**1810**	**4755**	**1778**
in %	**0.21**	**0.19**	**0.27**	**0.31**	**0.19**	**0.21**	**0.18**	**0.48**	**0.18**

	136-4 Jwrj	137-1 Jwrj	140-1 Jwrj	142-2 Jta	142-9 Jta	Jbc-2 Jb
	Unnormalized Major Elements (Weight %):					
SiO2	51.32	52.76	49.36	50.41	51.63	52.06
TiO2	1.238	1.186	1.156	1.156	1.068	0.847
Al2O3	13.89	14.30	14.33	14.49	14.41	15.04
FeO*	10.16	10.22	10.24	9.70	9.74	10.11
MnO	0.184	0.176	0.152	0.108	0.160	0.229
MgO	7.84	6.92	6.90	8.00	7.89	7.12
CaO	7.69	10.19	11.48	2.85	10.78	10.41
Na2O	3.37	2.18	1.59	4.72	1.58	2.03
K2O	0.79	0.75	0.43	0.55	0.69	0.36
P2O5	0.138	0.109	0.126	0.119	0.120	0.098
Sum	96.62	98.78	95.76	92.10	98.07	98.30
LOI %	2.73	0.88	3.61	7.23	1.62	1.07
	Major elements are normalized on a volatile-free basis, with total Fe expressed as FeO.					
	Normalized Major Elements (Weight %):					
SiO2	53.12	53.41	51.54	54.73	52.64	52.96
TiO2	1.280	1.200	1.210	1.250	1.090	0.862
Al2O3	14.37	14.47	14.96	15.73	14.70	15.30
FeO*	10.51	10.34	10.69	10.53	9.94	10.29
MnO	0.190	0.180	0.160	0.120	0.160	0.233
MgO	8.12	7.00	7.21	8.68	8.04	7.25
CaO	7.96	10.32	11.99	3.10	10.99	10.59
Na2O	3.49	2.20	1.66	5.12	1.61	2.06
K2O	0.82	0.76	0.45	0.60	0.71	0.36
P2O5	0.140	0.110	0.130	0.130	0.120	0.099
Total	100.00	100.00	100.00	100.00	100.00	100.00
	Unnormalized Trace Elements (ppm):					
Ni	82	70	78	99	92	54
Cr	268	223	271	300	342	166
Sc	39	38	36	37	37	44
V	276	278	259	271	260	282
Ba	1483	225	122	219	573	140
Rb	15	21	13	20	15	10
Sr	838	247	178	183	202	131
Zr	105	100	94	81	88	67
Y	24	23	23	56	22	25
Nb	7.8	8.3	6.5	7.1	6.3	3.4
Ga	16	16	16	15	17	18
Cu	126	119	114	24	107	69
Zn	92	80	78	81	76	84
Pb	7	5	3	3	4	5

	136-4 Jwrj	137-1 Jwrj	140-1 Jwrj	142-2 Jta	142-9 Jta	Jbc-2 Jb
Unnormalized Trace Elements (ppm):						
La	8	11	13	15	8	8
Ce	26	26	28	27	25	16
Th	3	3	3	1	3	2
Nd	15	13	14	18	13	9
U	2	1	2	2	1	1
sum tr.	3434	1509	1351	1458	1890	1134
in %	0.34	0.15	0.14	0.15	0.19	0.11
sum m+tr	96.97	98.93	95.89	92.25	98.26	98.41
M+Toxides	97.04	98.98	95.94	92.29	98.32	98.45
w/LOI	99.77	99.86	99.55	99.52	99.94	99.51
if Fe3+	100.90	101.00	100.68	100.60	101.02	100.64
Normalized Trace Elements (ppm):						
NiO	105.0	89.1	99.1	125.7	117.1	68.5
Cr2O3	391.2	326.2	395.6	437.7	500.2	242.9
Sc2O3	59.4	58.0	54.8	57.2	56.6	67.6
V2O3	405.9	409.0	380.9	398.1	381.9	414.9
BaO	1655.4	251.3	136.5	244.5	639.5	156.5
Rb2O	16.0	22.5	13.9	22.0	16.5	10.8
SrO	991.5	292.5	210.6	216.9	238.7	154.9
ZrO2	142.2	135.8	126.4	109.7	118.5	91.0
Y2O3	30.8	29.5	29.2	70.6	28.1	31.7
Nb2O5	11.1	11.9	9.3	10.2	9.0	4.9
Ga2O3	21.0	21.6	21.5	20.4	23.0	23.7
CuO	157.9	149.2	143.1	29.4	133.3	86.0
ZnO	115.1	99.8	97.5	100.7	94.7	104.7
PbO	7.5	5.7	2.9	2.7	3.8	5.3
La2O3	9.8	13.1	15.6	18.1	9.7	9.4
CeO2	32.0	32.5	34.8	33.7	31.1	20.2
ThO2	3.2	3.4	3.0	0.6	3.1	2.2
Nd2O3	17.8	14.9	16.1	20.6	14.9	10.0
U2O3	2.5	0.9	2.2	2.5	1.3	0.9
sum tr.	**4175**	**1967**	**1793**	**1921**	**2421**	**1506**
in %	**0.42**	**0.20**	**0.18**	**0.19**	**0.24**	**0.15**

APPENDIX IV. Petrographic descriptions, prepared by Allison Charney

Unpolished thin sections were prepared by Quality Thinsections, Inc., Tucson, AZ, and were viewed using standard petrographic microscopes. All descriptions and modal mineral abundances are based on best visual estimates. Micrograph illustrations below follow the convention of plane light images on left and crossed-nicols images on right.

In general, both basalt and diabase samples range in crystallinity from glassy and aphyric to hypocrystalline through holocrystalline. Many samples contain mesostasis. The degree of alteration varies on sample location, from minor along filled fractures to extensive and pervasive. The most abundant minerals consist of clinopyroxene and plagioclase with lesser olivine and orthopyroxene. Accessory minerals include an opaque phase, most likely magnetite or ilmenite, and apatite. Secondary alteration minerals include chlorite, calcite, quartz, zeolites, and altered glass products. Textures follow grain size and include phyric, glomerocrystic, diabasic, and subophitic.

In general, arkose samples range in grain size from medium-grained sandstone to pebble and cobble conglomerate. Although many locations contain lithic cobbles, care was taken to prepare samples of the finer matrix material. Samples range from fresh with iron-oxide staining to highly altered; many exhibit moderate melt/reaction textures. Major minerals include quartz, potassium feldspar, and plagioclase. Minor minerals include muscovite, biotite, zircon, schorl, and calcite. Lithic fragments include vein-quartz, potassium feldspar, and various metamorphic rock lithologies.

In general, basalt breccias are composed of sub-rounded to angular basalt fragments with a matrix of either arkose or basaltic ash and tuff (?). Cement is siliceous or calcareous and has been replaced in some samples by later hematite and various clay minerals.

New Haven Arkose (Trnh)

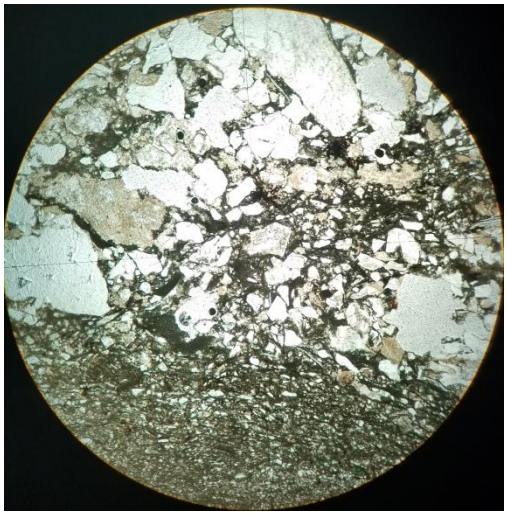

Samples 104 c&d Clastic, medium- to coarse-grained sand and lithic gravel, poorly sorted. Grains are comprised of angular to subrounded quartz, 50%, potassium feldspar, (25%), plagioclase feldspar (5%). Muscovite, minor zircon, and silty matrix material comprise 10% of the sample. Rock fragments comprise 10%. **Sample 104d** Contains layers with higher silt content and over all contains a greater abundance of rock fragments.

Right:104d; below: 104c. Width of view = 5 mm.

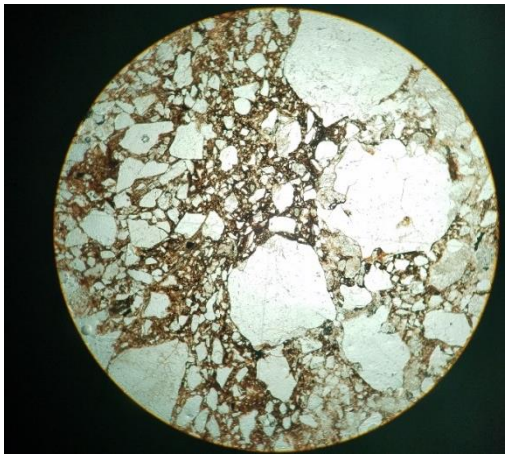

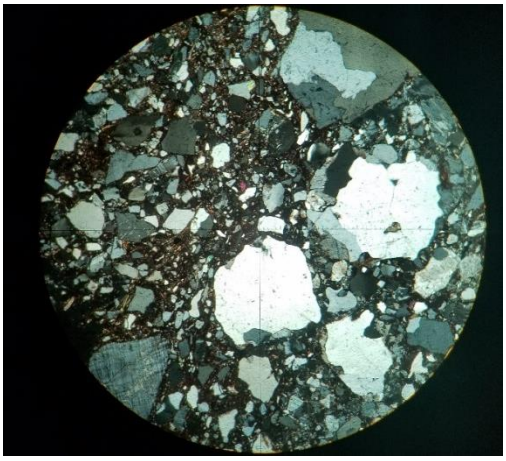

Sample 129.8 Garnet-bearing arkosic sandstone, medium-grained; garnets fine- to coarse-grained.

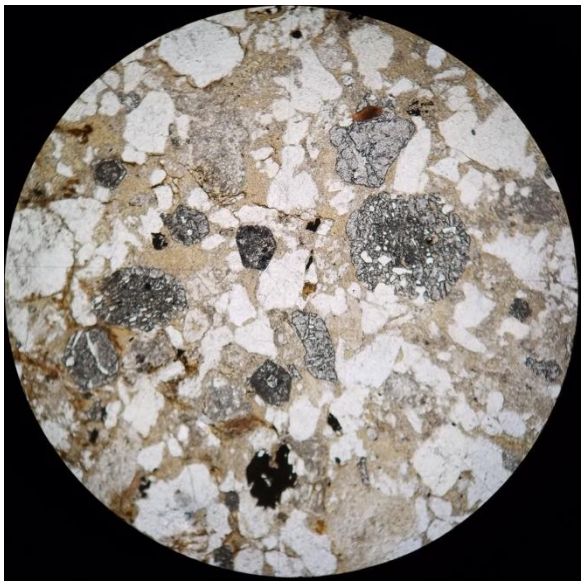

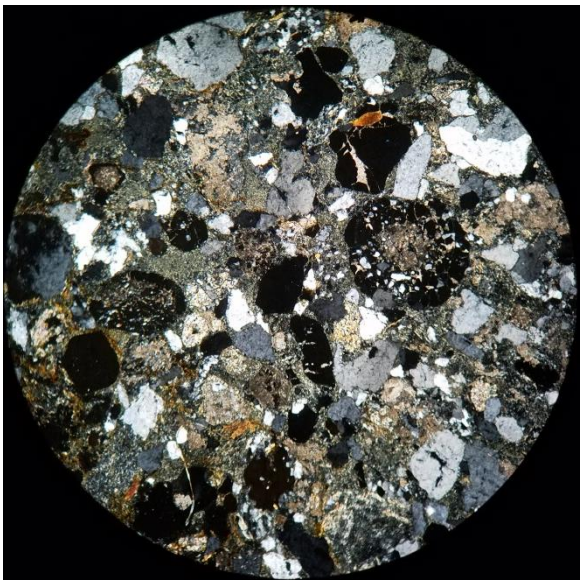

Width of view = 5 mm

Sandstone dike in intrusive diabase.

132-43B. Sandstone dike, 5 cm across cross-cuts fine-grained diabase dike. Sandstone medium- to coarse-grained, composed of quartz (~50%) K-feldspar, biotite and lithic fragments.

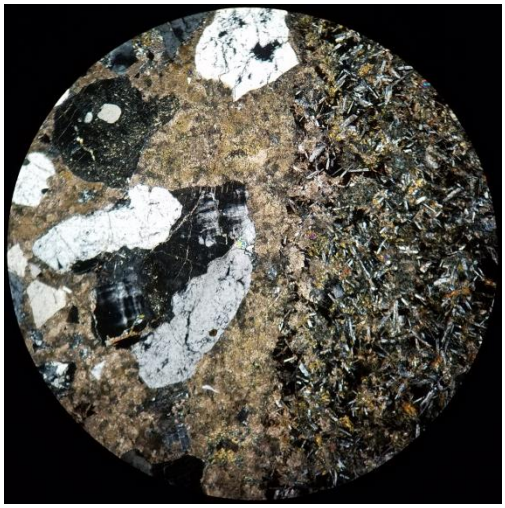

Width of view 5 mm.

Melted Arkose

Sample 108b Clastic, medium-grained sandstone that is partially melted and highly altered. The matrix is comprised of fine grained sedimentary material that has been partially melted and hydrothermally altered. The groundmass is composed of quartz, potassium feldspar and minor plagioclase. Potassium feldspar has been completely altered to various minerals. Quartz grains contain embayments and wisps that extend in the matrix.

Width of view = 5 mm; pl.

Sample 112 Clastic, medium-grained melted clastic material in contact with relatively fresh arkose. Highly altered and partially melted. The relatively fresh arkose is composed of quartz, muscovite mica, and very altered potassium feldspar. Some of the cement is calcite. The melted sediment is fine grained quartz with rare zircon and schorl set in a matrix of devitrified glass. Quartz grains contain embayments and wisps that extend in the matrix.

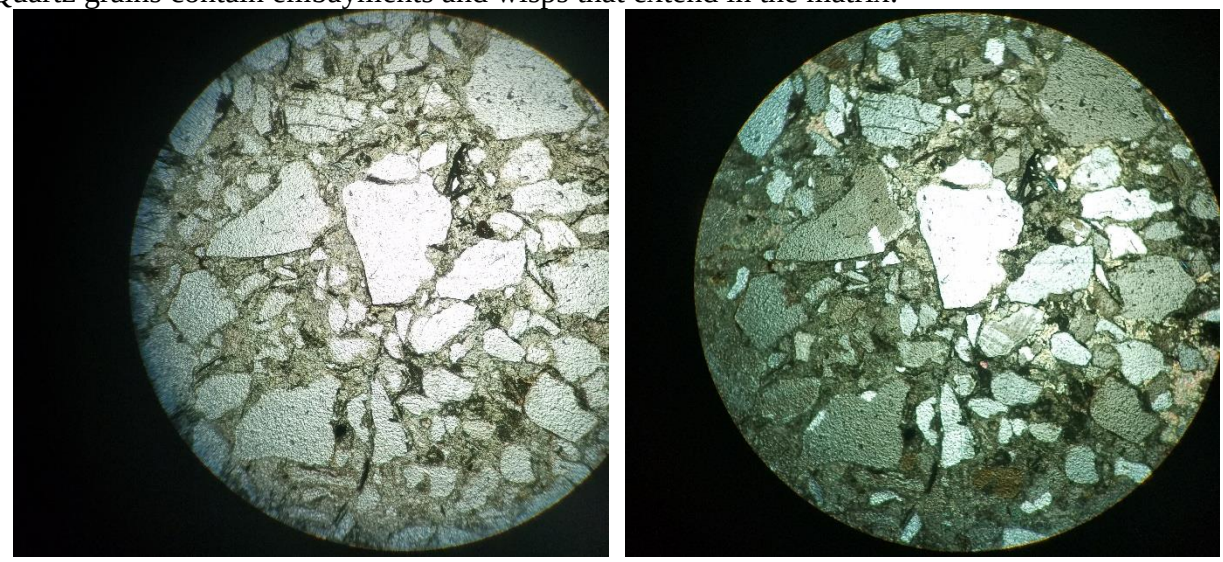

112.1. Width of view = 5 mm.

Sample 104.6 Clastic, medium-grained partially melted clastic sediments. The unmelted grains in the arkose are composed of quartz, plagioclase, and potassium feldspar. No muscovite is present, possibly completely melted out. Quartz grains contain embayments. Wisps of melt that extend in the matrix appear to be composed of noncotectic proportions of potassium feldspar, plagioclase, and quartz.

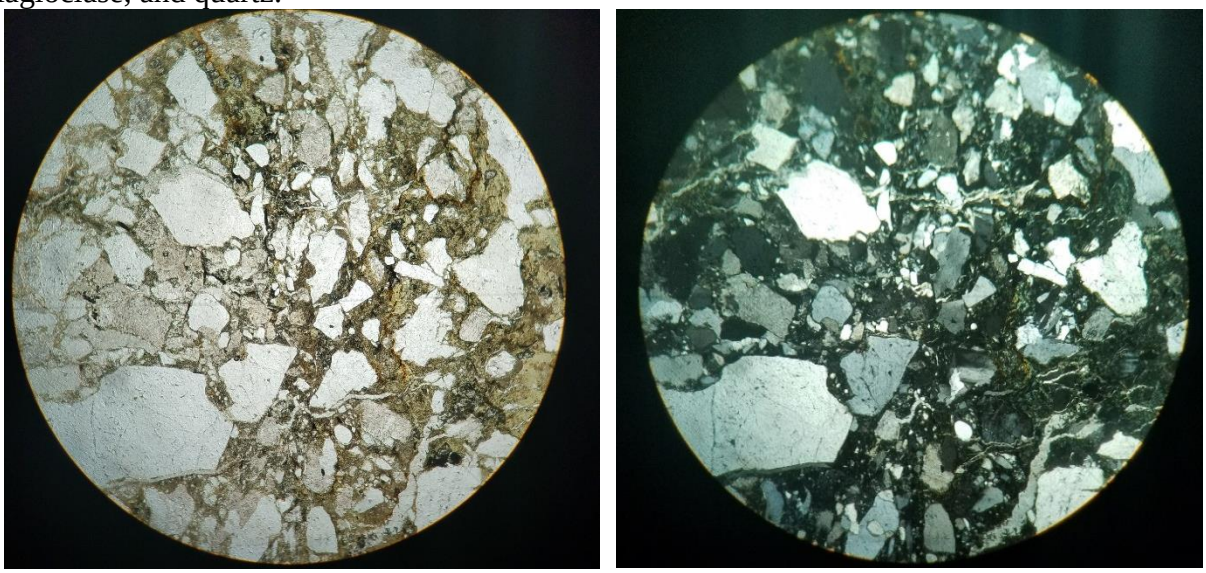

Width of view = 5 mm.

Talcott Basalt (Jta)

Sample 103-10: Very fine-grained vesicular basalt with plagioclase microlites and very round clinopyroxene glomerocrysts in devitrified glass; numerous partially resorbed quartz grains

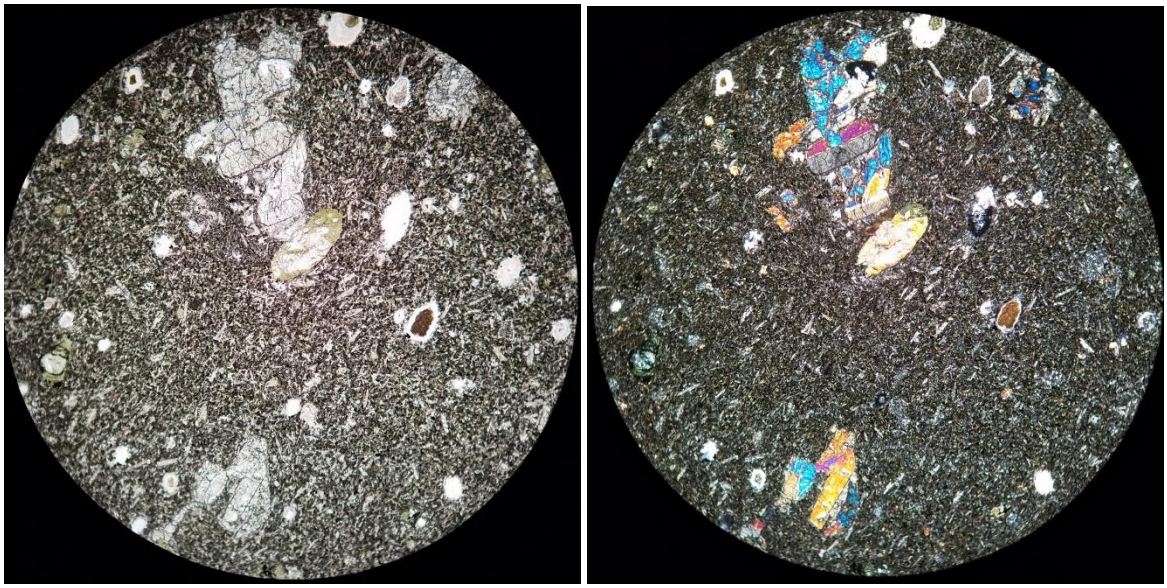

Left: Plane light, right, x-nicols; Field if view: 5 mm.

Sample 142.2 Very fine-grained basalt with relic olivine microphenocrysts (0.5 mm), and plagioclase microlites in altered devitrified glass.

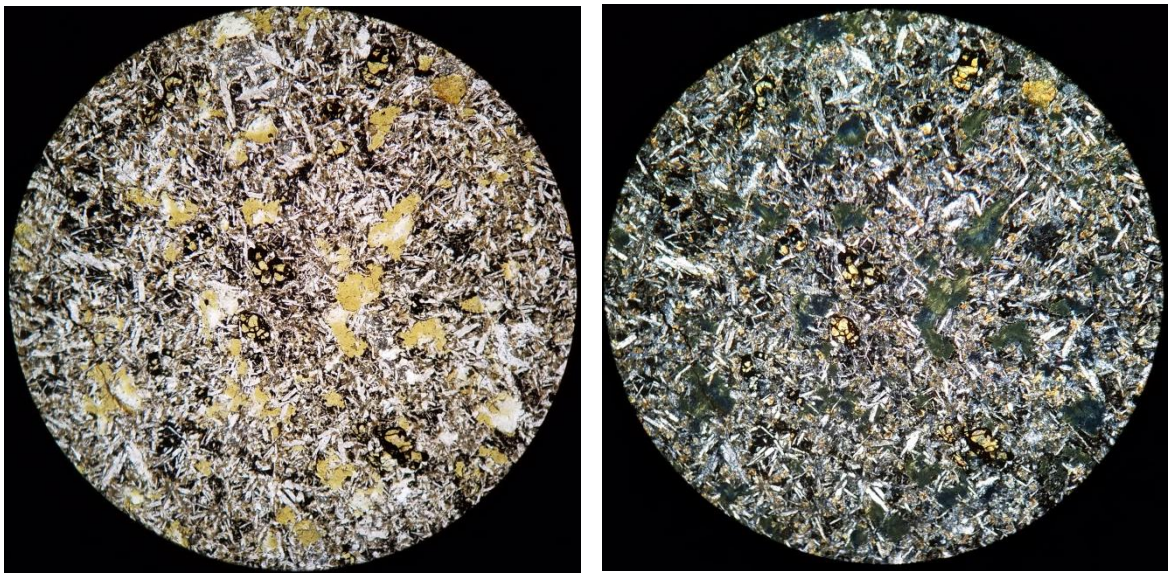

Left: Plane light, right, x-nicols; Field if view: 5 mm

Sample 142-9. Fine- to medium-grained weathered basalt, diabasic (?) texture, with clino-pyroxene phenocrysts and glomerocrysts (6 mm); few opaques remain, presumably dissolved by fluids.

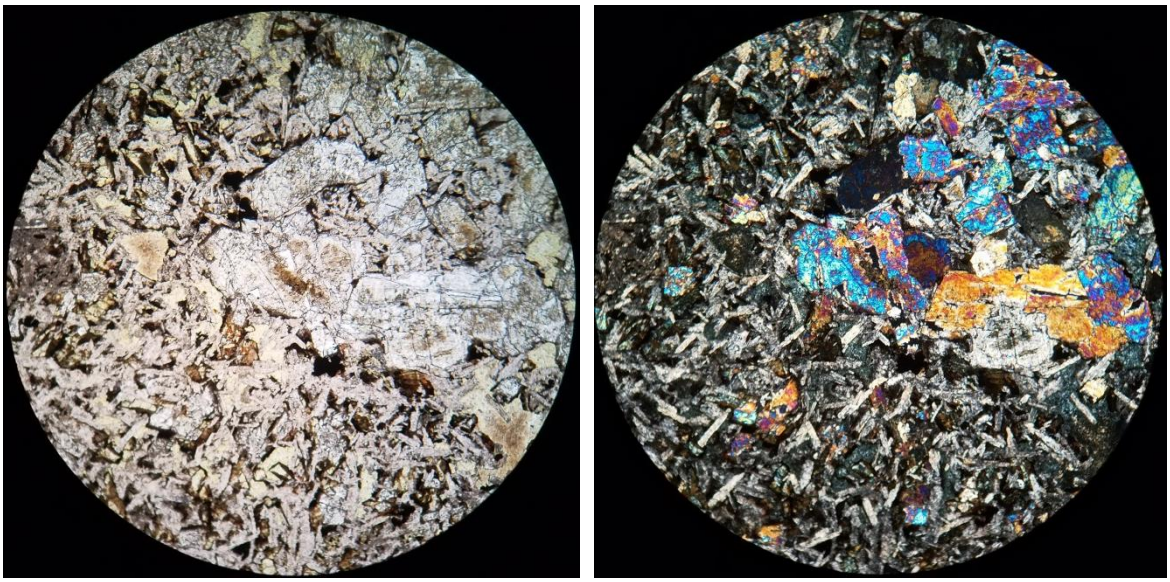

Left: Plane light, right, x-nicols; Field if view: 5 mm

Talcott Basalt Breccia (Jtab)

Sample 125.1 Clastic, containing angular to subrounded clasts of scoria and hypocrystalline basalt with a groundmass of volcanic ejecta and arkosic sediment. Mafic clasts are glassy to cryptocystalline, containing plagioclase microlites. Glassy fragments contain vesicles that are filled with calcite. Cryptocrystalline clasts contain microphenocrysts of euhdral olivine and broken plagioclase feldspar. Groundmass sediment is predominantly angular quartz grains. Additional images on next page.

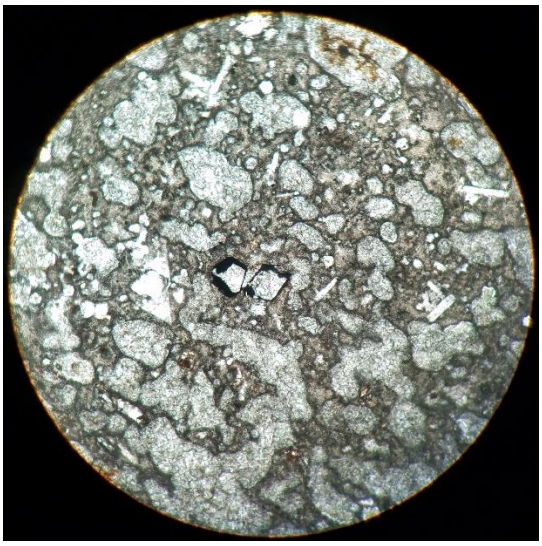

Width of view = 2 mm

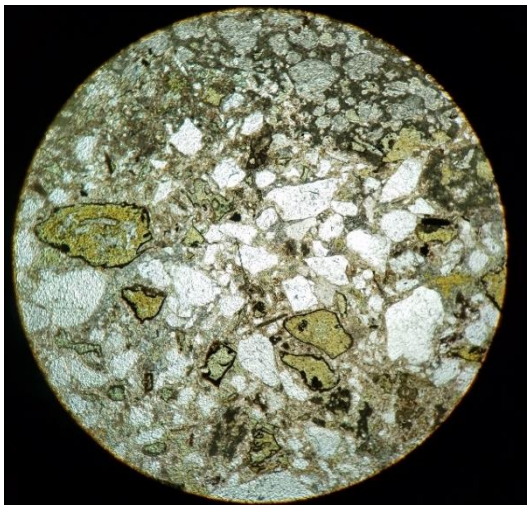

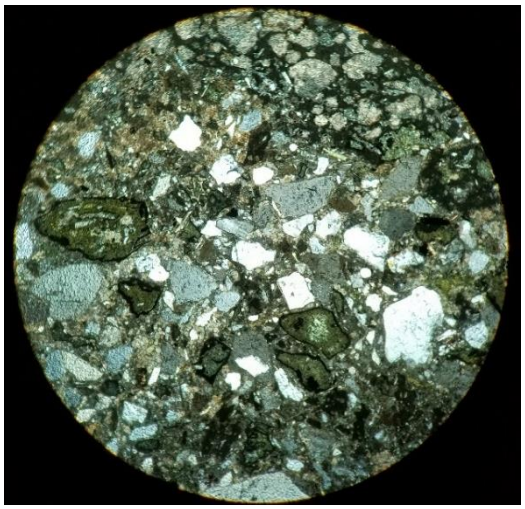

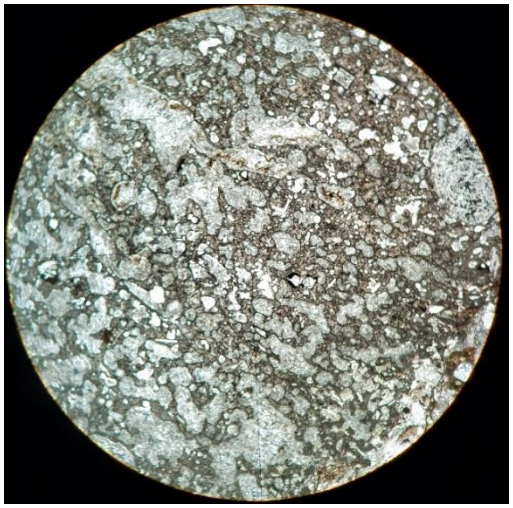

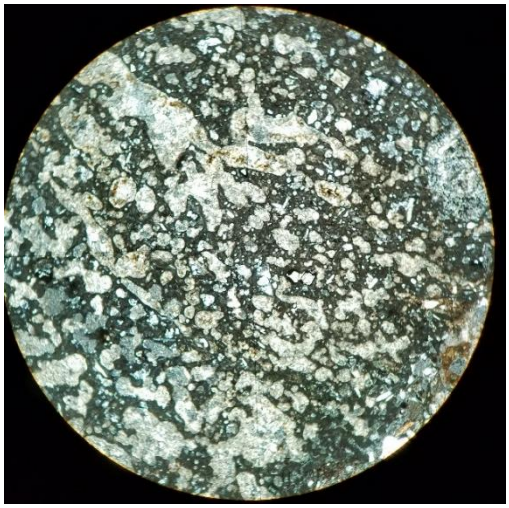

Sample 125-1; Width if view = 5 mm

Sample 126.1 Clastic, containing angular to subrounded clasts of scoria, hypocrystalline basalt, quartz, and schist with a groundmass of arkosic sediment, calcite cement, and hematite clays. Mafic clasts are glassy to cryptocystalline, containing plagioclase microlites. Glassy fragments contain vesicles filled with calcite?. Cryptocrystalline clasts contain microphenocrysts of euhdral olivine and plagioclase feldspar. Schist clasts are composed of muscovite and quartz. The groundmass is composed of quartz, potassium feldspar, plagioclase grains. Calcite cement is replaced in some areas by secondary hematite and iron-rich clay minerals.

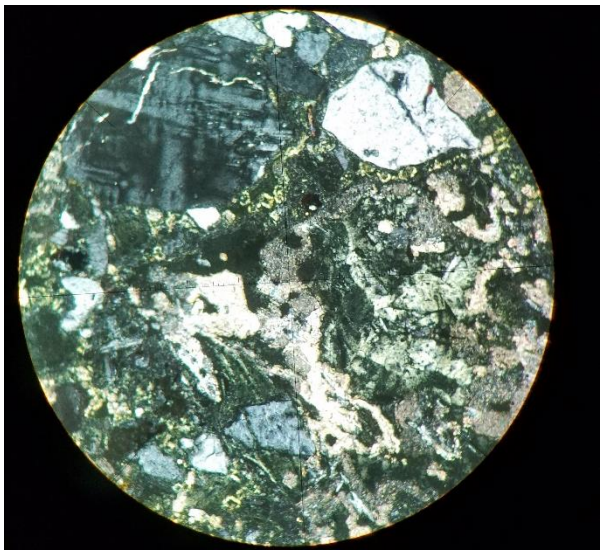

Width of view = 2 mm

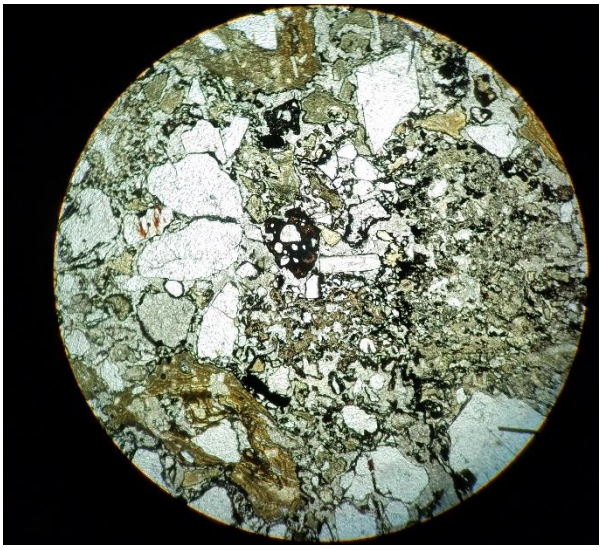

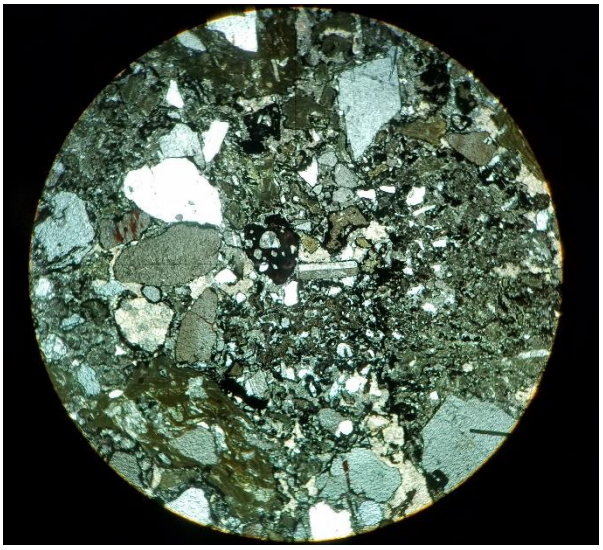

126.1 width of view = 5 mm

Sample 126.2 Clastic, containing angular to subrounded clasts of scoria, hypocrystalline basalt, and quartz with a groundmass of arkosic sediment, calcite cement, and hematite clays. Mafic clasts are glassy to cryptocystalline, containing plagioclase microlites. Glassy fragments contain calcite (?) filled amygdules. Cryptocrystalline clasts contain microphenocrysts of euhdral olivine and plagioclase feldspar. The groundmass is composed of quartz, potassium feldspar, plagioclase grains. Calcite cement is replaced in some areas by secondary hematite and iron-rich clay minerals.

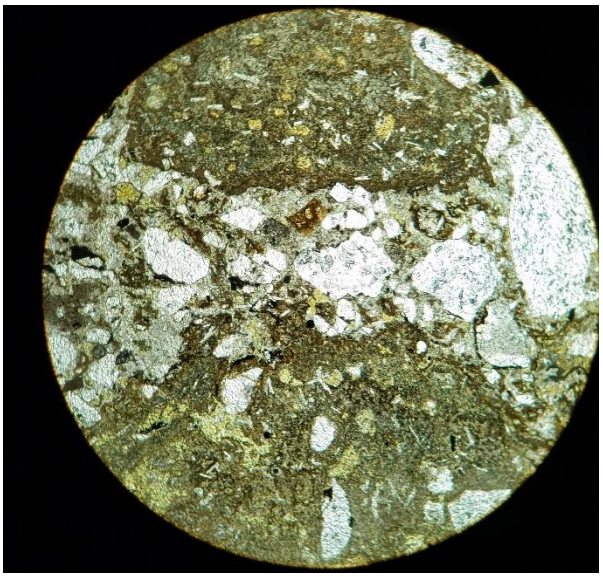

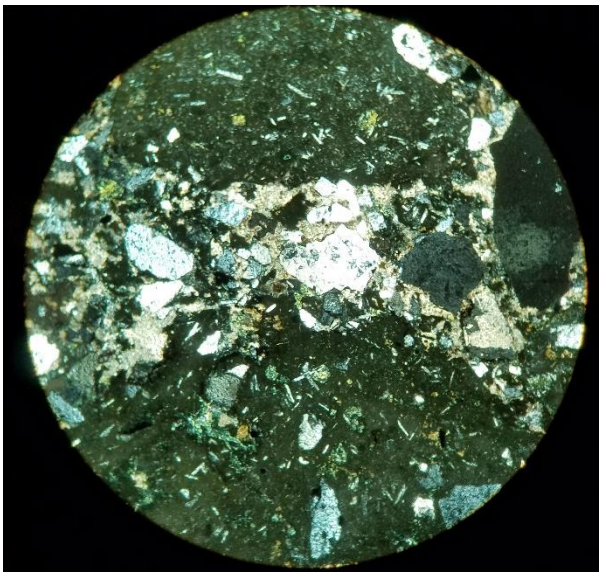

126.2 pl, xn; width of view = 5 mm

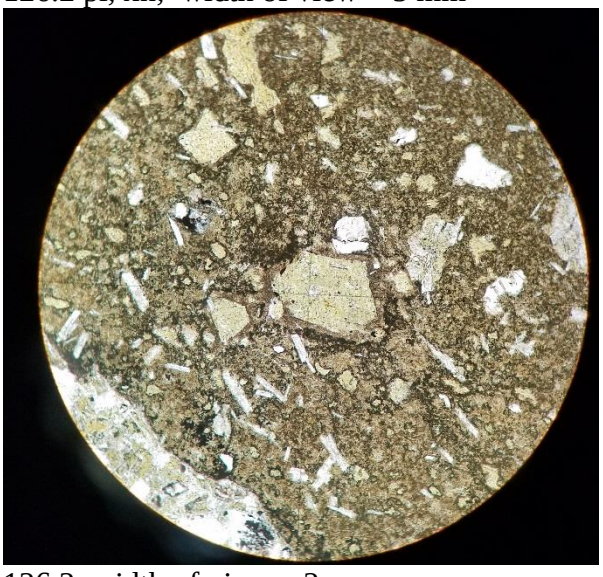

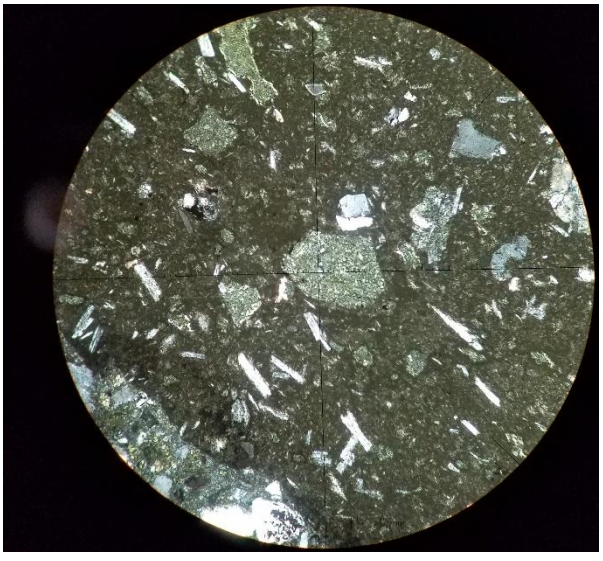

126.2; width of view = 2 mm

Holyoke Basalt (Jho)

Sample 111 Holocrystalline, coarse-grained. Highly Altered. Plagioclase, 40%, occurs as laths and are intergrown with augite clinopyroxene, 50%. Opaques, 10%, occur as subhedral? grains. No visible phenocrysts.
Width of view = 5 mm

Sample 113.3 Hypocrystalline, medium-grained with mesostasis and granophyre. Weakly altered. Plagioclase, 45%, occurs as laths that form chains, which surround stubby augite clinopyroxene grains (45%) and possible pigeonite grains. Opaque is most likely magnetite, 10%, and occurs as euhedral so semidendritic grains. Mesostasis and granophyre, 0.5%, fill interstices. Apatite occurs as needles in plagioclase. Phenocrysts are composed of plagioclase feldspar.

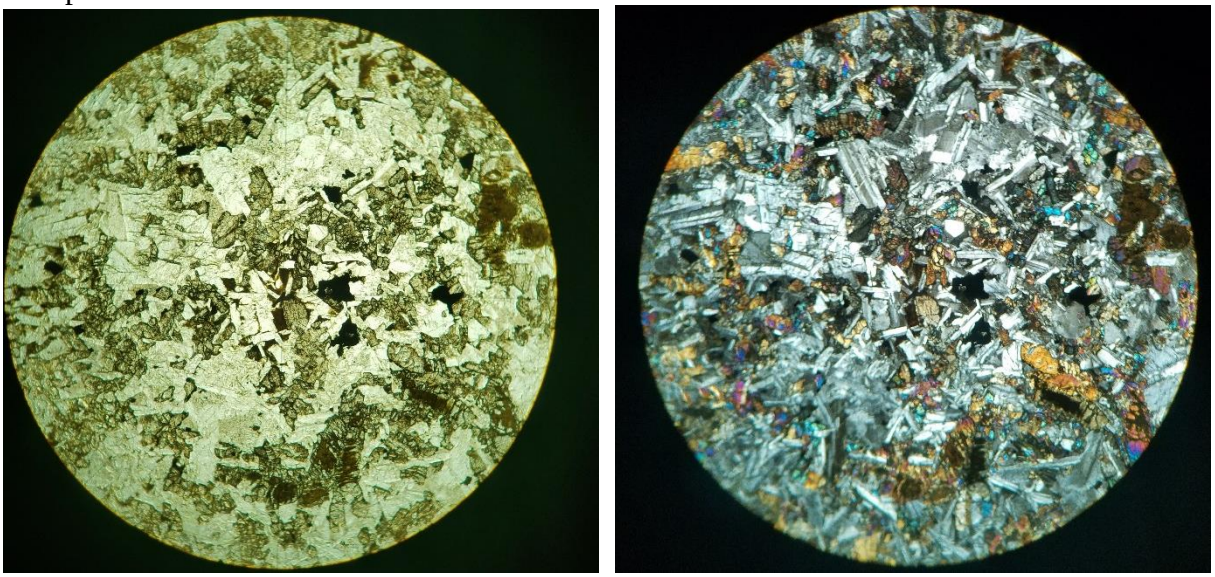

Width of view = 5 mm

Sample 115.3 Holocrystalline, coarse-grained to pegmatitic. Highly Altered. Plagioclase, 40%, occurs as laths and are intergrown with augite clinopyroxene, 50%. Opaques, 10%, occur as subhedral? grains. No visible phenocrysts. Segregation sheet.

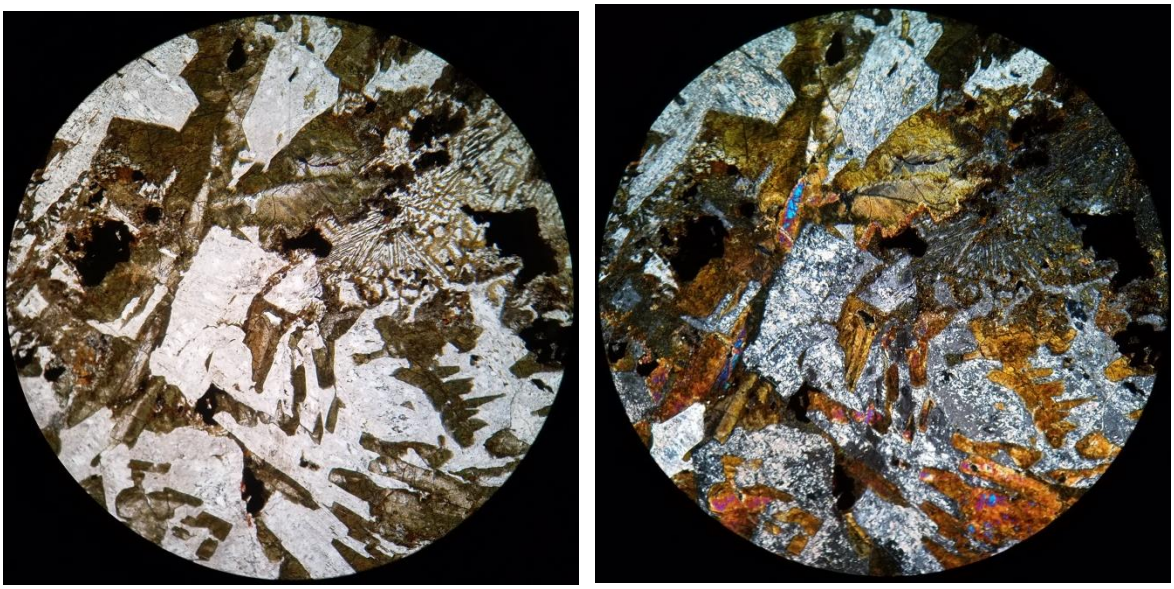

Left: Plane light, right, x-nicols; Field of view: 5 mm

Intrusive Diabase Dikes, Sills, and Stocks: West Rock diabase.

100.2. Very fine-grained subophitic with twinned clinopyroxene phenocrysts (2 mm); plagioclase laths (~40%) surrounded by clinopyroxene (`60%), very little mesostasis and opaques. One plagioclase glomerocryst.

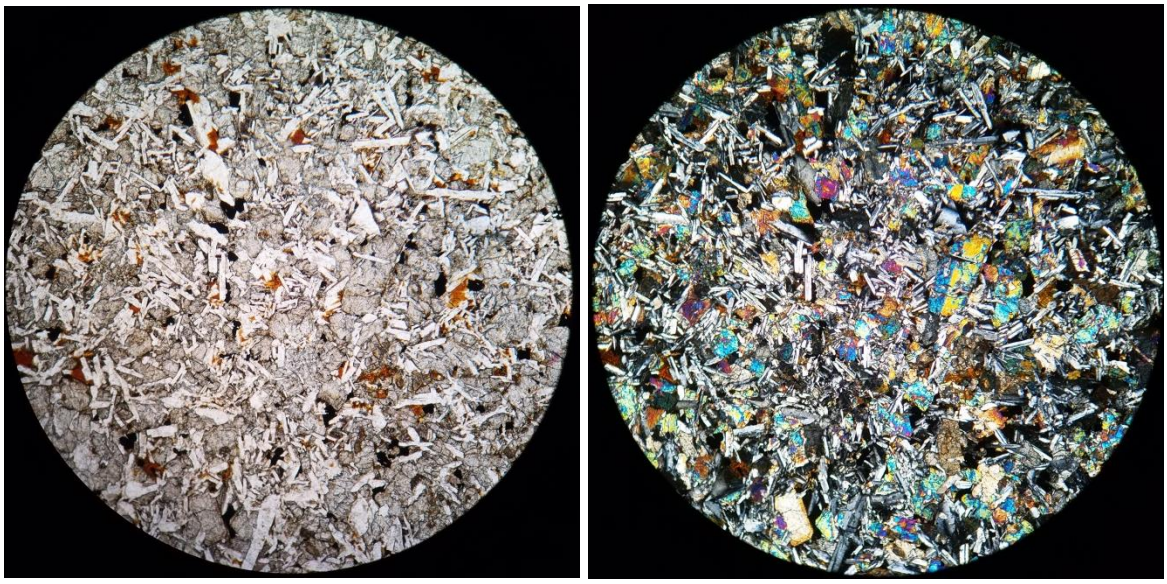

Width of view = 5 mm

Sample 100.7. Fine-grained diabase with about 10% mesostasis containing magnetite cubes, clinopyroxene oikocrysts (55%), plagioclase (35%); iddingsite (?) replacing unknown minerals.

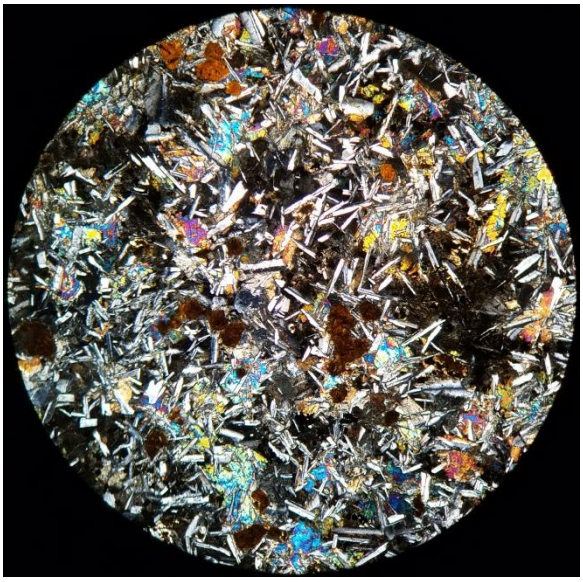

Sample 100-8. Contact between younger diabase (chilled margin) with older diabase. *Older diabase* is medium-grained with clinopyroxene phenocrysts (5%), scattered plagioclase phenocrysts and mesostasis (5%); clinopyroxene (some of which is hydrothermally altered)-plagioclase ratio about 60:40; areas of calcite and possible green-amphibole alteration; possible titanaugite(?) and olivine (?) pseudomorphs. *Younger diabase* is very fine-grained devitrified glass and glass with <5% clinopyroxene, plagioclase and olivine (?) phenocrysts (<5 mm).

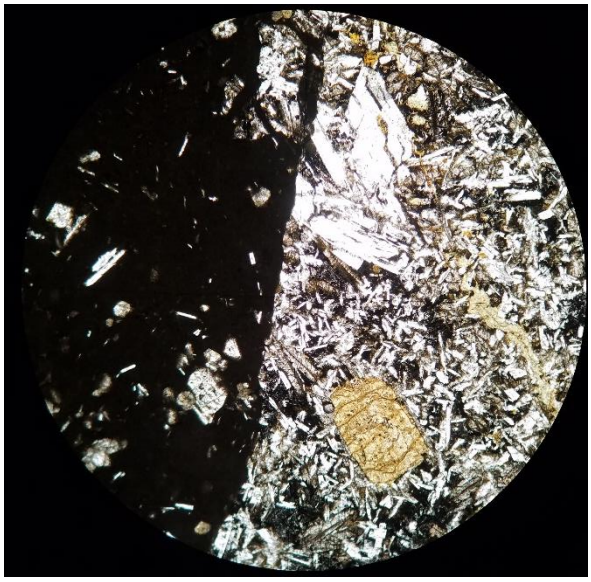

Plane light; width of view = 5 mm.

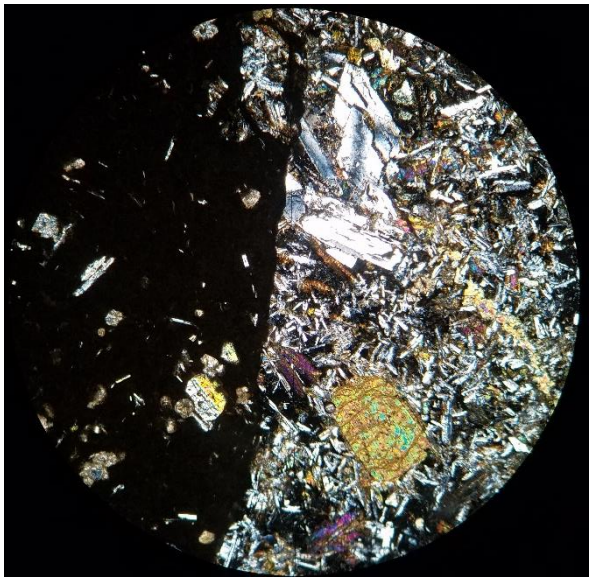

Crossed nicols.

Sample 100-8. *Older diabase*

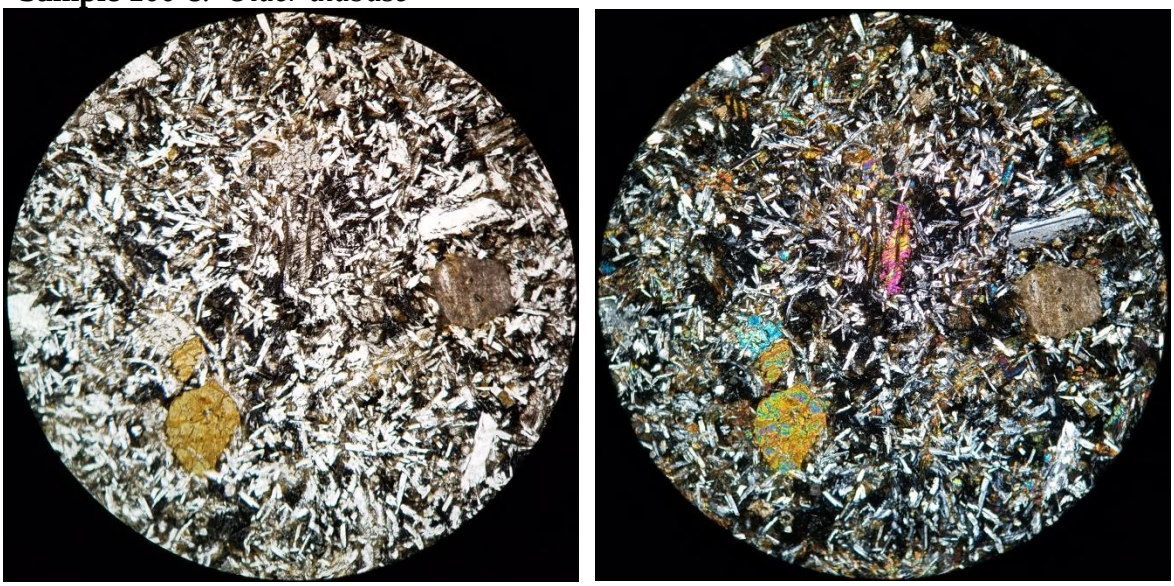

Width of view = 5 mm

Sample 100-8. *Younger diabase*

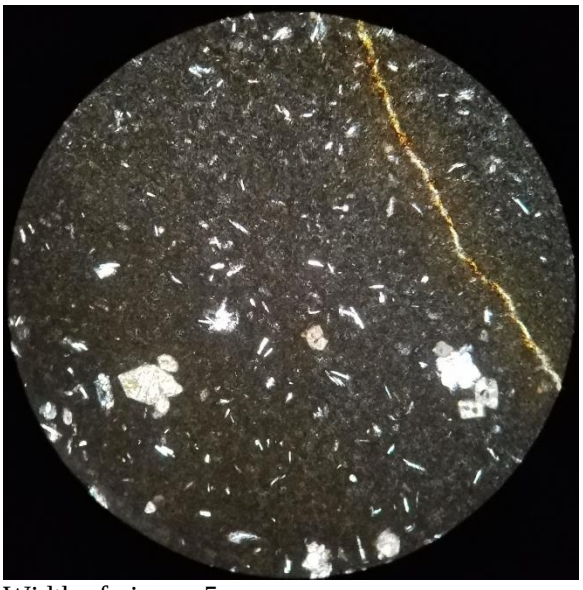

Width of view = 5 mm

Sample 101.3. Fine-grained diabase with large glomerocrysts of clinopyroxene and 5% mesostasis; diabasic texture with laths of plagioclase (50%) and smaller clinopyroxene (45%) crystals interstitial to plagioclase; possible olivine (?) pseduomorphs replaced by calcite.

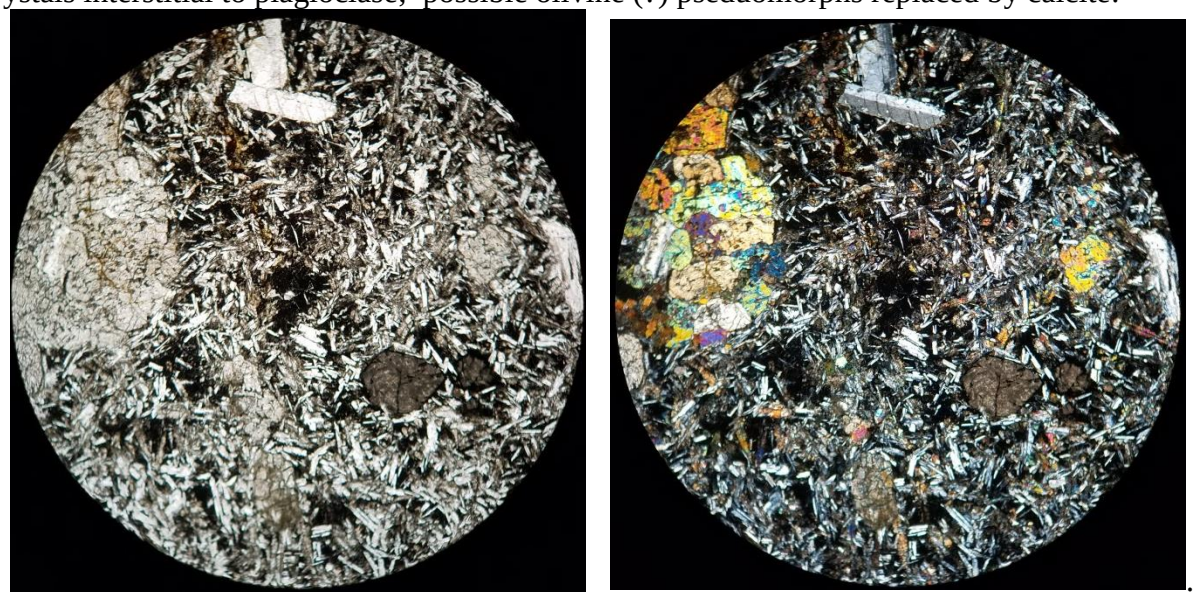

Width of view = 5 mm

Sample 104a. *Older diabase:* Hypocrystalline, fine- to medium-grained with up to 10% mesostasis. Minor Alteration. Plagioclase, 35%, occurs as laths and are intergrown with augite clinopyroxene, 55%. Opaques, 1%, occur as subhedral? grains. No visible phenocrysts.

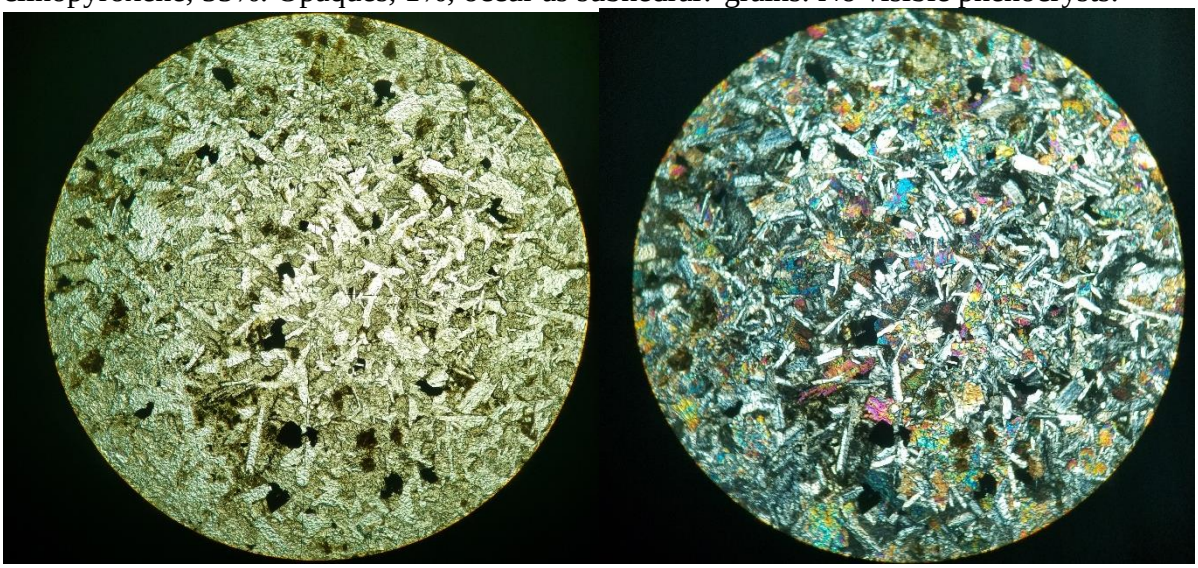

Width of view = 5 mm

Sample 104b *Younger diabase*: Hypocrystalline, fine-grained with up to 15% mesostasis. Moderate Alteration. Plagioclase, 65%, occurs as laths and are intergrown with smaller, equant augite clinopyroxene, 15%. Opaques, 1%, occur as subhedral? grains. Phenocrysts are glomerocrystic and composed of twinned pyroxene. Vesicles are filled with chert or microcrystalline quartz and zeolites.

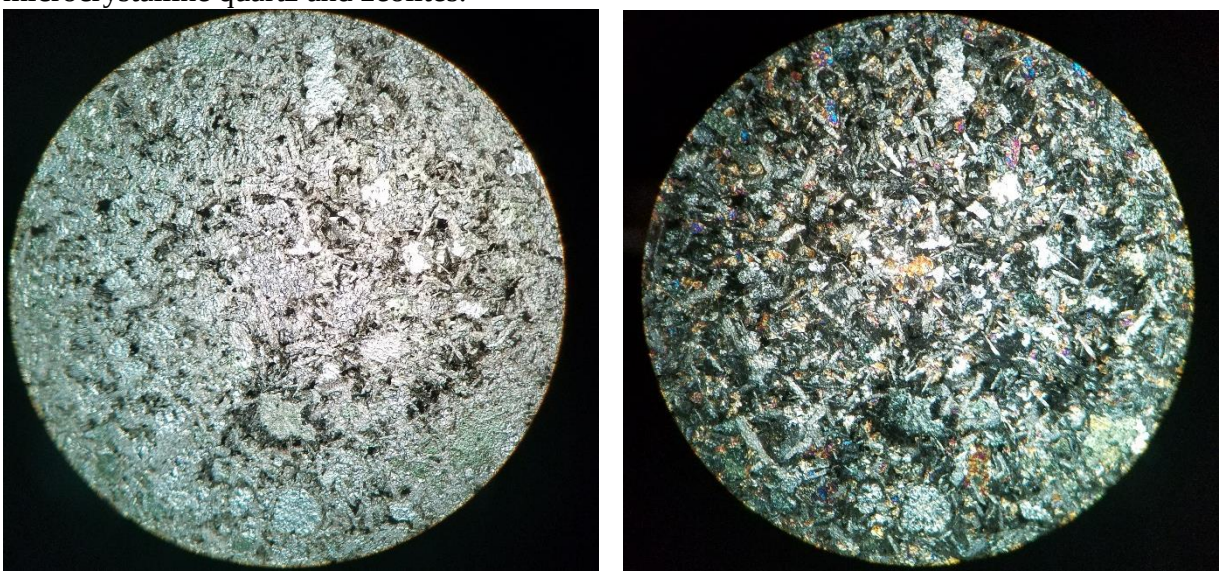

Width of view = 5 mm.

Sample 106.2 Hypocrystalline, fine-grained with up to 1% mesostasis. Moderate Alteration. Plagioclase, 65%, occurs as euhedral laths and are intergrown with stubby, equant augite, 35%, producing a subophitic texture. Magnetite 1%, occurs as subhedral grains. Phenocrysts, some glomerocrystic, are composed of twinned pyroxene. Many have been partially to nearly completely resorbed.

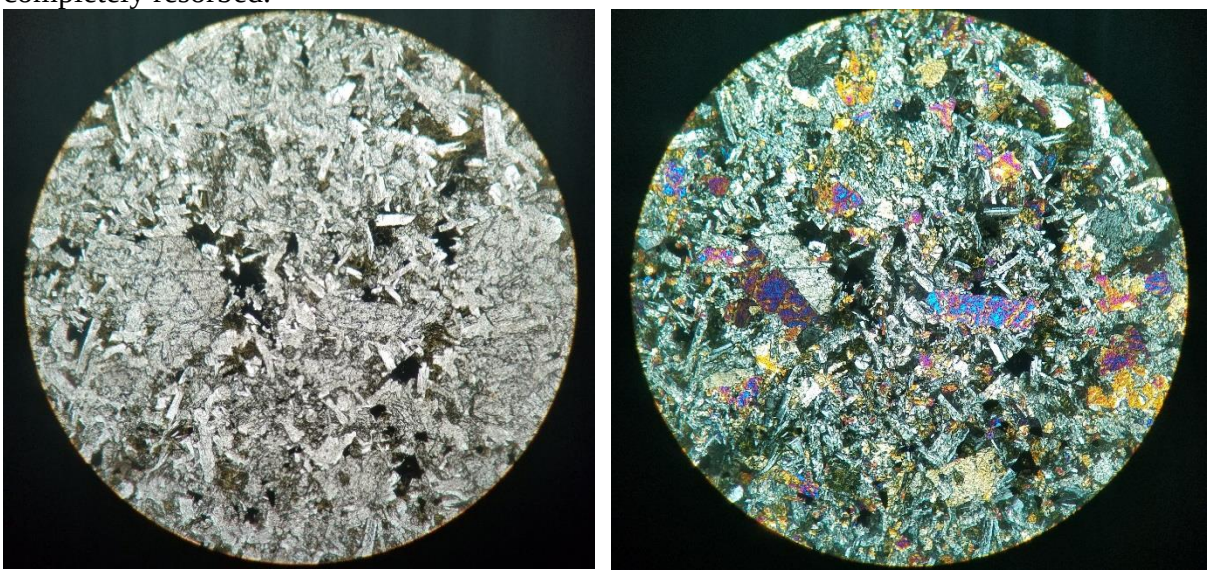

Width of view = 4 mm

Sample 107. Hypocrystalline, medium-grained with up to 1% mesostasis. Minor Alteration. Plagioclase, 65%, occurs as sub- to euhedral laths and are intergrown with augite, 35%, producing a subophitic texture with plagioclase laths partially enclosed by augite. Magnetite 1%, occurs as subhedral grains.

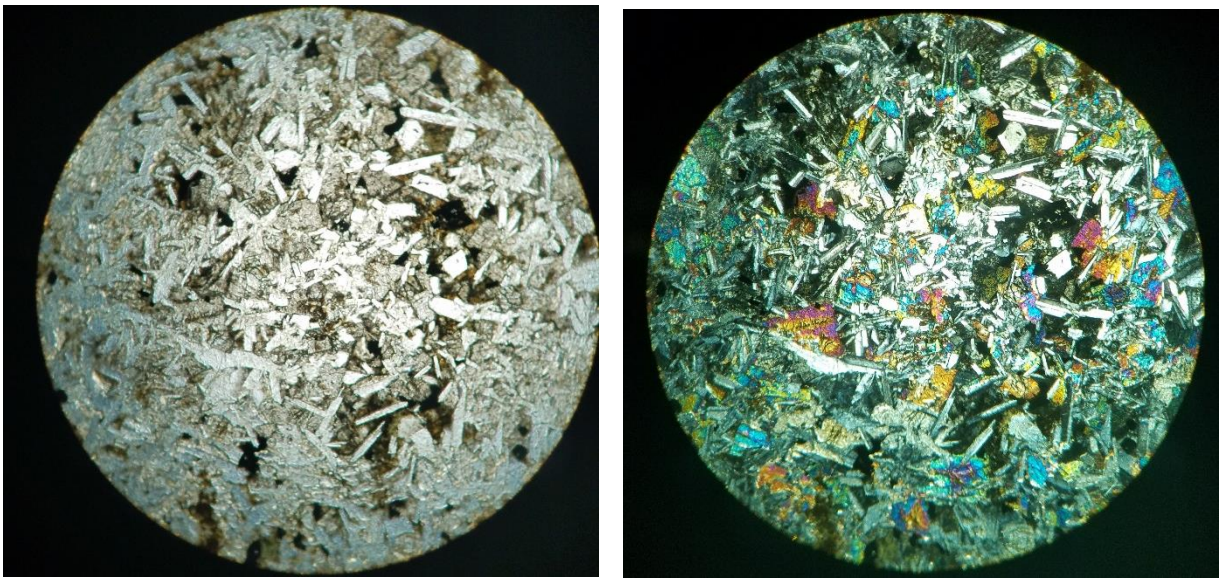

Width of view = 5 mm

Sample 107b.10 Glassy to hypocrystalline basalt in contact with melted sediment. Basalt is glassy and contains plagioclase microlites and vesicles filled with calcite or calcite and quartz. Along the contact, wisps of melted sediment connect together and are entrained into the basalt matrix. Sediment grains are comprised of quartz and minor plagioclase. There is no visible muscovite mica or potassium feldspar.

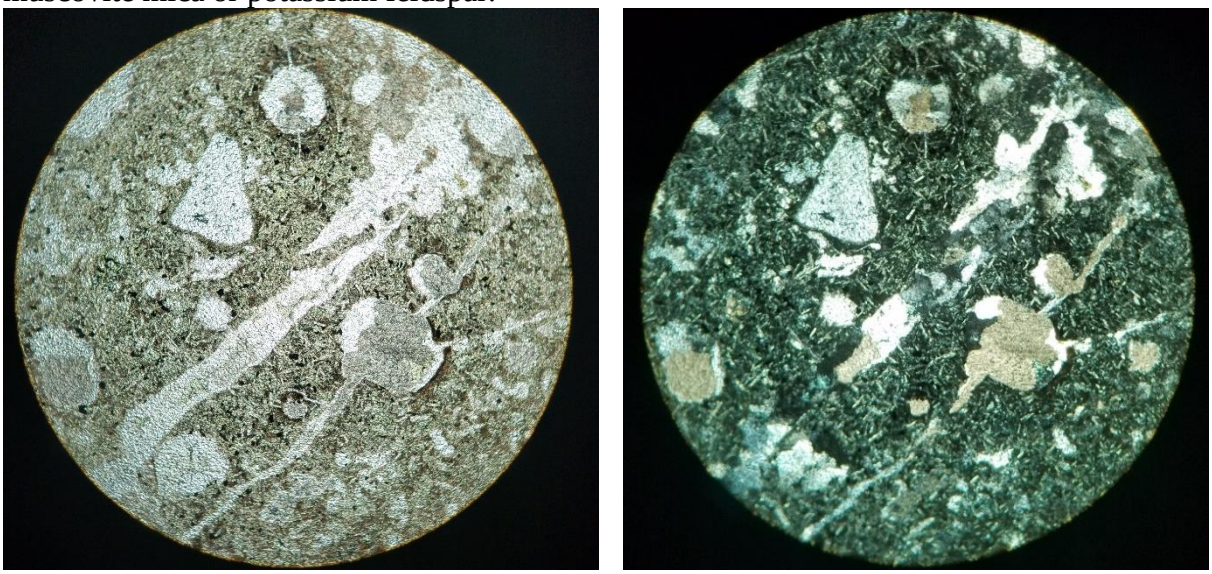

Width of view = 5 mm.

Sample 108b1 and 108b. Older diabase: Glassy to hypocrystalline basalt in contact with unmelted sediment. Basalt is glassy and contains microlites of plagioclase, olivine, and augite. The contact is chilled, follows arkose grain boundaries and does not intrude them. “Arkose was not entirely cemented at time of intrusion.”

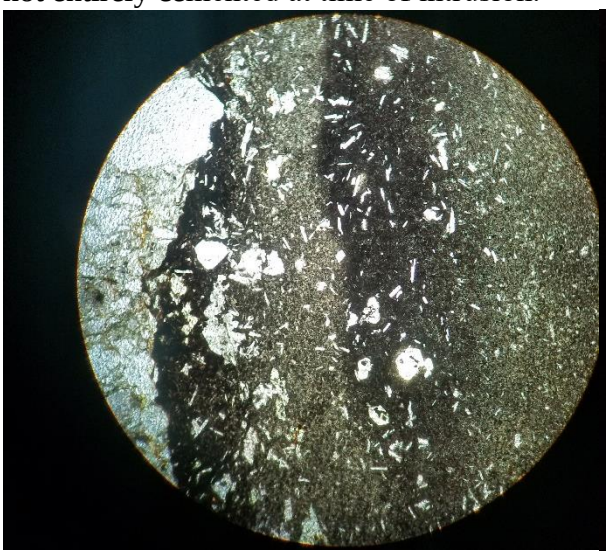

Width of view = 5 mm.

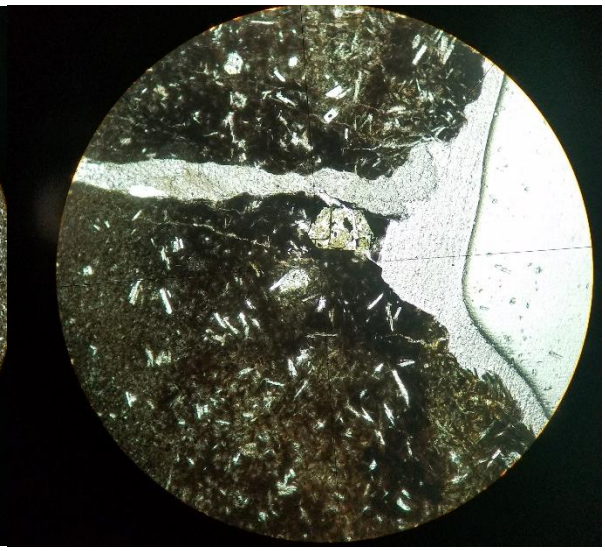

Width of view = 4 mm

Sample 108.5 Fine-grained with up to 5% mesostasis. Minor Alteration. Plagioclase, 45%, occurs as sub- to euhedral laths and are intergrown with augite, 50%, producing a subophitic texture with plagioclase laths partially enclosed by augite. Magnetite 1%, occur as subhedral grains. Phenocrysts are composed of twinned pyroxene.

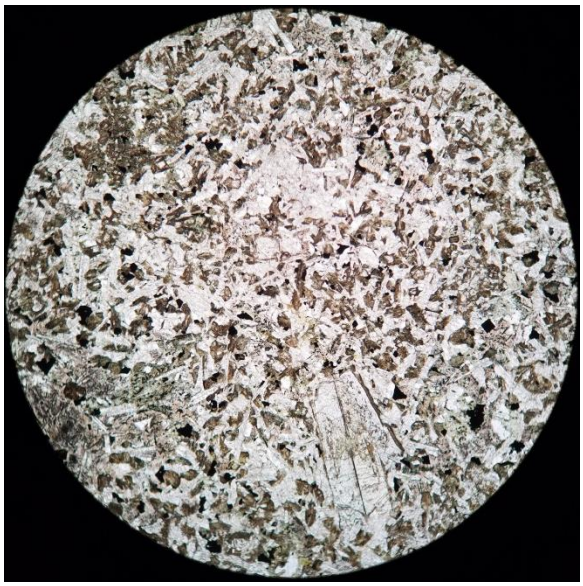

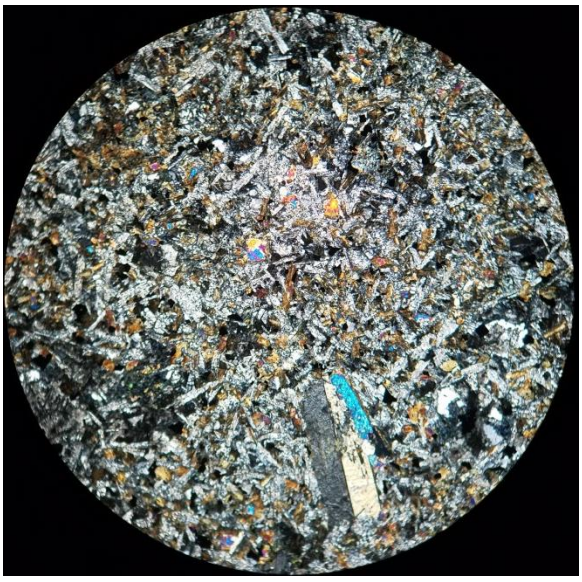

Width of view = 5 mm

Sample 112.1 Hypocrystalline, medium-grained with up to 5-8% mesostasis. Minor alteration. Plagioclase, 60-65%, occurs as sub- to euhedral laths and are intergrown with augite, 35%, producing a subophitic texture with plagioclase laths partially enclosed by augite. Magnetite 1-2%, occurs as subhedral grains. Phenocrysts are composed of twinned pyroxene.

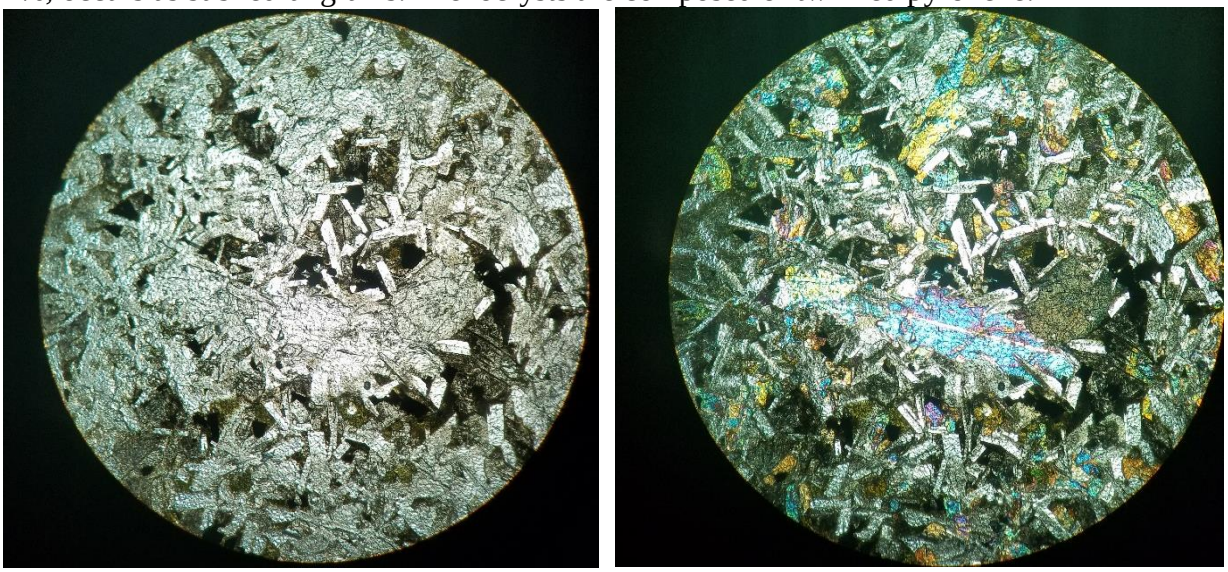

Width of view = 5 mm

Sample 116.2 Hypocrystalline, fine- to medium-grained with up to 0.1% mesostasis. Minor alteration. Plagioclase, 65%, occurs as sub- to euhedral laths and is intergrown with augite, 30%, producing a subophitic texture with plagioclase laths partially enclosed by augite. Magnetite 5%, occurs as subhedral grains, noticeably larger than the groundmass. Phenocrysts, some glomerocrystic, are composed of twinned pyroxene. Many have been partially resorbed.

Width of view = 5 mm

Sample 116.5 Hypocrystalline, fine- to medium-grained with up to 1% mesostasis. Minor alteration. Plagioclase, 60%, occurs as sub- to euhedral laths and is intergrown with augite, 40%, producing a subophitic texture with plagioclase laths partially enclosed by augite. Magnetite 1-2%, occurs as subhedral grains.

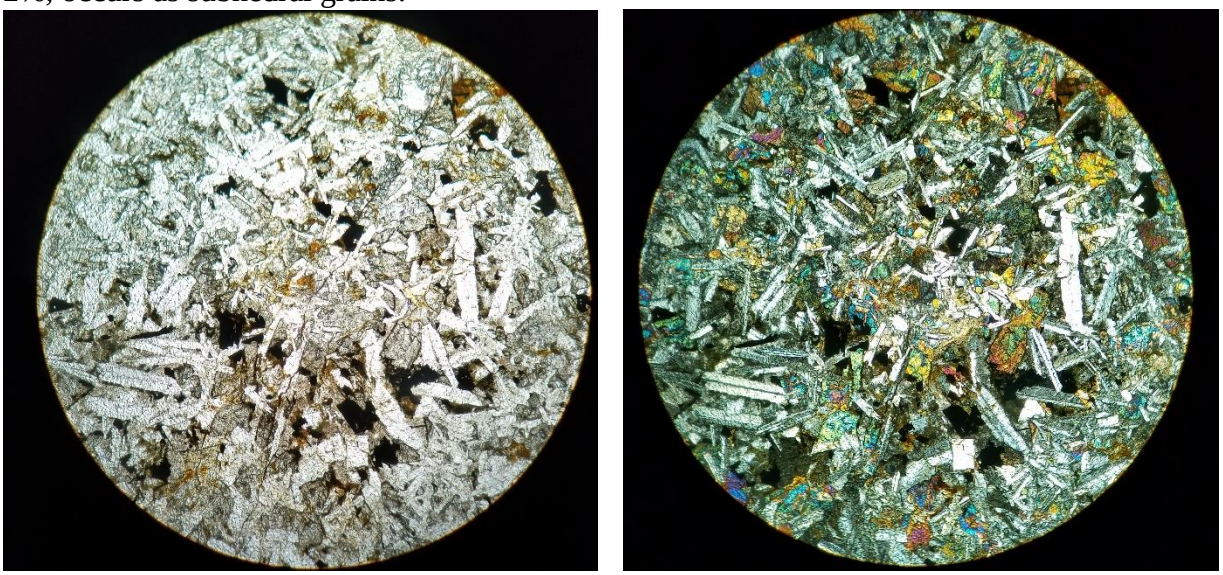

Width of view = 5 mm.

Sample 122.3 Holocrystalline, coarse-grained with granophyre. Weakly altered. Plagioclase, 60%, and augite clinopyroxene grains (35%) form a diabasic texture. Opaque is most likely magnetite, 1-2%, and occurs as anhedral to subhedral grains . Granophyre occurs as irregular blebs and fills interstices. No visible phenocrysts.

122.3. Width of view = 5 mm.

Sample 122.17 Hypocrystalline, medium grained. Moderate alteration. Plagioclase, 60%, and augite, 40%, are blocky in shape. Magnetite 1-2%, occurs as subhedral grains and is noticeably larger. Alteration products completely replace either orthopyroxene or olivine.

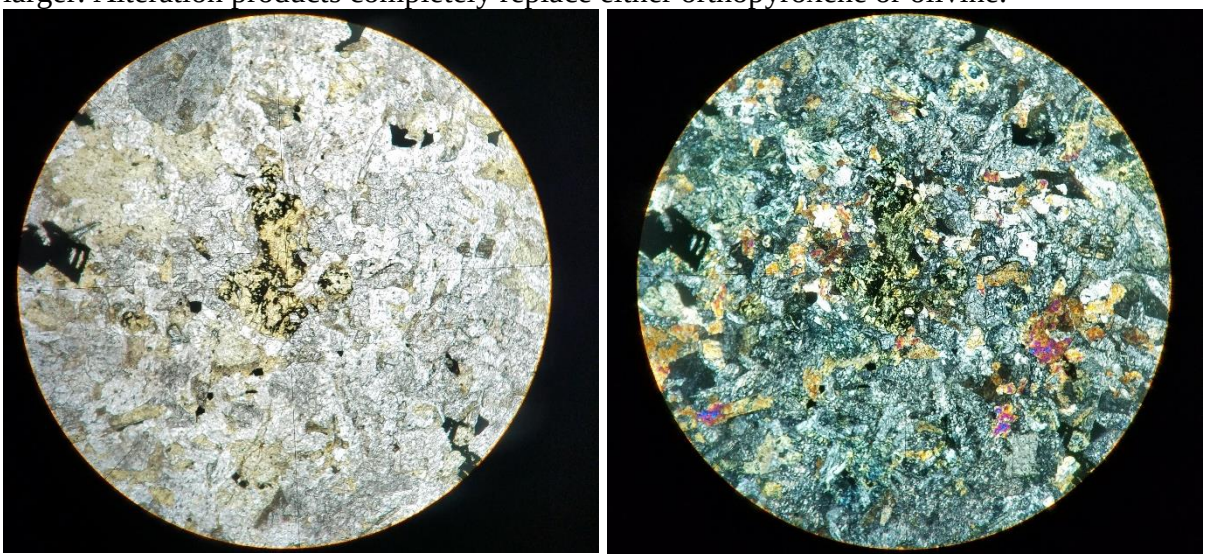

Width of view = 4 mm.

Sample 130w. Medium-grained ophitic diabase; 60% clinopyroxene, 35% plagioclase, 1% opaques, 5% altered mesostasis (with reddish orange alteration product) and locally similarly altered clinopyroxene.

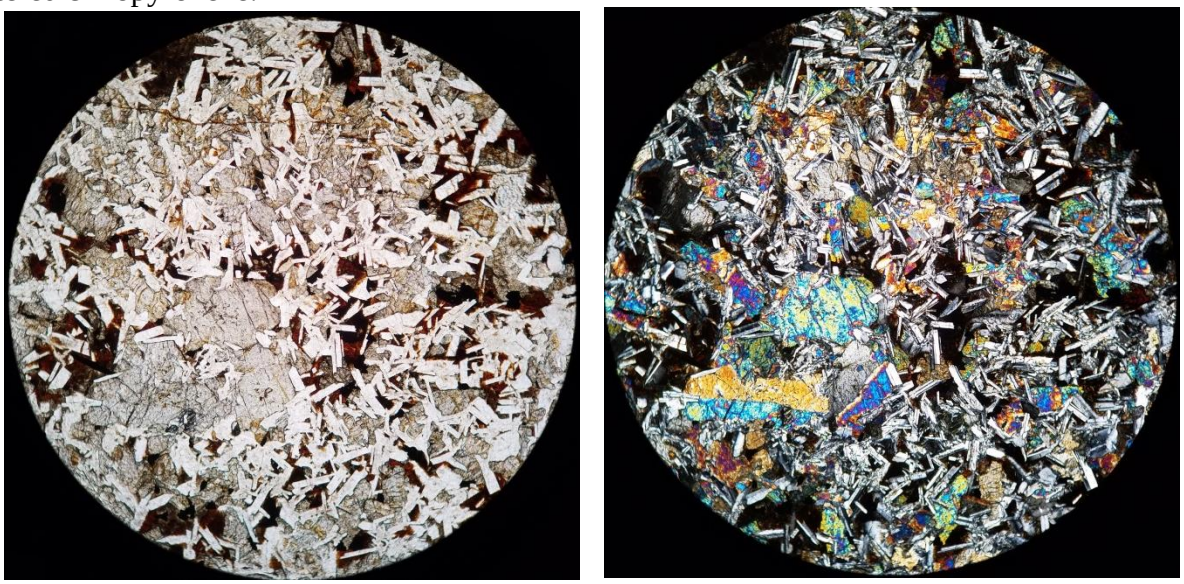

Width of view = 5 mm

Sample 131-6. Fine-grained, subophitic diabase with rare clinopyroxene phenocrysts (3.5 mm) and ~ 10% mesostasis; clinopyroxene (55%), plagioclase (35%), opaques with cubic morphology (~1%); reddish orange alteration of random clinopyroxene grains.

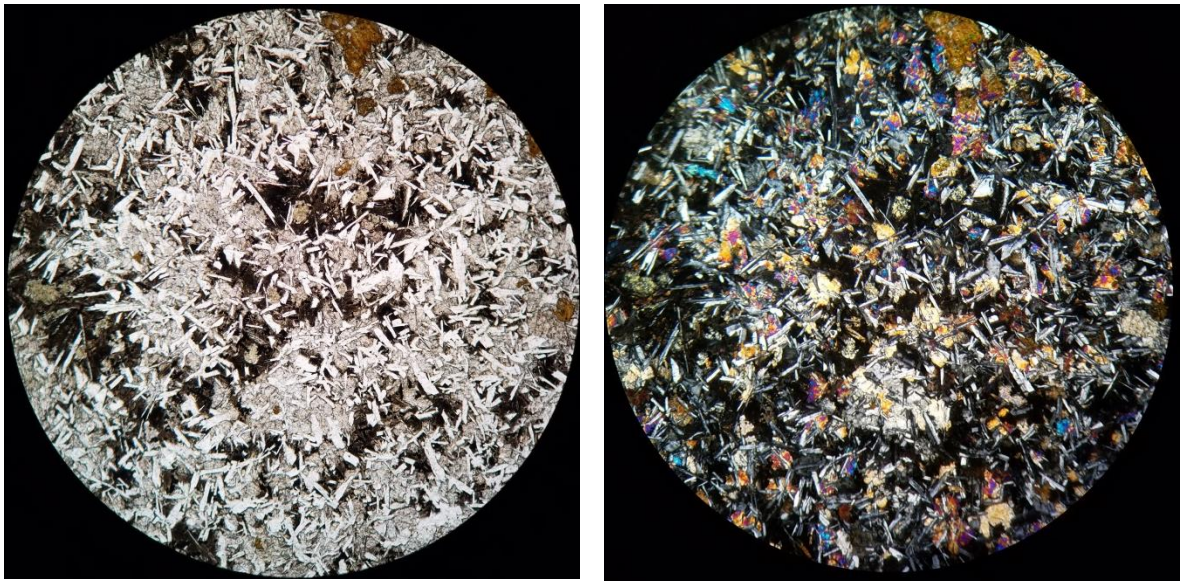

Width of view = 5 mm

Samples 131-14A, B. Contaminated diabase, very altered, with abundant sand-sized grains of quartz and lesser amounts of K-feldspar.

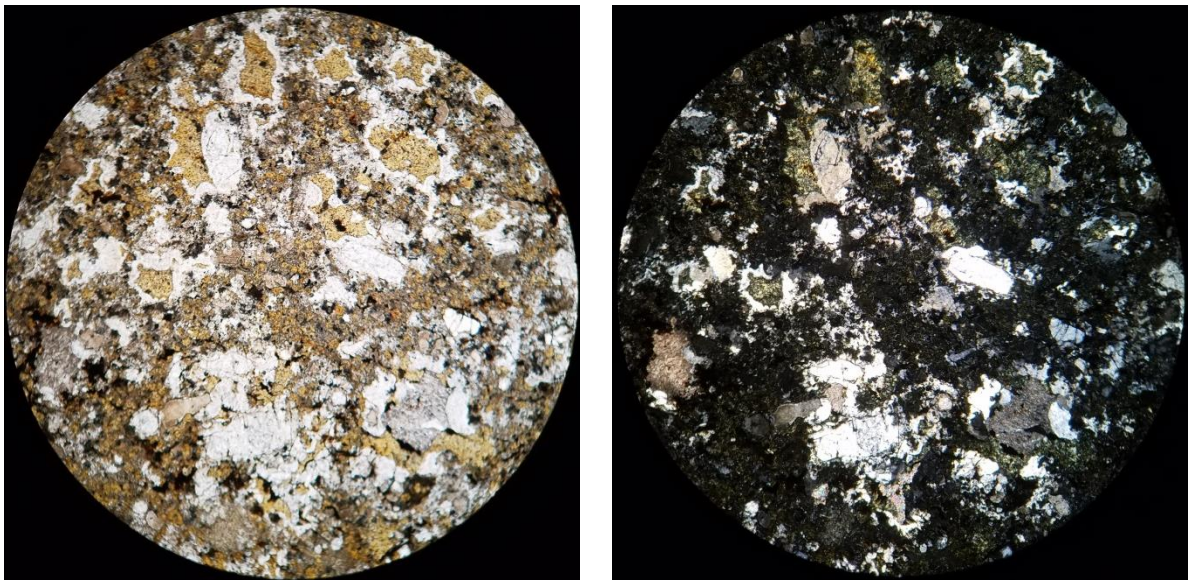

131.14A: Width of view = 5 mm

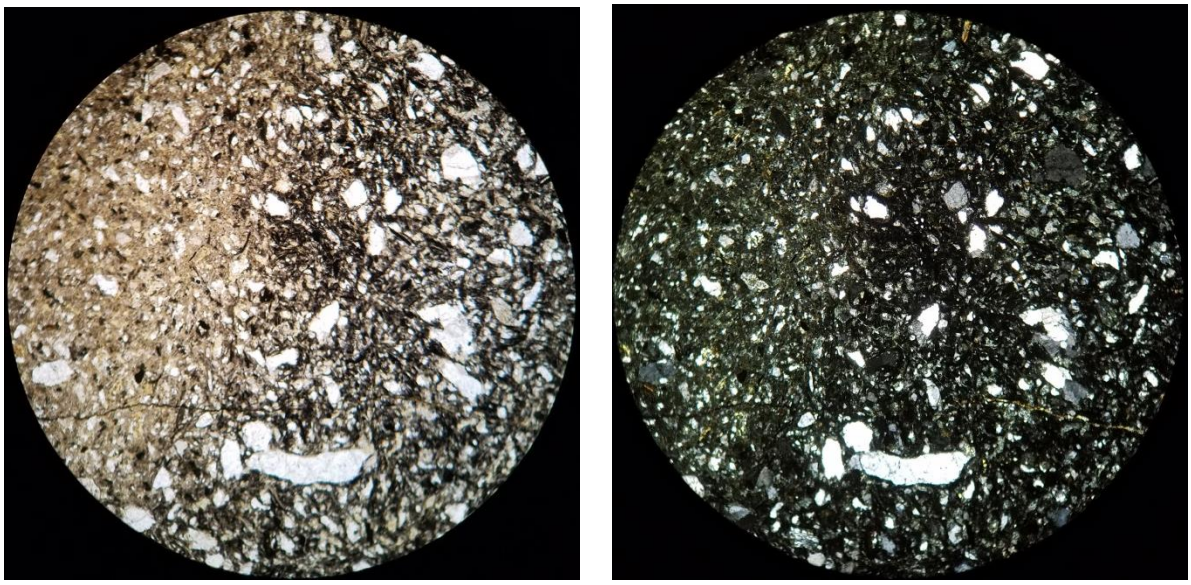

131.14B: Width of view = 5 mm

Sample 132B. Very fine-grained subophitic diabase with clinopyroxene phenocrysts (4-5 mm) and 5-10% mesostasis; clinopyroxene (55%) and plagioclase (35%) and about 1% opaques; one calcite filled amygdale; local widespread alteration of clinopyroxene and mesostasis to red-orange minerals.

Width of view = 5 mm

Sample 132C. Medium-grained subophitic diabase with <1% phenocrysts (0.5 mm) and <1% mesostasis; clinopyroxene (60%) and plagioclase (40%) and 1% opaques. Very minor calcite alteration

Width of view = 5 mm

Sample 132-2A. Fine-grained, subophitic diabase with 2-5% devitrified mesostasis containing clumps of opaques; 55% clinopyroxene, 40% plagioclase. 1 plagioclase phenocryst (1.5 mm).

Width of view = 5 mm

Sample 132-43. Medium-grained subophitic diabase with 2-5% crystallized mesostasis that has widespread alteration of red-orange mineral; clinopyroxene (55%) and plagioclase (40%) with ~1% opaques. 1 plagioclase phenocryst (1.7 mm).

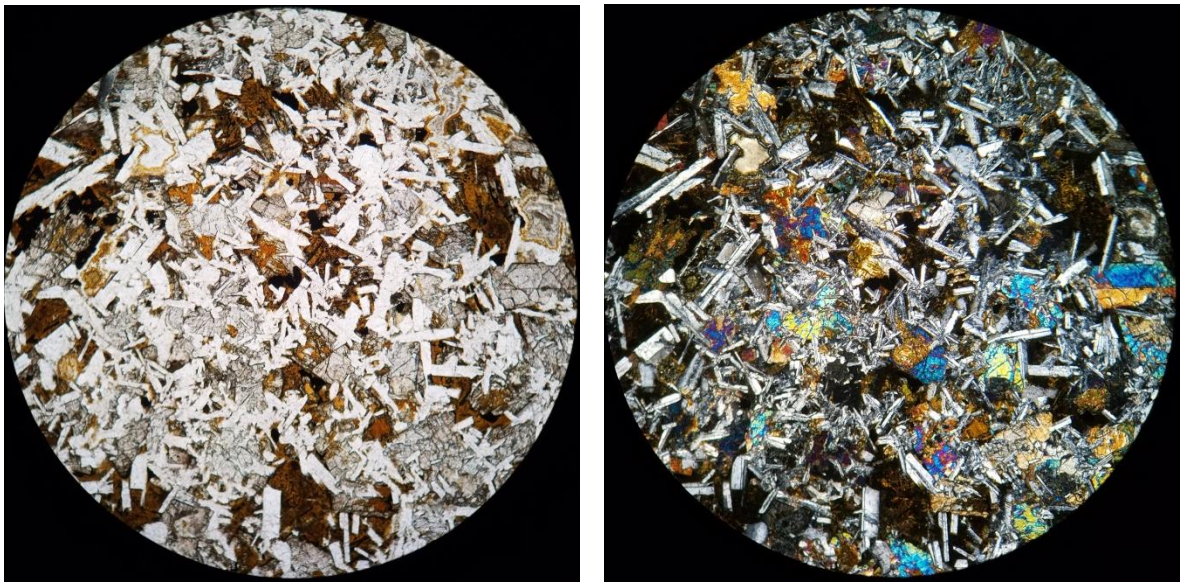

Width of view = 5 mm.

Sample 136-1. Very fine-grained diabase with small calcite filled amygdales; microlites mostly altered to calcite, some clinoperyxene microlites persist however; local calcite alteration. 50% devitrified glass.

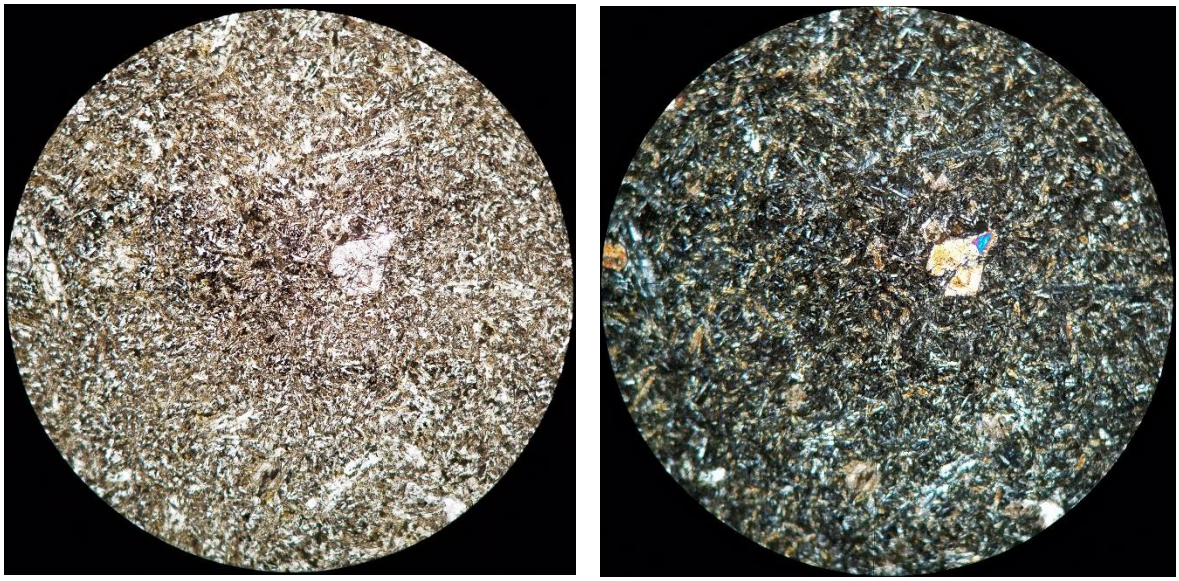

Width of view = 2 mm

Sample 136-4. Very fine-grained subophitic (?) diabase; ~20% mesostasis locally altered; clinopyroxene crystals locally altered to green mineral.

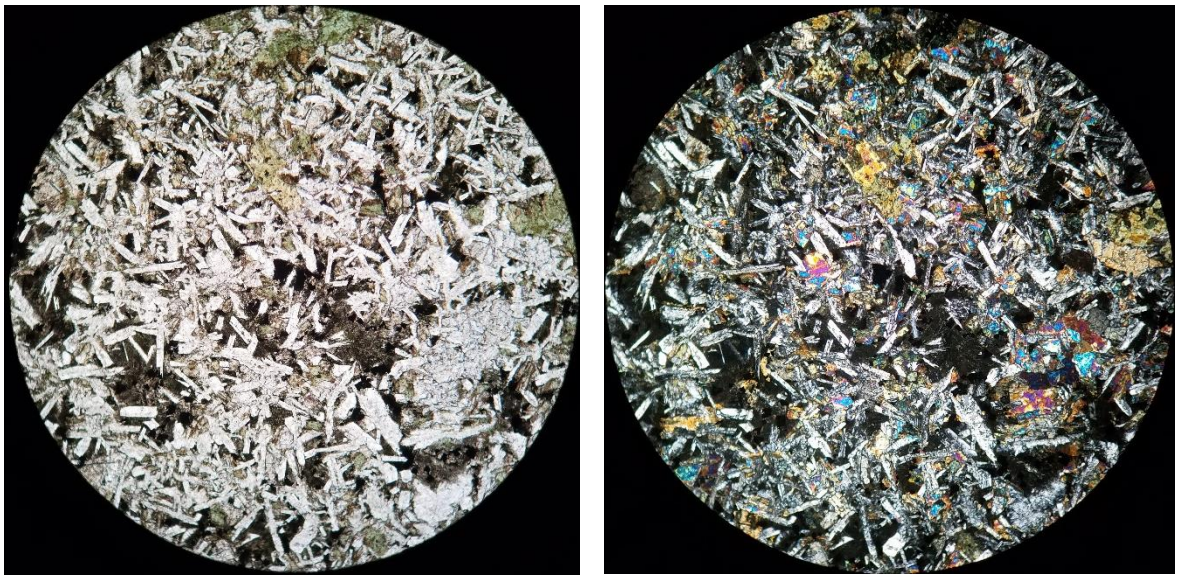

Width of view = 5 mm

Sample 137-1. Medium-grained diabase; diabasic (?) texture. Small stubby cllinopyroxene (~55%). Very large opaque minerals.

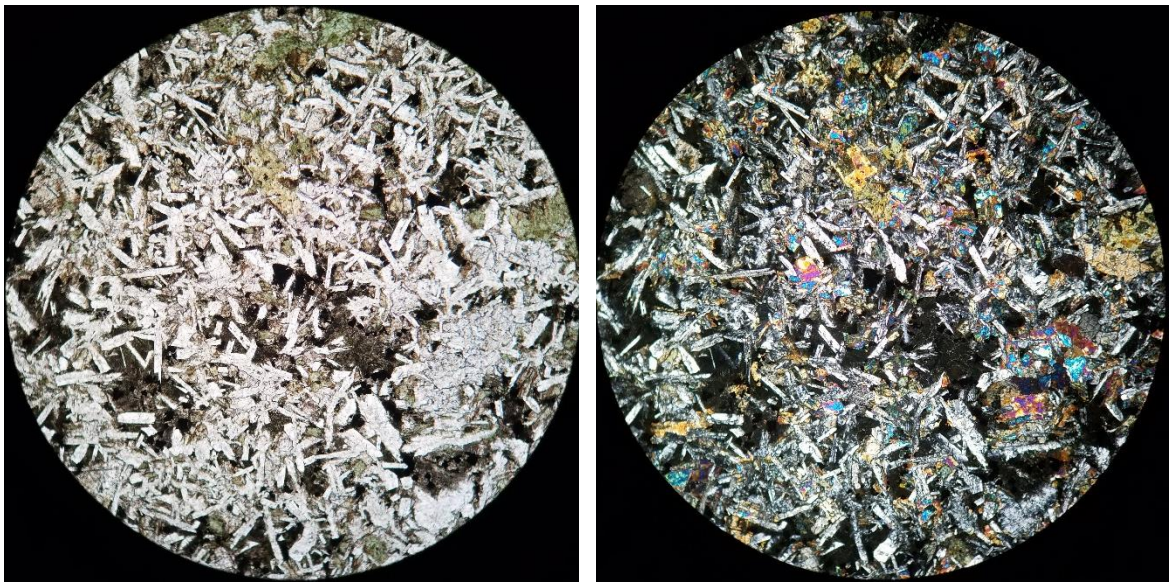

Width of view = 5 mm

Sample 140.1. Very fine-grained diabase with clinopyroxene and plagioclase microlites; medium-grained clinopyroxene and plagioclase glomerocrysts; local red-orange and calcitic alteration; no opaques.

Width of view = 5 mm

Sample 140-3A. Altered very fine-grained diabase, subophitic texture, ~15% mesostasis; clinopyroxene and plagioclase of equal abundance. One large plagioclase phenocryst.

Width of view = 5 mm

Buttress Diabase.

Sample 129-7. Very fine-grained subophitic diabase with <1% mesostasis; clinopyroxene (60%), plagioclase (40%), and 1% opaques.

Width of view = 5 mm.

Lamprophyre.

Sample 132-36A

Very fine-grained groundmass with phenocrysts, up to 1.5 cm of amphibole (1-3%). Groundmass composed of titanaugite, amphibole and magnetite with interstitial feldspar (mix of albite and K-feldspar).

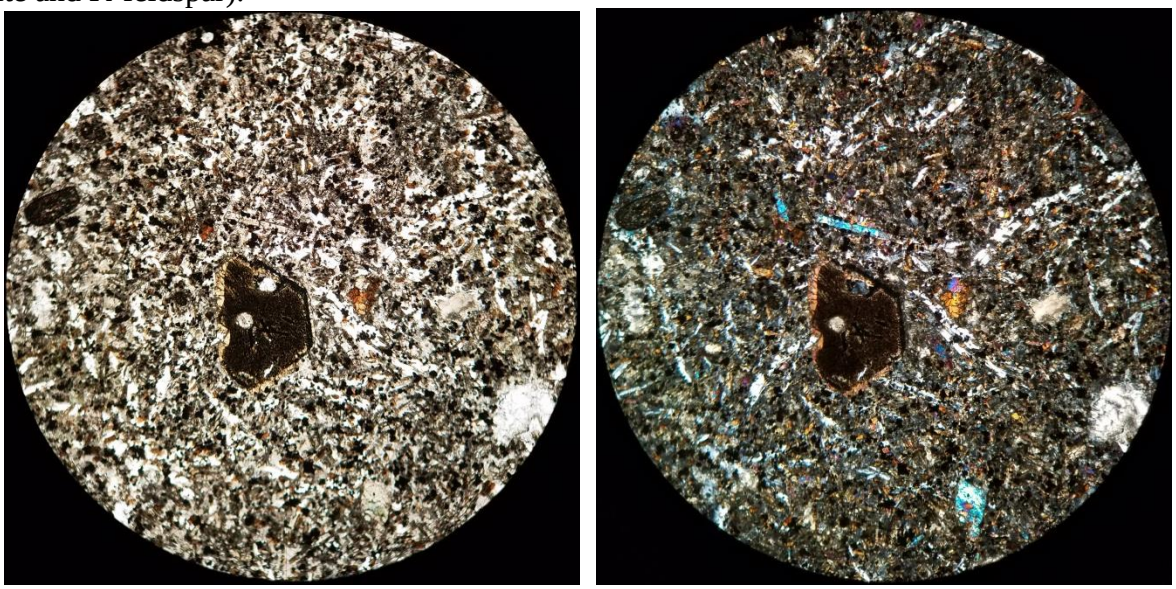

Width of view = 5 mm.

APPENDIX V. Structural Data

Local area map	Latitude	Longitude	Stratig. designat.	J O I N T S Strike	dip angle	#	Columnar/intersecting Joints Trend	Plunge	Observer *
100-1	41.4418470	-72.778969	Ji	300	90	1	318	68	AC, RS
100-1	41.4418470	-72.778969	Ji	320	90	1			AC, RS
100-1	41.4418470	-72.778969	Ji	35	20	1			AC, RS
100-2	41.4419040	-72.778881	Ji	228	66	1	324	70	AC, KT, RS
100-2	41.4419040	-72.778881	Ji	218	62	1			AC, KT, RS
100-2	41.4419140	-72.770321	Ji						AC, KT, RS
100-3	41.4416180	-72.779096	Ji	280	90	1			AC, KT, RS
100-3	41.4416180	-72.779096	Ji	260	90	1			AC, KT, RS
100-4	41.4416850	-72.778665	Ji	198	70	1			AC, KT, RS
100-5	41.4414660	-72.779286	Ji	28	73	1			AC, KT, RS
100-5	41.4414660	-72.779286	Ji	98	82	1			AC, KT, RS
100-7	41.4411510	-72.779108	Ji	106	90	1			AC, KT, RS
100-7	41.4411510	-72.779108	Ji	270	90	1			AC, KT, RS
100-9	41.4407700	-72.779994	Ji	300	90	1	290	70	AC, KT, RS
100-10	41.4402080	-72.780045	Ji	100	90	1			AC, KT, RS
100-10	41.4402080	-72.780045	Ji	90	70	1			AC, KT, RS
100-12	41.4407520	-72.778322	Ji	320	82	1			RS
100-12	41.4407520	-72.778322	Ji	16	82	1			RS
100-12a	41.4424770	-72.774208	Ji	282	82	1			RS, AC
100-14	41.4435160	-72.773385	Ji	290	90	1			RS, AC
100-16a	41.4431440	-72.772828	Ji	120	82	1			RS, AC
101-1	41.4362060	-72.780309	Ji	200	70				RS, AC
101-2	41.4364340	-72.780347	Ji	313	90				RS, AC
102	41.4338500	-72.782600	Ji	65	90	6			RV, JB
102	41.4338500	-72.782600	Ji	225	73	2			RV, JB
102	41.4338500	-72.782600	Ji	231	90	2			RV, JB
102	41.4338500	-72.782600	Ji	100	87	2			RV, JB
102	41.4338500	-72.782600	Ji	250	75	2			RV, JB
102	41.4338500	-72.782600	Ji	360	90	6			RV, JB
102	41.4338500	-72.782600	Ji	29	85	4			RV, JB
102	41.4338500	-72.782600	Ji	323	75	12			RV, JB
102	41.4338500	-72.782600	Ji	210	70	10			RV, JB
102	41.4338500	-72.782600	Ji	330	77	6			RV, JB
102	41.4312830	-72.784350	Ji	320	90	2			RV, JB
102	41.4312830	-72.784350	Ji	333	80	2			RV, JB
102	41.4312830	-72.784350	Ji	55	89	4			RV, JB
102	41.4312830	-72.784350	Ji	182	90	1			RV, JB
102	41.4312830	-72.784350	Ji	6	74	2			RV, JB
102	41.4307330	-72.784350	Ji	202	74	7			RV, JB
102	41.4307330	-72.784350	Ji	194	74	10			RV, JB
102	41.4307330	-72.784350	Ji	201	74	5			RV, JB
102	41.4307330	-72.784350	Ji	118	82	9			RV, JB
102	41.4307330	-72.784350	Ji	225	90	4			RV, JB

Local area map	Latitude	Longitude	Stratig. designat.	BEDDING Strike	BEDDING Dip	FAULTS Strike	FAULTS dip	Observer *
100-1	41.4418470	-72.778969	Ji					AC, RS
100-1	41.4418470	-72.778969	Ji					AC, RS
100-1	41.4418470	-72.778969	Ji					AC, RS
100-2	41.4419040	-72.778881	Ji					AC, KT, RS
100-2	41.4419040	-72.778881	Ji					AC, KT, RS
100-2	41.4419140	-72.770321	Ji			190	70	AC, KT, RS
100-3	41.4416180	-72.779096	Ji					AC, KT, RS
100-3	41.4416180	-72.779096	Ji					AC, KT, RS
100-4	41.4416850	-72.778665	Ji					AC, KT, RS
100-5	41.4414660	-72.779286	Ji					AC, KT, RS
100-5	41.4414660	-72.779286	Ji					AC, KT, RS
100-7	41.4411510	-72.779108	Ji					AC, KT, RS
100-7	41.4411510	-72.779108	Ji					AC, KT, RS
100-9	41.4407700	-72.779994	Ji					AC, KT, RS
100-10	41.4402080	-72.780045	Ji					AC, KT, RS
100-10	41.4402080	-72.780045	Ji					AC, KT, RS
100-12	41.4407520	-72.778322	Ji					RS
100-12	41.4407520	-72.778322	Ji					RS
100-12a	41.4424770	-72.774208	Ji					RS, AC
100-14	41.4435160	-72.773385	Ji					RS, AC
100-16a	41.4431440	-72.772828	Ji					RS, AC
101-1	41.4362060	-72.780309	Ji			200	40	RS, AC
101-2	41.4364340	-72.780347	Ji					RS, AC
102	41.4338500	-72.782600	Ji					RV, JB
102	41.4338500	-72.782600	Ji					RV, JB
102	41.4338500	-72.782600	Ji					RV, JB
102	41.4338500	-72.782600	Ji					RV, JB
102	41.4338500	-72.782600	Ji					RV, JB
102	41.4338500	-72.782600	Ji					RV, JB
102	41.4338500	-72.782600	Ji					RV, JB
102	41.4338500	-72.782600	Ji					RV, JB
102	41.4338500	-72.782600	Ji					RV, JB
102	41.4338500	-72.782600	Ji					RV, JB
102	41.4312830	-72.784350	Ji					RV, JB
102	41.4312830	-72.784350	Ji					RV, JB
102	41.4312830	-72.784350	Ji					RV, JB
102	41.4312830	-72.784350	Ji					RV, JB
102	41.4312830	-72.784350	Ji					RV, JB
102	41.4307330	-72.784350	Ji					RV, JB
102	41.4307330	-72.784350	Ji					RV, JB
102	41.4307330	-72.784350	Ji					RV, JB
102	41.4307330	-72.784350	Ji					RV, JB
102	41.4307330	-72.784350	Ji					RV, JB

Local area map	Latitude	Longitude	Stratig. designat.	J O I N T S Strike	dip angle	#	Columnar/intersecting Joints Trend	Plunge	Observer *
102	41.4307330	-72.784350	Ji	195	69	3			RV, JB
102	41.4307330	-72.784350	Ji	360	86	4			RV, JB
102	41.429901	-72.784649	Ji	336	85	1			RS
102	41.429901	-72.784649	Ji	320	90	1			RS
102	41.429901	-72.784649	Ji	135	90	1			RS
102	41.429901	-72.784649	Ji	150	88	1			RS
102	41.429901	-72.784649	Ji	168	60	1			RS
102	41.429901	-72.784649	Ji	190	75	1			RS
102	41.429953	-72.7842898	Trnh						RS
102	41.4300230	-72.784649	Ji	315	77	1			RS
103b-1	41.384063	-72.803415	Trnh	180	76	1			RS, RV, JB
103b	41.3849425	-72.803435	Trnh						RS, RV, JB
103b	41.3836469	-72.802118	Trnh						RS, RV, JB
103b	41.3836469	-72.802118	Trnh						RS, AC
103b-c	41.383987	-72.802969	Trnh						RS, AC
103b-a	41.383946	-72.802874	Trnh						RS, AC
103-14	41.379081	-72.805095	Trnh						RS, JB
103-11b	41.3778389	-72.807249	Trnh	156	26				RS, JB
103-11a	41.3777830	-72.807388	Trnh	62	18				
103	41.3777830	-72.807388	Trnh	182	18				
103	41.3790228	-72.807479							RS, JB
103-10	41.379634	-72.806977	Trnh						RS, JB
103	41.3791275	-72.807669	Trnh						RS, JB
104	41.3807403	-72.825478	Ji						RS, AC, JB, RV,MT
104	41.3807403	-72.825478							"
104	41.3801375	-72.825461	Ji	256	67	1			"
104	41.3801720	-72.825194							"
104	41.3806360	-72.825598	Trnh						"
104	41.3801833	-72.826008	Trnh						"
105	41.4389840	-72.824574	Trnh						RS, JB
106	41.4316830	-72.788283	Ji	280	90	2			RV, JB
106	41.4316830	-72.788283	Ji	325	72	7			RV, JB
106	41.4316830	-72.788283	Ji	225	74	9			RV, JB
106	41.4316830	-72.788283	Ji	290	85	10			RV, JB
106	41.4316830	-72.788283	Ji	305	74	4			RV, JB
106	41.4333830	-72.787267	Ji	119	86	5			RV, JB
106	41.4333830	-72.787267	Ji	300	82	8			RV, JB
106	41.4333830	-72.787267	Ji	10	90	10			RV, JB
106	41.4333830	-72.787267	Ji	315	90	4			RV, JB
106	41.4356000	-72.782533	Ji	279	82	1			RV, JB
106	41.4353313	-72.782558	Ji	284	90	1			RS, JB, RV, AC, MW
106	41.4350630	-72.782853	Ji	310	84	1			"
106	41.432306	-72.788237	Ji	328	78	1			"
106	41.4329180	-72.787679	Ji	6	90	1			"

Local area map	Latitude	Longitude	Stratig. designat.	B E D D I N G Strike	Dip	F A U L T S Strike	dip	Observer *
102	41.4307330	-72.784350	Ji					RV, JB
102	41.4307330	-72.784350	Ji					RV, JB
102	41.429901	-72.784649	Ji					RS
102	41.429901	-72.784649	Ji					RS
102	41.429901	-72.784649	Ji					RS
102	41.429901	-72.784649	Ji					RS
102	41.429901	-72.784649	Ji					RS
102	41.429901	-72.784649	Ji					RS
102	41.429953	-72.7842898	Trnh		105	5		RS
102	41.4300230	-72.784649	Ji					RS
103b-1	41.384063	-72.803415	Trnh	42	31			RS, RV, JB
103b	41.3849425	-72.803435	Trnh	32	27			RS, RV, JB
103b	41.3836469	-72.802118	Trnh	30	30			RS, RV, JB
103b	41.3836469	-72.802118	Trnh	310	24			RS, AC
103b-c	41.383987	-72.802969	Trnh	172	40			RS, AC
103b-a	41.383946	-72.802874	Trnh	133	72			RS, AC
103-14	41.379081	-72.805095	Trnh	274	37			RS, JB
103-11b	41.3778389	-72.807249	Trnh	336	26			RS, JB
103-11a	41.3777830	-72.807388	Trnh					
103	41.3777830	-72.807388	Trnh					
103	41.3790228	-72.807479				232	68	RS, JB
103-10	41.379634	-72.806977	Trnh	12	14			RS, JB
103	41.3791275	-72.807669	Trnh	12	22			RS, JB
104	41.3807403	-72.825478	Ji			344	84	RS, AC, JB, RV,MT
104	41.3807403	-72.825478				165	76	"
104	41.3801375	-72.825461	Ji					"
104	41.3801720	-72.825194				25	90	"
104	41.3806360	-72.825598	Trnh	142	24			"
104	41.3801833	-72.826008	Trnh	155	42			"
105	41.4389840	-72.824574	Trnh			60	22	RS, JB
106	41.4316830	-72.788283	Ji					RV, JB
106	41.4316830	-72.788283	Ji					RV, JB
106	41.4316830	-72.788283	Ji					RV, JB
106	41.4316830	-72.788283	Ji					RV, JB
106	41.4316830	-72.788283	Ji					RV, JB
106	41.4333830	-72.787267	Ji					RV, JB
106	41.4333830	-72.787267	Ji					RV, JB
106	41.4333830	-72.787267	Ji					RV, JB
106	41.4333830	-72.787267	Ji					RV, JB
106	41.4356000	-72.782533	Ji					RV, JB
106	41.4353313	-72.782558	Ji					RS, JB, RV, AC, MW
106	41.4350630	-72.782853	Ji					"
106	41.432306	-72.788237	Ji					"
106	41.4329180	-72.787679	Ji					"

Local area map	Latitude	Longitude	Stratig. designat.	J O I N T S Strike	dip angle	#	Columnar/intersecting Joints Trend	Plunge	Observer *
106	41.4329180	-72.787679	Ji	322	83	1			"
106	41.4318750	-72.788430	Ji	270	88	1			"
106	41.434371	-72.785573	Ji	326	83	1			"
106	41.4314580	-72.787908	Ji	40	82	1			"
106	41.432217	-72.788257	Trnh						"
106	41.431641	-72.789012	Trnh						"
107b				5	88	2			RV, JB
107b				289	90	3			RV, JB
107b1	41.4195260	-72.795669		59	74	1			RS, JB, RV
107b1	41.4195260	-72.795669		140	69	1			RS, JB, RV
107b1	41.4195260	-72.795669		69	68	1			RS, JB, RV
107b2	41.4182040	-72.794791							RS, JB, RV
107b	41.4182040	-72.794791		340	88	1			RS, JB, RV
107b	41.4160310	-72.793761		244	78	1			RS, JB, RV
107b	41.4160310	-72.793761		125	90	1			RS, JB, RV
107b	41.4160310	-72.793761		164	78	1			RS, JB, RV
107b	41.4132610	-72.794788		50	78	1			RS, JB, RV
107b	41.4154050	-72.793682	Trnh						RS, JB, RV
107b	41.4124860	-72.795025	Trnh						RS, JB, RV
107b-10	41.412870	-72.796458	Trnh						RS, JB, RV
108/108b	41.4214330	-72.786550	Trnh						RV, JB
108/108b	41.4209500	-72.786933		75	55	5			RV, JB
108/108b	41.4209500	-72.786933		30	60	5			RV, JB
108	41.4193980	-72.786848	Trnh						RS, JB, AC
108	41.4176110	-72.787417	Trnh						RS, JB, AC
108	41.4160390	-72.787653	Trnh						RS, JB, AC
108b	41.4205460	-72.787382							RS, JB, AC
108b	41.4215430	-72.786469							RS, JB, AC
108b	41.4213280	-72.786517							RS, JB, AC
108b	41.4204970	-72.786798	Trnh						RS, JB, AC
108b	41.4214000	-72.786042	Trnh						RS, JB, AC
108b	41.4220080	-72.784998	Trnh						RS, JB, AC
108b	41.4224720	-72.784856	Trnh						RS, JB, AC
109	41.4178380	-72.784721	Trnh						RS, JB, RV
110	41.4357550	-72.829263	Trnh						RS, JB
111	41.3909960	-72.775327	Jho	250	80	1			RS. AC, JB
111	41.3934450	-72.771009	Jho	278	65	1			RS. AC, JB
111	41.3959110	-72.769112	Jho	104	86	1			RS. AC, JB
111	41.3959110	-72.769112	Jho	180	88	1			RS. AC, JB
111	41.3959110	-72.769112	Jho	96	88	1			RS. AC, JB
112	41.3825710	-72.826430	Ji	4	90	1			RS, AC, RV
112	41.3825710	-72.826430	Ji	320	90	1			RS, AC, RV
112	41.3885010	-72.826959	Ji	60	90	1			RS, AC, RV
112	41.3885010	-72.826959	Ji	95	78	1			RS, AC, RV

Local area map	Latitude	Longitude	Stratig. designat.	B E D D I N G Strike	Dip	F A U L T S Strike	dip	Observer *
106	41.4329180	-72.787679	Ji					"
106	41.4318750	-72.788430	Ji					"
106	41.434371	-72.785573	Ji					"
106	41.4314580	-72.787908	Ji					"
106	41.432217	-72.788257	Trnh	36	16			"
106	41.431641	-72.789012	Trnh	44	22			"
107b								RV, JB
107b								RV, JB
107b1	41.4195260	-72.795669						RS, JB, RV
107b1	41.4195260	-72.795669						RS, JB, RV
107b1	41.4195260	-72.795669						RS, JB, RV
107b2	41.4182040	-72.794791				340	90	RS, JB, RV
107b	41.4182040	-72.794791						RS, JB, RV
107b	41.4160310	-72.793761						RS, JB, RV
107b	41.4160310	-72.793761						RS, JB, RV
107b	41.4160310	-72.793761						RS, JB, RV
107b	41.4132610	-72.794788						RS, JB, RV
107b	41.4154050	-72.793682	Trnh	28	12			RS, JB, RV
107b	41.4124860	-72.795025	Trnh	24	11			RS, JB, RV
107b-10	41.412870	-72.796458	Trnh	20	14			RS, JB, RV
108/108b	41.4214330	-72.786550	Trnh	270	30			RV, JB
108/108b	41.4209500	-72.786933						RV, JB
108/108b	41.4209500	-72.786933						RV, JB
108	41.4193980	-72.786848	Trnh	46	26			RS, JB, AC
108	41.4176110	-72.787417	Trnh	36	15			RS, JB, AC
108	41.4160390	-72.787653	Trnh	24	12			RS, JB, AC
108b	41.4205460	-72.787382				210	51	RS, JB, AC
108b	41.4215430	-72.786469				330	90	RS, JB, AC
108b	41.4213280	-72.786517				334	90	RS, JB, AC
108b	41.4204970	-72.786798	Trnh	28	26			RS, JB, AC
108b	41.4214000	-72.786042	Trnh	42	25			RS, JB, AC
108b	41.4220080	-72.784998	Trnh	62	12			RS, JB, AC
108b	41.4224720	-72.784856	Trnh	52	10			RS, JB, AC
109	41.4178380	-72.784721	Trnh	58	28			RS, JB, RV
110	41.4357550	-72.829263	Trnh	50	14			RS, JB
111	41.3909960	-72.775327	Jho					RS. AC, JB
111	41.3934450	-72.771009	Jho					RS. AC, JB
111	41.3959110	-72.769112	Jho					RS. AC, JB
111	41.3959110	-72.769112	Jho					RS. AC, JB
111	41.3959110	-72.769112	Jho					RS. AC, JB
112	41.3825710	-72.826430	Ji					RS, AC, RV
112	41.3825710	-72.826430	Ji					RS, AC, RV
112	41.3885010	-72.826959	Ji					RS, AC, RV
112	41.3885010	-72.826959	Ji					RS, AC, RV

Local area map	Latitude	Longitude	Stratig. designat.	J O I N T S Strike	dip angle	#	Columnar/intersecting Joints Trend	Plunge	Observer *
112	41.384346	-72.827035	Ji	41	90	1			RS, AC, RV
112	41.3819170	-72.825817	Ji	75	curved	7			RV, JB
112	41.3819170	-72.825817	Ji	175	curved	6			RV, JB
112	41.3819170	-72.825817	Ji	95	54	10			RV, JB
112	41.3819170	-72.825817	Ji	138	80	1			RV, JB
112	41.3819170	-72.825817	Ji	223	88	10			RV, JB
112	41.3819170	-72.825817	Ji	147	90	3			RV, JB
112	41.3819170	-72.825817	Ji	180	unknwn	5			RV, JB
112	41.3819170	-72.825817	Ji	217	unknwn	3			RV, JB
112	41.3819170	-72.825817	Ji	322	36	2			RV, JB
112	41.3819170	-72.825817	Ji	320	75	5			RV, JB
112	41.3819170	-72.825817	Ji	150	58	2			RV, JB
112	41.3819170	-72.825817	Ji	46	78	3			RV, JB
112	41.3819170	-72.825817	Ji	265	76	4			RV, JB
112	41.3819170	-72.825817	Ji	170	90	2			RV, JB
112	41.3819170	-72.825817	Ji	75	74	7			RV, JB
112	41.3819170	-72.825817	Ji	270	54	6			RV, JB
112	41.3866330	-72.827217	Ji	240	45	20			RV, JB
112	41.387533	-72.827134	Ji	240	66	6			RV, JB
112	41.3866330	-72.827217	Ji	295	70	2			RV, JB
112	41.3866330	-72.827217	Ji	215	81	4			RV, JB
112	41.3866330	-72.827217	Ji	323	58	3			RV, JB
112	41.3866330	-72.827217	Ji	350	81	8			RV, JB
112	41.3866330	-72.827217	Ji	30	85	3			RV, JB
112	41.387783	-72.827071	Ji	250	75	3			RV, JB
112	41.387783	-72.827071	Ji	160	81	3			RV, JB
112	41.387169	-72.827212	Ji	270	70	2			RV, JB
112	41.387169	-72.827212	Ji	15	87	2			RV, JB
112	41.3866330	-72.827217	Ji	260	54	3			RV, JB
112	41.3866330	-72.827217	Ji	0	75	10			RV, JB
113-2	41.398029	-72.769786	Jsm						
113	41.4001280	-72.769161	Jho	270	72	1			RS, JB, RV, AC
113-a	41.403063	-72.752596	Jho	278	82				
113	41.4013790	-72.766076	Jho	342	86	1			"
113	41.4013790	-72.766076	Jho	197	84	1			"
113	41.4013790	-72.766076	Jho	258	73	1			"
113	41.4013790	-72.766076	Jho	350	78	1			"
113	41.4013790	-72.766076	Jho	225	72	1			"
113-1	41.396247	-72.759657	Jho	350	85	2			RS, JB
113-1	41.396247	-72.759657	Jho	121	74	3			RS, JB
113-1	41.396247	-72.759657	Jho	239	77	4			RS, JB
113-2	41.396522	-72.761114	Jho	250	65	1			RS, JB
113-2	41.396522	-72.761114	Jho	70	90	4			RS, JB
113	41.3969130	-72.760950	Jho	129	80	7			RS, JB

Local area map	Latitude	Longitude	Stratig. designat.	BEDDING Strike	Dip	FAULTS Strike	dip	Observer *
112	41.384346	-72.827035	Ji					RS, AC, RV
112	41.3819170	-72.825817	Ji					RV, JB
112	41.3819170	-72.825817	Ji					RV, JB
112	41.3819170	-72.825817	Ji					RV, JB
112	41.3819170	-72.825817	Ji					RV, JB
112	41.3819170	-72.825817	Ji					RV, JB
112	41.3819170	-72.825817	Ji					RV, JB
112	41.3819170	-72.825817	Ji					RV, JB
112	41.3819170	-72.825817	Ji					RV, JB
112	41.3819170	-72.825817	Ji					RV, JB
112	41.3819170	-72.825817	Ji					RV, JB
112	41.3819170	-72.825817	Ji					RV, JB
112	41.3819170	-72.825817	Ji					RV, JB
112	41.3819170	-72.825817	Ji					RV, JB
112	41.3819170	-72.825817	Ji					RV, JB
112	41.3819170	-72.825817	Ji					RV, JB
112	41.3819170	-72.825817	Ji					RV, JB
112	41.3866330	-72.827217	Ji					RV, JB
112	41.387533	-72.827134	Ji					RV, JB
112	41.3866330	-72.827217	Ji					RV, JB
112	41.3866330	-72.827217	Ji					RV, JB
112	41.3866330	-72.827217	Ji					RV, JB
112	41.3866330	-72.827217	Ji					RV, JB
112	41.3866330	-72.827217	Ji					RV, JB
112	41.387783	-72.827071	Ji					RV, JB
112	41.387783	-72.827071	Ji					RV, JB
112	41.387169	-72.827212	Ji					RV, JB
112	41.387169	-72.827212	Ji					RV, JB
112	41.3866330	-72.827217	Ji					RV, JB
112	41.3866330	-72.827217	Ji					RV, JB
113-2	41.398029	-72.769786	Jsm	66	21			
113	41.4001280	-72.769161	Jho					RS, JB, RV, AC
113-a	41.403063	-72.752596	Jho					
113	41.4013790	-72.766076	Jho					"
113	41.4013790	-72.766076	Jho					"
113	41.4013790	-72.766076	Jho					"
113	41.4013790	-72.766076	Jho					"
113	41.4013790	-72.766076	Jho					"
113-1	41.396247	-72.759657	Jho					RS, JB
113-1	41.396247	-72.759657	Jho					RS, JB
113-1	41.396247	-72.759657	Jho					RS, JB
113-2	41.396522	-72.761114	Jho					RS, JB
113-2	41.396522	-72.761114	Jho					RS, JB
113	41.3969130	-72.760950	Jho					RS, JB

Local area map	Latitude	Longitude	Stratig. designat.	J O I N T S			Columnar/intersecting Joints		Observer *
				Strike	dip angle	#	Trend	Plunge	
113-2	41.396522	-72.761114	Jho	160	70	2			RS, JB
113-3	41.3971296	-72.760175	Jho	250	72	2			RS, JB
113-3	41.3971296	-72.760175	Jho	320	85	1			RS, JB
113-3	41.3971296	-72.760175	Jho	345	75	1			RS, JB
113-4	41.393447	-72.758871	Jho	240	75	5			RS, JB
113-4	41.393447	-72.758871	Jho	330	75	3			RS, JB
113-5	41.389627	-72.760156	Jho	257	85	1			RS, JB
113-5	41.389627	-72.760156	Jho	345	88	1			RS, JB
113-6	41.389939	-72.760237	Jho	240	90	3			RS, JB
113-6	41.389939	-72.760237	Jho	135	90	1			RS, JB
113-6	41.389939	-72.760237	Jho	310	85	2			RS, JB
113	41.3921320	-72.758671	Jho	320	90	5			RS, JB
113-8	41.393857	-72.757897	Jho	240	90	1			RS, JB
113-9	41.394805	-72.757074	Jho	333	90	1			RS, JB
113	41.3921320	-72.758671	Jho	233	79	1			RS, JB
115-2	41.380026	-72.767566	Jho	50	90	1			RS, JB
115-a	41.379004	-72.768086	Jho	318	76	1			RS, JB
115-a	41.379004	-72.768086	Jho	56	90	1			RS, JB
115	41.3782940	-72.767826	Jho	315	90	1			RS, JB
115-b	41.379472	-72.768498	Jho	58	90	1			RS, JB
115-d	41.376647	-72.767913	Jho	340	85	1			RS, JB
115-c	41.376989	-72.765627	Jho	54	90	1			RS, JB
115-1	41.378692	-72.765240	Jho	236	85	1			RS, JB
115-f	41.385104	-72.764726	Jho	55	90	1			RS, JB
115-e	41.383821	-72.764696	Jho	56	77	1			RS, JB
116	41.4279250	-72.791756	Ji	238	71	1			RS, JB, RV, MT
116	41.4279490	-72.793212	Ji	175	82	1			"
116	41.4279490	-72.793212	Ji	350	90	1			"
116	41.4261620	-72.793721	Ji	96	88	1			"
116	41.4261370	-72.796123	Ji	236	88	1			"
116	41.4241350	-72.798654	Trnh	346	85	1			"
116	41.4241350	-72.798654	Ji	176	82	1			"
116	41.4229210	-72.796564	Ji	70	90	1			"
116	41.4296640	-72.791726	Trnh						"
116	41.4273760	-72.794130	Trnh						"
116	41.4205620	-72.797534	Trnh						"
117	41.4113720	-72.804811	Ji	164	75	5			RS, RV
117	41.4113720	-72.804811	Ji	114	85	7			RS, RV
117	41.4113720	-72.804811	Ji	75	90	3			RS, RV
117	41.4113720	-72.804811	Ji	215	90	1			RS, RV
117	41.4113720	-72.804811	Ji	180	80	1			RS, RV
117	41.4113720	-72.804811	Ji	85	85	1			RS, RV
117	41.4116700	-72.804614	Ji	30	80	2			RS, RV
117	41.4133080	-72.804734	Ji	230	81	1			RS, RV

Local area map	Latitude	Longitude	Stratig. designat.	B E D D I N G		F A U L T S		Observer *
				Strike	Dip	Strike	dip	
113-2	41.396522	-72.761114	Jho					RS, JB
113-3	41.3971296	-72.760175	Jho					RS, JB
113-3	41.3971296	-72.760175	Jho					RS, JB
113-3	41.3971296	-72.760175	Jho					RS, JB
113-4	41.393447	-72.758871	Jho					RS, JB
113-4	41.393447	-72.758871	Jho					RS, JB
113-5	41.389627	-72.760156	Jho					RS, JB
113-5	41.389627	-72.760156	Jho					RS, JB
113-6	41.389939	-72.760237	Jho					RS, JB
113-6	41.389939	-72.760237	Jho					RS, JB
113-6	41.389939	-72.760237	Jho					RS, JB
113	41.3921320	-72.758671	Jho					RS, JB
113-8	41.393857	-72.757897	Jho					RS, JB
113-9	41.394805	-72.757074	Jho					RS, JB
113	41.3921320	-72.758671	Jho					RS, JB
115-2	41.380026	-72.767566	Jho					RS, JB
115-a	41.379004	-72.768086	Jho					RS, JB
115-a	41.379004	-72.768086	Jho					RS, JB
115	41.3782940	-72.767826	Jho					RS, JB
115-b	41.379472	-72.768498	Jho					RS, JB
115-d	41.376647	-72.767913	Jho					RS, JB
115-c	41.376989	-72.765627	Jho					RS, JB
115-1	41.378692	-72.765240	Jho					RS, JB
115-f	41.385104	-72.764726	Jho					RS, JB
115-e	41.383821	-72.764696	Jho					RS, JB
116	41.4279250	-72.791756	Ji					RS, JB, RV, MT
116	41.4279490	-72.793212	Ji					"
116	41.4279490	-72.793212	Ji					"
116	41.4261620	-72.793721	Ji					"
116	41.4261370	-72.796123	Ji					"
116	41.4241350	-72.798654	Trnh	50	17			"
116	41.4241350	-72.798654	Ji					"
116	41.4229210	-72.796564	Ji					"
116	41.4296640	-72.791726	Trnh	42	22			"
116	41.4273760	-72.794130	Trnh	80	12			"
116	41.4205620	-72.797534	Trnh	10	25			"
117	41.4113720	-72.804811	Ji					RS, RV
117	41.4113720	-72.804811	Ji					RS, RV
117	41.4113720	-72.804811	Ji					RS, RV
117	41.4113720	-72.804811	Ji					RS, RV
117	41.4113720	-72.804811	Ji					RS, RV
117	41.4113720	-72.804811	Ji					RS, RV
117	41.4116700	-72.804614	Ji					RS, RV
117	41.4133080	-72.804734	Ji					RS, RV

Local area map	Latitude	Longitude	Stratig. designat.	J O I N T S Strike	dip angle	#	Columnar/intersecting Joints Trend	Plunge	Observer *
117	41.4133080	-72.804734	Ji	290	80	1			RS, RV
117.6	41.413660	-72.804296	Ji	290	90	5			RS, RV
117.1	41.4108660	-72.804692	Trnh						RS, RV
117.5	41.4125930	-72.805604	Trnh						RS, RV
118	41.4022460	-72.816531	Ji	125	75	3			
118	41.4029320	-72.816178	Ji	130	85	3			
118	41.4029320	-72.816178	Ji	260	58	1			
118	41.4029320	-72.816178	Ji	26	62	5			
118	41.4052500	-72.814183	Ji	144	80	5			
118	41.4052500	-72.814183	Ji	270	75	1			
118	41.4052500	-72.814183	Ji	205	86	1			
118	41.4070330	-72.809600	Ji	10	76	1			
118	41.4070330	-72.809600	Ji	245	44	3			
118	41.4011590	-72.817846	Trnh						
118w	41.4101570	-72.817472	Trnh						RS, JB
118w	41.4209280	-72.812858	Trnh						RS, JB
118w	41.4056540	-72.817721	Trnh						RS, JB, AC, MW
118w	41.4056540	-72.817721	Ji-Brx						RS, JB
119	Loc3		Ji	230	88				RV, JB
119	5		Ji	35	71	5			RV, JB
119	6		Ji	302	88	1			RV, JB
119	6		Ji	310	88	1			RV, JB
119	6		Ji	305	88	1			RV, JB
119	7		Ji	206	40	3			RV, JB
119	8		Ji	25	70	7			RV, JB
119	9		Ji	230	65	5			RV, JB
119	10		Ji	60	52	6			RV, JB
119	11		Ji	82	88	10			RV, JB
119	41.3996020	-72.819771	Ji	125	78	1			RS, JB
120	41.4199880	-72.801399	Trnh						RS, JB, RV
120	41.4207920	-72.801796	Trnh						RS, JB, RV
120	41.420911	-72.802309	Trnh						RS, JB, RV
121	41.3880850	-72.770201	Jho	240	65				RS, JB, RV
121	41.3880850	-72.770201	Jho	225	82				RS, JB, RV
121	41.387203	-72.775523	Jsm						RS, JB, RV
121	41.3873990	-72.771107	Jsm						RS, JB, RV
122	41.4341460	-72.874105	Ji	350	90	17			??JB, RV
122	41.4341460	-72.874105	Ji	250	78	23			
122	41.4341460	-72.874105	Ji	345	87	7			
122	41.4341460	-72.874105	Ji	280	not meas	6			
122	41.4341460	-72.874105	Ji	355	88	7			
122	41.4341460	-72.874105	Ji	360	not meas	5			
122	41.4341460	-72.874105	Ji	10	88	3			
122	41.4341460	-72.874105	Ji	15	90	2			

Local area map	Latitude	Longitude	Stratig. designat.	B E D D I N G		F A U L T S		Observer *
				Strike	Dip	Strike	dip	
117	41.4133080	-72.804734	Ji					RS, RV
117.6	41.413660	-72.804296	Ji					RS, RV
117.1	41.4108660	-72.804692	Trnh	14	25			RS, RV
117.5	41.4125930	-72.805604	Trnh	5	21			RS, RV
118	41.4022460	-72.816531	Ji					
118	41.4029320	-72.816178	Ji					
118	41.4029320	-72.816178	Ji					
118	41.4029320	-72.816178	Ji					
118	41.4052500	-72.814183	Ji					
118	41.4052500	-72.814183	Ji					
118	41.4052500	-72.814183	Ji					
118	41.4070330	-72.809600	Ji					
118	41.4070330	-72.809600	Ji					
118	41.4011590	-72.817846	Trnh	24	26			
118w	41.4101570	-72.817472	Trnh	34	14			RS, JB
118w	41.4209280	-72.812858	Trnh	26	18			RS, JB
118w	41.4056540	-72.817721	Trnh	12	16			RS, JB, AC, MW
118w	41.4056540	-72.817721	Ji-Brx	26	16			RS, JB
119	Loc3		Ji					RV, JB
119	5		Ji					RV, JB
119	6		Ji					RV, JB
119	6		Ji					RV, JB
119	6		Ji					RV, JB
119	7		Ji					RV, JB
119	8		Ji					RV, JB
119	9		Ji					RV, JB
119	10		Ji					RV, JB
119	11		Ji					RV, JB
119	41.3996020	-72.819771	Ji			125	78	RS, JB
120	41.4199880	-72.801399	Trnh	6	14			RS, JB, RV
120	41.4207920	-72.801796	Trnh	60	11			RS, JB, RV
120	41.420911	-72.802309	Trnh	68	15			RS, JB, RV
121	41.3880850	-72.770201	Jho					RS, JB, RV
121	41.3880850	-72.770201	Jho					RS, JB, RV
121	41.387203	-72.775523	Jsm	52	12			RS, JB, RV
121	41.3873990	-72.771107	Jsm	50	15			RS, JB, RV
122	41.4341460	-72.874105	Ji					??JB, RV
122	41.4341460	-72.874105	Ji					
122	41.4341460	-72.874105	Ji					
122	41.4341460	-72.874105	Ji					
122	41.4341460	-72.874105	Ji					
122	41.4341460	-72.874105	Ji					
122	41.4341460	-72.874105	Ji					
122	41.4341460	-72.874105	Ji					

Local area map	Latitude	Longitude	Stratig. designat.	J O I N T S Strike	dip angle	#	Columnar/intersecting Joints Trend	Plunge	Observer *
122	41.4341460	-72.874105	Ji	340	80	4			
122	41.4341460	-72.874105	Ji	350	90	7			
122	41.4341460	-72.874105	Ji	255	not meas	1			
122	41.4341460	-72.874105	Ji	285	76	3			
122	41.4341460	-72.874105	Ji	80	75	13			
122-4	41.431043	-72.874146	Trnh						RS
122	41.4341180	-72.870933	Trnh						RS
122S	41.428468	-72.874677	Trnh						RS, JB
122S	41.428541	-72.874561	Trnh	310	74	1			RS, JB
122S	41.428541	-72.874561	Trnh	94	14	1			RS, JB
122S	41.4323700	-72.873120	Trnh						RS, JB
122S	41.430256	-72.874746	Trnh						RS, JB
122E	41.4315500	-72.869400	Ji	35	86	1			RS, JB
122E	41.4315500	-72.869400	Ji	160	85	1			RS, JB
122-12	41.432301	-72.869443	Ji	164	72				RS, JB
122-12	41.431043	-72.874146	Trnh						RS, JB
122E	41.4337710	-72.860288	Trnh						RS, JB
122E	41.4337710	-72.860288	Trnh						RS, JB
122-18	41.433995	-72.857777	Trnh						
122E	41.4296880	-72.863645	Trnh						RS, JB, AC
123	41.4004420	-72.788655	Trnh	210	63	3			RS, RV
123	41.4004420	-72.788655	Trnh	129	90	2			RS, RV
123	41.4004420	-72.788655	Trnh	125	70	2			RS, RV
123	41.4004420	-72.788655	Trnh	340	90	1			RS, RV
123	41.4010140	-72.788276	Trnh	210	90	3			RS, RV
123	41.4010140	-72.788276	Trnh	120	90	2			RS, RV
123	41.4010140	-72.788276	Trnh	180	90	1			RS, RV
123-3	41.401719	-72.788106	Trnh	125	90	1			RS, RV
123-3	41.401719	-72.788106	Trnh	270	90	1			RS, RV
123-3	41.401719	-72.788106	Trnh	350	90	1			RS, RV
123	41.4015860	-72.787960	Trnh	210	90	1			RS, RV
123	41.4015860	-72.787960	Trnh	10	90	1			RS, RV
124	41.3770110	-72.824056	Ji/Trnh	290	88	1			RS, JB
124	41.3770110	-72.824056	Ji/Trnh	310	90	1			RS, JB
124	41.3770110	-72.824056	Ji/Trnh	360	90	1			RS, JB
126-2	41.404277	-72.775350	Jtab						RS, JB
127	41.4196250	-72.870448	Trnh						RS, JB
129-1	41.4823050	-72.869684	Jb	355	82				RS, AC, JB, HS
129-1	41.4823050	-72.869684	Jb	204	76				"
129-2	41.4833050	-72.869115	Jb						"
129-4	41.4851990	-72.868226	Jb	40	78				"
129-7	41.4939390	-72.866469	Trnh						RS, JB, HS
129-9	41.4918490	-72.870697	Trnh						RS, JB, HS
130W-3	41.4678895	-72.866727	Jwr	242	70				AC, RS

Local area map	Latitude	Longitude	Stratig. designat.	BEDDING		FAULTS		Observer *
				Strike	Dip	Strike	dip	
122	41.4341460	-72.874105	Ji					
122	41.4341460	-72.874105	Ji					
122	41.4341460	-72.874105	Ji					
122	41.4341460	-72.874105	Ji					
122	41.4341460	-72.874105	Ji					
122-4	41.431043	-72.874146	Trnh	24	18			RS
122	41.4341180	-72.870933	Trnh	34	26			RS
122S	41.428468	-72.874677	Trnh	40	9			RS, JB
122S	41.428541	-72.874561	Trnh					RS, JB
122S	41.428541	-72.874561	Trnh					RS, JB
122S	41.4323700	-72.873120	Trnh	6	10			RS, JB
122S	41.430256	-72.874746	Trnh	35	17			RS, JB
122E	41.4315500	-72.869400	Ji					RS, JB
122E	41.4315500	-72.869400	Ji					RS, JB
122-12	41.432301	-72.869443	Ji					RS, JB
122-12	41.431043	-72.874146	Trnh	34	14			RS, JB
122E	41.4337710	-72.860288	Trnh	37	12			RS, JB
122E	41.4337710	-72.860288	Trnh	40	18			RS, JB
122-18	41.433995	-72.857777	Trnh	20	16			
122E	41.4296880	-72.863645	Trnh	60	17			RS, JB, AC
123	41.4004420	-72.788655	Trnh	20	34			RS, RV
123	41.4004420	-72.788655	Trnh					RS, RV
123	41.4004420	-72.788655	Trnh					RS, RV
123	41.4004420	-72.788655	Trnh					RS, RV
123	41.4010140	-72.788276	Trnh	25	24			RS, RV
123	41.4010140	-72.788276	Trnh					RS, RV
123	41.4010140	-72.788276	Trnh					RS, RV
123-3	41.401719	-72.788106	Trnh	26	20			RS, RV
123-3	41.401719	-72.788106	Trnh					RS, RV
123-3	41.401719	-72.788106	Trnh					RS, RV
123	41.4015860	-72.787960	Trnh					RS, RV
123	41.4015860	-72.787960	Trnh					RS, RV
124	41.3770110	-72.824056	Ji/Trnh	10	15			RS, JB
124	41.3770110	-72.824056	Ji/Trnh					RS, JB
124	41.3770110	-72.824056	Ji/Trnh					RS, JB
126-2	41.404277	-72.775350	Jtab	34	18			RS, JB
127	41.4196250	-72.870448	Trnh	37	13			RS, JB
129-1	41.4823050	-72.869684	Jb					RS, AC, JB, HS
129-1	41.4823050	-72.869684	Jb					"
129-2	41.4833050	-72.869115	Jb			359	78	"
129-4	41.4851990	-72.868226	Jb					"
129-7	41.4939390	-72.866469	Trnh	352	8			RS, JB, HS
129-9	41.4918490	-72.870697	Trnh	320	10			RS, JB, HS
130W-3	41.4678895	-72.866727	Jwr					AC, RS

Local area map	Latitude	Longitude	Stratig. designat.	J O I N T S Strike	dip angle	#	Columnar/intersecting Joints Trend	Plunge	Observer *
130W-3	41.4678895	-72.866727	Jwr	336	90				AC, RS
130FCC-1	41.465827	-72.857379	Jwr	212	67		42	46	AC, RS
130FCC-1	41.4656390	-72.857793	Jwr	120	90				AC, RS
130FCC-2	41.4692490	-72.864170	Jwr	74	90				RS
130FCC-3	41.4699670	-72.864580	Jwr	217	70		40	46	RS
130FCC-4	41.4697870	-72.866014	Jwr	149	80				RS
131-1	41.4588258	-72.840535	Jwr	328	82	1			RS, AC, HS
131-2	41.4590397	-72.841446	Jwr	328	90	1			RS, AC, HS
131-3	41.4587475	-72.841920	Trnh						RS, AC, HS
131-4	41.458252	-72.841857	Trnh						RS, AC,JB, HS
131-5	41.4587597	-72.841414	wr/nh	324	60				RS, AC, HS
131-6	41.459452	-72.839105	Jwr				120	90	
131-9	41.4624325	-72.843841	Trnh	222	74				RS, AC, HS
131-10	41.462091	-72.8457728	Ji				1	56	RS, AC, HS
131-10b	41.462984	-72.844717	Trnh						RS, AC, HS
131-11	41.4591778	-72.839997	Ji	336	76				RS, JB, HS
131-12	41.458346	-72.841685	Ji				116	78	RS, AC, JB, HS
131-12	41.458397	-72.841593	Ji				206	70	"
131-13	41.452835	-72.841266	Trnh						"
131-14	41.4627558	-72.848973	Jwr	210	41				"
131-15	41.4630939	-72.850390	Trnh				5	50	
131-D1	41.458020	-72.839840	Jwr				122	80	RS, AC
131-D1.1	41.458221	-72.839691	Jwr				136	65	RS, AC
131-D2	41.458882	-72.840227	Jwr				122	90	RS
131-D3	41.458419	-72.840705	Jwr				355	80	RS
131-D4	41.458067	-72.840623	Jwr				74	75	RS
131-D5	41.458229	-72.841292	Jwr				315	50	RS
132-1	41.4637319	-72.750593	Jwr	194	86				RS, AC
132-2	41.4649947	-72.751841	Jwr	248	82				RS, AC
132-2	41.4649947	-72.751841	Jwr	36	90				RS, AC
132-2	41.4649947	-72.751841	Jwr	340	82				RS, AC
132-2	41.464888	-72.751977	Jwr				258	82	RS, AC
132-2a	41.4644039	-72.751748	Jwr	6	90		282	68	RS, AC
132-2a	41.4644039	-72.751748	Jwr	356	90				RS, AC
132-2a	41.4644039	-72.751748	Jwr	308	90				RS, AC
132-3	41.4657594	-72.751825	Jwr	322	90				RS, AC
132-4	41.4661533	-72.751609	Jwr	341	90				RS, AC
132-5	41.4666053	-72.750947	Jwr	280	90		318	68	RS, AC
132-5	41.4666053	-72.750947	Jwr	160	80				RS, AC
132-6	41.4669294	-72.750131	Jwr				342	62	RS, AC
132-8	41.4670803	-72.749084	Jwr	274	80		340	70	RS, AC
132-10	41.4628114	-72.751154	Jwr	24	58				AC, RS
132-10	41.4628114	-72.751154	Jwr	92	90				AC, RS
132-11	41.4624303	-72.751344	Jwr	24	90				AC, RS

Local area map	Latitude	Longitude	Stratig. designat.	BEDDING		FAULTS		Observer *
				Strike	Dip	Strike	dip	
130W-3	41.4678895	-72.866727	Jwr					AC, RS
130FCC-1	41.465827	-72.857379	Jwr					AC, RS
130FCC-1	41.4656390	-72.857793	Jwr					AC, RS
130FCC-2	41.4692490	-72.864170	Jwr					RS
130FCC-3	41.4699670	-72.864580	Jwr					RS
130FCC-4	41.4697870	-72.866014	Jwr					RS
131-1	41.4588258	-72.840535	Jwr					RS, AC, HS
131-2	41.4590397	-72.841446	Jwr					RS, AC, HS
131-3	41.4587475	-72.841920	Trnh	40	12			RS, AC, HS
131-4	41.458252	-72.841857	Trnh	22	16			RS, AC,JB, HS
131-5	41.4587597	-72.841414	wr/nh					RS, AC, HS
131-6	41.459452	-72.839105	Jwr					
131-9	41.4624325	-72.843841	Trnh					RS, AC, HS
131-10	41.462091	-72.8457728	Ji					RS, AC, HS
131-10b	41.462984	-72.844717	Trnh	22	8			RS, AC, HS
131-11	41.4591778	-72.839997	Ji					RS, JB, HS
131-12	41.458346	-72.841685	Ji					RS, AC, JB, HS
131-12	41.458397	-72.841593	Ji					"
131-13	41.452835	-72.841266	Trnh	300	20			"
131-14	41.4627558	-72.848973	Jwr					"
131-15	41.4630939	-72.850390	Trnh					
131-D1	41.458020	-72.839840	Jwr					RS, AC
131-D1.1	41.458221	-72.839691	Jwr					RS, AC
131-D2	41.458882	-72.840227	Jwr					RS
131-D3	41.458419	-72.840705	Jwr					RS
131-D4	41.458067	-72.840623	Jwr					RS
131-D5	41.458229	-72.841292	Jwr					RS
132-1	41.4637319	-72.750593	Jwr					RS, AC
132-2	41.4649947	-72.751841	Jwr					RS, AC
132-2	41.4649947	-72.751841	Jwr					RS, AC
132-2	41.4649947	-72.751841	Jwr					RS, AC
132-2	41.464888	-72.751977	Jwr					RS, AC
132-2a	41.4644039	-72.751748	Jwr					RS, AC
132-2a	41.4644039	-72.751748	Jwr					RS, AC
132-2a	41.4644039	-72.751748	Jwr					RS, AC
132-3	41.4657594	-72.751825	Jwr					RS, AC
132-4	41.4661533	-72.751609	Jwr					RS, AC
132-5	41.4666053	-72.750947	Jwr					RS, AC
132-5	41.4666053	-72.750947	Jwr					RS, AC
132-6	41.4669294	-72.750131	Jwr					RS, AC
132-8	41.4670803	-72.749084	Jwr					RS, AC
132-10	41.4628114	-72.751154	Jwr					AC, RS
132-10	41.4628114	-72.751154	Jwr					AC, RS
132-11	41.4624303	-72.751344	Jwr					AC, RS

Local area map	Latitude	Longitude	Stratig. designat.	J O I N T S			Columnar/intersecting Joints		Observer *
				Strike	dip angle	#	Trend	Plunge	
132-12	41.4620778	-72.751432	Jwr	80	56				AC, RS
132-13	41.4619919	-72.751711	Jwr				300	40	AC, RS
132-14	41.4613533	-72.751635	Jwr	200	85				AC, RS
132-14	41.4613533	-72.751635	Jwr	95	90				AC, RS
132-15	41.4607531	-72.752066	Jwr	24	90				AC, RS
132-15	41.4607531	-72.752066	Jwr	60	80				AC, RS
132-17	41.4611628	-72.750786	Jwr	354	60				AC, RS
132-18	41.4638883	-72.752142	Jwr	168	78				AC, RS
132-18	41.4638883	-72.752142	Jwr	232	78				AC, RS
132-18	41.4638883	-72.752142	Jwr	292	72				AC, RS
132-19	41.4643456	-72.751952	Jwr				290	85	AC, RS
132-20	41.4584469	-72.751470	Jwr	300	90		340	18	KT, AC, RS
132-20	41.4584469	-72.751470	Ji	10	72				KT, AC, RS
132-21	41.4589233	-72.751508	Ji	88	90				KT, AC, RS
132-21	41.4589233	-72.751508	Ji	340	90				KT, AC, RS
132-21	41.4589233	-72.751508	Ji	125	90				KT, AC, RS
132-22	41.4587328	-72.755080	Ji	94	90				KT, AC, RS
132-22	41.4587328	-72.755080	Ji	105	90				KT, AC, RS
132-23	41.4595475	-72.754751	Ji	340	90				KT, AC, RS
132-23	41.4595475	-72.754751	Ji	94	90				KT, AC, RS
132-24	41.4604006	-72.754523	Ji	96	90				KT, AC, RS
132-24	41.4604006	-72.754523	Ji	334	90				KT, AC, RS
132-25	41.4577519	-72.749461	Trnh						KT, AC, RS
132-26	41.4618967	-72.754206	Ji	168	80				KT, AC, RS
132-26	41.4618967	-72.754206	Ji	100	90				KT, AC, RS
132-27	41.4607625	-72.762650	Trnh	150	80				KT, AC, RS
132-27	41.4607625	-72.762650	Trnh	180	90				KT, AC, RS
132-27	41.4607625	-72.762650	Trnh	198	78				KT, AC, RS
132-28	41.460058	-72.757989	Trnh						KT, AC, RS
132-29	41.4590661	-72.757589	Ji	144	75				KT, AC, RS
132-29	41.4590661	-72.757589		230	90				KT, AC, RS
132-30	41.4572744	-72.758804	Trnh	240	90				KT, AC, RS
132-30	41.4572744	-72.758804	Trnh	4	90				KT, AC, RS
132-32	41.4559214	-72.758614	Ji	16	90				KT, AC, RS
132-32	41.4559214	-72.758614	Ji	90	90				KT, AC, RS
132-32	41.4559214	-72.758614	Ji	320	90				KT, AC, RS
132-33	41.4582564	-72.755359	Ji	276	90		266	18	AC, KT, RS
132-34	41.4566267	-72.758154	Ji	76	22				AC, KT, RS
132-34	41.4566267	-72.758154	Ji	308	90				AC, KT, RS
132-34	41.4566267	-72.758154	Ji	40	90				AC, KT, RS
132-35	41.4557022	-72.758728	Ji	256	80				AC, KT, RS
132-35	41.4557022	-72.758728	Ji	10	90				AC, KT, RS
132-35	41.4557022	-72.758728	Ji	190	74				AC, KT, RS
132-36a	41.4546539	-72.759171	Kl	160	74				AC, KT, RS

Local area map	Latitude	Longitude	Stratig. designat.	B E D D I N G		F A U L T S		Observer *
				Strike	Dip	Strike	dip	
132-12	41.4620778	-72.751432	Jwr					AC, RS
132-13	41.4619919	-72.751711	Jwr					AC, RS
132-14	41.4613533	-72.751635	Jwr					AC, RS
132-14	41.4613533	-72.751635	Jwr					AC, RS
132-15	41.4607531	-72.752066	Jwr					AC, RS
132-15	41.4607531	-72.752066	Jwr					AC, RS
132-17	41.4611628	-72.750786	Jwr					AC, RS
132-18	41.4638883	-72.752142	Jwr					AC, RS
132-18	41.4638883	-72.752142	Jwr					AC, RS
132-18	41.4638883	-72.752142	Jwr					AC, RS
132-19	41.4643456	-72.751952	Jwr					AC, RS
132-20	41.4584469	-72.751470	Jwr					KT, AC, RS
132-20	41.4584469	-72.751470	Ji					KT, AC, RS
132-21	41.4589233	-72.751508	Ji					KT, AC, RS
132-21	41.4589233	-72.751508	Ji					KT, AC, RS
132-21	41.4589233	-72.751508	Ji					KT, AC, RS
132-22	41.4587328	-72.755080	Ji					KT, AC, RS
132-22	41.4587328	-72.755080	Ji					KT, AC, RS
132-23	41.4595475	-72.754751	Ji					KT, AC, RS
132-23	41.4595475	-72.754751	Ji					KT, AC, RS
132-24	41.4604006	-72.754523	Ji					KT, AC, RS
132-24	41.4604006	-72.754523	Ji					KT, AC, RS
132-25	41.4577519	-72.749461	Trnh	12	16			KT, AC, RS
132-26	41.4618967	-72.754206	Ji					KT, AC, RS
132-26	41.4618967	-72.754206	Ji					KT, AC, RS
132-27	41.4607625	-72.762650	Trnh					KT, AC, RS
132-27	41.4607625	-72.762650	Trnh					KT, AC, RS
132-27	41.4607625	-72.762650	Trnh					KT, AC, RS
132-28	41.460058	-72.757989	Trnh	40	17			KT, AC, RS
132-29	41.4590661	-72.757589	Ji					KT, AC, RS
132-29	41.4590661	-72.757589						KT, AC, RS
132-30	41.4572744	-72.758804	Trnh	11	12			KT, AC, RS
132-30	41.4572744	-72.758804	Trnh					KT, AC, RS
132-32	41.4559214	-72.758614	Ji					KT, AC, RS
132-32	41.4559214	-72.758614	Ji					KT, AC, RS
132-32	41.4559214	-72.758614	Ji					KT, AC, RS
132-33	41.4582564	-72.755359	Ji					AC, KT, RS
132-34	41.4566267	-72.758154	Ji					AC, KT, RS
132-34	41.4566267	-72.758154	Ji					AC, KT, RS
132-34	41.4566267	-72.758154	Ji					AC, KT, RS
132-35	41.4557022	-72.758728	Ji					AC, KT, RS
132-35	41.4557022	-72.758728	Ji					AC, KT, RS
132-35	41.4557022	-72.758728	Ji					AC, KT, RS
132-36a	41.4546539	-72.759171	Kl					AC, KT, RS

Local area map	Latitude	Longitude	Stratig. designat.	J O I N T S			Columnar/intersecting Joints		Observer *
				Strike	dip angle	#	Trend	Plunge	
132-40	41.4507686	-72.757054	Trnh						AC, RS
132-40b	41.4511556	-72.756919	Trnh						AC, RS
132-41	41.4532878	-72.758171	Ji	216	82				AC, RS
132-41	41.4532878	-72.758171	Ji	336	90				AC, RS
132-41	41.4532878	-72.758171	Ji	216	85				AC, RS
132-42	41.4528111	-72.759208	Ji	60	90				AC, RS
132-43	41.4522633	-72.759453	Ji	80	90				AC, RS
132-43	41.4522633	-72.759453	Ji	190	85				AC, RS
132-45	41.4515308	-72.759025	Ji	30	72				AC, RS
132-45	41.4515308	-72.759025	Ji	100	90				AC, RS
132-45	41.4515308	-72.759025	Ji	156	75				AC, RS
132-46	41.4502919	-72.759587	Ji	100	82				AC, RS
132-46	41.4502919	-72.759587	Ji	78	80				AC, RS
132-46	41.4502919	-72.759587	Ji	150	82				AC, RS
132-46	41.4502919	-72.759587	Ji	200	70				AC, RS
132-48	41.4489697	-72.758914	Trnh						AC, RS
132-49	41.4620650	-72.756907	Jwr	336	78				KT, AC, RS
132-50	41.4683560	-72.754058	Trnh						KT, AC, RS
133-1	41.4797236	-72.846439	Trnh						Jb, HS, RS
133-2	41.4788158	-72.844782	Trnh	218	64				Jb, HS, RS
135-1	41.4711700	-72.838972	Trnh	218	88				JB, HS, RS
135-2	41.4705933	-72.840252	Trnh						JB, HS, RS
136-2	41.4547681	-72.840601	Trnh						RS
136-3	41.4535328	-72.842792	Trnh						RS
136-4	41.4571628	-72.838467	Jwr	20	85				RS, AC
136-4	41.4571628	-72.838467	Jwr	300	80				RS, AC
137-1	41.4402533	-72.849777	Jwr				340	89	RS, AC
137-1	41.439067	-72.849901	Jwr	340	90				RS, AC
137-1	41.440434	-72.848590	Jwr	215	90				RS, AC
137-1	41.439699	-72.848608	Jwr	300	90				RS, AC
137-1	41.440703	-72.848744	Jwr	6	90				RS, AC
138-1	41.4547425	-72.783892	Trnh	242	84				HS, JB, RS
138-1	41.4547425	-72.783892	Trnh	260	82				HS, JB, RS
138-2	41.4523011	-72.787869	Trnh	214	90				HS, JB, RS
138-2	41.4523011	-72.787869	Trnh	250	90				HS, JB, RS
138-4	41.4494769	-72.787613	Trnh						HS, JB, RS
138-8	41.4511039	-72.786773	Trnh						RS, KT
139-1	41.4623089	-72.796822	Trnh						RS, KT
139-4	41.4649417	-72.795620	Ji	324	90				RS, KT
139-4	41.4649417	-72.795620	Ji	84	90				RS, KT
139-4	41.4649417	-72.795620	Ji	352	90		320	60	RS, KT, AC
139-5	41.4643011	-72.788921	Trnh						RS, KT
139-6	41.4725067	-72.792727	Trnh						RS, KT
140-1	41.4451297	-72.755950	Jwr				270	75	AC, RS

Local area map	Latitude	Longitude	Stratig. designat.	BEDDING		FAULTS		Observer *
				Strike	Dip	Strike	dip	
132-40	41.4507686	-72.757054	Trnh	15	5			AC, RS
132-40b	41.4511556	-72.756919	Trnh	36	10			AC, RS
132-41	41.4532878	-72.758171	Ji					AC, RS
132-41	41.4532878	-72.758171	Ji					AC, RS
132-41	41.4532878	-72.758171	Ji					AC, RS
132-42	41.4528111	-72.759208	Ji					AC, RS
132-43	41.4522633	-72.759453	Ji					AC, RS
132-43	41.4522633	-72.759453	Ji					AC, RS
132-45	41.4515308	-72.759025	Ji					AC, RS
132-45	41.4515308	-72.759025	Ji					AC, RS
132-45	41.4515308	-72.759025	Ji					AC, RS
132-46	41.4502919	-72.759587	Ji					AC, RS
132-46	41.4502919	-72.759587	Ji					AC, RS
132-46	41.4502919	-72.759587	Ji					AC, RS
132-46	41.4502919	-72.759587	Ji					AC, RS
132-48	41.4489697	-72.758914	Trnh	20	20			AC, RS
132-49	41.4620650	-72.756907	Jwr					KT, AC, RS
132-50	41.4683560	-72.754058	Trnh	38	12			KT, AC, RS
133-1	41.4797236	-72.846439	Trnh	56	27			Jb, HS, RS
133-2	41.4788158	-72.844782	Trnh	40	18			Jb, HS, RS
135-1	41.4711700	-72.838972	Trnh	24	20			JB, HS, RS
135-2	41.4705933	-72.840252	Trnh	16	18			JB, HS, RS
136-2	41.4547681	-72.840601	Trnh	44	18			RS
136-3	41.4535328	-72.842792	Trnh	40	16			RS
136-4	41.4571628	-72.838467	Jwr					RS, AC
136-4	41.4571628	-72.838467	Jwr					RS, AC
137-1	41.4402533	-72.849777	Jwr					RS, AC
137-1	41.439067	-72.849901	Jwr					RS, AC
137-1	41.440434	-72.848590	Jwr					RS, AC
137-1	41.439699	-72.848608	Jwr					RS, AC
137-1	41.440703	-72.848744	Jwr					RS, AC
138-1	41.4547425	-72.783892	Trnh	352	20			HS, JB, RS
138-1	41.4547425	-72.783892	Trnh					HS, JB, RS
138-2	41.4523011	-72.787869	Trnh	12	26			HS, JB, RS
138-2	41.4523011	-72.787869	Trnh					HS, JB, RS
138-4	41.4494769	-72.787613	Trnh	35	38			HS, JB, RS
138-8	41.4511039	-72.786773	Trnh	32	16			RS, KT
139-1	41.4623089	-72.796822	Trnh	14	14			RS, KT
139-4	41.4649417	-72.795620	Ji					RS, KT
139-4	41.4649417	-72.795620	Ji					RS, KT
139-4	41.4649417	-72.795620	Ji					RS, KT, AC
139-5	41.4643011	-72.788921	Trnh	352	8			RS, KT
139-6	41.4725067	-72.792727	Trnh	62	12			RS, KT
140-1	41.4451297	-72.755950	Jwr			184	74	AC, RS

Local area map	Latitude	Longitude	Stratig. designat.	J O I N T S			Columnar/intersecting Joints		Observer *
				Strike	dip angle	#	Trend	Plunge	
140-3	41.4465472	-72.756298	Jwr	184	78				AC, RS
140-3	41.4465472	-72.756298	Jwr	14	90				AC, RS
140-3	41.4465472	-72.756298	Jwr	96	90				AC, RS
140-7	41.4474406	-72.753734	Trnh						AC, RS
140-8	41.4474042	-72.763565	Jwr	278	40				AC, RS
140-8	41.4474042	-72.763565	Jwr	104	78				AC, RS
140-8	41.4474042	-72.763565	Jwr	284	66				AC, RS
140-8	41.4474042	-72.763565	Jwr	190	90				AC, RS
140-9	41.4452006	-72.764103	Trnh						AC, RS
141-1	41.4951300	-72.793844	Trnh	78	56				RS, IH
141-1	41.4951300	-72.793844	Trnh	224	60				RS, IH
141-3	41.4988397	-72.796592	Trnh	312	90				RS, IH
141-3	41.4988397	-72.796592	Trnh	276	90				RS, IH
141-4	41.4950008	-72.795892	Trnh	268	90				RS, IH
141-4	41.4950008	-72.795892	Trnh	204	90				RS, IH
141-4	41.4950008	-72.795892	Trnh	116	80				RS, IH
142-3	41.488147	-72.761683	Trnh						RS
142-3	41.488213	-72.761860	Trnh	300	80				RS
142-4	41.4871833	-72.769367	Trnh						RS
142-5	41.4920875	-72.756546	Trnh						RS, IH
142-6	41.4968761	-72.755358	Trnh	146	84				RS, IH
142-6.5	41.4961256	-72.755766	Trnh						RS, IH
142-7	41.4976406	-72.758438	Trnh						RS, IH
142-8	41.4961689	-72.754341	Trnh	32	90				RS, IH
142-8	41.4961689	-72.754341	Trnh	300	90				RS, IH
142-9	41.4981197	-72.752953	Jta	4	79				RS, IH
142-9	41.4981197	-72.752953	Jta	34	90				RS, IH
142-9	41.4981197	-72.752953	Jta	68	90				RS, IH
WoodsHill	41.4125490	-72.771571	Trnh						RS, JB
Rte17	41.3972430	-72.786838	Trnh						
S-1	41.497364	-72.790208	Trnh						
S-2	41.443059	-72.754334	Trnh						
S-3	41.442301	-72.787799	Trnh						
S-4	41.427571	-72.808020	Trnh						
S-5	41.430208	-72.8104	Trnh						
S-6	41.407297	-72.8329	Trnh						
S-7	41.405078	-72.804857	Trnh						
S-8	41.396815	-72.792461	Trnh						
S-9	41.375049	-72.803791	Trnh						
S-10	41.431975	-72.853507	Trnh						

Local area map	Latitude	Longitude	Stratig. designat.	BEDDING		FAULTS		Observer *
				Strike	Dip	Strike	dip	
140-3	41.4465472	-72.756298	Jwr			290	85	AC, RS
140-3	41.4465472	-72.756298	Jwr					AC, RS
140-3	41.4465472	-72.756298	Jwr					AC, RS
140-7	41.4474406	-72.753734	Trnh	5	5			AC, RS
140-8	41.4474042	-72.763565	Jwr					AC, RS
140-8	41.4474042	-72.763565	Jwr					AC, RS
140-8	41.4474042	-72.763565	Jwr					AC, RS
140-8	41.4474042	-72.763565	Jwr					AC, RS
140-9	41.4452006	-72.764103	Trnh	18	14			AC, RS
141-1	41.4951300	-72.793844	Trnh	348	16			RS, IH
141-1	41.4951300	-72.793844	Trnh					RS, IH
141-3	41.4988397	-72.796592	Trnh	18	14			RS, IH
141-3	41.4988397	-72.796592	Trnh					RS, IH
141-4	41.4950008	-72.795892	Trnh	1	11			RS, IH
141-4	41.4950008	-72.795892	Trnh					RS, IH
141-4	41.4950008	-72.795892	Trnh					RS, IH
142-3	41.488147	-72.761683	Trnh	32	18			RS
142-3	41.488213	-72.761860	Trnh					RS
142-4	41.4871833	-72.769367	Trnh	42	14			RS
142-5	41.4920875	-72.756546	Trnh	10	18			RS, IH
142-6	41.4968761	-72.755358	Trnh	14	20			RS, IH
142-6.5	41.4961256	-72.755766	Trnh	8	18			RS, IH
142-7	41.4976406	-72.758438	Trnh	4	16			RS, IH
142-8	41.4961689	-72.754341	Trnh	358	18			RS, IH
142-8	41.4961689	-72.754341	Trnh					RS, IH
142-9	41.4981197	-72.752953	Jta					RS, IH
142-9	41.4981197	-72.752953	Jta					RS, IH
142-9	41.4981197	-72.752953	Jta					RS, IH
WoodsHill	41.4125490	-72.771571	Trnh	45	18			RS, JB
Rte17	41.3972430	-72.786838	Trnh	18	16			
S-1	41.497364	-72.790208	Trnh	15	15			
S-2	41.443059	-72.754334	Trnh	350	15			
S-3	41.442301	-72.787799	Trnh	12	10			
S-4	41.427571	-72.808020	Trnh	36	15			
S-5	41.430208	-72.8104	Trnh	24	15			
S-6	41.407297	-72.8329	Trnh	24	15			
S-7	41.405078	-72.804857	Trnh	10	15			
S-8	41.396815	-72.792461	Trnh	19	25			
S-9	41.375049	-72.803791	Trnh	20	10			
S-10	41.431975	-72.853507	Trnh	30	10			

* AC: Allison Charney, HS: Heidi Salg; IH: Ian Hillenbrand, JB: James Bogart, KT: Kaitlin Taylor; MT: Margaret Thomas, MW: Madeleine Weinsteiger, RV: Rebecca VanderLeest, RS: Randolph Steinen. **Should be read +/-108o

APPENDIX VI. Water well data used to constrain fault locations and outcrop pattern of Talcott Basalt, NE corner of map											
Town	**#**	**Street**	**Lat**	**Long**	**Elev (FT)**	**YieldGPM**	**Lithol.**	**El T/Trap**	**El B/Trap**	**Thickness**	**Fm at Surf**
Wallingford	8	High Hill Road	41.470676	-72.757721	313		30-205 Red rock				Trnh
Wallingford	10	High Hill Road	41.47113	-72.757721	328		18-135 Shale				Trnh
Wallingford	150	High Hill Road			469	15	30-405 Bed rock				Trnh
Wallingford	152	High Hill Road	41.48325	-72.753098	458	8	10-150 Red rock				Trnh
Wallingford	154	High Hill Road	41.483307	-72.753471	460	5	10-160 Red rock				Trnh
Wallingford	156	High Hill Road	41.483391	-72.754021	454	15+	19-160 Red rock				Trnh
Wallingford	160	High Hill Road	41.484264	-72.753792	458	15	11-150 Brownstone				Trnh
Wallingford	164	High Hill Road	41.48472	-72.75339	458	7	15-150 Shale				Trnh
Wallingford	182	High Hill Road	41.48646	-72.75273	467	15	10-155 Sandstone				Trnh
Wallingford	188	High Hill Road	41.47808	-72.752594	470	14	8-50 Redrock, 50-60 Ledge, 60-120 Redrock				Trnh
Wallingford	192	High Hill Road	41.48748	-72.75246	474	20	10-155 Sandstone				Trnh
Wallingford	194	High Hill Road	41.4879	-72.752501	476	10	22-120 Shale				Trnh
Wallingford	196	High Hill Road	41.48835	-72.75222	479	10	19-136 Shale				Trnh
Wallingford	198	High Hill Road	41.48866	-72.75179	485	10	19-150 Red rock				Trnh
Wallingford	202	High Hill Road	41.490112	-72.751228	550	12	18-200 Trap rock				Trnh
Wallingford	210	High Hill Road	41.491676	-72.751389	542		18-68 Trap rock, 68-150 Gray shale?, 150-185 Red shale		357		Jta
Wallingford	322	High Hill Road	41.494034	-72.751495	502	10	11-40 Shale, 40-210 Trap rock, 210-250 Sandstone	462	292	170	Jsm
Wallingford	324	High Hill Road	41.494984	-72.749733	502	10	8-48 Red rock, 48-155 Blue ledge	454			Jsm
Wallingford	326	High Hill Road	41.48456	-72.75145	549	3.5	13-430 Red Rock				Jsm
Wallingford	328	High Hill Road	41.494971	-72.75145	551	25	9-350 Trap rock			>341	Jta
Wallingford	344	High Hill Road	41.495686	-72.751808	540	6	17-110 Trap rock, 110-270 red rock		430		Jta
Wallingford	5	Valley View	41.484756	-72.751297			18-40 Traprock, 40-175 Shale				Jta
Wallingford	6	Valley View	41.48511	-72.75218	475	15	10-140 Red shale				
Wallingford	9	Valley View	41.485165	-72.751137	498	9	8-51 Blue traprock, 51-175 Red traprock		447?		Jta?
Wallingford	10	Valley View	41.485416	-72.7519	485	20	20-165 Red rock				
Wallingford	14	Valley View	41.485813	72.751762	488	8	10-24 Soft sandstone, 24-183 Sandstone				
Wallingford	17	Valley View	41.485973	-72.750839	524	12+	0-90 Traprock, 90-160 Red rock		434		Jta
Wallingford	18	Valley View	41.486317	-72.751579	495	10	19-150 Shale				
Wallingford	21	Valley View	41.48637	-72.750702	531	9	12-200 Traprock and shale				Jta
Wallingford	22	Valley View	41.48674	-72.75168	513	15	8-40 Traprock, 40-163 sandstone		473		Jta
Wallingford	25	Valley View	41.486767	-72.750702	533	12	18-65 Trap rock, 65-75 shale, 75-160 Traprock, 160-185 Shale		373		Jta
Wallingford	26	Valley View	41.487103	-72.75145	523	20	8-15 Soft Trap rock, 15-62 Hard traprock, 62-65, rotten traprock, 65-113 red sandstone		458		Jta
Wallingford	29	Valley View	41.48719	-72.75061	525	15+	10-102 Trap rock, 102-140 Brnstone		423		Jta
Wallingford	30	Valley View	41.487526	-72.751297	532	20	4-82 Trap rock, 82-183 sandstone		450		Jta
Wallingford	32	Valley View	41.487923	-72.75115	541	12	6-160 red shale				
Wallingford	33	Valley View	41.4876	-72.75022	525	6	25-100 trap rock, 100-125 Shale, 125-165 Trap rocl, 160-180 shale and coarse sand				Jta
Wallingford	34	Valley View	41.488422	-72.750977		56	9-140 red shale				
Wallingford	34.5	Valley View	41.489267	-72751386	530	10	8-265 gray shale and red rock				
Wallingford	35	Valley View	41.488075	-72.750035	532	12	4-124 Top rock, 124-170 red rock, 170-180 Top rock		408		Jta
Wallingford	36	Valley View	41.488964	-72.750793	537	15	4-181 Red rock				
Wallingford	37	Valley View	41.488522	-72.750145	527	7	20-175 Trap rock				Jta
Wallingford	38	Valley View	41.48988	-72.75058	529	25	12-305 Red rock				
Wallingford	39	Valley View	41.489071	-72.750008	512	7	10-140 trap rock, 140-320 Red rock				Jta
Wallingford	40	Valley View	41.490562	-72.750328	520		5-180 red rock				
Wallingford	41	Valley View	41.48967	-72.74958	509	3	22-350 Red rock and trap				
Wallingford	43	Valley View	41.490238	-72.749565	505	100	13-28 Red rock, 28-80 Shale, 80-175 Trap rock, 175-200 Sandstone	425	330	95	Jsm
Wallingford	44	Valley View	41.491299	-72.750191	528	10	15-25 Red rock, 25-185 Trap rock	503			Jsm

Town	#	Street	Lat	Long	Elev (FT)	YieldGPM	Lithol.	El T/Trap	El B/Trap	Thickness	Fm at Surf
Wallingford	45	Valley View	41.49056	-72.74928	503	100	30-225 Granite				
Wallingford	47	Valley View	41.49099	-72.749405	504	8	12-24 Weathered rock, 24-310 Sandstone				
Wallingford	3	Cliffside	41.483452	-72.749176	473	5	15-175 Soft traprock, 175-243 Red sandstone		298		Jta
Wallingford	4	Cliffside	41.4846	-72.750069	502	10	10-127 Traprock				Jta
Wallingford	7	Cliffside	41.484753	-72.749054	484	2	6-230 Traprock, 230-303 Red sandstone		254		Jta
Wallingford	8	Cliffside	41.485	-72.75001	509	7	6-180 Red shale				
Wallingford	11	Cliffside	41.48518	-72.748901	475	11	19-175 Trap, 175-205 Red rock		300		Jta
Wallingford	12	Cliffside	41.485352	-72.749802	509	30	8-160 Red shale				
Wallingford	15	Cliffside	41.48551	-72.74865	472	10.5	14-120 Top rock, 120-130 Red rock, 130-155 Top rock				Jta
Wallingford	16	Cliffside	41.485752	-72.749634	507	6	8-220 Red shale				
Wallingford	19	Cliffside	41.485989	-72.748711	470	10	16-25 Broken ledge, 25-119 Traprock, 119-129 Brnstone,128-162 Traprock				
Wallingford	20	Cliffside	41.486111	-72.749496	500	10	18-150 Top rock				Jta
Wallingford	24	Cliffside	41.486618	-72,749,359	496	21	9-180 Red shale				
Wallingford	27	Cliffside	41.486824	-72.748482	465	12	15-30 Red rock, 30-183 Traprock	435			Jsm
Wallingford	28	Cliffside	41.486984	-72.749268	487	5	8-200 Traprock, 200-270 Sandstone		287		Jta
Wallingford	31	Cliffside	41.487152	-72.74839	460	10	25-125 Red rock, 125-140 Top rock, 140-150 Red rock				Jsm
Wallingford	32	Cliffside	41.48741	-72.74926	479	8	23-30 Red rock, 30-150 Top rock	449			Jsm
Wallingford	35	Cliffside	41.487518	-72.748184	441	12	48-105 Red rock, 105-155 Top rock	336			Jsm
Wallingford	36	Cliffside	41.487896	-72.748039	478	4.5	10-130 Trap rock, 130-243 Sandstone		348		Jta
Wallingford	38	Cliffside	41.48832	-72.749	483	10	22-205 Red rock				
Wallingford	39	Cliffside	41.487961	-72.748093	444	50	31-120 Red shale				
Wallingford	40	Cliffside	41.48888	-72.7488	478	7	30-245 Granite				
Wallingford	41	Cliffside	41.488522	-72.747932	445	20	10-43 Red soil and Gravel, 43-155 Redrock				
Wallingford	42	Cliffside	41.489681	-72.74881	477	100	7-60 Redrock, 60-100 Shale, 100-200 Traprock	377			
Wallingford	43	Cliffside	41.489418	-72.747833	445	7	41-160 Red shale				
Wallingford	46	Cliffside	41.492302	-72.750053	508	18	5-80 Redrock, 80-145 Traprock	428			Jsm
Wallingford	47	Cliffside	41.490559	-72.748344	466	25	12-65 Red shale, 65-140 Traprock	401			Jsm
Wallingford	48	Cliffside	41.492245	-72.750656	541	10	8-180 Red shale				
Wallingford	49	Cliffside	41.490929	-72.748528	472	10	8-20 Red shale, 20-200 Red rock				
Wallingford	51	Cliffside	41.49137	-72.74848	475	30	15-70 Red rock, 70-160 Traprock, 160-275 Sandstone	405	315	90	Jsm
Wallingford	52	Cliffside	41.49219	-72.75139	538	8	19-180 Shale				
Wallingford	53	Cliffside	41.491661	-72.748856	482	15	8-140 Red shale				
Wallingford	55	Cliffside	41.49215	-72.74882	491	20	5-80 Redrock, 80-100 Top rock, 100-145 Redrock				Jsm
Wallingford	57	Cliffside	41.49259	-72.74898	492	12	8-140 Red shale				
Wallingford	59	Cliffside	41.49284	-72.749369		25	18-35 Seamy redrock, 35-60 Redrock, 60-200 Gray and black shale				
Wallingford	61	Cliffside	41.4935	-72.749374	504	10	20-105 Ledge				
Wallingford	63	Cliffside	41.493107	-72.750098	509	30	31-220 Red shale				
Wallingford	65	Cliffside	41.493111	-72.75061	531	40	21-180 Red shale				
Wallingford	7	Whisk Key Wind Road	41.48973	-72.751297	465	12	5-100 Trap, 100-182 Sandstone		365		Jta
Wallingford	8	Whisk Key Wind Road	41.484398	-72.751138	474	7.5	16-70 Traprock, 70-125 Shale		404		Jta
Wallingford	11	Whisk Key Wind Road	41.483471	-72.750916	467	10	18-40 Traprock, 40-140 Shale		427		Jta
Wallingford	14	Whisk Key Wind Road	41.484203	-72.750328	490	8	23-80 Traprock				Jta
Wallingford	17	Whisk Key Wind Road	41.48524	-72.750328	475	6	8-55 Traprock, 55-70 Redrock, 70-140 Traprock, 140-390 Sandstone		335		Jta
Wallingford	19	Whisk Key Wind Road	41.483727	-72.749313	483	6.5	16-100 Traprock, 100-120 Shale, 120-150 Traprock				Jta
Wallingford	21	Whisk Key Wind Road	41.482944	-72.748123	476?	2	30-340 Bedrock				

Town	#	Street	Lat	Long	Elev (FT)	YieldGPM	Lithol.	El T/Trap	El B/Trap	Thickness	Fm at Surf
Wallingford	27	Whisk Key Wind Road	41.483868	-72.748253	456	4	34-145 Traprock, 145-160 Shale, 160-190 Traprock				Jta
Wallingford	31	Whisk Key Wind Road	41.483833	-72.74765	435	9	26-60 Red rock, 60-130 Traprock	375			
Wallingford	34	Whisk Key Wind Road	41.484547	-72.748001	449	8	16-106 Top rock, 106-110 ?		343		Jta
Wallingford	35	Whisk Key Wind Road	41.484116	-72.747147	420	15	22-60 Red rock, 60-190 Trap	360			Jsm
Wallingford	39	Whisk Key Wind Road	41.484413	-72.74675	413	25	6-180 Red shale				
Wallingford	42	Whisk Key Wind Road	41.484962	-72.747803	438	10	6-180 Red shale				
Wallingford	46	Whisk Key Wind Road	41.485332	-72.747696	438	NR	25-200 Red rock and trap rock				
Wallingford	50	Whisk Key Wind Road	41.485733	-72.747559	436	6	13-55 Red rock, 55-230 Traprock, 230-265 Sandstone	381	206	175	Jsm
Wallingford	54	Whisk Key Wind Road	41.486183	-72.747513	420	30	10 Red shale				
Wallingford	60	Whisk Key Wind Road	41.486511	-72.747284	421	13	16-95 Red rock, 95-180 Traprock	326			Jsm
Wallingford	4	Marie Lane	41.481232	-72.753563	481	10	10-240 Red shale				
Wallingford	6	Marie Lane	41.481262	-72.753006	486	6	12-200 Red shale				
Wallingford	7	Marie Lane	41.480339	-72.751717	504	3	90-405 Granite				
Wallingford	8	Marie Lane	41.4814	-72.75197	483	2	50-405 Shale				
Wallingford	9	Marie Lane	41.479897	-72.751297	507	15	95-305 Granite				
Wallingford	10	Marie Lane	41.481525	-72.570793	471	10+	NR				
Wallingford	11	Marie Lane	41.479317	-72.751488	509	15	110-405 Shale				
Wallingford	12	Marie Lane	41.48106	-72.750587	483	60	24-45 Broken Trap, 45-100 Traprock, 100-540 Sandstone		383		Jta
Wallingford	14	Marie Lane	41.480568	-72.750237	484	4	40-345 Sandstone				
Wallingford	15	Marie Lane	41.478672	-72.751717	485	10	60-81 Fractured bedrock, 81-300 Bedrock				
Wallingford	16	Marie Lane	41.47996	-72.74973	483	10	56-91 Conglom- erate, 91-203 Sandstone				
Wallingford	18	Marie Lane	41.479385	-72.749565	480	50	79-570 Sandstone				
Wallingford	1	Hemingway Dr.	41.473129	-72.751007	390	2	32-405 Granite				Trnh
Wallingford	2	Hemingway Dr.	41.473961	-72.751205	419	4	11-345 Granite				
Wallingford	3	Hemingway Dr.	41.473431	-72.749962	384	6	21-265 Granite				
Wallingford	4	Hemingway Dr.	41.474354	-72.750053	421	4	32-325 Granite				
Wallingford	5	Hemingway Dr.	41.47403	-72.749176	377	3	32-225 Shale				
Wallingford	6	Hemingway Dr.	41.475079	-72.749825	439	10+	53-305 Red shale				
Wallingford	8	Hemingway Dr.	41.475712	-72.749496	450	20+	53-245 Sandstone				
Wallingford	10	Hemingway Dr.	41.476269	-72.749687	462	7	53-365 Granite				
Wallingford	11	Hemingway Dr.	41.47543	-72.74812	416	30	50-265 Shale				
Wallingford	12	Hemingway Dr.	41.476677	-72.750198	467	2	32-405 Granite				
Wallingford	14	Hemingway Dr.	41.477379	-72.750237	469	15	45-365 Shale				
Wallingford	15	Hemingway Dr.	41.476009	-72.748482	433	4.5	15-20 Sandstone, 20-365 Red rock				
Wallingford	16	Hemingway Dr.	41.477962	-72.751058	477	3	53-365 Red shale and traprock				
Wallingford	17	Hemingway Dr.	41.476624	-72.748764	445	15	53-365 Shale				
Wallingford	18	Hemingway Dr.	41.487096	-72.750015	472	2	70-365 Sandstone				
Wallingford	21	Hemingway Dr.	41.477779	-72.749016	457	15	70-245 Shale				
Wallingford	23	Hemingway Dr.	41.478577	-72.74913	461	2	74-445 Shale				
Wallingford	3	Quarry Run Court	41.471886	-72.74659	337	15	44-130 Shale				Trnh
Wallingford	4	Quarry Run Court	41.473213	-72.748909	367	50	20-305 Shale				
Wallingford	5	Quarry Run Court	41.472225	-72.74733	341	4	32-345 Shale				
Wallingford	6	Quarry Run Court	41.473473	-72.747864	349	12	30-140 Red shale				
Wallingford	7	Quarry Run Court	41.742694	-72.746941	335	6	20-245 Red shale				
Wallingford	8	Quarry Run Court	41.474621	-72.747551	357	20	31-120 Red shale				
Wallingford	9	Quarry Run Court	41.473354	-72.746574	339	30	34-140 Red shale				
Wallingford	11	Quarry Run Court	41.473747	-72.745506	340	4	25-32 Weathered sandstone, 32-310 Sandstone				
Wallingford	15	Quarry Run Court	41.474358	-72.745392	339	9	25-300 ___ rock				
Wallingford	17	Quarry Run Court	41.474373	-72.745987	343	30	30-245 Shale				
Wallingford	19	Quarry Run Court	41.475582	-72.743973	340	30	12-23 Gray r ock, 23-405 Brown and gray rock				
Wallingford	8	North Branford Rd	41.43522	-72.75252	439	40	10-310 Red rock				Trnh
Wallingford	9	North Branford Rd	41.435444	-72.755676	462	10	18-180 Red shale				
Wallingford	9s	North Branford Rd	41.435444	-72.755676	462	10	50-305 Bedrock				
Wallingford	10	North Branford Rd	41.435989	-72.75264	449	20	10-330 Red sandstone				
Wallingford	11	North Branford Rd	41.43504	-72.75412	453	22	31-190 Red shale				
Wallingford	14	North Branford Rd	41.435383	-72.749474	441	30	10-30 Soft sandstone, 30-350 Sandstone				
Wallingford	15	North Branford Rd	41.435993	-72.755409	457	20+	60-205 Red rock				
Wallingford	17	North Branford Rd	41.435848	-72.754211	458	15	41-205 Red rock				
Wallingford	19	North Branford Rd	41.436474	-72.755119	458	15	32-285 Granite				

Town	#	Street	Lat	Long	Elev (FT)	YieldGPM	Lithol.	El T/Trap	El B/Trap	Thickness	Fm at Surf
Wallingford	21	North Branford Rd	41.436543	-72.753822	451	10	6-330 Red sandstone				
Wallingford	23	North Branford Rd	41.436909	-72.754959	447	20	16-160 Red shale				
Wallingford	25	North Branford Rd	41.437252	-72.753654	436	25	8-25 Seamy rock, 25-264 Sandstone				
Wallingford	67	North Branford Rd	41.441002	-72.750305	396	15	6-140 Red shale				
Wallingford	102	North Branford Rd	41.439167	-72.752319	369	10	6-130 Red rock, 130-160 Blue rock, 160-200 top rock				
Wallingford	104	North Branford Rd	41.43996	-72.751808	390	8	115-200 Red rock				
Wallingford	106	North Branford Rd	41.44072	-72.751419	403	8	20-120 Red rock				
Wallingford	132	North Branford Rd	41.442852	-72.753876	490	5	2-35 Rusted sandstone, 35-430 Sandstone				
Wallingford	134	North Branford Rd	41.442539	-72.751534	398	20	5-115 Red rock, 115-200 Soft rock				
Wallingford	140	North Branford Rd	41.443119	-72.751343	400	20	125-225 Red rock				
Wallingford	144	North Branford Rd	41.44371	-72.751251	410	10	15-150 Red rock, 150-200 Top rock				
Wallingford	148	North Branford Rd	41.444088	-72.75219	437	12	6-202 Brownstone				
Wallingford	152	North Branford Rd	41.444454	-72.751389	416	14	4-200 Red sandstone				
Wallingford	457	North Branford Rd	41.464584	-72.746849	375	9	70-250 Red rock				
Wallingford	525	North Branford Rd	41.468502	-72.747147	320	30	6-140 Red shale				
Wallingford	15	South Branford Rd	41.429409	-72.756401	455	50	35-50 Seamy rock, 50-190 Sandstone				Trnh
Wallingford	17	South Branford Rd	41.428791	-72.755852	444	18	53-205 Sandstone				
Wallingford	19	South Branford Rd	41.428364	-72.756035	460	35	88-310 Sandstone				
Wallingford	46	South Branford Rd	41.430679	-72.754669	415	12	Illegable				
Wallingford	48	South Branford Rd	41.430222	-72.754898	413	15	38-115 Red rock				
Wallingford	68	South Branford Rd	41.427326	-72.754852	402	12	58-80 Red rock				
Wallingford	72	South Branford Rd	41.426788	-72.754807	400	100	46-160 Red sandstone				
Wallingford	76	South Branford Rd	41.425999	-72.7537	387	30	43-265 Red rock				
Wallingford	80	South Branford Rd	41.424152	-72.751373	386	15+	20-125 Red rock				
Wallingford	92	South Branford Rd	41.422894	-72.752892	347	15+	35-115 Red rock				
Wallingford	96	South Branford Rd	41.422279	-72.752892	350	10	46-125 Red rock				
Wallingford	100	South Branford Rd	41.421288	-72.75412	359	30	18-124 Red sandstone				
Wallingford	2	Bartholomew Rd	41.439713	-72.750526	422	15	2-300 Red slate				
Wallingford	3	Bartholomew Rd	41.43882	-72.751419	434	8.5	5-210 Red rock				
Wallingford	4	Bartholomew Rd	41.438335	-72.748627	381	6	5-210 Red rock				
Wallingford	5	Bartholomew Rd	41.437267	-72.750328	414	5+	15-300 Red rock				
Wallingford	6	Bartholomew Rd	41.437271	-72.748436	392	7	45-105 Gray shale, 105-350 Red shale				
Wallingford	8	Bartholomew Rd	41.437351	-72.749405	400	48	55-375 Granite				
Wallingford	1264	Whirl Wind Hill Rd	41.439117	-72.768234	322	4	20-305 Red rock				Trnh
Wallingford	1290	Whirl Wind Hill Rd	41.438751	-72.766432	325	2	8-320 Red sandstone				
Wallingford	1300	Whirl Wind Hill Rd	41.439587	-72.765892	298	20	4-180 Red rock				
Wallingford	1339	Whirl Wind Hill Rd	41.435165	-72.769806	387	10	4-250 Red rock				
Wallingford	1345	Whirl Wind Hill Rd	41.435703	-72.763863	329	3	30-305 Red rock				
Wallingford	1349	Whirl Wind Hill Rd	41.434525	-72.763123	321	1	19-390 Red sandstone				
Wallingford	1397	Whirl Wind Hill Rd	41.434258	-72.758331	425	17	10-160 Red rock				
Wallingford	1678	Whirl Wind Hill Rd	41.435051	-72.746384	425	25	21-45 Rotten ledge, 45-223 Red sandstone				
Wallingford	1680	Whirl Wind Hill Rd	41.436268	-72.745583	431	11	24-160 Red shale				
NoBranford	14	Foote Hill Road	41.390244	-72.804276	168	35	5-185 Red rock				Trnh
NoBranford	44	Foote Hill Road	41.389072	-72.802666	216	12	31-225 Red rock				Trnh
NoBranford	50	Foote Hill Road	41.389464	-72.801918	238	8.5	50-165 Red rock				Trnh
NoBranford	75	Foote Hill Road	41.387584	-72.799934	238	20	5-220 Red shale				Trnh
NoBranford	80	Foote Hill Road					No report				Trnh
NoBranford	90	Foote Hill Road	41.388019	-72.798732	207		12-450 Sandstone				Trnh
NoBranford	118	Foote Hill Road	41.385727	-72.794975	155	18	81-160 red shale				Trnh
NoBranford		Foote Hille Road				15+	15-130 Red rock				
NoBranford	1070	Middletown Ave	41.382101	-72.815659	74	5	48-305 Basalt				Ji
NoBranford	1151	Middletown Ave	41.380031	-72.804367	200	4	20-405 Bedrock (red rock?)				Trnh
NoBranford	1171	Middletown Ave	41.38063	-72.8031	188	12	10-170 Trap, red rock, sandstone				Ji?
NoBranford	1226	Middletown Ave	41.382712	-72.802583	251	12	10-205 Red rock, brownstone				Trnh
NoBranford	1344-67	Middletown Ave				14	68-180 Red shale				
NoBranford	1345	Middletown Ave	41.389457	-72.794044	155	20	40-180 Red shale				
NoBranford	1355	Middletown Ave				30	88-260 Red shale				
NoBranford	1387	Middletown Ave				30	25-200 sandstone				
NoBranford	1395	Middletown Ave				12	34-143 Red rock				
NoBranford	1444	Middletown Ave.	41.395203	-72.789925	180	18+	12-185 Red rock				
NoBranford	26-48	Old Post Rd.	41.396188	-72.791899	250	18/30	5-175 Sandstone, 175-Traprock				Trnh
NoBranford	70	Old Post Road	41.398208	-72.791051	262	10+	90-160 Sandstone				Trnh
NoBranford	78	Old Post Road	41.398827	-72.790863	263	200+	35-245 Red rock				Trnh

Town	#	Street	Lat	Long	Elev (FT)	YieldGPM	Lithol.	El T/Trap	El B/Trap	Thickness	Fm at Surf
NoBranford	79	Old Post Road	41.398591	-72.790377	245	20+	14-32 Seamy ledge, 32-290 Sandstone				Trnh
NoBranford	80	Old Post Road	41.399132	-72.793514	255	10+	14-187 Red rock				Trnh
NoBranford	82	Old Post Road				15	20-220 Red rock				
NoBranford	116	Old Post Road				30	30-20 bedrock				
NoBranford	117	Old Post Road				10+	20-148 Red rock				
NoBranford	126	Old Post Road				10	32-115 Red rock				
NoBranford	131	Old Post Road				25	49-160 Sandstone				
NoBranford	133	Old Post Road				15+	23-110 Red rock				
NoBranford	156	Old Post Road				6	79-220 Red shale				
NoBranford	158	Old Post Road	41.404983	-72.78573	284	15	27-160 Red rock				Trnh
NoBranford	186	Old Post Road				30	11-110 Red rock				
NoBranford	104	Oxbow Lane	41.413188	-72.760447	314	6	8-244 Sandstone				Trnh
NoBranford	108	Oxbow Lane				5	30-405 Sandstone				
NoBranford	112	Oxbow Lane	41.413084	-72.762426	354	2	6-310 Sandstone				Trnh
NoBranford	114	Oxbow Lane				12	4-260 Red shale				
NoBranford	118	Oxbow Lane				15	35-190 Red rock				
NoBranford	122	Oxbow Lane				10	73-250 Red rock				
NoBranford	125	Oxbow Lane				1.5	125-405 Shale				
NoBranford	126	Oxbow Lane				15	80-245 Red rock				
NoBranford	129	Oxbow Lane				8	116-305 Red rock				
NoBranford	130	Oxbow Lane				10	60-184 Red rock				
NoBranford	133	Oxbow Lane				4	66-300 Red rock				
NoBranford	137	Oxbow Lane				10+	23-220 Red rock				
NoBranford	138	Oxbow Lane				10	53-265 Sandstone				
NoBranford	141	Oxbow Lane				12	50-405 Red rock				
NoBranford	142	Oxbow Lane				10+	70-285 Red rock				
NoBranford	145	Oxbow Lane				5	55-340 Sandstone				
NoBranford	149	Oxbow Lane				6	60-345 Red rock				
NoBranford	149	Oxbow Lane				12	30-305 Red rock				
NoBranford	7	St. Monica Drive	41.387654	-72.804611	177	15	8-150 Red rock				Trnh
NoBranford	9	St. Monica Drive				12	5-125 Red rock				
NoBranford	10	St. Monica Drive				8.5	38-205 Red rock				
NoBranford	17	St. Monica Drive				12	5-155 Red rock				
NoBranford	25	St. Monica Drive				20	15-206 Red rock				
NoBranford	29	St. Monica Drive					No rpt				
NoBranford	31	St. Monica Drive				20	12-250 Sandstone				
NoBranford	34	St. Monica Drive				30	68-165 Red rock				
NoBranford	37	St. Monica Drive				12	55-490 Sandstone				
NoBranford	823	Totoket Road	41.372545	-72.799643	145	30	22-205 Trap				Jta
NoBranford	833	Totoket Road	41.373601	-72.80155	190	8	12-148 Trap and red rock				Jta
NoBranford	848	Totoket Road	41.372735	-72.801368	213	10+	10-230 Redrock				
NoBranford	849	Totoket Road	41.374761	-72.800422	173	12	23-130 Trap rock				Jta
NoBranford	857	Totoket Road				3	24-305 granite, redrock				
NoBranford	857	Totoket Road				12	42-235 granite				
NoBranford	881	Totoket Road	41.37637	-72.799794	169	15	8-105 Trap rock				Jta
NoBranford	882	Totoket Road	41.376912	-72.800766	198	35	10-185 Red rock				
NoBranford	884	Totoket Road	41.377214	-72.800464	189	35	8-185 Red rock				
NoBranford	886	Totoket Road				12	13-305 Red rock				
NoBranford	888	Totoket Road				3	8-305 Red rock				
NoBranford	889	Totoket Road	41.376737	-72.798204	134	9+	35-130 Trap rock, 130-180 redrock				Jta
NoBranford	927	Totoket Road	41.30852	-72.796935	132	10	80-305 granite				
NoBranford	931	Totoket Road	41.381401	-72.796754	142	50	78-125 gray granite				Jta
NoBranford	933	Totoket Road	41.382054	-72.796681	151	100	125-185 Red rock				
NoBranford	180	Village Street	41.37362	-72.806936	213	70	51-125 Red rock				Trnh
NoBranford	180	Village Street				100+	91-345 Red rock				
NoBranford	200	Village St.	41.374533	-72.806434	197	15	15-170 Red rock				Trnh
NoBranford	204	Village St.	41.375458	-72.80716	198	10+	15-150 Red rock				Trnh
NoBranford	211	Village St.				20	3-230 granite				
NoBranford	215	Village St.	41.37733	-72.807815	178	10	9-140 Red shale				Trnh
NoBranford	225	Village St.; 30 ft east of house; 2005	41.378023	-72.807086	221	15	4-185 Red rock, 185-203 Traprock, 203-310 Red rock.				Trnh
NoBranford	225	Village St.; 41 ' n. of house, 2009	41.378226	-72.807359	222	15	3-370 Red rock				
NoBranford	235	Village St.?				12	15-95 traprock, 95-310 red rock				
NoBranford	264	Village St.	41.379016	-72.808791	97	4	50-410 Sandstone				Trnh
NoBranford	273	Village St.	41.380014	-72.808075	120	15	34-205 Red rock				Trnh
NoBranford	290	Village St.	41.38104	-72.809012	85						Trnh

Town	#	Street	Lat	Long	Elev (FT)	YieldGPM	Lithol.	El T/Trap	El B/Trap	Thickness	Fm at Surf
NoBranford	330	Village St.				25	5-65 Red rock				
NoBranford	384	Village St.					0-97				
NoBranford	399	Village St.					geothermal wells				
NoBranford	468	Village St.				35	8-140 Red shale				
NoBranford	470	Village St.				5	5-240 Sandstone				
NoBranford	472	Village St.					soil				
NoBranford	472	Village St.				15+	10-145 Red rock				
NoHaven		Knight Lane, Lot 1				20	11-320 Shale				Trnh
NoHaven	7	Knight Lane, Lot 2				9	12-148 Red rock, 148-365 granite				Trnh
NoHaven	11	Knight Lane, Lot 3				2	20-365 granite				Trnh
NoHaven		Knight Lane, Lot 9				8	4-22 Trap, 23-385 trap + red rick				Jwr
NoHaven	23	Knight Lane, Lot 10				4	4-44 Red rock, 22-385 red + trap				Trnh
NoHaven	29	Knight Lane, Lot 11				4	22-200 Red rock, 200-385 red + trap				Trnh
NoHaven	33	Knight Lane, Lot 12				7.5	19-42 Soft red rock 42-305 Red gray rock				Trnh
NoHaven	38	Knight Lane, Lot 13				9	12-21 Bed rock, 21-365 bedrock				Trnh
NoHaven	34	Knight Lane, Lot 14				12	30-120 sandstone, 150-510 trap rock				Trnh
NoHaven	30	Knight Lane, Lot 15				9	3-13 bedrock, 13-23 grey rock, 23-365 red and grey rock				Trnh
NoHaven	26	Knight Lane, Lot 16				7.5	0-21 red rock, 21-405 red rock				Trnh
NoHaven		Knight Lane, Lot 17				9	5-21 red rock, 21-385 red rock				Trnh
NoHaven		Knight Lane, Lot 18				5	30-41 red rock, 41-405 red grey rock				Trnh
NoHaven	6	Knight Lane, Lot 19				11	red rock				Trnh
NoHaven	19	Knight Lane, Lot ?				8	5-23 grey rock, 23-305 red				Jwr
Hamden	155	Chestnut Lane	Location?			8	6-160 Trap rock				
Hamden	167	Chestnut Lane	Location?			8	trap rock				
Hamden	185	Chestnut Lane	Location?			2.5	3-310 trap rock				
Hamden	325	Chestnut Lane	Location?			6	41-63 v. soft sandstone, 63-115 grey sandstone, 115-510 traprock				
Hamden	354	Chestnut Lane	Location?			12	10-350 bedrock				

APPENDIX VII. Additional illustrations enhancing text figures.

A.

B.

Figure VII-1. A. Mosaic of tabular sill-like body at Lufbery Park, northeast of field (location 131-6 on area map 131), showing cooling columns on left oriented approximately perpendicular to sandstone/diabase contact (arrow) that become near vertical away from the contact. Hammer about 30 cm for scale. B. Detail of contact. Shape of body interpreted to be tabular based on this contact. Body is >200 m long.

Figure VII-2. Sill-like body at southeastern-facing slope at Lufbery Park (area 131) illustrating irregular contact of sill with overlying sandstone and columnar jointing (A., B., and C.). Local brecciation of the sandstone (C.) occurs where either "load structures" formed, forcing lobes of sandstone downward into the diabase, or small upward migrating tongues of diabase became detached. Precarious slopes precluded our placing scales in all but B where yellow pencil is about 15 cm in length. Approximately 10 cm of plastic clipboard seen at base of C.

Figure VII-3. Contact of diabase with sandstone near entrance ramp into Lufbery Park (see area 131 Detail). Sand is incorporated in diabase in zone several cm inboard from contact. Also globules of diabase are incorporated along edge of sandstone contact. Both observations suggest sandstone was poorly or completely unlithified at time of intrusion.

Figure VII-4. Columnar joints at area 131 southeast-facing escarpment at Lufbery Park. Large poison ivy leaves approximately 15 cm for scale.

Figure VII-5. Mosaic of round-topped tongue of diabase at southwestern part of Lufbery Park (area 131) showing changing trend and plunge of columnar joints (see detailed map for area 131). Columns on eastern side (right side) trend and plunge 260-70^{o}, on western side 116-78^{o}.

Figure VII-6A. Patten Road cut (area 104 looking southeast). Photograph, approximately 10 m in height, of dikes of West Rock diabase. Schematic drawing of same, with diabase shaded light pink for older dike and darker pink for columnar jointed younger dike (yellow box shows approximate area of text figure 12A). Gray sandstone to east (left) of dike is faulted. We infer that hydrothermal fluids flowing through the fractures altered the sandstone to produce dark gray color. Relict bedding is dips toward west at low angles. Reddish-brown sandstone on east (far left, that) dips 22 degrees west; this is interpreted as drag caused by down-to-the-west faulting. Reddish-brown sandstones on west side dip more steeply to west; this is interpreted as normal drag along the fault system.

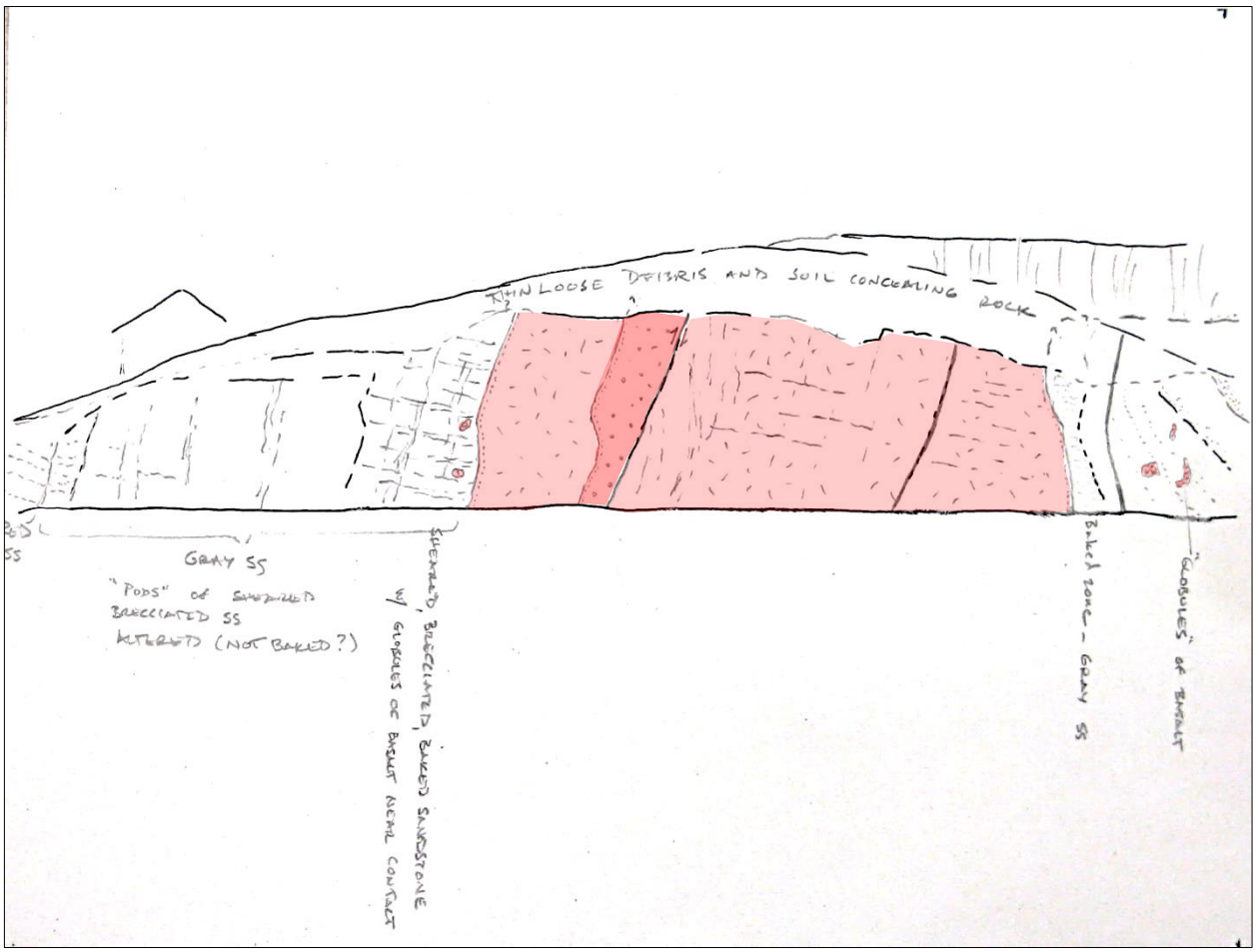

Figure VII-6B. West side of outcrop showing west dipping sandstone and siltstone on west side of fault zone. Reddish-gray sandstone behind street-light on above mosaic are in mid left of lower mosaic.

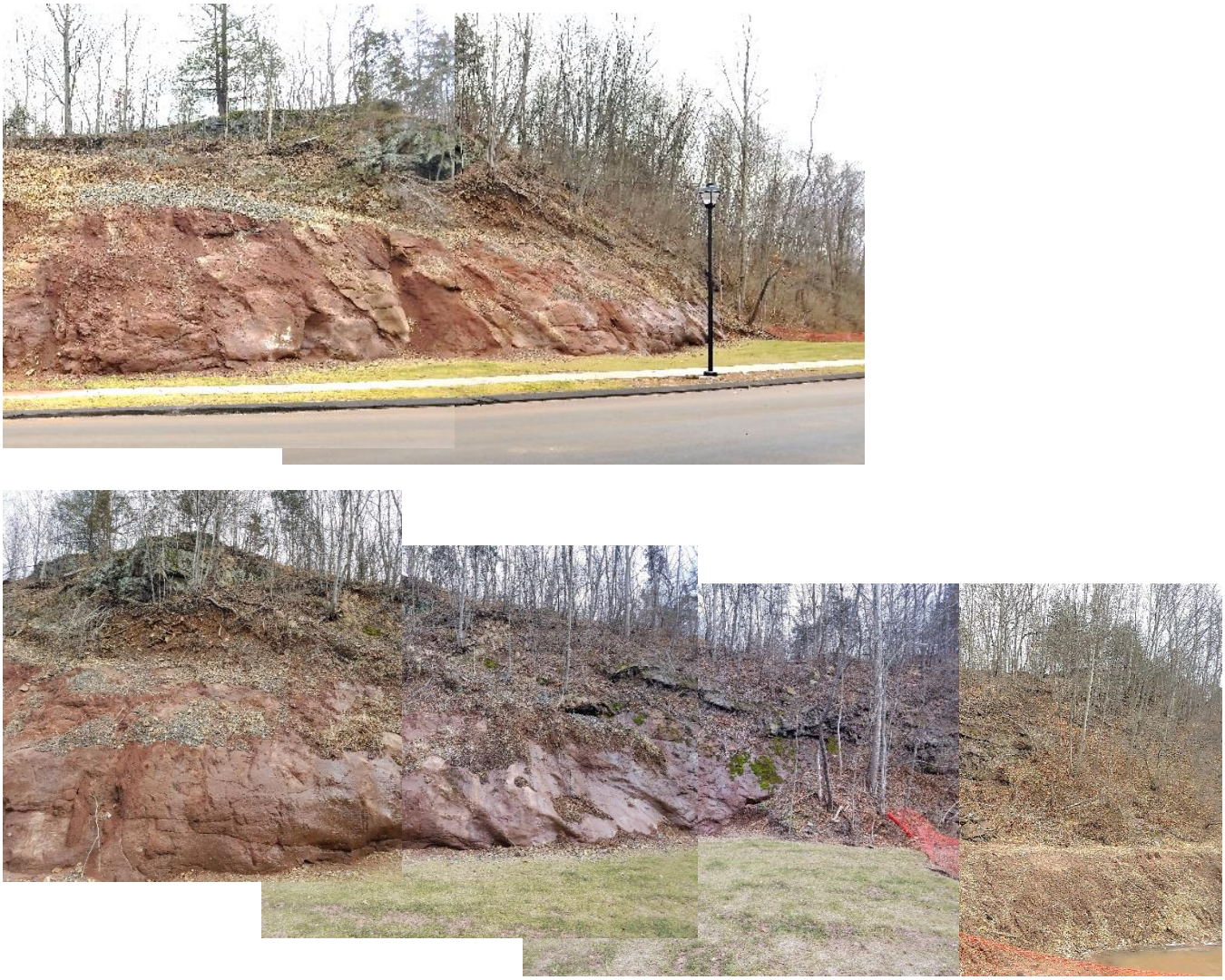

Figure VII-7

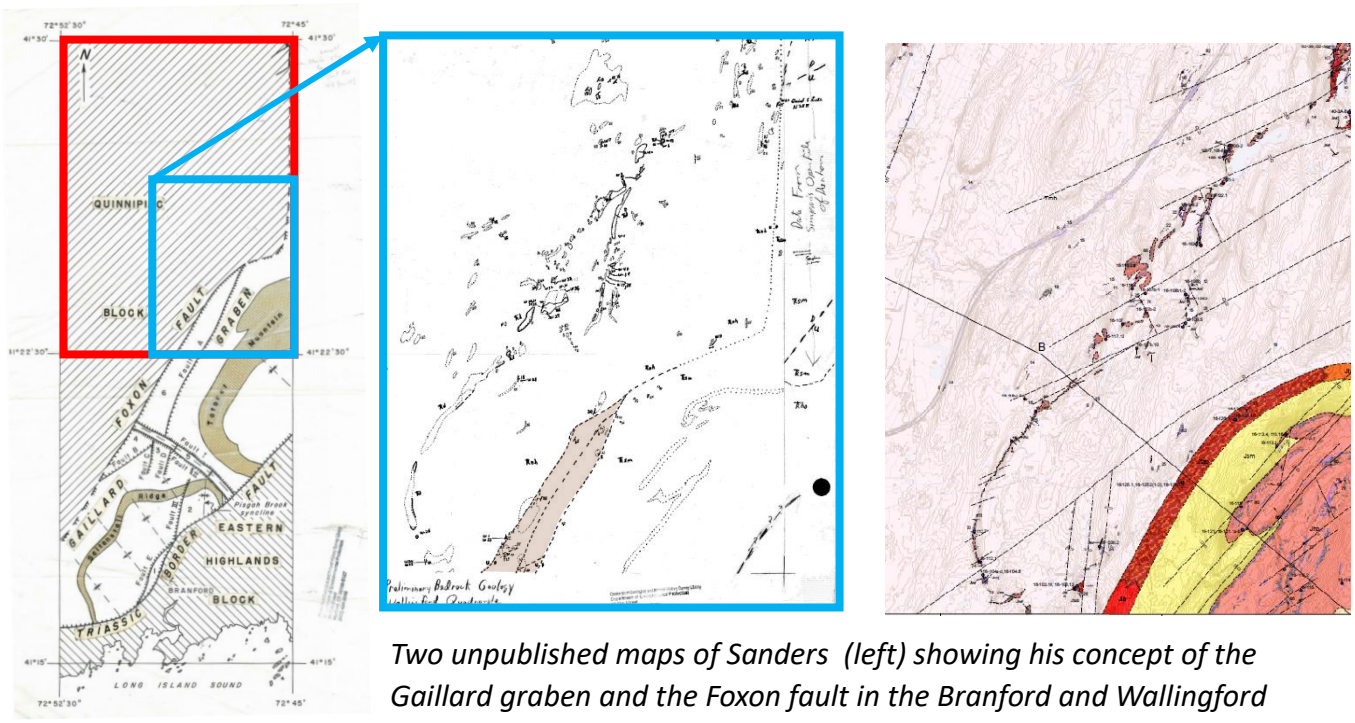

Two unpublished maps of Sanders (left) showing his concept of the Gaillard graben and the Foxon fault in the Branford and Wallingford quadrangles. Our map (right) of the area outlined by blue rectangle.

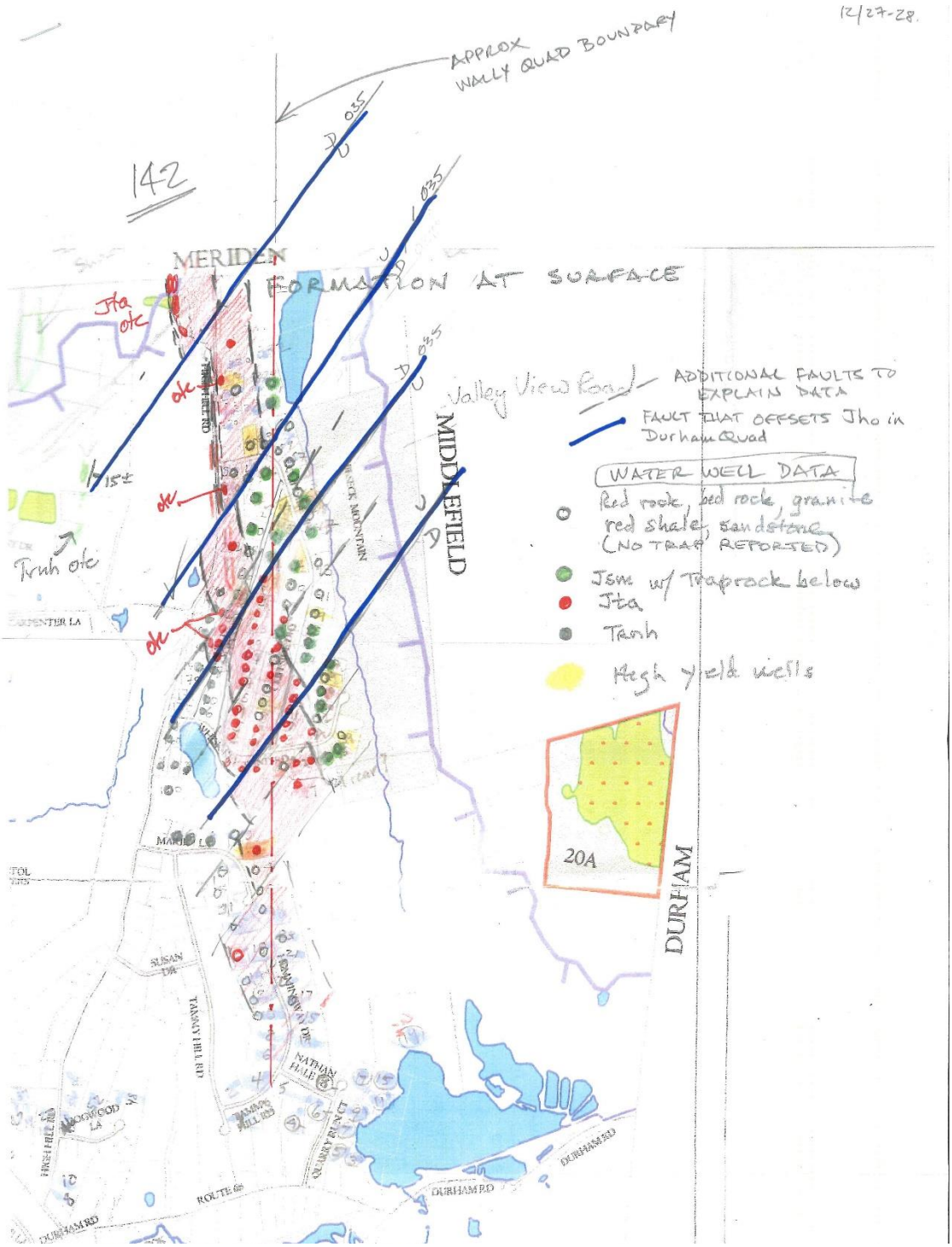

Figure VII-8. Work sketch map of water well data, NE-corner of quadrangle and part of Durham quadrangle. Compare with final map shown as Figure I-59 in Appendix I.

Appendix VIII. Location information for illustrations and Figures.

Figure number	Local area #	Location confidence[1]	Latitude	Longitude
Figure 1	map			
Figure 2	diagram			
Figure 3A, B	123	A	41.400327	-72.788725
3C	116	A	41.424098	-72.798511
3D	110	B	41.43547	-72.82896
Figure4A	141	C	41.4987	-72.79854
4B	135	A	41.472077	-72.829207
4C	135	A	41.479434	-72.82773
4D	141	C	41.4994	-72.79612
4E	141	C	41.4999	-72.79529
Figure 5B	103	A	41.379132	-72.8058398
5C	103	A	41.411658	-72.787522
5D, E	103	A	41.3788556	-72.808318
Figure 6A	126	A	41.404123	-72.775716
6B	126	A	41.403704	-72.775326
6C	126	A	41.404203	-72.775754
6D, E, F	Durham	A	41.433495	-72.722326
Figure 7A, B	121	A	41.386042	-72.773093
Figure 9A, B	115	B	41.37804	-72.76548
9C	114	A	41.388899	-72.758809
9D	113?	C	41.397	-72.761
Figure 10A	112	B	41.38204	-72.82565
10B	112	B	41.38281	-72.82666
10C	112	C	41.3848	-72.827
Figure 11A	107	B	41.41642	-72.79923
11B, C	107	B	41.41646	-72.799201
11D	106	B	41.43458	-72.783003
Figure 12A, B	104	A	41.380541	-72.825599
12C	100	A	41.440886	-72.779501
12D	131	B	41.461382	-72.841095
Figure 13A	130	A	41.463116	-72.849805
13B	131	A	41.458018	-72.842173
13C	131	A	41.459878	-72.839036
13D	131	A	41.495055	-72.890067
Figure 14	102/108/108s	map		
Figure 15A	129S	B	41.48171	-72.83728
15B	129	D	41.4812	-72.8708
Figure 16A, B	129S	E		
Figure 17A, B	129S	D	41.48122	-72.8708
Figure 18A, B, C	Boulder Knoll, Cheshire	E		
18D	Boulder Knoll, Cheshire	D	41.4737	-72.8767

Figure number	Local area #	Location confidence[1]	Latitude	Longitude
Figure 19A	129S	B	41.481662	-72.870563
19B, C	Boulder Knoll, Cheshire	D	41.47306	-72.8773
Figure 20A	Boulder Knoll, Cheshire	E		
20B	129S	B	41.481742	-72.870679
20C, D	Boulder Knoll, Cheshire	E		
Figure 21A-E	Boulder Knoll, Cheshire	E		
Figure 22A, B	Boulder Knoll, Cheshire	B	41.475892	-72.875558
22C, D	Boulder Knoll, Cheshire	E		
Figure 23	129S	B	41.48171	-72.83728
Figure 24A-D	129S	B	41.481641	-72.870694
Firgure 25	129S	B	41.481687	-72.87059
Figure 26	129S	A	41.4766	-72.874938
Figure 27A	129C	map		
27B, C	129C	A	41.503949	-72.981672
27D	129C	A	41.485525	-72.868211
Figure 28A, B	129C	A	41.485594	-72.867968
Figure 29	132	map		
Figure 30	132	D		
Figure 31	132	D		
Figure 32A	132	D		
32B	132	D		
32C	132	D		
Figure 33, 34		diagrams		
Figure 35	126, Durham	map		
Figure 36A, B	103b	A	41.383532	-72.800877
Figure 37-40		diagrams		
Figure VII-1	131	A	41.459878	-72.839036
Figure VII-2	131	A	41.458321	-72.841182
Figure VII-3	131	A	41.458765	-72.841389
Figure VII-4	131	A	41.495055	-72.890067
Figure VII-5	131	A	41.458337	-72.841662
Figure VII-6	104	A	41.380541	-72.825599

A. Location confidence:

A. Recorded by field or camera GPS

B. Not recorded, accurate location on ArcGIS map

C. Not recorded, approximately located on ArcGIS map

D. Not recorded, approximately located on Local Area map

E. Not recorded, location W of quadrangle boundry in Boulder Knoll City Park, Cheshire

Bedrock Geology of the Wallingford Quadrangle, New Haven County, Connecticut

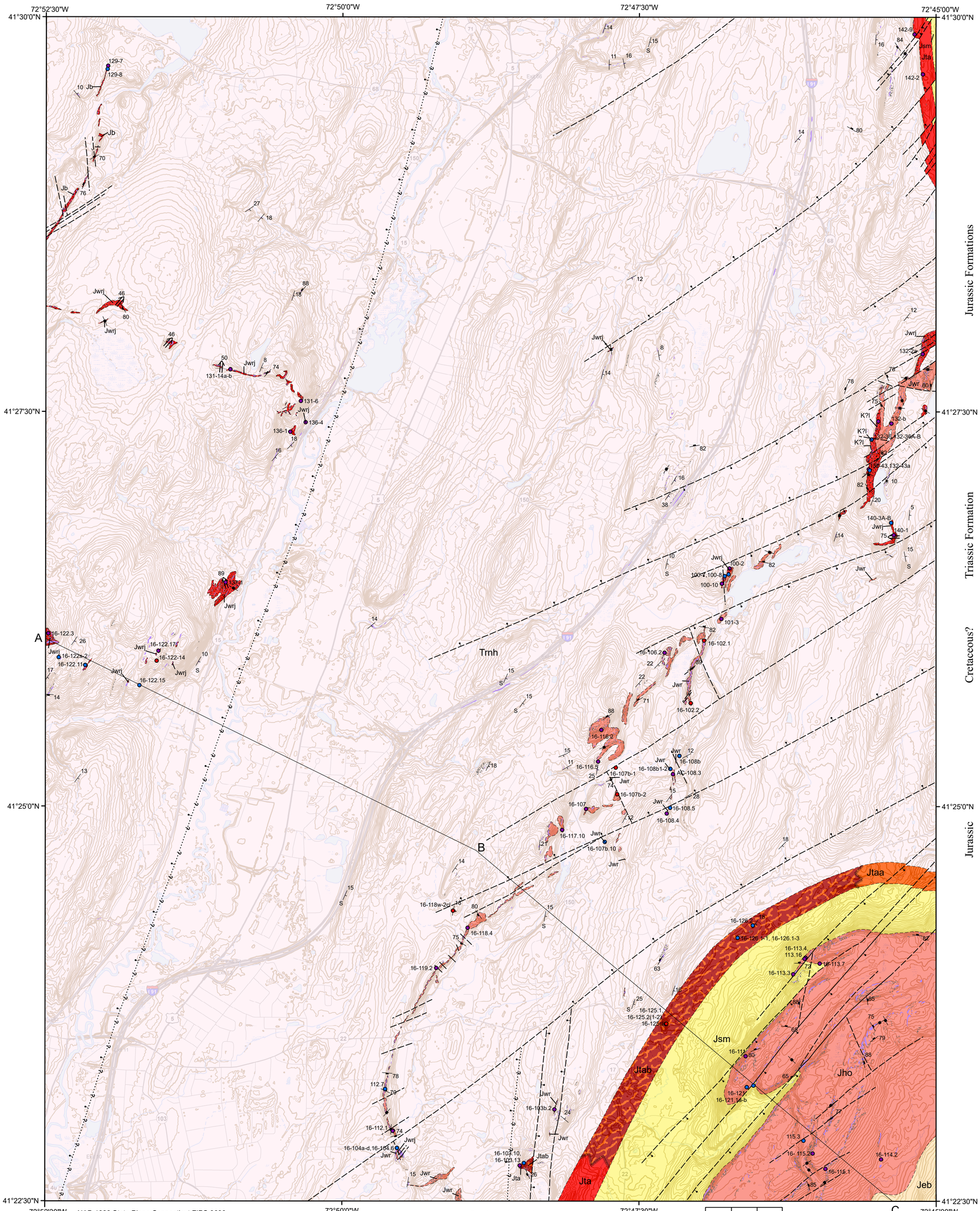

Explanation

Areas of outcrop shown in purple; areas with numerous small outcrops and bedrock near the surface are shown by stippled overprint. Grain-size descriptors follow customary usage.

Jurassic Formations

Jeb — East Berlin Formation

Maroon siltstone and fine-grained sandstone (Sanders, 1972b). Not exposed in Wallingford quadrangle; closest exposures in Branford quadrangle (Sanders, 1972b) along northeast shore of Lake Gaillard ~100 m south of Wallingford quadrangle boundary.

Jho — Holyoke Basalt

Basalt, gray, dark gray and greenish gray on freshly broken surface, weathers to tea-brown patina. Composed of gray plagioclase feldspar laths up to 0.5 mm in length and dark gray stubby pyroxene crystals ~0.5 mm in length in a gray groundmass. Base not exposed in quadrangle; top vesicular with local soil pockets; top exposed in Crooked Creek near southeast corner of quadrangle. Lower third with columnar joints and segregation sheets composed of ferro-diorite. Curvilinear columnar entablature reported in some locations. Vesicles and amygdules reported in upper part of unit. Ridge-forming and generally cliff-forming. Approximately 200 m thick.

Jsm — Shuttle Meadow Formation

Reddish-brown to grayish-red siltstone and very fine-grained sandstone with rare medium-grained sandstone lenses overlying scour surfaces. Sandstone ripple-stratified. Poorly exposed in quadrangle; only positively correlated Shuttle Meadow Formation seen below (but not in contact with) Holyoke Basalt in Gulf Brook and its tributary and an unnamed intermittent stream north and east of Northford Village. Approximately 150 m thick based on width of outcrop.

Jta, Jtaa, Jtab — Talcott Basalt

Dark bluish gray massive or pillowed basalt (Jta) and volcaniclastic breccia (Jtab). Base exposed at only one location; top not exposed in quadrangle. Pillow basalt exposed only in southern part of quadrangle where it is fine-grained and even textured; vesicles and pillows reported in other locations, but not seen elsewhere in the Wallingford quadrangle. Basalt flows better exposed to south in Branford quadrangle. Volcaniclastic breccia is more common and exposed from the southern edge of the quadrangle to the eastern edge just north of Totoket Mountain. Breccia consists of rounded to angular clasts of scoria and both massive and vesicular basalt. Some basalt clasts have chilled margins. Breccia also contains sedimentary clasts and matrix, dominantly quartz and feldspar, typical of arkosic sediments. Immediately north of Totoket Mountain Talcott Basalt is extensively altered and crops out poorly (Jtaa). Locally and in subsurface renderings Talcott Basalt is undifferentiated (Jt). Thickness approximately 140 m based on width of outcrop.

Triassic Formation

Trnh — New Haven Arkose

Poorly exposed arkosic conglomerate and conglomeratic sandstone; coarse- to fine-grained arkosic sandstone and siltstone. Coarser grained rocks found generally on the eastern side of quadrangle where they are ridge-forming and locally may be exposed as low cliffs; lenticular beds, internally mostly unbedded with rare tabular cross-bedding; gray to pinkish gray, poorly sorted; may contain cobbles up to 30 cm. Finer grained rocks found in stream valleys and artificial exposures along highways in central and west side of quadrangle; well bedded with cross-bedding and ripple lamination; generally brick-red with local pale green reduction spots and white caliche nodules. New Haven Arkose is host rock for all Jurassic intrusive rocks found in quadrangle. Neither top nor base exposed. Thickness not determined.

Intrusive Rocks

Cretaceous?

K?l — Lamprophyre

Gray to black, 1-2 m dikes intruded into the West Rock Diabase in the east-central portion of quadrangle. Composed of finely crystalline lamprophyre with phenocrysts, up to 3 cm in diameter, of biotite, amphibole, and clinopyroxene, set in a groundmass of amphibole, titanaugite, magnetite and late feldspar. Dike centers contain irregularly shaped vesicles and calcite-filled amygdules.

Jb — Buttress Diabase

Buttress Dike. Diabase dikes, fine- to medium-grained, massive to locally brecciated, locally vesicular and/or amygdaloidal. Interpreted, based on chemical affinities, to have fed the Holyoke Basalt (Philpotts and Martello, 1986). Consists of plagioclase laths and phenocrysts and clinopyroxene phenocrysts and aggregate grains, commonly with mesostasis. Dikes form discontinuous ridges in the northwestern corner of quadrangle and continue southwestward into the Mount Carmel quadrangle where they cross-cut dikes and sills of West Rock Diabase. Extensive breccia consists of non-vesicular diabase fragments. May have diabase or sedimentary matrix. Considered autobreccia by Philpotts and Martello (1986). Sedimentary rocks locally contaminate the diabase. Several local areas of Cu-mineralization.

Jurassic

Jwr, Jwrj — West Rock Diabase

Fairhaven and Cross-Rocks Dike. Diabase dikes and sills, fine- to medium- grained, massive to locally brecciated, locally vesicular and/or amygdaloidal. Consists of plagioclase laths and phenocrysts, clinopyroxene phenocrysts and aggregate grains, commonly with mesostasis. Chilled margins contain olivine microcrysts. Diabase dikes interpreted, based on chemical affinities, to have fed the Talcott Basalt (Philpotts and Martello, 1986). Dikes form ridge-lines common to the area. Local breccia consists of non-vesicular diabase fragments, mostly angular, lacking chilled margins, with or without sedimentary matrix. Formed by two pulses of intrusion; where diabase from both pulses is exposed in contact, the younger diabase displays chilled margins and columnar jointing. Rocks from both intrusive events have the same mineralogical and chemical composition. Sedimentary rocks locally contaminate the diabase.

Contact — Solid where observed, dashed where inferred, hatched where gradational.

Fault — Showing sense of movement where interpreted. Solid where observed, dashed where inferred, stippled and queried where location uncertain.

Rocks Close to Surface

Numerous small outcrops or abundant broken rock at surface; slightly darker pattern is outcrop reported by Porter (1960) that is no longer accessible for various reasons.

- Strike and dip of bedding.
- Strike and dip of bedding measured by Sanders (1972b) at inaccessible outcrop.
- Strike and dip of inclined joints.
- Strike of vertical joints.
- Entrance to collapsed adit.
- Trend and plunge of columnar joints or line of intersection of two or more joint sets.
- Location of sample corresponding to thin section (blue), geochemical analysis (red), or both (purple).

NAD 1983 State Plane Connecticut FIPS 0600
Lambert Conformal Conic
Contours.....CTDEEP, 2011...http://www.ct.gov/deep
Hydrography...CTDEEP, 2005...http://www.ct.gov/deep
Roads.....CTDEEP, 2006...http://www.ct.gov/deep

Scale 1:24,000

0.5 0.25 0 0.5 1 Miles
1 0.5 0 1 2 Kilometers
4,500 2,250 0 4,500 9,000 Feet

MN
13° 28'
2019 MAGNETIC NORTH DECLINATION AT MAP CENTER

1 SOUTHINGTON
2 MERIDEN
3 MIDDLETOWN
4 MOUNT CARMEL
5 DURHAM
6 NEW HAVEN
7 BRANFORD
8 GUILDFORD

LOCATION OF QUADRANGLE

Randolph Steinen (1,2) and Allison Charney (3)

Assisted by: James Bogart (1), Rebecca VanderLeest (2), Heidi Salg (3), Kaitlin Taylor (3), and Ian Hillenbrand (1)

Final Cartography by: Taryn Isenburg (1)

2021

Author Affiliations
1. Connecticut Geological Survey, Department of Energy and Environmental Protection
2. University of Connecticut, Department of Geosciences
3. Central Connecticut State University, Department of Geological Sciences

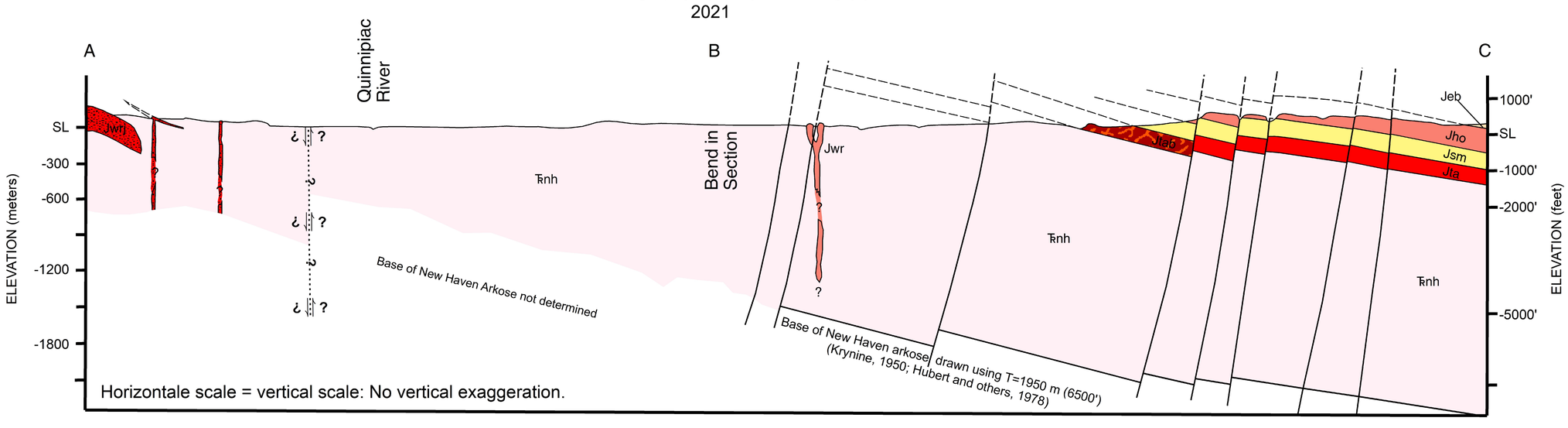

Funded in part by the United States Geological Survey National Cooperative Geologic Mapping Program under State Map award number G16AC00180, 2016

Produced by the Connecticut Geological Survey, Department of Energy and Environmental Protection
www.ct.gov/deep/geology